Journal of Applied Mechanics

(Contributions of the ASME Applied Mechanics Division)

Stresses in a Tube Under High Radial Temperature Variation . . . . . Chieh-Chien Chang and Wen-Hwa Chi 101

Stresses and Deformations of Hinged Shells . . . . . G. Herrmann and I. M. Chamorro, Jr. 109

Maximum Deflection of Membranes . . . . . P. S. Shaw and M. Perrone 117

Bending of Plates by Concentrated Couples and Forces . . . . . Yi-Yuan Yu 129

Plastic Flow in a Notched Bar . . . . . E. H. Lee 140

Transformations of Tension Beam a Bar to a Plate . . . . . J. N. Goodier and C. S. Hsu 147

A Curved Bar With Tangential Boundary Loads . . . . . Ning-Gan Wu and C. W. Nelson 151

On the Equations of Motion of Cylindrical Shells . . . . . P. M. Naghdi and J. G. Berry 160

Vibrations of Shells in an Acoustic Medium . . . . . H. H. Bleich and M. L. Baron 167

Frequencies and Modes of Cylindrical Shells . . . . . M. L. Baron and H. H. Bleich 178

On the Thickness of Normal Shock Waves in a Perfect Gas . . . . . A. H. Shapiro and S. J. Kline 185

Brief Notes

The Delayed Hot-Wire Problem . . . . . Walter Kinzel 193

Plastic Potential Theory and Prandtl Bearing Capacity Solution . . . . . R. T. Shield 193

Comparison of the Hardening Produced in a Yield-Point Steel by Uniaxial Loading Under Static and Under Dynamic Conditions . . . . . D. R. Harvey and M. P. White 194

Note on the Problem of Vibrations of Slightly Curved Bars . . . . . Eric Reissner 195

General Solution for Nonuniform Hinged-End Columns . . . . . L. E. Bissell 196

Method of Computing Principal Strains . . . . . N. J. Talbot 197

Use of Double-Exposure Photography in Photoelasticity . . . . . W. M. Kosh and R. A. Sage 198

Discussion on previously published papers by E. Lenkey, N. C. Dahl, P. Dergarabedian, E. A. Anderson, J. Mitchell, J. E. Jackson, D. S. Wood, and D. S. Clark 199

Book Reviews 202

JUNE, 1954

VOL. 21, NO. 2

Transactions of The American Society of Mechanical Engineers

Journal of Applied Mechanics

Papers Contributed to the Transactions by the ASME Applied Mechanics Division

EXECUTIVE COMMITTEE OF THE APPLIED MECHANICS DIVISION

N. M. Newmark, *Chairman* — N. J. Hoff, *Secretary*

John M. Lessells, *Technical Editor*

Published Quarterly by

The American Society of Mechanical Engineers

Publication Office, 20th and Northampton Streets, Easton, Pa.
Editorial Department at the Headquarters of the Society, 29 West Thirty-Ninth Street, New York 18, N. Y.

OFFICERS OF THE SOCIETY

Lewis K. Sillcox, *President*

James L. Kaw, *Treasurer* — C. E. Davies, *Secretary*
E. J. Kates, *Assistant Treasurer*

PUBLICATIONS COMMITTEE

Paul T. Norton, Jr., *Chairman* — Glennon A. Stetson, *Editor*
K. W. Clements, *Mgr. Editor*

By-Law: The Society shall not be responsible for statements or opinions advanced in papers or . . . printed in its publications (B13, Par. 4).

Published quarterly by The American Society of Mechanical Engineers. Publication office at 20th and Northampton Streets, Easton, Pa. The editorial department is located at the headquarters of the Society, 29 West Thirty-Ninth Street, New York, 18, N. Y. Cable address, "Dynamic, New York." Price $1.50 a copy, $5.00 a year; to members $2.50 a year, single copy price to members, $1.00. Changes of address must be received at Society headquarters seven weeks before they are to be effective on the mailing list. Please send old as well as new address. . . . By-Law: The Society shall not be responsible for statements or opinions advanced in papers or . . . printed in its publications (B13, Par. 4). . . . Entered as second-class matter March 14, 1955, at the Post Office at Easton, Pa., under the act of August 24, 1912. . . . Copyright, 1956, by The American Society of Mechanical Engineers. Reprints from this publication may be made on condition that full credit be given the JOURNAL OF APPLIED MECHANICS and the author, and that date of publication be stated.

Stresses in a Metal Tube Under Both High Radial Temperature Variation and Internal Pressure[1]

By CHIEH-CHIEN CHANG[2] AND WEN-HWA CHU,[3] COLLEGE PARK, MD.

The paper treats the stress distribution in a metal tube which is subject to a very high radial temperature variation and pressure. The radial temperature distribution across the tube wall and the variations of the modulus of elasticity and the coefficient of thermal expansion are obtained from experimental data, and all these effects of temperature are taken into account in the calculations.[4] The fundamental equations in the case of plane strain and plane stress can be formulated as the nonhomogeneous Whittaker differential equations. The corresponding solutions are obtained by the method of variation of parameters and in terms of Kummer series. An example is shown, and the stress distribution across the wall is given. For comparison, the stress distribution of the case of constant modulus of elasticity and coefficient of expansion is included.

Nomenclature

The following nomenclature is used in the paper:

A', B' = const
a, b, c = const
a' = coefficient of linear thermal expansion
E = modulus of elasticity
E^* = const
e_{11}, e_{22}, e_{33} = direct strains along radial, tangential, and axial directions
e_4 = thermal expansion at temperature, T
$F(\rho) = -e^{\rho} E \dfrac{de_4}{d\rho}$
g, h = const
$k = -\left(\dfrac{1}{2} + \dfrac{\mu'}{a}\right)$
$m = 1/a$
$M_{k,\pm m}(z)$ = confluent hypergeometric function
p = pressure
r, θ, x = cylindrical co-ordinates
$R(\rho) = -\dfrac{e^{\rho} E}{1-\mu}\dfrac{de_4}{d\rho}$
$\bar{R}(z) = R(\rho)$
$S_{k,\pm m}(-z)$ = Kummer's series
T = temperature, deg F
$z = -\dfrac{b}{a} e^{a\rho}$
δ = const
μ = Poisson's ratio
$\mu' = \dfrac{\mu}{1-\mu}$
$\rho = \log r$
σ_{11}, σ_{22}, σ_{33} = direct stresses along r, θ, x direction, respectively
ϕ = stress function (defined by Equation [4])
$\psi = \phi(-az)^{1/2} e^{z/2}$
$\bar{\psi}$ = defined by Equation [16]

Subscripts:

o = outside
i = inside

Superscripts:

1 = thermal stresses (no pressure applied)
2 = additional stresses due to pressure applied
21 = additional stresses attributed to internal pressure
22 = additional stresses attributed to external pressure

Introduction

The stresses of a finite-length circular tube with high radial temperature variation across the tube wall and uniform internal pressure constitute a complicated two-dimensional problem even within the range of elastic theory, since the stress distribution depends both on the axial and the radial distance. To simplify the problem to a one-dimensional one, two limiting cases may be considered. One is to assume that the tube is infinitely long, so that the strain is independent of the axial distance and the so-called plane-strain theory becomes valid. This affords a good approximation of the stress distribution in the central section of a long tube. The stresses in an infinitely long tube under uniform pressure without temperature gradient are well known (1). Timoshenko (2) gives further the thermal stresses for the cases in which the variation of mechanical properties of the material with temperature can be neglected.

The other limiting case is to assume that the tube is infinitely short or becomes virtually a thin ring, so that the plane-stress theory becomes valid. To a first approximation, the stresses are assumed to be independent of axial distance. Timoshenko also gives the thermal stresses of such a thin ring for the case where

[1] This problem was initiated by Prof. Guy Bryan, The Johns Hopkins University, during consulting work done for Van Zelm Associates, Inc., Baltimore, Md.

[2] Formerly, Research Contract Director, The Johns Hopkins University, Consultant to Air Research and Development Command, USAF. Now, Research Professor, Institute for Fluid Dynamics and Applied Mathematics, University of Maryland.

[3] Formerly, Research Assistant, Aeronautics Department, The Johns Hopkins University. Now, Institute for Fluid Dynamics and Applied Mathematics, University of Maryland.

[4] After completing the original manuscript, reference (7)[5] became available in which Dr. Hilton treats the same thermal stress problem with a method based upon the assumption that Poisson's ratio is exactly 1/2. In our analysis the Poisson's ratio need not be any particular constant and the method can be extended easily to the case where Poisson's ratio is temperature dependent.

[5] Numbers in parentheses refer to Bibliography at end of paper.

Contributed by the Applied Mechanics Division and presented at the Annual Meeting, New York, N. Y., November 29–December 4, 1953, of THE AMERICAN SOCIETY OF MECHANICAL ENGINEERS.

Discussion of this paper should be addressed to the Secretary, ASME, 29 West 39th Street, New York, N. Y., and will be accepted until July 12, 1954, for publication at a later date. Discussion received after the closing date will be returned.

NOTE: Statements and opinions advanced in papers are to be understood as individual expressions of their authors and not those of the Society. Manuscript received by ASME Applied Mechanics Division, August 18, 1952. Paper No. 53—A-4.

the mechanical properties of the material do not change with temperature. Lees (3) investigates the thermal stresses in tubes and takes into account the variation of the thermal-expansion coefficient with temperature. However, in the case where high temperature and pressure are applied to the inner wall of the tube and the outer wall is maintained at a very low temperature, both the expansion coefficient and the modulus of elasticity are functions of the temperature. Naturally, both become functions of the radial distance across the wall thickness. Further complication likely is introduced by the possible existence of plastic behavior instead of elastic behavior in a part of the material. The modulus of elasticity would then be a function of strain as well as temperature. A nonlinear differential equation rather than a linear one is involved in the general problem.

For preliminary investigation, the present analysis deals with the limiting cases mentioned, in which the material is homogeneous and isotropic and the temperature differences across the wall are not too high so that the theory of elasticity can be applied. The inner wall is heated to a high temperature, while the outer wall is maintained at 0 F. The radial temperature variations are measured experimentally. The modulus of elasticity is given graphically as a function of temperature. Owing to lack of test data, Poisson's ratio is assumed to be a constant for the present. Under these circumstances, the problem can be formulated as a linear, nonhomogeneous differential equation of the second order, which can be transformed into a Whittaker's equation within a certain approximation. The general solution can be obtained by the method of variation of parameters. The arbitrary constants are determined completely by the given pressure exerted on the internal and external boundaries.

For simplicity, the solution is decomposed into two parts: One gives the thermal stresses resulting solely from temperature variations with no boundary pressure, and the other gives the additional stresses caused by boundary pressures. Following the superposition principle of linear differential equations with linear boundary conditions, the actual stress components in the cases where both pressure and temperature variation exist are the sum of the corresponding components contributed by each part.

As an example, a metal tube subject to a temperature of 400 F at the inner wall and to internal and external pressures is studied. Of course, the method given in this paper can be used for the case of the tube subject to much higher temperature as long as the elastic behavior of the material can be assumed to exist.

Formulation of the "Plane-Strain" Problem and the "Plane-Stress" Problem

A tube made of homogeneous isotropic material is subjected to pressures inside and outside the tube wall and also to a differential temperature distribution across the wall. The stress distribution within the tube depends both on the radial distance and the longitudinal distance along the axis, although the temperature and pressure distribution are axially symmetric. In order to simplify the analysis, two limiting cases are considered; i.e., (*a*) the tube is infinitely long, and (*b*) the tube is infinitely short. In the theory of elasticity (4) the former is called the plane-strain problem and the latter is called the plane-stress problem. The mathematical problem in the first case involves a single independent variable, namely, the radial distance r, while only to a first approximation do the stresses in the second case depend solely on the radial distance. This approximation is valid for sufficiently small $l/(r_o - r_i)$, l being the length of the tube (virtually, height of a thin ring).

(*a*) *Plane-Strain Problem—Infinitely Long Tube.* In the plane-strain problem, both the stresses and the strains are functions of the radial distance r from the tube axis. Owing to the axial symmetry of the loading, all the shear stresses and strains are zero. Then, if e_{11}, e_{22}, e_{33} are the direct strains, and σ_{11}, σ_{22}, σ_{33} the direct stresses, respectively, along the radial, tangential, and axial directions of the tube, the equation of equilibrium with no body force can be written (1) as

$$\frac{d\sigma_{11}}{dr} + \frac{\sigma_{11} - \sigma_{22}}{r} = 0 \quad \ldots\ldots [1]$$

and the stress-strain relations are

$$\left.\begin{aligned} e_{11} &= \frac{1}{E}(\sigma_{11} - \mu\sigma_{22} - \mu\sigma_{33}) + e_t \\ e_{22} &= \frac{1}{E}(\sigma_{22} - \mu\sigma_{33} - \mu\sigma_{11}) + e_t \\ e_{33} &= \frac{1}{E}(\sigma_{33} - \mu\sigma_{11} - \mu\sigma_{22}) + e_t \end{aligned}\right\} \quad \ldots\ldots [2]$$

where E is modulus of elasticity, μ is Poisson's ratio, e_t is thermal expansion at temperature T(deg F).

Obviously, e_{33} is a constant everywhere in the tube wall. Both E and μ may be functions of temperature. The total thermal expansion at temperature T is

$$e_t = \int_{T_0}^{T} a'\, dT$$

where a' is the coefficient of the linear thermal expansion and is also a function of temperature. T_0, as the lower limit of the foregoing integration, may be chosen as zero for simplicity.

The compatibility equations (reference 2) give

$$e_{22} - e_{11} + r\frac{de_{22}}{dr} = 0 \quad \ldots\ldots [3]$$

Equation [1] is automatically satisfied if a stress function ϕ is introduced so that

$$\left.\begin{aligned} \sigma_{11} &= \frac{\phi}{r} \\ \sigma_{22} &= \frac{d\phi}{dr} \end{aligned}\right\} \quad \ldots\ldots [4]$$

It is noted that from Equation [2]

$$\sigma_{33} = e_{33}E - e_tE + \mu(\sigma_{11} + \sigma_{22}) \quad \ldots\ldots [5a]$$

where the constant longitudinal strain e_{33} is determined by the condition that the resultant axial force over any cross-sectional area is zero, i.e.

$$\int_{r_i}^{r_o} \sigma_{33} r\, dr = 0 \quad \ldots\ldots [5b]$$

r_i and r_o being the inside and outside diameter of the tube, respectively.

Making use of Equations [2] and [4], we can write Equation [3] in terms of the stress function ϕ so that the fundamental differential equation governing ϕ is

$$\left.\begin{aligned} &\frac{d^2\phi}{d\rho^2} - \left(\frac{d\ln E}{d\rho} + \frac{1}{1-\mu^2}\frac{d\mu^2}{d\rho}\right)\frac{d\phi}{d\rho} \\ &\quad - \left(1 + \frac{1}{1-\mu^2}\frac{d\mu}{d\rho} + \frac{1}{1-\mu^2}\frac{d\mu^2}{d\rho}\right. \\ &\quad \left. - \frac{\mu}{1-\mu}\frac{d\ln E}{d\rho}\right)\phi = e^{\rho}\left[-\frac{E}{1-\mu}\frac{de_t}{d\rho}\right. \\ &\quad \left. + \frac{(e_{33} - e_t)E}{1-\mu^2}\frac{d\mu}{d\rho}\right] \end{aligned}\right\} \quad \ldots [6]$$

where $\rho = \ln r$ is introduced to simplify the equation. It is a nonhomogeneous linear equation of second order, if both E and μ are functions of temperature only, and thus are independent of the stress, i.e., ϕ. It is understood that the temperature is a function of r or ρ. E and μ can be written directly as functions of ρ.

So far there are no test data on the variation of the value of μ with temperature. Assume μ is independent both of temperature and ρ. Then Equation [6] reduces to

$$\frac{d^2\phi}{d\rho^2} - \frac{d \ln E}{d\rho}\frac{d\phi}{d\rho} - \left(1 - \frac{\mu}{1-\mu}\frac{d \ln E}{d\rho}\right)\phi = R(\rho) \ldots [7]$$

where

$$R(\rho) = -\frac{e^\rho E}{1-\mu}\frac{de_4}{d\rho} \ldots [8]$$

The boundary conditions are $\sigma_{11} = -p$ on the wall, or in terms of ϕ they are

$$\phi = -r_o p_o \text{ at } r = r_o \ldots [9a]$$

$$\phi = -r_i p_i \text{ at } r = r_i \ldots [9b]$$

(*b*) *Plane-Stress Problem—Infinitely Short Tube.* Suppose that a very short tube is subjected to thermal strain and pressure, both being independent of axial distance z and the angular position θ. To a first approximation, we postulate that the stresses are independent of the axial distance z. Stresses σ_{33}, σ_{23}, σ_{31} are zero everywhere, since they are zero on the end surfaces. Owing to axial symmetric conditions, the stresses also are independent of θ. Stresses σ_{11}, σ_{12}, σ_{22} are, therefore, functions of r only. Furthermore, the condition that no torque is applied implies $\sigma_{12} = 0$ everywhere. The equation of compatibility, Equation [3], has to be satisfied, while the other equations of compatibility involving derivatives with respect to z and the assumption of $\sigma_{33} = \sigma_{23} = \sigma_{31} = 0$ are disregarded in this approximation. Therefore the equations to be satisfied are the Equation of Compatibility [3], the Equation of Equilibrium [1], and Equations [2], the relations between stresses and strains. Again, a stress function can be defined by Equation [4] as in the previous case, and likewise governed by the following differential equation in order to satisfy Equations [2] and [3] with $\sigma_{33} = 0$ (not $e_{33} = \text{const}$)

$$\frac{d^2\phi}{d\rho^2} - \frac{d \ln E}{d\rho}\frac{d\phi}{d\rho} - \left(1 + \frac{d\mu}{d\rho} - \mu\frac{d \ln E}{d\rho}\right)\phi = -Ee^\rho\frac{de_4}{d\rho} \ldots [10]$$

A comparison of Equation [10] with [6] shows that only when $e_4 = 0$, $E = \text{const}$, $\mu = \text{const}$, is the differential Equation [10] identical with Equation [6], and the solution of a plane-strain problem an approximate solution to the plane-stress problem of the same boundary conditions. If the variation of μ is negligible, Equation [10] reduces to

$$\frac{d^2\phi}{d\rho^2} - \frac{d \ln E}{d\rho}\frac{d\phi}{d\rho} - \left(1 - \mu\frac{d \ln E}{d\rho}\right)\phi = F(\rho) \ldots [11]$$

where

$$F(\rho) = -e^\rho E\frac{de_4}{d\rho}$$

Solutions

In general, the nonhomogeneous Equations [7] and [11] cannot be solved easily if E is an arbitrary function of r. However, for a particular alloy steel under consideration, the experimental relation between the modulus of elasticity E and the temperature T is shown in Fig. 1. An approximate temperature-distribution curve for a tube made of this material was determined experimentally under certain conditions, Fig. 2. Based on these data, the curve $(d \ln E)/(d\rho)$ versus ρ is constructed graphically, Fig. 3. The differential Equations [7] and [11] will be solved in a

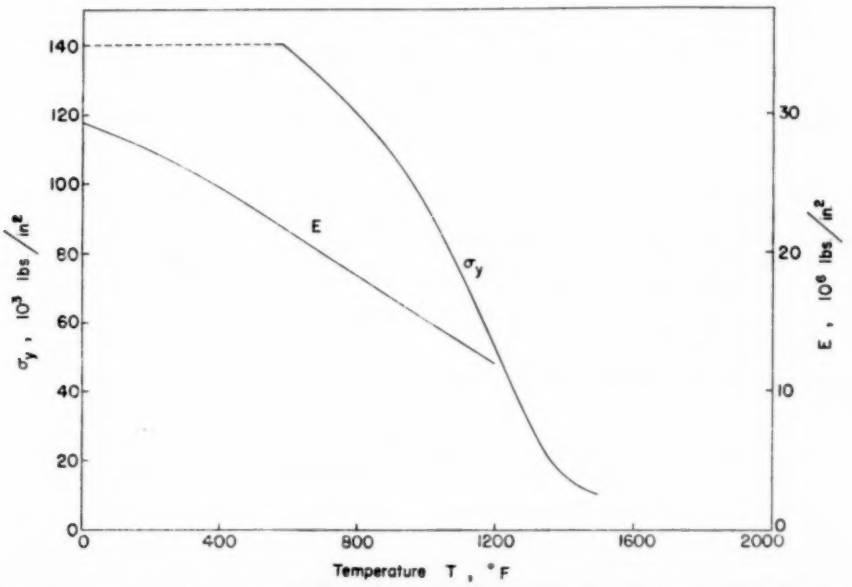

Fig. 1 Variation of Modulus of Elasticity E and Tensile Yielding Stress σ_y Versus Temperature T of a Typical Alloy Steel

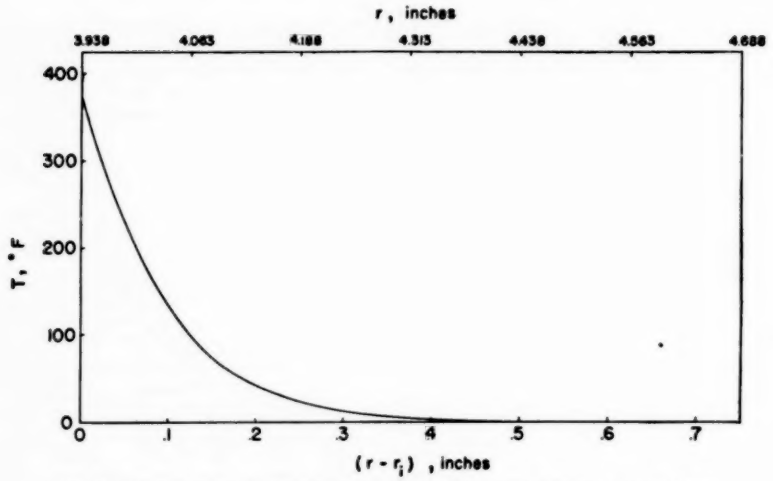

FIG. 2 TEMPERATURE DISTRIBUTION IN TUBE WALL FOR TYPICAL ALLOY STEEL (r_i = 3.938 in. r_o = 4.688 in.)

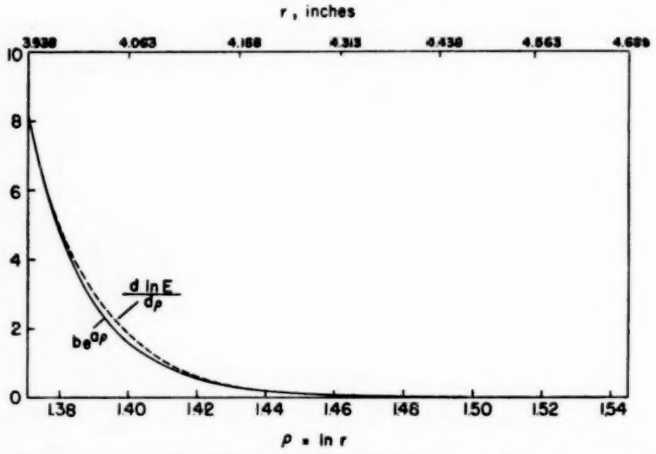

FIG. 3 VARIATION OF $d \ln E/d\rho$ ACROSS WALL THICKNESS FOR TYPICAL ALLOY STEEL (r_i = 3.938 in. r_o = 4.688 in.)

quite general fashion so that the treatment may not be limited only to materials of this kind.

Several simple expressions have been tried to represent the curve, $(d \ln E)/(d\rho)$. It is found that $be^{a\rho}$ fits the curve satisfactorily by adjusting the two free constants a and b. With this approximation as shown in Fig. 3, the next question is whether Equations [7] and [11] can be reduced to forms of differential equations for which the solutions are known.

For simplicity, introduce two new variables z and ψ to replace ρ and ϕ, respectively, as

$$z = -\frac{b}{a} e^{a\rho} = -\frac{1}{a} \frac{d \ln E}{d\rho} \quad \ldots\ldots [12]$$

and

$$\psi = \phi(-az)e^{z/2} \quad \ldots\ldots [13]$$

where the constant a is found to be negative and the constant b positive in practical cases. For the plane-strain problem Equation [7] can be transformed to

$$\frac{d^2\psi}{dz^2} + \left(-\frac{1}{4} + \frac{-\frac{1}{2} - \frac{\mu'}{a}}{z} + \frac{\frac{1}{4} - \frac{1}{a^2}}{z^2} \right) \psi = \bar{R}(z)e^{z/2}(-az)^{-3/2} \quad \ldots\ldots [14]$$

where

$$\bar{R}(z) = R(\rho)$$

$$\mu' = \frac{\mu}{1 - \mu}$$

The complementary equation of Equation [14] with $\bar{R}(z) = 0$ can be identified as Whittaker's equation if

$$-\frac{1}{2} - \frac{\mu'}{a} = k, \quad \frac{1}{a} = m$$

The complete solution of Equation [14] may be shown as

$$\psi = AM_{k,m}(z) + BM_{k,-m}(z) + \bar{\psi} \quad \ldots\ldots [15]$$

where A and B are two constants to be determined, $M_{k,\pm m}(z)$ are confluent hypergeometric functions (5) and

$$\psi = \frac{a}{2} M_{k,m}(z) \int_0^z \bar{R}(z) \frac{(-az)^{1/3} e^{z/2}}{a^2 z^2} M_{k,-m}(z)\, dz - \frac{a}{2} M_{k,-m}(z) \int_0^z \bar{R}(z) \frac{(-az)^{1/3} e^{z/2}}{a^2 z^2} M_{k,m}(z)\, dz \quad [16]$$

which can be derived by the method of variation of parameters (6) without much difficulty.

The problem now is how to evaluate the stresses. Kummer's first formula (5) gives

$$\left.\begin{aligned} M_{k,-m}(z) &= z^{1/3-1/a} e^{z/2} S_{k,-m}(-z) \\ M_{k,m}(z) &= z^{1/3+1/a} e^{z/2} S_{k,m}(-z) \end{aligned}\right\} \quad [17]$$

where the Kummer's series can be written as

$$S_{k,-m}(-z) = 1 + \frac{1+\mu'}{a-2} z + \left(\frac{1+\mu'}{a-2}\right)\left(\frac{1+\mu'-a}{2a-2}\right)\frac{z^2}{2!} + \cdots$$

$$S_{k,m}(-z) = 1 + \frac{\mu'-1}{a+2} z + \left(\frac{\mu'-1}{a+2}\right)\left(\frac{\mu'-1-a}{2a+2}\right)\frac{z^2}{2!} + \cdots$$

Then, $R(\rho) = \bar{R}(z)$ must be expressed analytically in terms of z. For the material used, the curve of the coefficient of linear thermal expansion a' versus temperature T and the graphically integrated curve $e_4 \left(= \int_0^T a'dT\right)$ versus T are both shown in Fig. 4. Value of e_4 is further determined graphically as a function of ρ in Fig. 5. As a good approximation, e_4 can be represented by $ce^{g\rho}$, Fig. 5, where c and g are constants. On the other hand, by integrating $(d \ln E)/(d\rho)$

$$E \cong E^* e^{\overset{b}{e}^{a\rho}} = E^* e^{-z} \quad [18]$$

where E^* is a constant determined to give a satisfactory representation of the graphically constructed curve E. This curve is also shown in Fig. 5 for comparison. Therefore Equation [8] can be expressed as

$$R(\rho) = \bar{R}(z) = hz^\delta e^{-z} \quad [19]$$

where

$$h = \frac{-gcE^*}{1-\mu}\left(\frac{-a}{b}\right)^\delta$$

a known constant and

$$\delta = \frac{1+g}{a}$$

another known constant. Making use of Equations [15] to [19] as well as Equation [13], one finds after some simplification

$$\phi = A' z^m S_{k,m}(-z) + B' z^{-m} S_{k,-m}(-z) - \frac{U(z)}{(-2a)} S_{k,m}(-z) + \frac{V(z)}{(-2a)} S_{k,-m}(-z) \quad [20]$$

where

$$U(z) = z^m \int_0^z \bar{R}(z) z^{-1-m} e^z S_{k,-m}(-z)\, dz = hz^\delta \left[\frac{1}{\delta - m} + \left(\frac{1+\mu'}{a-2}\right)\frac{z}{\delta - m + 1} + \left(\frac{1+\mu'}{a-2}\right)\left(\frac{1+\mu'-a}{2a-2}\right)\frac{z^2}{2!(\delta-m+2)} + \cdots\cdots + \frac{1+\mu'}{a-2}\frac{1+\mu'-a}{2a-2}\cdots\cdots\frac{1+\mu-(n-1)a}{na-2}\frac{z^n}{n!(\delta-m+n)} + \cdots\cdots\right]$$

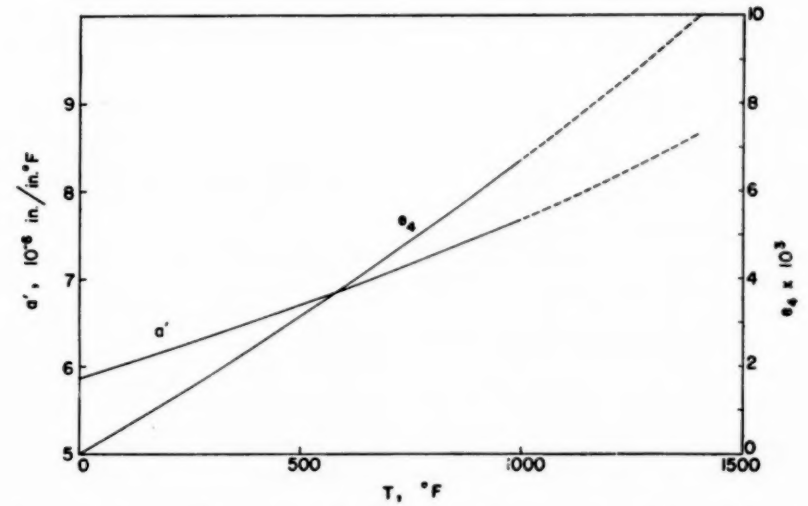

FIG. 4 VARIATION OF COEFFICIENT OF LINEAR THERMAL EXPANSION a' AND THERMAL STRAIN e_4 WITH TEMPERATURE T OF TYPICAL ALLOY STEEL

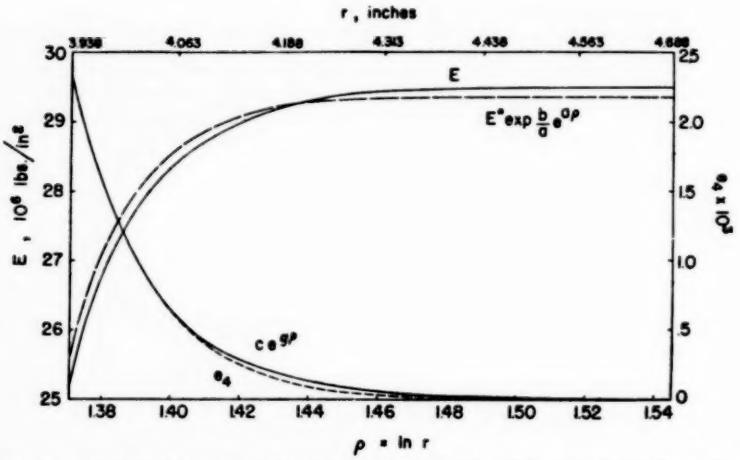

FIG. 5 VARIATION OF MODULUS OF ELASTICITY E AND THERMAL STRAIN e_4 ACROSS TUBE WALL

$$V(z) = z^{-m} \int_0^z \bar{R}(z)\, z^{-1+m}\, e^z\, S_{k,m}(-z)\, dz$$

$$= h\, z^{\delta}\left[\frac{1}{\delta+m} + \frac{\mu'-1}{a+2}\,\frac{z}{\delta+m+1} + \frac{\mu'-1}{a+2}\,\frac{\mu'-1-a}{2a+2}\,\frac{z^2}{2!(\delta+m+2)} + \cdots\cdots + \frac{\mu'-1}{a+2}\,\frac{\mu'-1-a}{2a+2}\cdots\cdots\frac{\mu'-1-(n-1)a}{na+2}\,\frac{z^n}{n!(\delta+m+n)} + \cdots\cdots\right]$$

$$A' = A\,(-a)^{-1/a}$$

$$B' = B\,(-a)^{-1/a}$$

A' and B' are the only remaining constants to be determined from the boundary conditions. It is obvious that the radial stress σ_{11} can be obtained from Equations [4] and [20]. In so far as the tangential stress σ_{22} is concerned, it can be obtained from Equation [4] by differentiating Equation [20]

$$\sigma_{22} = A'\frac{z^m}{r}\left[S_{k,m}(-z) - (-az)\frac{d}{dz}S_{k,m}(-z)\right] - B'\frac{z^{-m}}{r}\left[S_{k,-m}(-z) + (-az)\frac{d}{dz}S_{k,-m}(-z)\right] - \frac{U(z)}{(-2a)r}\left[S_{k,m}(-z) - (-az)\frac{d}{dz}S_{k,m}(-z)\right] - \frac{V(z)}{(-2a)r}\left[S_{k,-m}(-z) + (-az)\frac{d}{dz}S_{k,-m}(-z)\right] \cdots\cdots [21]$$

From Equations [4], [5a], and [5b], it is easy to show that for the plane-strain case

$$\sigma_{22} = \frac{E\int_{r_i}^{r_o} e_4\, Er\, dr - E\int_{r_i}^{r_o}\mu\left(\phi + r\frac{d\phi}{dr}\right)dr}{\int_{r_i}^{r_o} Er\, dr} - e_4 E + \frac{\mu}{r}\left(\phi + r\frac{d\phi}{dr}\right) \cdots\cdots [22]$$

So far the discussion has been on the plane-strain problem. Similar solutions can be obtained easily for the plane-stress case. Comparing Equation [7] with Equation [11], one finds that μ takes the place of μ' and $(1-\mu)h$ takes the place of h as

$$F(\rho) = -rE\frac{de_4}{d\rho} = (1-\mu)R(\rho)$$

Therefore a change of μ' to μ and h to $(1-\mu)h$ in the preceding results gives the approximate solution for the plane-stress problem, except that the arbitrary constants in the stress function have to be redetermined to satisfy the boundary conditions. Of course, $\sigma_{33} = 0$ here while the other stress components are calculated from Equations [4], [20], and [21].

Owing to the linearity of the differential equation and the boundary conditions, the stress function ϕ may be decomposed into two parts. The first part, $\phi^{(1)}$ is independent of the boundary pressure and is the stress function for thermal stresses (when no pressure is applied on the boundaries). The second part $\phi^{(2)}$ is the stress function for the additional stresses due to boundary pressure and may be decomposed further into two parts: $\phi^{(21)}$, proportional to p_i and $\phi^{(22)}$, proportional to p_o. Correspondingly we have

$$\sigma = \sigma^{(1)} + \sigma^{(2)} \text{ and } \sigma^{(2)} = \sigma^{(21)} + \sigma^{(22)}$$

Example. The physical constants determined by the properties of the material and temperature distribution for a tube of 7.876 in. ID and 9.376 in. OD are as follows:

$\mu = 0.3$	$E^* = 2.935 \times 10^7$
$a = -55.48$	$h = 6.070 \times 10^7$
$b = 8.560 \times 10^{32}$	$\delta = 7.249 \times 10^3$
$c = 7.643 \times 10^{21}$	$\mu' = 4.286 \times 10^3$
$g = -41.22$	

With Equations [20] to [22], the stress components are calculated in both the plane-strain case and the plane-stress case. The results are plotted in Figs. 6 to 10. Comparisons also are made in the figures with the known results in the plane-strain case where E and a' are assumed to be constant. In calculating these stresses (2) graphical integration of $\int_{r_i}^{r} Tr\, dr$ has been employed. The constants E and a' are taken to be the average values $\bar{E}$ ($\cong 27 \times 10^6$ psi) and a' ($\cong 6.2 \times 10^{-6}$ per deg F) over the temperature range covered.

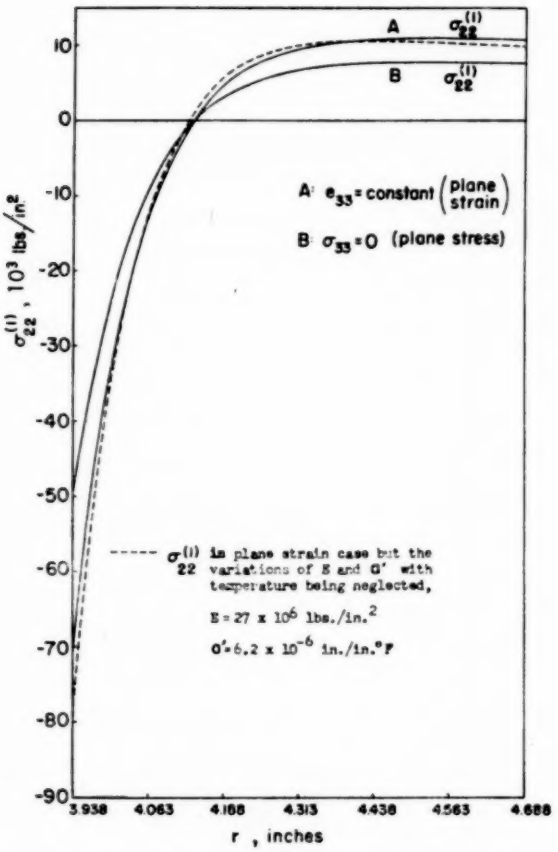
A $\sigma_{22}^{(1)}$
B $\sigma_{22}^{(1)}$
A: e_{33} = constant (plane strain)
B: σ_{33} = 0 (plane stress)
$\sigma_{22}^{(1)}$ in plane strain case but the variations of E and α' with temperature being neglected,
E = 27 x 10⁶ lbs./in.²
α' = 6.2 x 10⁻⁶ in./in.°F
$\sigma_{22}^{(1)}$, 10³ lbs/in.²
r, inches

FIG. 6 THERMAL STRESS $\sigma_{22}^{(1)}$ IN TANGENTIAL DIRECTION ACROSS TUBE WALL WITH ONLY TEMPERATURE GRADIENT AND NO PRESSURE APPLIED

With no applied pressure, the thermal stress $\sigma_{22}^{(1)}$ in the tangential direction is shown in Fig. 6. The curve for the plane-strain case (curve A) is similar in shape to that for plane-stress case (curve B). The equilibrium condition $\int_{r_i}^{r_o} \sigma_{22}^{(1)}\, dr = 0$ can be used as a check. Since only a small portion of the tube near the inner wall is at relatively high temperature, $\sigma_{22}^{(1)}$ decreases rapidly to rather high compression at the inner wall. The magnitude of the maximum compression is about 70×10^3 psi and 50×10^3 psi, respectively, in the plane-strain and plane-stress case and is roughly 7 times the maximum tension in both cases in the particular example. Curve C for the plane-strain case based on constants E and α' is shown for comparison. Since the effect of fast-decreasing modulus of elasticity exceeds that of increasing thermal-expansion coefficient with increasing temperature, the maximum thermal compression $\sigma_{22}^{(1)}$, Fig. 6, is 10 per cent lower than that calculated on the basis of constant modulus of elasticity and constant thermal-expansion coefficient.

The additional stress $\sigma_{22}^{(2)}$ in the tangential direction is shown in Fig. 7. The magnitude of either of $\sigma_{22}^{(21)}$ and $\sigma_{22}^{(22)}$ across the tube wall remains practically the same in the plane-stress case as in the plane-strain case, and each can be represented by a single curve in the present example. The known results of $\sigma_{22}^{(2)}$ (reference 1) with E assumed constant turn out to be independent of E and are the same in both the plane-strain case and

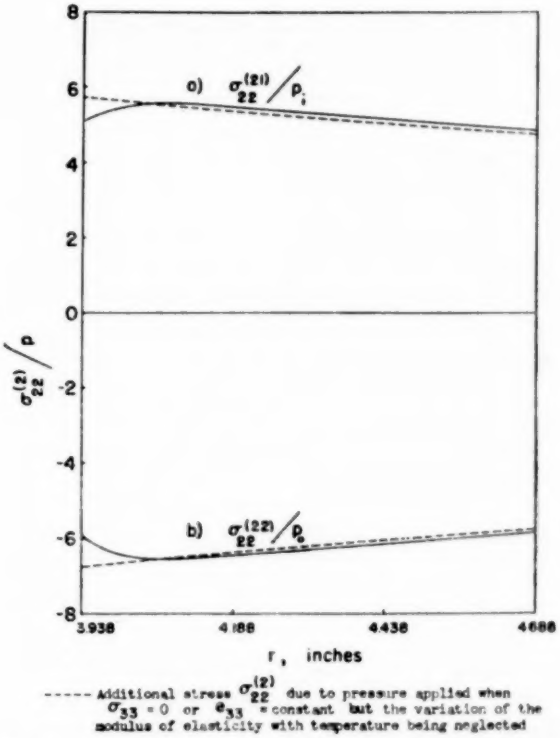
a) $\sigma_{22}^{(21)}/p_i$
b) $\sigma_{22}^{(22)}/p_o$
$\sigma_{22}^{(2)}/p$
r, inches
Additional stress $\sigma_{22}^{(2)}$ due to pressure applied when σ_{33} = 0 or e_{33} = constant but the variation of the modulus of elasticity with temperature being neglected

FIG. 7 ADDITIONAL STRESS $\sigma_{22}^{(2)}$ DUE TO PRESSURE APPLIED (*a*, Internal pressure; *b*, external pressure.)

the plane-stress case. Naturally, the internal pressure contributes tension to the tube in the θ-direction, while the external pressure contributes compression. It is found that the magnitudes of the stresses $\sigma_{22}^{(21)}$, $\sigma_{22}^{(22)}$ are slightly larger than those calculated by assuming E = const, except for a small region near the inner wall where they are considerably less. From equilibrium of forces

$$\frac{1}{r_i}\int_{r_i}^{r_o} \frac{\sigma_{22}^{(21)}}{p_i}\, dr = 1$$

and

$$\frac{1}{r_o}\int_{r_i}^{r_o} \frac{\sigma_{22}^{(22)}}{p_o}\, dr = 1$$

which can be used for checking purposes.

The thermal stress $\sigma_{11}^{(1)}$ in the radial direction, is shown in Fig. 8. Since no pressure is applied at either $r = r_i$ or $r = r_o$, $\sigma_{11}^{(1)}$ is zero at both $r = r_i$ and $r = r_o$. The magnitude of $\sigma_{11}^{(1)}$ is not of significant order and is roughly the same whether the variation of E with temperature is considered or not.

The additional stress $\sigma_{11}^{(2)}$ in the radial direction is shown in Fig. 9. The magnitude of $\sigma_{11}^{(21)}/p_i$ due to internal pressure decreases from unity to zero, while that of $\sigma_{11}^{(22)}/p_o$ due to external pressure increases from zero to unity with increase of radial distance. The value of $\sigma_{11}^{(2)}$ based on the temperature-dependent E does not deviate significantly from the constant E-case.

Furthermore, the thermal stress $\sigma_{33}^{(1)}$ in the axial direction is shown in Fig. 10. The magnitude of $\sigma_{33}^{(1)}$ in the plane-strain

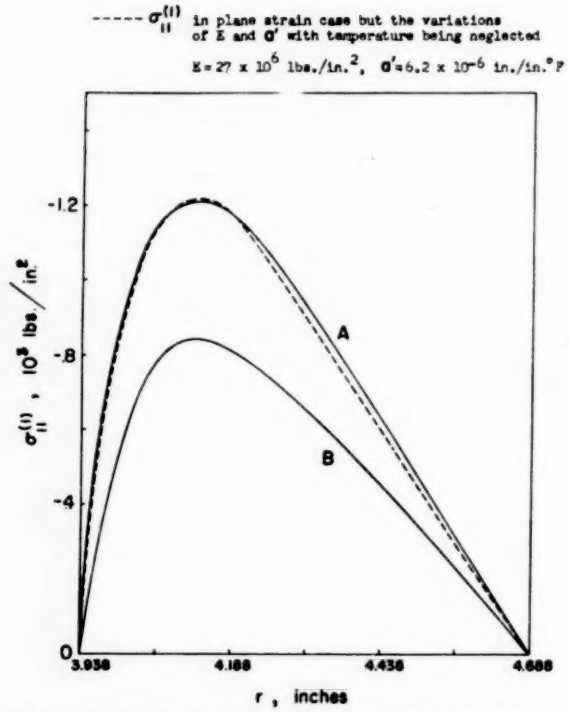

FIG. 8 THERMAL STRESS $\sigma_{11}^{(1)}$ IN RADIAL DIRECTION ACROSS TUBE WALL WITH ONLY TEMPERATURE GRADIENT AND NO PRESSURE APPLIED

(A, Plane-strain case; B, plane-stress case.)

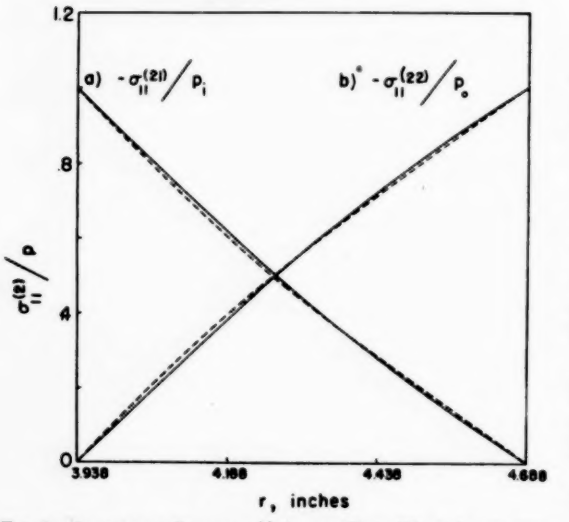

FIG. 9 ADDITIONAL STRESS $\sigma_{11}^{(2)}$ ACROSS TUBE WALL ATTRIBUTED TO (a) INTERNAL PRESSURE p_i, (b) EXTERNAL PRESSURE p_o

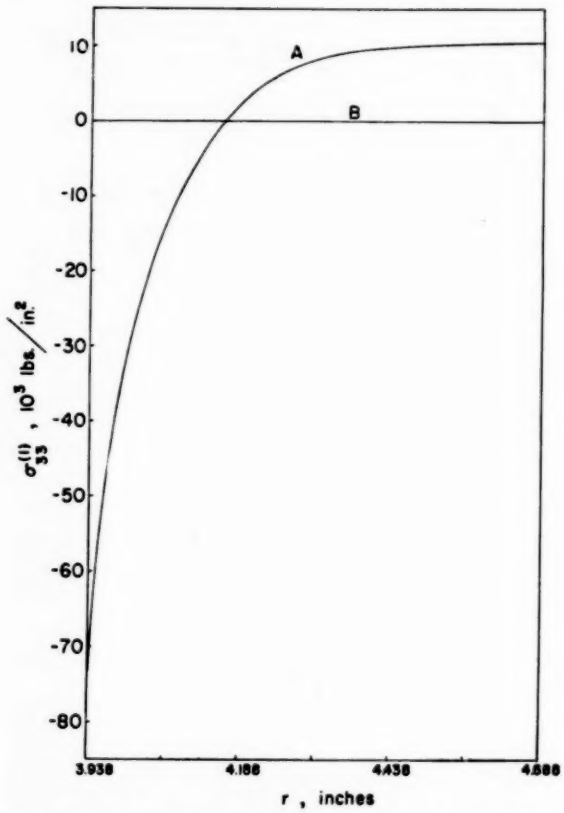

FIG. 10 THERMAL STRESS $\sigma_{33}^{(1)}$ IN AXIAL DIRECTION ACROSS TUBE WALL WITH ONLY TEMPERATURE GRADIENT AND NO PRESSURE APPLIED

(A, Plane-strain case; B, plane-stress case.)

case is roughly the same as that of $\sigma_{22}^{(1)}$. The distribution of $\sigma_{33}^{(1)}$ based on constant E has not been calculated for the present temperature distribution and the curves for the additional stress $\sigma_{33}^{(2)}$ also have been omitted.

BIBLIOGRAPHY

1 "A Treatise on the Mathematical Theory of Elasticity," by A. E. H. Love, Dover Publications, New York, N. Y., pp. 56–90, 78, 108, 143–146.

2 "Theory of Elasticity," by S. Timoshenko, McGraw-Hill Book Company, Inc., New York, N. Y., first edition, 1934, pp. 67, 364–376.

3 "The Thermal Stress in Solid and in Hollow Circular Cylinders Concentrically Heated," by C. H. Lees, Proceedings of the Royal Society, London, England, series A, vol. 101, 1922, p. 411.

4 "An Introduction to the Theory of Elasticity," by R. V. Southwell, Oxford University Press, London, England, second edition, 1941, pp. 400, 403.

5 "A Course of Modern Analysis," by E. T. Whittaker and G. N. Watson, The Macmillan Company (American edition), New York, N. Y., 1948, pp. 337–338.

6 "A Treatise on Differential Equations," by A. R. Forsyth, Macmillan and Company, Ltd., London, England, 1885, pp. 100-101.

7 "Thermal Stresses in Bodies Exhibiting Temperature-Dependent Elastic Properties," by H. H. Hilton, JOURNAL OF APPLIED MECHANICS, Trans. ASME, vol. 74, 1952, pp. 350–354.

Stresses and Deformations of Flanged Shells

By G. HORVAY[1] and I. M. CLAUSEN, JR.,[2] SCHENECTADY, N. Y.

Simple formulas are given for the effect of a flange on the deformations and stresses of an attached shell.

1 Introduction

AMONG the principal functions of a shell is containment of pressure, whether gas or liquid. The membrane stress caused in a shell by such pressure is the primary design criterion. However, near regions of rapid change of shape, or near an end, the shell incurs additional stresses. These usually are called discontinuity stresses or edge-load stresses which a shell, designed for membrane action only, is often not prepared to take. The reinforcement which must be provided to secure adequate behavior for discontinuity stresses may take the shape of a hoop ring or bracket support or may rely on thicker wall construction in a transition region. At an end the reinforcement (as well as means for attachment to the supporting structure) is usually provided by a flange, Fig. 1.

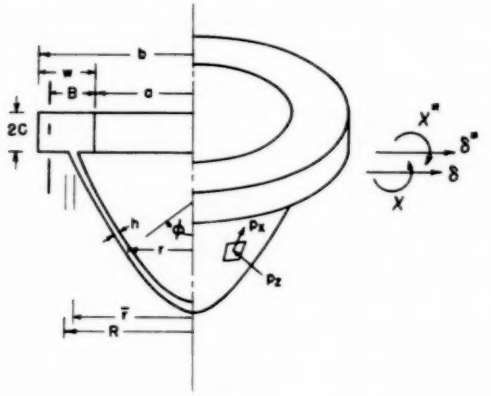

FIG. 1

Determination of the reinforcement provided by a flange is thus a basic and recurrent design problem. While this subject has been discussed extensively in the literature (1*a*)[3] and also in various codes, there does not seem to be available a simple, quick, yet reliable procedure for solution of the problem when the shell is noncylindrical. The scheme of calculation, developed in this paper, aims at filling this gap. The analysis involves the following steps:

1 Consider the shell and flange severed at their juncture and determine the misalignments of (and the stresses in) the two members under the direct loads or the temperature variations they experience (membrane analysis).

2 Calculate the internal reactions necessary to re-establish continuity of shell and flange. (In Fig. 4, $\mathfrak{M}$, H', and $\mathfrak{M}^*$, $H^{*\prime}$ are the moment and force reactions acting on shell and flange, respectively, per inch of shell periphery.)

3 Determine the stresses and displacements induced by these internal reactions (edge-load analysis).

4 Superpose the stresses and displacements so obtained on those determined in 1.

There is only one not entirely clear-cut step in the analysis. This entails recognition of the fact that while the edge moments $\mathfrak{M}$ and $\mathfrak{M}^*$ of Fig. 2 balance, the effective edge forces $\mathfrak{K}$ and $\mathfrak{K}^*$ add up to zero only when the shell is cylindrical at the juncture.

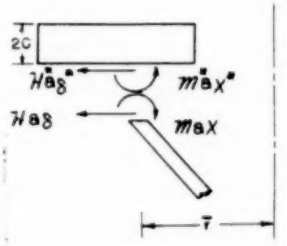

FIG. 2

In Section 2 we derive the formulas for the internal actions $\mathfrak{M}$, $\mathfrak{K}$, $\mathfrak{M}^*$, $\mathfrak{K}^*$ that must be developed at the common edge of shell and flange if the rotational and translational misalignments $\chi\dagger$ and $\delta\dagger$ are to be eliminated. Once these actions are known both the shell problem and the flange problem become statically determinate and can be handled by conventional methods.

In Section 3 we list the formulas which relate flange deformation and stress to applied moment and force.

In Section 4 we list the formulas which relate shell deformation and stress to applied moment and force.

In Section 5 we consider the effect of axial temperature variations.

In Section 6 we illustrate the use of the method by an example which involves weight, pressure, and temperature loadings. The example is somewhat artificial. Its purpose is to illuminate a number of features which could not otherwise be assembled into a single problem.

Our analysis considers only axisymmetrical loading and is based on the following additional assumptions:

(*a*) The shell is axisymmetric, thin-walled, not too flat near the flange edge ($\varphi \gtrsim \pi/4$), and its parameters (thickness, etc.), vary but slowly.

(*b*) The flange dimensions are small compared to the flange radius. More precisely, $(w/R)^2$ and $\mu w/R$ are negligible compared to 1.

---

[1] Development Engineer, General Electric Company, Knolls Atomic Power Laboratory. Mem. ASME. The Knolls Atomic Power Laboratory is operated by the General Electric Company for the Atomic Energy Commission. The work reported here was carried out under contract No. W-31-109 Eng. 52.

[2] Formerly, Member, Advanced Engineering Program; at present, Technical Engineer, Accessory Turbine Engineering, Aircraft Gas Turbine Division, General Electric Company. Assoc. Mem. ASME.

[3] Numbers in parentheses refer to the Bibliography at the end of the paper.

Contributed by the Applied Mechanics Division and presented at the Annual Meeting, New York, N. Y., November 29–December 4, 1953, of The American Society of Mechanical Engineers.

Discussion of this paper should be addressed to the Secretary, ASME, 29 West 39th Street, New York, N. Y., and will be accepted until July 12, 1954, for publication at a later date. Discussion received after the closing date will be returned.

Note: Statements and opinions advanced in papers are to be understood as individual expressions of their authors and not those of the Society. Manuscript received by ASME Applied Mechanics Division, April 13, 1953. Paper No. 53—A-43.

(*c*) Stresses and deformations are computed on a filastic basis.[4]

(*d*) Stress concentrations are disregarded.

(*e*) The loads are sufficiently small so that higher than first powers of the ensuing deformations are negligible.

Assumption (*a*) is conventional. Bending theories for non-axisymmetric shells have not yet reached the stage where they may be readily adapted to the problems of engineering design. The other assumptions of (*a*) could perhaps be relaxed at the cost of enormously increasing the required calculational labor. Recent work by E. Reissner and collaborators (2, 3) has brought very flat shells, as well as shells with fairly rapidly varying parameters within the scope of accessible analysis; some thick-walled shell theory is discussed in (4*a*). But inclusion of such considerations would conflict with our aim of presenting results immediately applicable to design practice.

When the shell is thin-walled and none too flat, one may, as is shown in reference (5) or (6), replace the shell at the juncture to the flange (in edge load analysis) by a tangent conical shell and still get reliable results. The formulas used may be called "zeroth" approximation formulas for "discontinuity" or "edge-load" analysis; they disregard variations of the attenuation length or of other shell parameters in the edge region. More accurate formulas are given in references (2) and (3), and some special ones in references (6) and (4*b*).

Assumption (*b*) is rather innocuous. Most flanges adhere to this assumption rather well. The assumption insures that flange sections displace and rotate rigidly. For greater accuracy the assumption may be dropped. This creates little extra labor.

Assumption (*c*) states that if the stresses and deformations involved are past the proportional limit, we nevertheless calculate as if the stress-strain curve continued linearly indefinitely. Clearly the results so obtained are based on a fictitious extension of the elastic range; to refer to these fictitious elastic conditions we shall use the abridged expression, "filastic conditions." To calculate in any other manner would greatly extend the work involved.

Assumption (*d*) implies that at sudden transitions in contours where discontinuity stresses arise, there also arise stress concentrations, sometimes of considerable magnitude, which we shall persistently disregard. These stress concentrations (which are significant over distances of about $2h$ from the edge—in contrast to the effect of edge loads[5] which are significant over distances of about $2l$) can be greatly reduced by use of adequate fillets, and they can be analyzed most satisfactorily by experimental methods. Much valuable information has been assembled by Heywood (7). In any given design one should be careful to check whether, under alternating loading, the regions of stress concentrations have adequate strength. Further information on the subject can be found in a recent report (8) which gives an exhaustive survey of the present state of art and numerous references.

Assumption (*e*) insures that (in Fig. 6) we may neglect the contribution $(R - \bar{r})\chi^{*2}/2$ to the horizontal flange displacement in comparison with the contribution $c\chi^*$. For very wide flanges this may turn out to be a poor approximation.

2 Flange and Shell Interaction

Fig. 1 shows a flanged shell and defines the flange dimensions a (inside radius), b (outside radius), $R = (a + b)/2$ (mean radius), $a + B$ (bolt circle radius), w (flange width), $2c$ (flange height). The figure also illustrates the shell parameters r (radius to mid-plane), latitude angle φ, and wall thickness h. The edge value, $\bar{r}$ of r, is usually, but not always, equal to a. (Edge values of shell quantities will be denoted by bars.)

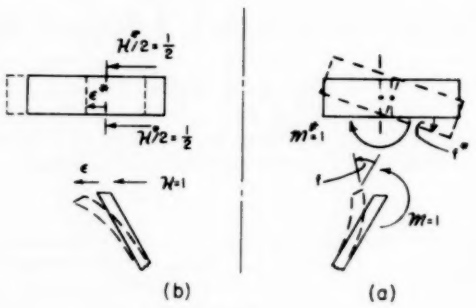

Fig. 3

Fig. 2 shows the flange severed from the shell. We refer to the edge value $\bar{\chi}$ of shell rotation χ under unit applied edge moment $\mathfrak{M}$ as "flexibility" and denote it by f, as illustrated in Fig. 3(*a*). We refer to the edge value of shell displacement δ under unit applied horizontal edge force $\mathfrak{C}$ as "expansivity" and denote it by ϵ, as illustrated in Fig. 3(*b*). Positive convention for $\mathfrak{M}$, χ, $\mathfrak{C}$, δ is defined in Fig. 2. The edge loads $\mathfrak{M}$ and $\mathfrak{C}$ imposed by flange on shell are, in general, specified as so many lb in/in, or so many lb/in at radius $\bar{r}$. The expressions of f and ϵ will be established in Section 4.

We denote rotation and displacement of flange where it joins the shell by χ^* and δ^*. Positive convention for χ^*, δ^*, and the edge loads $\mathfrak{M}^*$, $\mathfrak{C}^*$ imposed by shell on flange are defined in Fig. 2.

We refer to the rotation χ^* of the flange under unit applied moment as flange flexibility and denote it by f^* as in Fig. 3(*a*). We refer to the displacement δ^* of the flange under unit force applied at flange mid-plane as expansivity and denote it by ϵ^* as in Fig. 3(*b*). $\mathfrak{M}^*$ and $\mathfrak{C}^*$ are, in general, specified as so many lb in/in or so many lb/in at radius $\bar{r}$.

For narrow flanges (which obey assumption *b*) the displacement δ^* for a mid-plane force and the rotation χ^* due to a moment load are the same for all points of the cross section. When assumption (*b*) is dropped this is no longer true, and in this case f^*, ϵ^* will be understood to refer to displacement and rotation at radius $\bar{r}$. The expressions of f^* and ϵ^* will be derived in Section 3.

In general, we shall be concerned with moment $\mathfrak{M}^*$, force $\mathfrak{C}^*$, transmitted by shell to flange at radius $\bar{r}$, at the lower edge of the flange, as in Fig. 2. The consequent flange displacements are

$$\left.\begin{aligned} \chi^* &= f^*(\mathfrak{M}^* - c\mathfrak{C}^*) \\ \delta^* &= \epsilon^*\mathfrak{C}^* - c\chi^* \\ \hat{\delta}^* &= \epsilon^*\mathfrak{C}^* + c\chi^* \end{aligned}\right\} \quad \ldots\ldots\ldots [1a, b, c]$$

Here δ^* denotes the lower edge displacement, $\hat{\delta}^*$ the displacement of the upper edge of the flange. Equations [1] presuppose that assumption (*e*) of small rotation angle χ^* is obeyed.

Similarly, we shall be concerned with the effects of force $\mathfrak{C}$ and moment $\mathfrak{M}$ transmitted by flange to shell. The consequent deformations, forces, and moments will be enumerated in Section 4. Here we merely state that $\mathfrak{C}$ and $\mathfrak{M}$ cause edge rotation and edge displacement

$$\left.\begin{aligned} \bar{\chi} &= f\left[\mathfrak{M} - \frac{1}{2}\mathfrak{C}l_e\right] \\ \bar{\delta} &= \epsilon\left[-\frac{\mathfrak{M}}{l_e} + \mathfrak{C}\right] \end{aligned}\right\} \quad \ldots\ldots\ldots [2a, b]$$

[4] For definition of "filasticity" see later comments pertaining to assumption (*c*).

[5] See Equation [3] for definition of l.

In the foregoing

$$l = [3(1-\mu^2)]^{-1/4}\sqrt{\bar{r}h/\sin\bar{\varphi}}, \quad l_v = l\sin\bar{\varphi}\,. \quad [3a, b]$$

are the "attenuation length" of the shell and its vertical component, respectively. For $\mu = 0.3$, l has the value

$$l = 0.778\sqrt{\bar{r}h/\sin\bar{\varphi}}\,. \quad [3c]$$

In the foregoing we have enumerated the edge deformations of flange and shell under edge loads $\mathfrak{M}^*$, $\mathfrak{C}^*$ and $\mathfrak{M}$, $\mathfrak{C}$, respectively.

We are now ready to handle the flange-shell interaction problem.

When shell and flange are severed, the shell incurs, under the distributed meridional and normal loads $p_x(x)$, $p_z(x)$, psi, which act on it (see Fig. 1), membrane displacement and rotation δ_m, χ_m.[6] Under the prescribed temperature distribution $\vartheta(x)$ it incurs, furthermore, displacement and rotation δ_ϑ, χ_ϑ. The edge values of these deformations are $\bar{\delta}_m$, $\bar{\chi}_m$ and $\bar{\delta}_\vartheta$, $\bar{\chi}_\vartheta$, respectively. Their resultants will be denoted simply by δ_1, χ_1

$$\delta_1 = \bar{\delta}_m + \bar{\delta}_\vartheta, \quad \chi_1 = \bar{\chi}_m + \bar{\chi}_\vartheta\,. \quad [4]$$

Under the action of the given applied loads the flange incurs displacement and rotation δ_m^*, χ_m^*, and under the given temperature distributions it incurs displacement and rotation δ_ϑ^*, χ_ϑ^*. The resultant flange deformation at the place where it joins the shell, thus is

$$\delta_1^* = \delta_m^* + \delta_\vartheta^*, \quad \chi_1^* = \chi_m^* + \chi_\vartheta^*\,. \quad [5]$$

In general, we shall find that the membrane and temperature deformations cause misalignments in flange and shell. Consequently edge loads $\mathfrak{M}^*$, $\mathfrak{C}^*$ must be developed, giving rise to additional flange deformations χ_2^*, δ_2^*; and edge loads $\mathfrak{M}$, $\mathfrak{C}$ must be developed giving rise to additional shell deformations χ_2, δ_2, with edge values $\bar{\chi}_2$, $\bar{\delta}_2$ (for simplicity we shall denote the latter briefly by χ_2, δ_2) such that for the resultant edge deformations

$$\left.\begin{aligned} \bar{\chi} &= \chi_1 + \chi_2, & \bar{\delta} &= \bar{\delta}_1 + \bar{\delta}_2 \\ \chi^* &= \chi_1^* + \chi_2^*, & \delta^* &= \delta_1^* + \delta_2^* \end{aligned}\right\} \quad [6]$$

the "continuity conditions"

$$\bar{\chi} + \chi^* = 0, \quad \bar{\delta} = \bar{\delta}^*\,. \quad [7a, b]$$

of shell and flange be re-established: total shell rotation compensate for total flange rotation; total shell displacement be equal to total flange displacement.

Observing that χ_1^*, δ_1^*, χ_1, δ_1 are known from membrane and temperature analysis, χ_2^*, δ_2^*, χ_2, δ_2 have known Expressions [1], [2] in terms of edge loads, the continuity Equations [7] constitute two equations for the four unknowns $\mathfrak{M}^*$, $\mathfrak{C}^*$, $\mathfrak{M}$, $\mathfrak{C}$.

We need two more equations for determining the four unknown reactions. One is

$$\mathfrak{M} = \mathfrak{M}^*\,. \quad [8a]$$

and expresses moment balance at the juncture of flange and shell. The other is

$$\mathfrak{C} + \mathfrak{C}^* + \mathfrak{U}\cot\bar{\varphi} = 0\,. \quad [8b]$$

and expresses force balance at the juncture. In the foregoing $\mathfrak{U}$ is the vertical force, lb/in, which acts between flange and shell, as in Fig. 4. It has the value

$$\mathfrak{U} = W/2\pi\bar{r}\,. \quad [9]$$

[6] Subscripts m, ϑ, and e are used to denote membrane action, temperature action, and edge-load action, respectively, when such distinction appears desirable. x is the meridional co-ordinate, see Fig. 7.

where W is the resultant downward force (weight) supported by the flange.

We arrive at Equation [8b] as follows: The vertical force $\mathfrak{U}$ which acts on the shell edge is decomposed into a meridional force

$$N_{xm} = \mathfrak{U}/\sin\varphi\,. \quad [10]$$

(N_{xm} is our membrane solution at the edge), and a horizontal force $-\mathfrak{U}\cot\bar{\varphi}$. The forces H' and $H^{*\prime}$ which—due to continuity requirements—are called into action at shell and flange edge must balance

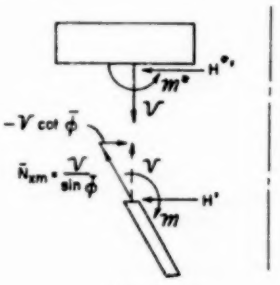

Fig. 4

$$H' + H^{*\prime} = 0\,. \quad [11]$$

the same as the moments $\mathfrak{M}$, $\mathfrak{M}^*$ balance in Equation [8a]. Denoting the resultant horizontal force of H' and of $-\mathfrak{U}\cot\bar{\varphi}$ by $\mathfrak{C}$

$$\mathfrak{C} = H' - \mathfrak{U}\cot\bar{\varphi}\,. \quad [12a]$$

and denoting the resultant edge load force on the flange by $\mathfrak{C}^*$

$$\mathfrak{C}^* = H^{*\prime}\,. \quad [12b]$$

the force balance Equation [11] reduces to [8b].

To summarize, we analyze the flanged shell as follows: (*a*) We calculate the edge deformations of flange and shell, when these are considered as severed, under the given distributed loads and temperature distributions. (*b*) We calculate the four edge loads required to re-establish continuity from the four Equations [7a, b], [8a, b]. (*c*) We calculate the effects of these edge loads stresswise and deformationwise. (*d*) We superimpose the results of (*a*) and (*c*).

Before proceeding to establishment of the formulas for f^*, ϵ^*, f, ϵ we shall slightly simplify step (*b*). Expressing $\mathfrak{M}^*$ and $\mathfrak{C}^*$ by Equations [8] in terms of $\mathfrak{M}$ and $\mathfrak{C}$, we write Equations [7a, b] on the basis of Equation [6] and the Expressions [1] for χ_2^*, δ_2^*, and Expressions [2] for χ_2, δ_2 in the form

$$\left.\begin{aligned} (f^* + f)\mathfrak{M} + (f^*c - fl_v/2)\mathfrak{C} &= -\chi\dagger \\ (f^*c - \epsilon/l_v)\mathfrak{M} + (f^*c^2 + \epsilon^* + \epsilon)\mathfrak{C} &= -\delta\dagger \end{aligned}\right\} \quad [13a, b]$$

where

$$\left.\begin{aligned} \chi\dagger &= \chi_1 + \chi_1^* + f^*c\mathfrak{U}\cot\bar{\varphi} \\ \delta\dagger &= \bar{\delta}_1 - \delta_1^* + (f^*c^2 + \epsilon^*)\mathfrak{U}\cot\bar{\varphi} \end{aligned}\right\} \quad [13c, d]$$

are known quantities. We shall refer to $\chi\dagger$, $\delta\dagger$ as the rotational and translational "misalignments" which must be eliminated by suitable edge loads $\mathfrak{M}$, $\mathfrak{C}$, $\mathfrak{M}^*$, $\mathfrak{C}^*$. When the misalignments are zero, then so are the edge actions.

By virtue of the identities

$$\epsilon = fl_v^2/2, \quad \epsilon^* = f^*c^2/3\,. \quad [14a, b]$$

to be established further below in Equations [25] and [22], we

may write solution of Equations [13a, b] in terms of the "flexibility ratio"

$$\rho_f = f/f^* \quad [15a]$$

and "expansivity ratio"

$$\rho_\epsilon = \epsilon^*/\epsilon \quad [15b]$$

as follows

$$\left.\begin{aligned} f\mathfrak{M} &= t_{MX}\chi\dagger + t_{M\delta}\delta\dagger/l_\epsilon \\ f\mathfrak{C}l_\epsilon &= t_{HX}\chi\dagger + t_{H\delta}\delta\dagger/l_\epsilon \end{aligned}\right\} \quad [16a,b]$$

where the "influence coefficients" t are given by

$$\left.\begin{aligned} t_{MX} &= -(1 + 4\rho_\epsilon)\rho_f/\Delta \\ t_{M\delta} &= t_{HX} = (\sqrt{6\rho_\epsilon\rho_f} - \rho_f)/\Delta \\ t_{H\delta} &= -2(1 + \rho_f)/\Delta \\ \Delta &= 1 + \rho_\epsilon + \rho_f/2 + \sqrt{6\rho_\epsilon\rho_f} + 4\rho_\epsilon\rho_f \end{aligned}\right\} \quad [17]$$

The coefficients $-t_{MX}$, $-t_{M\delta} = -t_{HX}$, $-t_{H\delta}$ are plotted in Fig. 5(a, b, c) versus ρ_f (for constant ρ_ϵ, full lines), and versus ρ_ϵ (for constant ρ_f, dashed lines), in the most frequently occurring range, $0.01 \leq \rho_\epsilon, \rho_f \leq 1.0$. These graphs are not drawn in sufficient detail to permit quantitative use; they serve merely as an aid in estimating the trends certain design changes may produce. The coefficients should be calculated from the simple Expressions [17].

3 Flange Action

We now proceed to derive the flexibility and expansivity formulas f^*, ϵ^* for the flange and establish the expressions of flange stresses.

We shall denote the flange cross-section area and the moment of inertia by A and I, respectively

$$A = 2cw, \quad I = 2c^3w/3 \quad [18a, b]$$

Let a moment $\mathfrak{M}^* = 1$ lb in/in be applied, at radius a, at the inner face of the flange. Then it follows from reference (4c) that the inside face of the flange rotates an angle

$$f_a^* = \frac{a^2}{EI}\left[1 + \left(\frac{1}{2} + \mu\right)\frac{w}{R} + \frac{1 + \mu}{2}\frac{w^2}{aR}\right] \quad [19a]$$

Likewise, it follows from reference (1b) that on applying the force $\mathfrak{C}^* = 1$ lb/in to the flange, at inside radius a, uniformly distributed over height $2c$, the internal face of the flange displaces outward an amount

$$\epsilon_a^* = \frac{aR}{EA}\left[1 + \mu\frac{w}{R} + \frac{w^2}{4R^2}\right] \quad [19b]$$

If the ratio w^2/aR is negligible compared to 1 then Formulas [19a, b] reduce to

$$f_a^* = \frac{Ra}{EI}\left(1 + \mu\frac{w}{R}\right), \quad \epsilon_a^* = \frac{Ra}{EA}\left(1 + \mu\frac{w}{R}\right) \quad [20]$$

In this approximation the outside face of the flange—at radius b—deforms, due to the loads applied at the inner face, the amounts

$$f_b^* = \frac{Ra}{EI}, \quad \epsilon_b^* = \frac{Ra}{EA} \quad [21a]$$

respectively. Clearly, the flange does not deform rigidly. There exists a distortion due to Poisson ratio effect. However, if we consider also $\mu w/R$ as negligible, then the deformation of the inner face

$$f_a^* = \frac{Ra}{EI}, \quad \epsilon_a^* = \frac{Ra}{EA} \quad [21b]$$

becomes the same as that of the outer face. In this approximation, therefore, the flange cross section moves and rotates rigidly. Moreover, the rotation occurs about the centroid of the section. One likewise shows that if $\mathfrak{M}^* = 1$ lb in/in and $\mathfrak{C}^* = 1$ lb/in are, in the same fashion, applied at radius $\bar{r}$, as in Fig. 2, then Expressions [21] must be replaced by

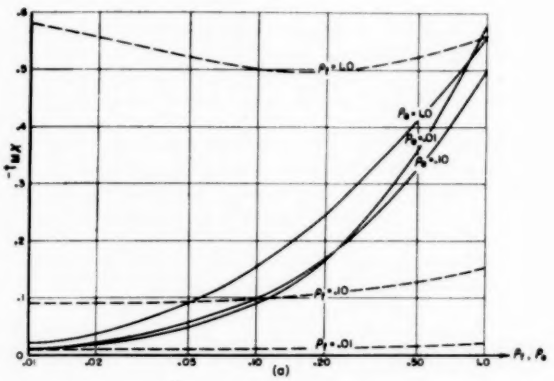

FIG. 5(a)

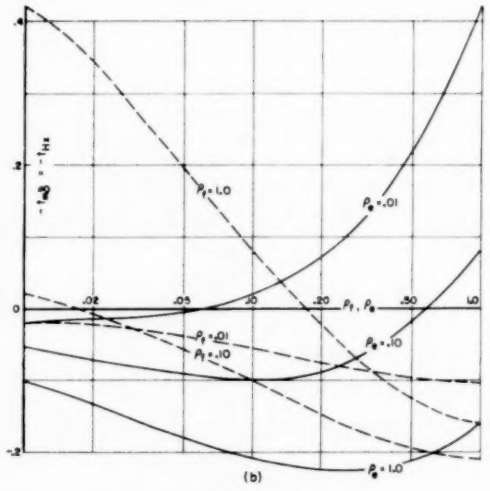

FIG. 5(b)

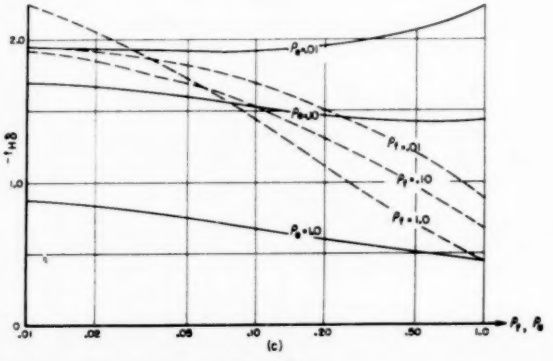

FIG. 5(c)

$$f^* = \frac{R\bar{r}}{EI}, \quad \epsilon^* = \frac{R\bar{r}}{EA} \ldots\ldots\ldots [22a, b]$$

These are the flange flexibility and expansivity expressions for loads applied at radius $\bar{r}$. The rotation still occurs about the centroid.

The foregoing considerations were based on the assumption that the rotation angle χ^* is small. If it is not small then Equations [1*a*, *b*] must be replaced in accordance with Fig. 6 by

$$\left.\begin{aligned} \chi^* &= f^*[\mathfrak{M}^* - \{c + (R - \bar{r})\chi^*\}\mathfrak{C}^*] \\ \delta^* &= \epsilon^*\mathfrak{C}^* - c\chi^* + (R - \bar{r})\chi^{*2}/2 \end{aligned}\right\} \ldots [23a, b]$$

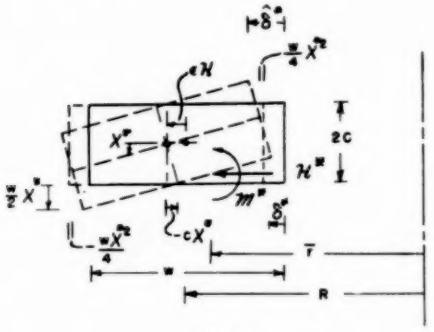

FIG. 6

This makes the problem nonlinear and complicated. In what follows we shall assume that the linearization of Expressions [23] to those of [1] is always permissible.

When the flange cross section rotates rigidly, as it does in our approximation, then the only stresses the flange experiences are hoop stresses, arising from the displacements δ^* and $\hat{\delta}^*$ of lower and upper edge. According to whether δ^* or $\hat{\delta}^*$ is numerically larger, the stress at the lower inside corner, or the upper inside corner of the flange

$$\sigma^* = E\delta^*/a, \quad \hat{\sigma}^* = E\hat{\delta}^*/a \ldots\ldots\ldots [24a, b]$$

will be the largest stress in the flange.

4 Shell Action

It was shown in Equation [10] of reference (5) that under edge loads $\mathfrak{M}$ and $\mathfrak{C}$, as in Fig. 7, a non-too flat shell incurs deformations δ, χ

$$\left.\begin{aligned} \delta/fl_s &= -\frac{1}{2}\mathfrak{M}\,F_3(n) + \frac{1}{2}\mathfrak{C}l_sF_4(n) \\ \chi/f &= \mathfrak{M}\,F_4(n) - \frac{1}{2}\mathfrak{C}l_sF_1(n) \end{aligned}\right\} \ldots\ldots [25][7]$$

$$\nabla = -\delta \cot \varphi$$

and moments and forces M_x, M_θ, H, N_x, N_θ

$$\left.\begin{aligned} M_x &= \mathfrak{M}F_1(n) - \mathfrak{C}l_sF_2(n) \\ Hl_s &= 2\mathfrak{M}F_2(n) + \mathfrak{C}l_sF_3(n) \\ M_\theta &= \mu M_x, \quad N_x = H\cos\varphi \\ N_\theta &= Eh\delta/r = (3.30/h)[-\mathfrak{M}F_3(n) + \mathfrak{C}l_sF_4(n)] \end{aligned}\right\} [26]$$

(in the expression of N_θ we used $\mu = 0.3$), where

$$\left.\begin{aligned} F_1 &= \sqrt{2}\,e^{-n}\cos(n - \pi/4), \quad F_2 = e^{-n}\sin n \\ F_3 &= -\sqrt{2}\,e^{-n}\sin(n - \pi/4), \quad F_4 = e^{-n}\cos n \end{aligned}\right\} . [27]$$

[7] Formulas [25], [26] may be deduced also from equations [35]–[44] of reference (3), utilizing his equations [57]–[61] and making suitable simplifications.

are damped sinusoidals, tabulated as functions φ, ζ, ψ, θ in reference (1*c*), and as functions A, B, C, D in reference (6). In the foregoing

$$f = l/D \ldots\ldots\ldots [28a]$$

is the flexibility of the shell

$$D = Eh^3/12(1 - \mu^2) \ldots\ldots\ldots [28b]$$

is the stiffness of the shell, and n denotes the distance from the edge—along a meridian—in number of attenuation lengths

$$n = (\bar{x} - x)/l \ldots\ldots\ldots [29]$$

Symbol x is the meridional co-ordinate of a shell point as in Fig. 7, $\bar{x}$ that of the shell edge.

It was shown likewise in reference (5) Equation [1] that under

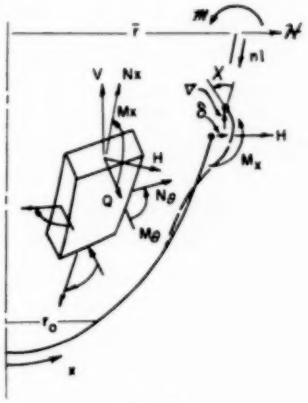

FIG. 7

distributed loads p_x, p_z the shell incurs a vertical force V lb/in

$$2\pi r\,V(x) = 2\pi r_0V_0 - \int_{x_0}^{x} 2\pi r p_z\,dx,$$

$$p_v = p_x\sin\varphi + p_z\cos\varphi \ldots\ldots [30a]$$

it incurs membrane forces

$$N_x = V/\sin\varphi, \quad N_\theta = -rp_v/\sin\varphi - rN_x/R_x\sin\varphi \ldots [30b, c]$$

displaces horizontally

$$\delta = r(N_\theta - \mu N_x)/Eh \ldots\ldots\ldots [31a]$$

and rotates

$$\chi = [(N_x - \mu N_\theta)/Eh - r/R_x\sin\varphi]\cot\varphi - d\,(\delta/\sin\varphi)/dx \ldots\ldots [31b]$$

In the foregoing, R_x is the radius of curvature of the meridian.

In Section 6 we shall need the edge values of Expressions [30], [31] for the case of a conical shell ($R_x = \infty$, $\tilde{\varphi} = \varphi$) subject (*a*) to weight loading

$$2\pi\bar{r}\bar{V} = W, \quad p_x = p_z = 0 \ldots\ldots [32a]$$

(*b*) to liquid pressure-loading

$$p_x = 0, \quad p_z = -\gamma d \ldots\ldots [32b]$$

as indicated in Fig. 9. Term d denotes the depth below the surface of the liquid.

For Case (*a*) we find

$$\left.\begin{aligned} \mathfrak{U} &= \bar{V} = W/2\pi\bar{r}, \ \bar{N}_x = \bar{V}/\sin\varphi, \ \bar{N}_\theta = 0 \\ \bar{\delta} &= -\mu W/2\pi Eh\sin\varphi, \ \bar{\chi} = W\cot\varphi/2\pi\bar{r}Eh\sin\varphi \end{aligned}\right\} [33a, b, c, d, e_1]$$

For Case (*b*) Formulas [33*a*, *b*, *c*, *d*] hold unchanged (W now denotes the total weight of the supported liquid) only the $\bar{\chi}$ expression must be changed to

$$\chi = (W \cot \varphi + 2W')/2\pi r E h \sin \varphi \quad \ldots\ldots [33e_2]$$

where

$$W' = \gamma \pi r^3 \quad \ldots\ldots [34]$$

Consequently, the resultant shell deformations are

$$\chi = \chi_m + \chi_\vartheta + \chi_e, \quad \delta = \delta_m + \delta_\vartheta + \delta_e \quad \ldots\ldots [35a, b]$$

where we included also contributions from temperature deformations. In the narrow edge region, where χ_e, δ_e change rapidly, the membrane quantities vary but slowly and can be replaced by their edge values

$$\text{Near edge: } \chi \simeq \chi_m + \chi_\vartheta + \chi_e, \quad \delta \simeq \overset{*}{\delta}_m + \overset{*}{\delta}_\vartheta + \delta_e \quad \ldots\ldots [35c, d]$$

Farther away from the edge the variation of the membrane quantities cannot be ignored, but here δ_e, χ_e are negligible

$$\text{Away from edge: } \chi \simeq \chi_m + \chi_\vartheta, \quad \delta \simeq \delta_m + \delta_\vartheta \quad \ldots\ldots [35e, f]$$

Similarly, the shell stresses have expressions[8]

$$\left.\begin{aligned} \sigma_x &= (N_{xm} + N_{x\vartheta} + N_{xe})/h \mp 6M_x/h^2 \\ &= \sigma_{xm} + \sigma_{x\vartheta} + \sigma_{xt} + \sigma_{xb} \\ \sigma_\vartheta &= (N_{\vartheta m} + N_{\vartheta\vartheta} + N_{\vartheta e})/h \mp 6M_\vartheta/h^2 \\ &= \sigma_{\vartheta m} + \sigma_{\vartheta\vartheta} + \sigma_{\vartheta t} + \sigma_{\vartheta b} \end{aligned}\right\} \quad [36a, b]$$

The first three terms in these expressions represent uniform stresses across the shell wall, the last terms represent bending stresses. Upper sign holds for inner fiber, lower sign for outer fiber. Approximations equivalent to Equations [35*c*, *d*, *e*, *f*] hold also for the stresses. We shall refer to these as Equations [36*c*, *d*] and [36*e*, *f*] respectively.

5 Temperature Effects

We restrict ourselves to the case when the temperature variation, ϑ, in both shell and flange is linear in the axial direction, and has a discontinuity at the juncture, as in Fig. 8. Then severance

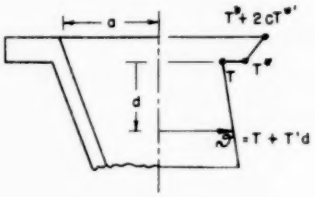

Fig. 8

of flange and shell leads to shell deformations

$$\overset{*}{\delta}_\vartheta = \bar{r}\alpha T, \quad \overline{\chi}_\vartheta = \bar{r}\alpha T' \quad \ldots\ldots [37a, b]$$

and flange deformations at the juncture

$$\delta_\vartheta^* = \bar{r}\alpha T^*, \quad \overline{\chi}_\vartheta^* = \bar{r}\alpha T^{*\prime} \quad \ldots\ldots [38a, b]$$

and does not create any stresses.

6 Numerical Example

We have chosen for illustration of the principles a rather unconventional example. But this will enable us to pinpoint a number of considerations which otherwise would not arise in a single problem. The 132-in-diam vessel shown in Fig. 9 is of $^3/_8$ in. wall thickness throughout, of 96 in. depth in the cylindrical portion, of 12 in. depth in the conical flare (of 45 deg inclination), and is supported by a 6-in-wide flange along a bolt circle of 81 in. radius. The vessel (including bottom plate) weighs 12,000 lb. It contains liquid of specific density 250 pcf.[8a] The upper part of the shell is cooled at the rate of 10 deg F per vertical inch; on the other hand, the flange is maintained at constant temperature. Suitable fillets at C and D eliminate the necessity for considering stress concentrations.

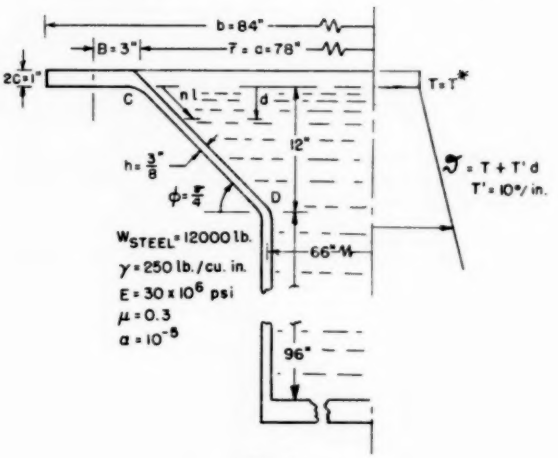

Fig. 9

The Problem. To find the stresses and deformations in the vessel near the flange region. (Because the knuckle is separated from the flange by more than two attenuation lengths, we can disregard the interaction of the two effects. Determination of strengthening required at the knuckle is a separate problem and is not considered in this paper.)

To correlate the example with the text, primes will be appended to the present equations to indicate the earlier equation into which the numerical substitutions were made.

(*a*) *Shell Parameters*

$$l = \text{attenuation length} = 0.778\sqrt{78 \times 0.375/0.707} = 5.00 \text{ in} \quad \ldots\ldots [3c']$$

$$l_v = \text{vertical component of } l = 0.707l = 3.54 \text{ in} \quad \ldots\ldots [3b']$$

$$D = \text{stiffness} = 2.75 \times 10^6 \times 0.375^3 = 144{,}000 \text{ lb-in}^2\text{/in} \quad \ldots\ldots [28b']$$

$$f = \text{flexibility} = 5/144{,}000 = 0.0346 \times 10^{-3} \text{ in/lb in.} \quad \ldots\ldots [28a']$$

$$\epsilon = \text{expansivity} = 0.5 \times 0.0346 \times 10^{-3} \times 3.54^2 = 0.216 \times 10^{-3} \text{ in/(lb/in)} \quad \ldots\ldots [14a']$$

(*b*) *Flange Parameters*

$$A = \text{area} = 2 \times 0.5 \times 6 = 6 \text{ in.}^2 \quad \ldots\ldots [18a']$$

$$I = \text{moment of inertia} = (2/3)\,0.5^3 \times 6 = 0.5 \text{ in.}^4 \quad \ldots\ldots [18b']$$

$$f^* = \text{flexibility} = 81 \times 78/30 \times 10^6 \times 0.5 = 0.421 \times 10^{-2} \text{ in/lb in.} \quad \ldots\ldots [22a']$$

[8] Subscript t stands for tension due to edge loads $\mathfrak{M}$, $\mathfrak{C}$, subscript b stands for bending; we distinguish $\sigma_{xbi} = -6M_x/h^2$ and $\sigma_{xbo} = +6M_x/h^2$ (bending stress for inner fiber, outer fiber), and similarly we distinguish $\sigma_{\vartheta bi}$, $\sigma_{\vartheta bo}$.

[8a] pci in the figure should read pcf.

ϵ^* = expansivity = $81 \times 78/30 \times 10^6 \times 6 = 0.0351 \times 10^{-3}$ in/(lb/in) ..... [22b']

(c) Interaction Parameters

ρ_f = flexibility ratio = $0.346/0.421 = 0.0822$ ..... [15a']

ρ_ϵ = expansivity ratio = $0.0351/0.216 = 0.1625$ ..... [15b']

Influence coefficients

$$\left.\begin{aligned} \Delta &= 1 + 0.1625 + 0.0411 + 0.2831 + 0.0534 = 1.540 \\ t_{M\chi} &= -0.0881,\ t_{M\delta} = t_{H\chi} = 0.1305,\ t_{H\delta} = -1.406 \end{aligned}\right\} \quad \text{..... [17']}$$

(d) Applied Loads

W_{cyl} = weight of liquid in cylindrical portion = $250\pi\,(65.8/12)^2 \times 96/12$ = 191,000 lb

W_{cone} = weight of liquid in conical portion = $(250/3)\pi \times 107.7$ = 27,000 lb

W_l = total weight of liquid = 191,000 + 27,000 = 218,000 lb

W_s = weight of steel container = 12,000 lb

W = total supported weight = $W_l + W_s$ ..... [39]

= 230,000 lb ..... [39']

W' = weight $\gamma\pi\bar{r}^2$ of liquid = 33,000 lb ..... [34']

Temperature gradient in shell = T' = 10 deg F drop toward flange per vertical inch

$\mathcal{U}$ = vertical load per inch acting at flange-shell juncture

= $230{,}000/2\pi \times 78 = 0.4694 \times 10^3$ lb/in .. [33a']

$M^*_{applied}$ = moment applied to flange = $-\mathcal{U}B$ ..... [40]

= $-0.4694 \times 10^3 \times 3 = -1.408 \times 10^3$ in. lb/in (at radius a) ..... [40']

(e) Edge Deformations of Severed Shell

1 Membrane deformation

χ_m = $(230{,}000 + 66{,}000)/2\pi \times 77.8 \times 0.375 \times 30 \times 10^6 \times 0.707$

= 0.0001 rad ..... [33e$_1$', e$_2$']

$\bar{\delta}_m$ = −0.00138 in. ..... [33d']

2 Temperature deformation

$\bar{\chi}_\vartheta$ = $10^{-5} \times 78 \times 10 = 0.0078$ rad ..... [37b']

$\bar{\delta}_\vartheta$ = 0 ..... [37a']

(f) Deformations of Severed Flange

χ_m^* = $f^* M^*_{applied} = -0.4213 \times 1.408 = -0.594$ ..... [1a']

$\bar{\delta}_m^*$ = $-c\chi_m^* = 0.594/2 = 0.297$ in. ..... [1b']

(g) Misalignments

$\chi\dagger$ = $\bar{\chi}_m + \bar{\chi}_\vartheta + \chi_m^* + \chi_\vartheta^* + f^* c\mathcal{U}\cot\varphi$
= $0.0001 + 0.0078 - 0.594 + 0 + 0.0990 = -0.487$ ..... [13c']

$\delta\dagger$ = $\bar{\delta}_m + \bar{\delta}_\vartheta - \delta_m^* - \delta_\vartheta^* + (c + \epsilon^*/f^* c) f^* c\mathcal{U}\cot\varphi$
= $-0.00138 + 0 - 0.297 - 0 + 0.066 = -0.232$ in. ..... [13d']

(h) Edge Reactions

$\mathfrak{M}$ = $(t_{M\chi}/f)\chi\dagger + (t_{M\delta}/fl_v)\delta\dagger$
= $(-0.0881/0.0346)(-487) + (0.1305/0.1226) \times (-232) = 990$ in. lb/in ..... [16a']

$\mathfrak{C}$ = $(t_{H\chi}/fl_v)\chi\dagger + (t_{H\delta}/fl_v^2)\delta\dagger$
= $(0.1305/0.1226)(-487) + (-1.406/0.432)(-232)$
= 240 lb/in ..... [16b']

$\mathfrak{M}^*$ = 990 in. lb/in ..... [8a']

$\mathfrak{C}^*$ = $-240 - 469 = -710$ lb/in ..... [8b']

(i) Resultant Flange Deformations and Stresses

χ^* = $f^*(M^*_{applied} + \mathfrak{M}^* - c\mathfrak{C}^*)$
= $0.4213\,(-1.408 + 0.990 + 0.355) = -0.0266$ .. [1a']
(rotation which causes shell sagging)

δ^* = $\epsilon^*\mathfrak{C}^* - c\chi^*$
= $-0.0351 \times 0.710 + 0.5 \times 0.0266 = -0.0116$ in. .. [1b']
(radial shrinkage of lower flange edge)

$\hat{\delta}^*$ = $\epsilon^*\mathfrak{C}^* + c\chi^*$
= $-0.0249 - 0.0133 = -0.0382$ in ..... [1c']
(radial shrinkage of upper flange edge)

σ = $E\delta^*/a$
= $30 \times 10^6 \times 0.0116/78 = -4500$ psi ..... [24a']
(hoop compression of lower edge)

$\hat{\sigma}$ = $E\hat{\delta}^*/a = -14{,}700$ psi ..... [24b']
(hoop compression of upper edge)

(j) Resultant Shell Deformations

$$\left.\begin{aligned} \bar{\chi} &= \bar{\chi}_m + \bar{\chi}_\vartheta + f\mathfrak{M} - fl_v\mathfrak{C}/2 \\ &= 0.0001 + 0.0078 + 0.0346 \times 0.990 \\ &\quad -0.1226 \times 0.240/2 = 0.0273 \end{aligned}\right\} \quad \text{..... [35a', 2a']}$$

$$\left.\begin{aligned} \bar{\delta} &= \bar{\delta}_m + \bar{\delta}_\vartheta - \epsilon(\mathfrak{M}/l_v) + \epsilon\mathfrak{C} \\ &= -0.00138 + 0 - 0.216(0.990/3.54) \\ &\quad + 0.216 \times 0.240 = -0.0098 \text{ in.} \end{aligned}\right\} \quad \text{..... [35b', 2b']}$$

The slight discrepancy between the present values and the flange values given in the foregoing equations must be attributed to inaccuracy due to slide-rule calculations.

(k) Resultant Shell Stresses

1 Membrane stresses in edge region. Meridional tension due to $N_{xm} = \mathcal{U}/\sin\varphi$ is

σ_{xm} = $(469/0.707)/0.375 = 1800$ psi ..... [36']

Azimuthal tension due to $N_{\theta m} = 0$ is

$\sigma_{\theta m} = 0$ ..... [36']

2 Edge values of edge load stresses (filastic). Meridional bending stress σ_{xbi} and σ_{xbo} due to edge load action is

σ_{xbi} = $-6 \times 900/0.375^2 = -42{,}500$ psi ..... [36']
(inner surface, compression)

σ_{xbo} = +42,500 psi ..... [36']
(outer surface, tension)

Meridional tensile stress σ_{xt} is

$\sigma_{xt} = \mathfrak{C}\cos\varphi/h$

= $240 \times 0.707/0.375 = 450$ psi (tension) ..... [36']

Hoop tensile stress σ_θ is

$$\sigma_{\theta_t} = 3.30\,(-\mathfrak{M} + 3\mathfrak{C}l_e)/h^2$$
$$= 3.30\,(-990 + 240 \times 3.54)/0.375^2 = -3300 \text{ psi} \quad [26']$$
(hoop compression)

Hoop bending stress is

$$\sigma_{\theta_b} = \mu\sigma_{xb} = \begin{cases} -0.3 \times 42{,}500 = -12{,}800 \text{ psi} \\ \text{(compression, inner surface)} \\ +12{,}800 \text{ psi (tension, outer surface)} \end{cases} \quad [36']$$

3 Edge values of combined shell stresses (filastic)
Meridional

$$\begin{cases} \sigma_{xm} + \sigma_{xt} + \sigma_{xbi} \\ = 1800 + 550 - 42{,}500 = -40{,}200 \text{ psi} \\ \text{(compression, inner surface)} \\ \sigma_{xm} + \sigma_{xt} + \sigma_{xbo} \\ = 1800 + 550 + 42{,}500 = 44{,}800 \text{ psi} \\ \text{(tension, outer surface)} \end{cases} \quad [36']$$

Hoop

$$\begin{cases} \sigma_{\theta_m} + \sigma_{\theta_t} + \mu\sigma_{xbi} \\ = 0 - 3300 - 12{,}800 = -16{,}100 \text{ psi} \\ \text{(compression, inner surface)} \\ \sigma_{\theta_m} + \sigma_{\theta_t} + \mu\sigma_{xbo} \\ = 0 - 3300 + 12{,}800 = 9500 \text{ psi} \\ \text{(tension, outer surface)} \end{cases} \quad [36']$$

4 Edge-load stresses at distance $0.75l_e$ below edge. At the edge the horizontal force $\mathfrak{C}$ causes no bending stresses. Its maximum stresses are produced where $e^{-n} \sin n$ is maximum. This occurs at a distance $n = d/l_e \simeq 0.75$, i.e., $0.75l_e \sim 2.7$ in. below the edge, when measured vertically, or $0.75l \sim 3.7$ in. away from the edge, when measured along the meridian. It is always desirable to check stresses 2/3 to 3/4 attenuation lengths away from the edge, because of the possibility of an increase in stresses a slight distance away from the edge.

At $n = 3/4$ Formula [26] gives

$$M_x = 0.6683\mathfrak{M} - 0.3223\mathfrak{C}l_e$$
$$= 661 - 274 = 380 \text{ lb in/in} \quad [26']$$

This moment creates bending stresses

$$\sigma_{xb} = \mp 6M_x/h^2 \simeq \mp 16{,}100 \text{ psi}$$

on inner and outer surfaces. The meridional tensile stress at $n = 0.75$ can be disregarded, while the hoop stress at distance $0.75l$ from the edge is

$$\sigma_{\theta_t} = 3.30\,(-0.0243\mathfrak{M} + 0.346\,3\mathfrak{C}l_e)/h^2$$
$$= 6300 \text{ psi (hoop tension)} \quad [26']$$

In the present example the stresses are, at $n = 3/4$, appreciably below their edge values. Beyond $n = 3/4$ location the stresses can be expected to fall off still more rapidly and, at $2.5l \sim 12.5$ in. distance, ~ 8.6 in. depth, their values will be roughly 10 per cent of the edge values. Clearly, the discontinuities at the flange and at the knuckle leave each other unaffected, and thus the two conditions can be evaluated independently.

BIBLIOGRAPHY

1 "Strength of Materials," by S. Timoshenko, D. Van Nostrand Company, Inc., New York, N. Y., vol. 2, 1940, (*a*) p. 180; (*b*) p. 241, and (*c*) p. 5.

2 "On the Theory of Thin Elastic Shells," by E. Reissner, Reissner Anniversary Volume, J. W. Edwards, Ann Arbor, Mich., 1949, p. 231.

3 "On Asymptotic Integration in Shell Theory," by F. B. Hildebrand, Proc. Symposia in Applied Mathematics, McGraw-Hill Book Company, Inc., New York, N. Y., vol. 3, 1950.

4 "Theory of Plates and Shells," by S. Timoshenko, McGraw-Hill Book Company, Inc., New York, N. Y., 1940, (*a*) p. 459; (*b*) p. 473, and (*c*) p. 64.

5 "Membrane and Bending Analysis of Axisymmetrically Loaded Axisymmetrical Shells," by G. Horvay and I. M. Clausen, submitted to the JOURNAL OF APPLIED MECHANICS.

6 "Beams on Elastic Foundation," by M. Hetenyi, University of Michigan Press, Ann Arbor, Mich., 1946.

7 "Designing by Photoelasticity," by R. B. Heywood, Chapman and Hall, London, England, 1952, pp. 320–330.

8 "Report on the Design of Pressure Vessel Heads," *Welding Journal*, Research Supplement, January, 1953.

A Numerical Solution for the Nonlinear Deflection of Membranes[1]

By F. S. SHAW[2] and N. PERRONE,[3] BROOKLYN, N. Y.

A numerical method of solution for the nonlinear deflection of thin flat membranes subjected to normal forces as well as forces in the plane of the membrane has been given by Hencky. The equations he solved were first derived by Föppl, and they also follow directly from the von Kármán nonlinear plate equations on formally making the plate stiffness zero. Föppl's equations are two in number, one being of fourth order and the other second. The unknown quantities are a stress function and the normal displacement. Hencky's method of solution does not seem capable of easy generalization. The same class of membrane problems is reconsidered here. By casting the problem entirely in terms of displacement components three simultaneous nonlinear second-order partial differential equations are obtained, and a technique is here devised by means of which these equations can be solved without difficulty using finite-difference approximations in conjunction with a relaxation-iteration procedure. Various simple preliminary examples are discussed, after which an example involving a rectangular region is considered in complete detail. The technique devised can be used for a region of any shape, including the case where the boundary is curved, and also for any arbitrary given load system.

1 DERIVATION OF GOVERNING EQUATIONS

Introduction

1 A numerical solution for the large deflection of thin flat membranes which are subjected to normal forces as well as external edge forces in the plane of the membrane has been considered by Hencky (1).[4] The equations he solved follow directly from the von Kármán large deflection flat-plate equations on making the plate stiffness identically zero.

The von Kármán equations for the large deflection of a thin flat plate of uniform thickness are (2)

$$\left.\begin{aligned} \nabla^4 F &= E(w_{,xy}^2 - w_{,xx}w_{,yy}) \\ \nabla^4 w &= (h/D)\{(q/h) + F_{,yy}w_{,xx} + F_{,xx}w_{,yy} - 2F_{,xy}w_{,xy}\} \end{aligned}\right\} \quad \ldots [1]$$

where

[1] The results presented in this paper were obtained in the course of research sponsored by the Office of Naval Research under Contract N6onr-26308 with the Polytechnic Institute of Brooklyn.

[2] Associate Professor, Polytechnic Institute of Brooklyn, Department of Aeronautical Engineering and Applied Mechanics.

[3] Research Assistant, Polytechnic Institute of Brooklyn, Department of Aeronautical Engineering and Applied Mechanics.

[4] Numbers in parentheses refer to the Bibliography at the end of the paper.

Contributed by the Applied Mechanics Division and presented at the Annual Meeting, New York, N. Y., November 29–December 4, 1953, of The American Society of Mechanical Engineers.

Discussion of this paper should be addressed to the Secretary, ASME, 29 West 39th Street, New York, N. Y., and will be accepted until July 12, 1954, for publication at a later date. Discussion received after the closing date will be returned.

Note: Statements and opinions advanced in papers are to be understood as individual expressions of their authors and not those of the Society. Manuscript received by ASME Applied Mechanics Division, April 2, 1953. Paper No. 53—A-36

∇^4 is the biharmonic operator, i.e.

$$\nabla^4 F = F_{,xxxx} + 2F_{,xxyy} + F_{,yyyy}$$

w is the lateral (i.e., normal) deflection, $q = q(x, y)$ is the applied normal load intensity, h is the plate thickness, D its stiffness, E is Young's modulus for the plate material, and F is a stress function related to the forces per unit length in the plane of the plate by the formulas

$$N_{xx} = hF_{,yy}, \quad N_{yy} = hF_{,xx}, \quad N_{xy} = -hF_{,xy}$$

By formally making the stiffness zero, there follows from Equations [1] the two simultaneous nonlinear equations in the membrane deflection and the stress function, namely

$$\left.\begin{aligned} \nabla^4 F &= E(w_{,xy}^2 - w_{,xx}w_{,yy}) \\ (q/h) + F_{,yy}w_{,xx} + F_{,xx}w_{,yy} - 2F_{,xy}w_{,xy} &= 0 \end{aligned}\right\} \quad \ldots [2]$$

which are the equations solved numerically by Hencky (1). The equations themselves were first obtained by Föppl (3).

Of the two Equations [2], one is second order and the other is fourth order. While techniques exist for solving fourth-order partial differential equations by numerical means (4), the difficulties to be overcome are rather greater than those associated with a second-order operator. Accordingly, the Hencky membrane problem is here considered numerically in terms only of displacement components rather than in the Föppl formulation. By so doing the differential equations corresponding to Equations [2] become all of second order with, however, the price that they are three in number instead of two.

It must be emphasized that the problem being discussed here is that of a membrane, i.e., a thin flat structural element of constant small but finite thickness and possessing zero bending stiffness. From this viewpoint, although such a membrane may be regarded almost everywhere as an approximation to a very thin flat plate, the essential connection between the two, namely, the edge boundary-layer effect discussed by Friedrichs (5), is automatically precluded from consideration.

Governing Equations

2 Although the nonlinear deflection of a membrane is discussed by Timoshenko (2), it is of interest to reformulate the problem in detail here. To do so[5] we consider a thin, flat unstrained membrane of arbitrary contour C and region R in the x_1, x_2-plane. The membrane is to be loaded by a (compressive) force of intensity $p = p(x_1, x_2)$ which will act in the x_3-direction.

Let u_i $(i = 1, 2, 3)$ be the resulting displacement components in the directions of the x_i-axes. More particularly, we assume $u_\alpha = u_\alpha(x_1, x_2)$ everywhere, $(\alpha = 1, 2)$; $u_3 = u_3(x_1, x_2)$ on middle surface of membrane. We impose the restriction, however, that squares and products of derivatives of u_1 and u_2 are small compared with those of u_3 and so can be neglected.

[5] It is convenient to use Cartesian tensors in this connection. Thus we identify x_1, x_2, x_3 with the usual Cartesian co-ordinates x, y, z, and displacement components u_1, u_2, u_3 with the familiar u, v, w-components.

With these assumptions, the general nonlinear strain-displacement relations[6]

$$e_{ij} = (u_{i,j} + u_{j,i} + u_{k,i}u_{k,j})/2, \quad (i,j,k = 1, 2, 3) \ldots\ldots [3]$$

reduce to

$$\left.\begin{aligned} e_{11} &= (u_{1,1} + u_3^2{}_{,1})/2 \\ e_{22} &= (u_{2,2} + u_3^2{}_{,2})/2 \\ e_{12} &= (u_{1,2} + u_{2,1} + u_{3,1}u_{3,2})/2 \\ e_{13} &= (u_{3,1} + u_{3,1}u_{3,3})/2 \\ e_{23} &= (u_{3,2} + u_{3,2}u_{3,3})/2 \end{aligned}\right\} \ldots\ldots\ldots [4]$$

and e_{33} is as yet unspecified.

Next, we assume that the normal stress σ_{33} is zero everywhere, and so, from the general linear stress-strain law

$$\sigma_{ij} = \frac{E}{1+\nu}\left\{e_{ij} + \frac{\nu}{1-2\nu} e_{kk}\,\delta_{ij}\right\}, \quad (i,j,k = 1, 2, 3) \ldots\ldots [5]$$

deduce that

$$e_{33} = -e_{\alpha\alpha}\nu/(1-\nu), \quad (\alpha = 1, 2) \ldots\ldots\ldots [4a]$$

Here, E is Young's modulus and ν is Poisson's ratio.

For equilibrium it is then necessary that, in the absence of body forces, the potential energy V

$$V = \frac{1}{2}\int_V \sigma_{ij}e_{ij}\,dV - \int_{S_B} T_i u_i\,dS \ldots\ldots\ldots [6]$$

be stationary for arbitrary variation in displacements. In this expression $\sigma_{ij} = \sigma_{ij}(e_{ij})$ via the stress-strain law Equation [5], and an S_B surface is one for which

$$\int_S u_i \delta T_i\,dS$$

vanishes. This minimum potential-energy principle is usually stated and proved for linear strain-displacement relations; however, with suitable interpretation it is true for the nonlinear Relations [3] also.

Using Equation [5], Equation [6] becomes

$$V = \frac{E}{2(1+\nu)}\int_V \left(e_{ij}e_{ij} + \frac{\nu}{1-2\nu} e_{ii}e_{jj}\right) dV - \int_{S_B} T_i u_i\,dS$$

$$= \frac{E}{2(1+\nu)}\int_V \left(e_{ij}e_{ij} + \frac{\nu}{1-2\nu} e_{ii}e_{jj}\right) dV$$

$$- \int_R p\,u_3\,dA - \int_{\bar{S}} T_i u_i\,dS \ldots\ldots [7]$$

where R is the plan-form area of the membrane, i.e., the region in the x_1, x_2-plane bounded by the membrane contour C, $\bar{S}$ is the edge surface of the membrane, i.e., the surface formed by the contour C and the membrane thickness h, and $p = p(x_1, x_2)$ is the surface traction applied in the x_3-direction on the membrane surface $x_3 = -h/2$.

Using Expressions [4] and [4a], and neglecting the effects of σ_{13}, σ_{23}, on substitution we obtain

$$\frac{E}{2(1+\nu)}\int_V \left(e_{ij}e_{ij} + \frac{\nu}{1-2\nu} e_{ii}e_{jj}\right) dV - \int_R p\,u_3\,dA$$

$$= \frac{E}{2(1+\nu)}\int_V \left(e_{\alpha\beta}e_{\alpha\beta} + \frac{\nu}{1-\nu} e_{\alpha\alpha}e_{\beta\beta}\right) dV - \int_R p\,u_3\,dA$$

$$= \frac{Eh}{2(1+\nu)}\int_R \left\{\frac{1}{4}(u_{\alpha,\beta} + u_{\beta,\alpha} + u_{3,\alpha}u_{3,\beta})^2 + \frac{\nu}{4(1-\nu)}(2u_{\alpha,\alpha} + u_{3,\alpha}u_{3,\alpha})(2u_{\beta,\beta} + u_{3,\beta}u_{3,\beta}) - \frac{2(1+\nu)}{Eh}\,p\,u_3\right\} dA, \quad (\alpha,\beta = 1, 2) \ldots\ldots [8]$$

For equilibrium we require $\delta V = 0$. Using Equations [7] and [8], and considering first all the terms involving only integrals over the region R, equating δV to zero leads to a set of three simultaneous nonlinear equilibrium equations expressed in terms of displacement components u_i. If, now, we write u, v, w instead of $u_i (i = 1, 2, 3)$, and x, y in lieu of x_α, $(\alpha = 1, 2)$, these equations are

$$\nabla^2 u + (u_{,xx} - \nu u_{,yy}) + (1+\nu)v_{,xy} = -\{(1+\nu)w_{,y}w_{,xy} + 2w_{,x}w_{,xx} + (1-\nu)w_{,x}w_{,yy}\}$$

$$\nabla^2 v + (v_{,yy} - \nu v_{,xx}) + (1+\nu)u_{,xy} = -\{(1+\nu)w_{,x}w_{,xy} + 2w_{,y}w_{,yy} + (1-\nu)w_{,y}w_{,xx}\}$$

$$w_{,xx}(3w_{,x}^2 + w_{,y}^2) + w_{,yy}(w_{,x}^2 + 3w_{,y}^2) + 4w_{,x}w_{,y}w_{,xy} = -\{w_{,x}(2u_{,xx} + u_{,yy} + v_{,xy}) + w_{,y}(2v_{,yy} + v_{,xx} + u_{,xy}) + \nu w_{,x}(v_{,xy} - u_{,yy}) + \nu w_{,y}(u_{,xy} - v_{,xx})\} - 2\{w_{,xx}(u_{,x} + \nu v_{,y}) + (1-\nu)w_{,xy}(u_{,y} + v_{,x}) + w_{,yy}(v_{,y} + \nu u_{,x})\} - 2(1-\nu^2)p/Eh \ldots\ldots [9]$$

Here $w_{,x}^2$ (for example) means $(\partial w/\partial x)^2$.

Boundary Conditions

3 The term so far ignored in obtaining the variation of V, namely

$$-\int_{\bar{S}} T_i u_i\,dS$$

contributes only to the prescription of possible boundary conditions for this problem. To this term there will be added, as a result of the computation that gave Equations [9], other $\bar{S}$ edge-surface integral terms also, and as a result of all of these terms it will be found that various types of boundary conditions are possible.

One of these sets of conditions is the requirement

$$u = 0 = v = w \text{ on } C \ldots\ldots\ldots\ldots\ldots [10]$$

and these are the conditions we will use here. Other alternative possibilities will refer to various edge-traction specifications; however, these will not be considered here.

4 For later use it is convenient to write down, explicitly, expressions for the stress components in terms of displacements. From Equations [4] we have

$$\left.\begin{aligned} e_{xx} &= u_{,x} + w_{,x}^2/2 \\ e_{yy} &= v_{,y} + w_{,y}^2/2 \\ e_{xy} &= (u_{,y} + v_{,x} + w_{,x}w_{,y})/2 \\ e_{zz} &= -(e_{xx} + e_{yy})\nu/(1-\nu) \end{aligned}\right.$$

Hence, using the stress-strain law, Equation [5], it follows immediately that the stress components of interest are given by

[6] Note that the summation convention is being used. Thus where a letter subscript is repeated it is implied that the repeated subscript is to be given all possible values (i.e., 1, 2, 3 here) and then the quantities involved are to be summed. For example

$$u_{k,i}u_{k,j} = \sum_k u_{k,i}u_{k,j} = u_{1,i}u_{1,j} + u_{2,i}u_{2,j} + u_{3,i}u_{3,j}$$

$$\left.\begin{aligned}\sigma_{xx} &= \{E/2(1-\nu^2)\}\{2(u_{,x}+\nu v_{,y})+(w_{,x}{}^2+\nu w_{,y}{}^2)\}\\ \sigma_{yy} &= \{E/2(1-\nu^2)\}\{2(v_{,y}+\nu u_{,x})+(w_{,y}{}^2+\nu w_{,x}{}^2)\}\\ \sigma_{xy} &= \{E/2(1+\nu)\}\{u_{,y}+v_{,x}+w_{,x}w_{,y}\}\end{aligned}\right\}\quad..[11]$$

NONDIMENSIONALITY

5 Before discussing the numerical solution to any problem it is advisable to recast the governing Equations [9] in nondimensional form. To do this, we put

$$\left.\begin{aligned}x &= \xi L, \quad y = \eta L\\ u &= \bar{u}L, \quad v = \bar{v}L, \quad w = \bar{w}L, \quad h = \bar{h}L\end{aligned}\right\}\quad.....[12]$$

where L is a representative dimension of the membrane, e.g., the length of one side. With these substitutions we have

$$\frac{\partial}{\partial x} = \frac{1}{L}\frac{\partial}{\partial \xi},\ldots\ldots$$

$$\frac{\partial^2}{\partial x^2} = \frac{1}{L^2}\frac{\partial^2}{\partial \xi^2},\ldots\ldots$$

and so

$$\frac{\partial w}{\partial x} = \frac{\partial \bar{w}}{\partial \xi},\ldots\ldots$$

$$\frac{\partial^2 w}{\partial x^2} = \frac{1}{L}\frac{\partial^2 \bar{w}}{\partial \xi^2},\ldots\ldots$$

Using these, the three differential Equations [9] become

$$\left.\begin{aligned}&(\bar{u}_{,\xi\xi}+\bar{u}_{,\eta\eta})+(\bar{u}_{,\xi\xi}-\nu\bar{u}_{,\eta\eta})+(1+\nu)\bar{v}_{,\xi\eta}\\ &\quad=-\{(1+\nu)\bar{w}_{,\eta}\bar{w}_{,\xi\eta}+2\bar{w}_{,\xi}\bar{w}_{,\xi\xi}+(1-\nu)\bar{w}_{,\xi}\bar{w}_{,\eta\eta}\}\\ &(\bar{v}_{,\xi\xi}+\bar{v}_{,\eta\eta})+(\bar{v}_{,\eta\eta}-\nu\bar{v}_{,\xi\xi})+(1+\nu)\bar{u}_{,\xi\eta}\\ &\quad=-\{(1+\nu)\bar{w}_{,\xi}\bar{w}_{,\xi\eta}+2\bar{w}_{,\eta}\bar{w}_{,\eta\eta}+(1-\nu)\bar{w}_{,\eta}\bar{w}_{,\xi\xi}\}\\ &\bar{w}_{,\xi\xi}(3\bar{w}_{,\xi}{}^2+\bar{w}_{,\eta}{}^2)+\bar{w}_{,\eta\eta}(\bar{w}_{,\xi}{}^2+3\bar{w}_{,\eta}{}^2)+4\bar{w}_{,\xi}\bar{w}_{,\eta}\bar{w}_{,\xi\eta}\\ &\qquad=-K\\ &-\{\bar{w}_{,\xi}(2\bar{u}_{,\xi\xi}+\bar{u}_{,\eta\eta}+\bar{v}_{,\xi\eta})+\bar{w}_{,\eta}(2\bar{v}_{,\eta\eta}+\bar{v}_{,\xi\xi}+\bar{u}_{,\xi\eta})\\ &\qquad+\nu\bar{w}_{,\xi}(\bar{v}_{,\xi\eta}-\bar{u}_{,\eta\eta})+\nu\bar{w}_{,\eta}(\bar{u}_{,\xi\eta}-\bar{v}_{,\xi\xi})\}\\ &-2\{\bar{w}_{,\xi\xi}(\bar{u}_{,\xi}+\nu\bar{v}_{,\eta})+(1-\nu)\bar{w}_{,\xi\eta}(\bar{u}_{,\eta}+\bar{v}_{,\xi})\\ &\qquad+\bar{w}_{,\eta\eta}(\bar{v}_{,\eta}+\nu\bar{u}_{,\xi})\}\end{aligned}\right\}\quad..[13]$$

where K is the nondimensional quantity

$$K = 2(1-\nu^2)p/E\bar{h}.....[13a]$$

For any given problem the number K is specified completely. For computational purposes, however, it is convenient to be able to choose instead of K some other number, say, D, which is more suited to the problem.

To facilitate this choice we introduce other weighted nondimensional displacement components

$$\bar{u} = \underline{u}(K/D)^{3/4}, \quad \bar{v} = \underline{v}(K/D)^{3/4}, \quad \bar{w} = \underline{w}(K/D)^{1/4}..[14]$$

If the applied load is assumed to be uniform, substitution of Equations [14] in [13] yields

$$\left.\begin{aligned}&(\underline{u}_{,\xi\xi}+\underline{u}_{,\eta\eta})+(\underline{u}_{,\xi\xi}-\nu\underline{u}_{,\eta\eta})+(1+\nu)\underline{v}_{,\xi\eta}\\ &\quad=-\{(1+\nu)\underline{w}_{,\eta}\underline{w}_{,\xi\eta}+2\underline{w}_{,\xi}\underline{w}_{,\xi\xi}+(1-\nu)\underline{w}_{,\xi}\underline{w}_{,\eta\eta}\}\\ &(\underline{v}_{,\xi\xi}+\underline{v}_{,\eta\eta})+(\underline{v}_{,\eta\eta}-\nu\underline{v}_{,\xi\xi})+(1+\nu)\underline{u}_{,\xi\eta}\\ &\quad=-\{(1+\nu)\underline{w}_{,\xi}\underline{w}_{,\xi\eta}+2\underline{w}_{,\eta}\underline{w}_{,\eta\eta}+(1-\nu)\underline{w}_{,\eta}\underline{w}_{,\xi\xi}\}\\ &\underline{w}_{,\xi\xi}(3\underline{w}_{,\xi}{}^2+\underline{w}_{,\eta}{}^2)+\underline{w}_{,\eta\eta}(\underline{w}_{,\xi}{}^2+3\underline{w}_{,\eta}{}^2)+4\underline{w}_{,\xi}\underline{w}_{,\eta}\underline{w}_{,\xi\eta}\\ &=-D-\{\underline{w}_{,\xi}(2\underline{u}_{,\xi\xi}+\underline{u}_{,\eta\eta}+\underline{v}_{,\xi\eta})+\underline{w}_{,\eta}(2\underline{v}_{,\eta\eta}+\underline{v}_{,\xi\xi}\\ &\quad+\underline{u}_{,\xi\eta})+\nu\underline{w}_{,\xi}(\underline{v}_{,\xi\eta}-\underline{u}_{,\eta\eta})+\nu\underline{w}_{,\eta}(\underline{u}_{,\xi\eta}-\underline{v}_{,\xi\xi})\}\\ &-2\{\underline{w}_{,\xi\xi}(\underline{u}_{,\xi}+\nu\underline{v}_{,\eta})+(1-\nu)\underline{w}_{,\xi\eta}(\underline{u}_{,\eta}+\underline{v}_{,\xi})\\ &\qquad+\underline{w}_{,\eta\eta}(\underline{v}_{,\eta}+\nu\underline{u}_{,\xi})\}\end{aligned}\right\}\quad..[15]$$

where D is any arbitrary number. For finite-difference work it is convenient (as will be seen later) to choose D in the form

$$D = n^4\underline{D}$$

where $\underline{D}$ is a large whole number, and n is the number of subdivisions or meshes into which the representative length L is divided when making the finite-difference approximations.

From Equations [15] it can be seen that, although for nonlinear problems of this class superposition does not hold, if for a particular shaped region a solution can be obtained to [15] then by using Equations [12], [13a], and [14] we have available also the solutions for all problems of that geometrical family shape and for all magnitudes of uniform load.[7]

6 Finally, using Equations [12], [13a], and [14], the stress components, Equations [11], can be written in the form

$$\left.\begin{aligned}\sigma_{xx} &= [E/2(1-\nu^2)](K/D)^{2/4}\,\underline{\sigma}_{\xi\xi}\\ \sigma_{yy} &= [E/2(1-\nu^2)](K/D)^{2/4}\,\underline{\sigma}_{\eta\eta}\\ \sigma_{xy} &= [E/2(1+\nu)](K/D)^{2/4}\,\underline{\sigma}_{\xi\eta}\end{aligned}\right\}\quad.....[16]$$

where $\underline{\sigma}_{\xi\xi}$, $\underline{\sigma}_{\eta\eta}$, $\underline{\sigma}_{\xi\eta}$ are nondimensional stress components given by

$$\left.\begin{aligned}\underline{\sigma}_{\xi\xi} &= \{2(\underline{u}_{,\xi}+\nu\underline{v}_{,\eta})+(\underline{w}^2{}_{,\xi}+\nu\underline{w}^2{}_{,\eta})\}\\ \underline{\sigma}_{\eta\eta} &= \{2(\underline{v}_{,\eta}+\nu\underline{u}_{,\xi})+(\underline{w}^2{}_{,\eta}+\nu\underline{w}^2{}_{,\xi})\}\\ \underline{\sigma}_{\xi\eta} &= \{\underline{u}_{,\eta}+\underline{v}_{,\xi}+\underline{w}_{,\xi}\underline{w}_{,\eta}\}\end{aligned}\right\}\quad.....[17]$$

As part of the results of any problem it will be of interest to compute the principal stresses. Using the relations

$$\sigma_1, \sigma_2 = (\sigma_{xx}+\sigma_{yy})/2 \pm \{(\sigma_{xx}-\sigma_{yy})^2/4+\sigma^2{}_{xy}\}^{1/2}$$

we can rewrite them in the form

$$\sigma_1, \sigma_2 = [\{E/2(1-\nu^2)\}(K/D)^{2/4}]\underline{\sigma}_1, \underline{\sigma}_2.....[18]$$

where $\underline{\sigma}_1$, $\underline{\sigma}_2$ are the nondimensional principal stresses and are given by

$$\sigma_1, \sigma_2 = (\underline{\sigma}_{\xi\xi}+\underline{\sigma}_{\eta\eta})/2 \pm \{(\underline{\sigma}_{\xi\xi}-\underline{\sigma}_{\eta\eta})^2/4+(1+\nu)^2\underline{\sigma}^2{}_{\xi\eta}\}^{1/2}.....[19]$$

2 SOLUTION OF MODIFIED w PROBLEM

PRELIMINARY, SIMPLIFIED TEST PROBLEM

7 To solve particular problems numerically we will first introduce finite-difference equivalents for the various derivatives in Equations [15] and will then solve the resulting sets of nonlinear, algebraic, simultaneous equations by a combined relaxation-iteration technique.

As an aid in solving these equations we act on the plausible assumption that, since the w-displacements are large relative to the other two, a solution to the third of Equations [15] obtained on holding u and v zero everywhere should yield a w-displacement pattern which will not differ appreciably from that of the complete solution to the three simultaneous Equations [15]. Thus a solution of this artificial, restricted w-problem should be a good starting point from which to attempt the complete solution of Equations [15].

Initially, then, we concentrate attention on the third of Equations [15] in which it is assumed that both u and v will remain zero.[8] In this circumstance that equation becomes

[7] This implies that if the deflection pattern is obtained experimentally, in principle it is only necessary to obtain the pattern for a uniform load of one chosen magnitude. Obviously, the extension to nonuniform loads is immediately possible.

[8] The implication is that all points on the membrane middle surface deflect vertically only, which means that, although vertical equilibrium is satisfied, horizontal is not.

$$w_{,\xi\xi}(3w_{,\xi}^2 + w_{,\eta}^2) + w_{,\eta\eta}(w_{,\xi}^2 + 3w_{,\eta}^2) + 4w_{,\xi}w_{,\eta}w_{,\xi\eta} = -D \quad [20]$$

and we consider the solution of this equation, together with the condition that $w = 0$ on the boundary C, as a problem in itself. Since, from now on we will only be considering nondimensional problems, in the following it will be convenient[9] to drop the bars under the nondimensional displacements w, x, y. In any places in which doubt could result the independent variable, x or ξ, and so on, will be indicated; consequently, no confusion should arise.

8 Before discussing the general method of solving Equation [20] two special problems are of interest. They are the solutions to Equation [20] for an infinite strip and for a circular region since, for a uniformly applied normal surface traction, exact solutions are readily obtainable. With these known they can be used to give an indication of the accuracy of finite-difference solutions.

We consider, first, the infinite strip

$$-L/2 \leq x \leq L/2, \quad -\infty \leq y \leq \infty$$

i.e.

$$-1/2 \leq \xi \leq 1/2, \quad -\infty \leq \eta \leq \infty$$

Since the behavior of w is now independent of η, Equation [20] becomes

$$3w_{,\xi\xi}w_{,\xi}^2 = -D$$

or

$$(w^3)_{,\xi,\xi} = -D \quad [21]$$

Keeping in mind symmetry, we have as boundary conditions

$$\left.\begin{aligned} w(\xi) &= 0 \text{ for } \xi = -1/2, 1/2 \\ \text{with the consequence that} & \\ w_{,\xi} &= 0 \text{ for } \xi = 0 \end{aligned}\right\} \quad [22]$$

The solution of Equation [21] with boundary conditions [22] is[10]

$$w(\xi) = (3/4)D^{1/3}\{(1/2)^{4/3} - \xi^{4/3}\} \quad [23]$$

9 As already mentioned, to obtain an approximate numerical solution to Equations [21] and [22] we first cast Equation [21] in finite-difference form. To do this let the points i, $i = 0, 1 \ldots, n$ be points uniformly spaced a distance a apart in the interval $-1/2 \leq \xi \leq 1/2$. Thus, with n subintervals we have

$$na = 1$$

Let points b, d, e, f, g, be any consecutive five of these points, and let the (nondimensional) normal displacements there be w_b, w_d, w_e, w_f, w_g. In addition, let α and β be points midway between d and e, and e and f, respectively, see Fig. 1.

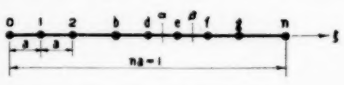

FIG. 1

Then we have as an approximation

$$(w,_\xi)_\beta = (w_f - w_e)/(\xi_f - \xi_e) = (w_f - w_e)/a$$

and

$$(w,_\xi)_\alpha = (w_e - w_d)/a$$

In the same way we can write

$$\{(w^3,_\xi),_\xi\}_e = \{(w^3,_\xi)_\beta - (w^3,_\xi)_\alpha\}/a = \{(w_f - w_e)^3 - (w_e - w_d)^3\}/a^4$$

Hence, at point e, instead of Equation [21] we have a finite-difference approximation

$$(w_f - w_e)^3 - (w_e - w_d)^3 + a^4D = 0 \quad [24a]$$

Similarly, at points d and f the finite-difference equations are

$$\left.\begin{aligned} (w_e - w_d)^3 - (w_d - w_b)^3 + a^4D &= 0 \\ (w_g - w_f)^3 - (w_f - w_e)^3 + a^4D &= 0 \end{aligned}\right\} \quad [24b]$$

and there will be one such equation for each internal point of subdivision of the interval $[-1/2, 1/2]$.

10 To solve this set of simultaneous, nonlinear, algebraic equations by relaxation methods (6) we first must obtain residual and relaxation operators. The former follows immediately. From Equations [24a] and [24b] we have

$$\left.\begin{aligned} (w_e - w_d)^3 - (w_d - w_b)^3 + a^4D &= R_d \\ (w_f - w_e)^3 - (w_e - w_d)^3 + a^4D &= R_e \\ (w_g - w_f)^3 - (w_f - w_e)^3 + a^4D &= R_f \end{aligned}\right\} \quad [25]$$

where R_i, $i = 1, \ldots, d, e, f, \ldots, n-1$, is the error, or residual, at each internal point i for any given set of displacements $\{w_i\}$ which is not a solution to the complete set of Equations [28].

Continuing, from Equations [25] we obtain

$$\begin{aligned} dR_d &= 3(w_e - w_d)^2(dw_e - dw_d) - 3(w_d - w_b)^2(dw_d - dw_b) \\ dR_e &= 3(w_f - w_e)^2(dw_f - dw_e) - 3(w_e - w_d)^2(dw_e - dw_d) \\ dR_f &= 3(w_g - w_f)^2(dw_g - dw_f) - 3(w_f - w_e)^2(dw_f - dw_e) \end{aligned}$$

from which, for $dw_e \neq 0$, $dw_i = 0$ for $i \neq e$, it follows that

$$\begin{aligned} dR_d &= 3(w_e - w_d)^2 dw_e \\ dR_e &= -3\{(w_f - w_e)^2 + (w_e - w_d)^2\}dw_e \\ dR_f &= 3(w_f - w_e)^2 dw_e \end{aligned}$$

and all the remaining dR_i are zero.

It is convenient now to introduce a different subscript notation for naming the subdivision or mesh points. Let point c be the central point of any group of three consecutive points, with points r and l the immediately adjacent right and left points, respectively. Then, from Equations [25] the general residual operator is

$$(w_r - w_c)^3 - (w_c - w_l)^3 + a^4D = R_c \quad [26]$$

and the general relaxation operator is made up from the components

$$\left.\begin{aligned} dR_l &= 3(w_c - w_l)^2 dw_c \\ dR_c &= -3\{(w_r - w_c)^2 + (w_c - w_l)^2\}dw_c \\ dR_r &= 3(w_r - w_c)^2 dw_c \end{aligned}\right\} \quad [27]$$

Following the relaxation literature the relaxation operator can be presented graphically as in Fig. 2. We see that the general operator depends in a nonlinear manner on the instantaneous magnitudes of w associated with the three points, or star, centered

[9] For printing purposes.
[10] See Appendix 1.

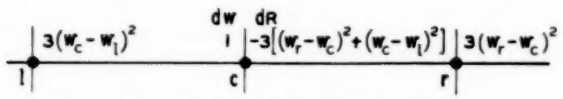

FIG. 2 GENERAL RELAXATION OPERATOR

at point c. This is a complication introduced by the nonlinearity of Equation [21], and it slows down considerably the speed of relaxing in the residual-liquidation process. Thus, for each individual residual-liquidation step, the local relaxation operator component magnitudes must be calculated afresh.

General details of the relaxation process will not be discussed here; further amplification can be obtained elsewhere (6, 7, 8). However, it can be said that this feature just mentioned, that is, the changing nature of the operator, need not be adhered to rigidly for computation purposes. For instance, when the displacement w at the various mesh points are approaching the solution of the set of finite-difference equations, the numbers $(w_c - w_l)^3$, and so on, can be regarded as remaining sensibly constant for several relaxation steps even though, in fact, they do not do so. Hence, after a time it only becomes necessary to recalculate the magnitudes of the relaxation operators every now and again and, although in between such revisions the operators will be incorrect and use of them will introduce errors into the residuals, these errors usually will be small. If this modified procedure is adopted, as a consequence it becomes necessary to compute the correct values of the residuals fairly frequently by means of Equation [26].

One other point should be noted. Since Equation [21] involves the first derivative of w, for the current and similar problems possessing symmetry the interval $[-1/2, 1/2]$ must be subdivided into an odd number of equal intervals. The center point of $[-1/2, 1/2]$ cannot be a mesh point, for if it were no relaxation operator would be available with which to manipulate the residual at that point.

11 For the infinite strip being discussed the interval $[-1/2, 1/2]$ was subdivided into eleven equal intervals, so that

$$n = 11, \quad a = 1/11$$

Because of symmetry it was necessary only to consider the range

$$0 \leq \xi \leq 1/2$$

and the boundary conditions [22] were satisfied by keeping $w_{11} = 0$ and $w_5 = w_6$ throughout the relaxation process. The value of D in Equation [21] was chosen as

$$D = 3000(11)^4$$

so that

$$a^4 D = 3000$$

No difficulty was experienced in obtaining a solution, and convergence of the relaxation process was fairly rapid even though a poor initial set of displacements was chosen deliberately. In fact, the chief time-consuming factor was the changing nature of the relaxation operator.

The solution to the problem, together with the corresponding displacements computed from the analytical solution, Equation [23], is given in Table 1. As can be seen the agreement is excellent.

Having obtained a solution, one question presents itself immediately: Since the finite-difference equations are nonlinear, why should the foregoing procedure lead to the desired answer?

To investigate this the interval $[-1/2, 1/2]$ was subdivided into five equal parts and the associated finite-difference equations written down using Equation [23]. Since the deflection is zero at the end points, symmetry reduced the number of independent unknowns to two. Solution of these two simultaneous cubic equations showed that only one set of roots was real.

TABLE 1 SOLUTION OF TEST PROBLEM AND DISPLACEMENTS

	Displacement					
	w_0, w_{11}	w_1, w_{10}	w_2, w_9	w_3, w_8	w_4, w_7	w_5, w_6
Relaxation solution	0	24.72	47.65	68.46	86.61	101.01
Analytical solution	0	24.68	47.56	68.35	86.49	100.75

SECOND SIMPLIFIED PROBLEM

12 The second simplified problem of interest is that for which the region is a circle of radius R. Again, the loading is taken as constant, and the edge displacement w as zero.

To solve this problem it is convenient to transform Equation [20] to (r, θ) co-ordinates. On so doing, and noting that the deflection is independent of θ, Equation [20] reduces to[11]

$$\left(\frac{1}{r} + \frac{d}{dr}\right)\left(\frac{dw}{dr}\right)^3 = -2(1 - \nu^2)p/Eh \quad \ldots\ldots [28]$$

To make Equation [28] nondimensional put

$$r = \xi R, \quad w = \bar{w}R, \quad h = \bar{h}R, \quad 2(1 - \nu^2)p/E\bar{h} = K$$

which transforms Equation [28] to

$$\left(\frac{1}{\xi} + \frac{d}{d\xi}\right)\left(\frac{d\bar{w}}{d\xi}\right)^3 = -K$$

For computational purposes again we put

$$\bar{w} = \psi(K/D)^{1/3}$$

where D is any arbitrary constant. This yields the desired equation

$$\left(\frac{1}{\xi} + \frac{d}{d\xi}\right)\left(\frac{d\psi}{d\xi}\right)^3 = -D, \quad 0 \leq \xi \leq 1 \quad \ldots\ldots [29]$$

with boundary conditions

$$\left.\begin{aligned} \psi &= 0 \text{ for } \xi = 1 \\ \psi_{,\xi} &= 0 \text{ for } \xi = 0 \end{aligned}\right\} \quad \ldots\ldots [30]$$

The solution to Equations [29] and [30] is[12]

$$\psi = (3/4)(D/2)^{1/3}(1 - \xi^{4/3}) \quad \ldots\ldots [31]$$

Again, with the understanding that only nondimensional quantities are involved, we can drop the bar from ψ and write $\psi = w(\xi)$, or simply $= w$.

13 To derive a finite-difference approximation to Equation [29] the procedure follows that already discussed. Referring again to Fig. 1, for $(d/d\xi)w^3{}_{,\xi}$ we have

$$\{(w^3{}_{,\xi})_{,\xi}\}_c = \{(w_r - w_c)^3 - (w_c - w_l)^3\}/a^4$$

However, for the remaining term $w^3{}_{,\xi}/\xi$ it is necessary to use an interval of $2a$. This yields

$$\{w^3{}_{,\xi}/\xi\}_c = \{(w_r - w_l)/2a\}^3/\xi_c$$

so that for any central point c of a three-point approximation the finite-difference equation corresponding to Equation [29] is

$$(w_r - w_c)^3 - (w_c - w_l)^3 + (w_r - w_l)^3/8(\xi_c/a) = -Da^4 \ldots [32]$$

[11] See Appendix 2.
[12] See Appendix 3.

where $a = 2/n$ and n is the number of intervals into which the domain of 2ξ (i.e., the nondimensional diameter) is subdivided.

The method of solving the set of finite-difference equations of which Equation [32] is a typical member is identical with that already outlined. It will not be discussed further. To specify the problem completely n was taken to be 11; i.e., the unit diameter was subdivided into eleven equal intervals, see Fig. 3, so that

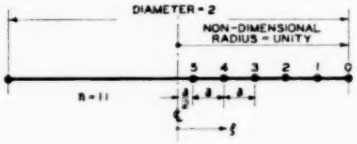

FIG. 3

$$a = 2/11$$

and D was chosen to be $3000\ (11/2)^4$. The numerical solution obtained, together with corresponding results computed from the analytical Solution [31], are given in Table 2.

TABLE 2 SOLUTION OF SECOND SIMPLIFIED PROBLEM

	Displacements $w(\xi)$					
	w_0	w_1	w_2	w_3	w_4	w_5
Relaxation solution	0	19.76	38.19	55.08	70.18	83.47
Analytical solution	0	19.58	37.74	54.23	68.61	79.94

14 This relaxation solution is not as accurate as that obtained for the infinite strip problem. This is because the finite-difference approximation to the first term in the governing differential Equation [29] is less accurate than the second.

Accordingly, for interest it was decided to decrease the subdivision length a and so obtain a second approximation. On taking $n = 25$ and retaining D as $3000\ (11/2)^4$ the second solution is given in Table 3. Here the agreement is much better.

TABLE 3 ALTERNATE SOLUTION TO SIMPLIFIED PROBLEM

	Displacements $w(\xi)$												
	w_0	w_1	w_2	w_3	w_4	w_5	w_6	w_7	w_8	w_9	w_{10}	w_{11}	w_{12}
Relaxation solution	0	8.9	17.53	25.9	33.97	41.75	49.2	56.3	63.0	69.2	74.7	79.6	84.0
Analytical solution	0	8.77	17.29	25.54	33.51	41.17	48.5	55.46	62.00	68.08	73.60	78.42	82.21

THIRD SIMPLIFIED PROBLEM

15 With the two foregoing problems as guides for technique we consider, finally, a finite two-dimensional simplified $w(\xi, \eta)$-problem. Except for the fact that the residual and relaxation operators become more cumbersome the general method of solution will remain unaltered.

Let R be some closed finite region in the (ξ, η)-plane with boundary B. The problem is to solve the equation

$$w_{,\xi\xi}(3w_{,\xi}^2 + w_{,\eta}^2) + w_{,\eta\eta}(w_{,\xi}^2 + 3w_{,\eta}^2) + 4w_{,\xi}w_{,\eta}w_{,\xi\eta} = -D. \quad [20]$$

in R, with boundary condition that on B

$$w = 0. \quad [33]$$

To derive a set of finite-difference equations corresponding to Equation [20] let a square mesh of lines be superposed on R, the lines being parallel to the ξ and η-axes, and the squares being of side length a. Let Fig. 4 represent portion of R, and let the point c be any internal point of the mesh.

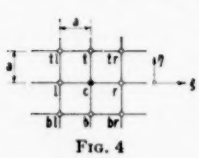

FIG. 4

With point c as center let a set of nine mesh points be named as shown, and let the $w(\xi, \eta)$-displacement at point c be w_c, and so on. Then, from Fig. 4, we have finite-difference approximations

$$(w,_\xi)_c = (w_r - w_l)/2a$$

$$(w,_\eta)_c = (w_t - w_b)/2a$$

$$(w,_{\xi\xi})_c = (w_r + w_l - 2w_c)/a^2$$

$$(w,_{\eta\eta})_c = (w_t + w_b - 2w_c)/a^2$$

$$(w,_{\xi\eta})_c = (w_{tr} - w_{tl} + w_{bl} - w_{br})/4a^2$$

Using these, an approximation to Equation [20], evaluated at point c, is

$$(w_r + w_l - 2w_c)\{3(w_r - w_l)^2 + (w_t - w_b)^2\} + (w_t + w_b - 2w_c)\{3(w_t - w_b)^2 + (w_r - w_l)^2\} + (w_r - w_l)(w_t - w_b)(w_{tr} - w_{tl} + w_{bl} - w_{br}) = -4a^4D. \quad [34]$$

and there is one such equation for each nonboundary mesh point c in R.

16 The derivation of the residual and relaxation operators need not be discussed in detail; the procedure follows that already given. For the general residual operator we have immediately

$$(w_r + w_l - 2w_c)\{3(w_r - w_l)^2 + (w_l - w_b)^2\} + (w_t + w_b - 2w_c)\{3(w_t - w_b)^2 + (w_r - w_l)^2\} + (w_r - w_l)(w_t - w_b)(w_{tr} - w_{tl} + w_{bl} - w_{br}) + 4a^4D = R_c \quad [35]$$

To write down the relaxation operator in general form it is convenient to introduce further meaning into the subscript notation used in naming the mesh points in Fig. 4. Point c is, of course, any mesh point defined by the mesh superposed on R. Point c is also the center point[13] of the general nine-point star c, l, r, t, b, tr, tl, bl, br, and it is obvious that the letters r, l, t, b stand for right, left, top, bottom, respectively, implying that (for example) point tr is the point immediately adjacent and top-right to c.

However, on a nine-point star with center point c, the point r to the right of c is also the center point for another similar set of nine points not specifically indicated on Fig. 4; and, relative to point r as center, the point c shown in Fig. 4 is the l point. Without introducing further letters we can indicate this by using a set of curly braces with subscripts inside and also outside the right-hand brace. For example, in the quantity

$$\{(w_r - w_l)(\ldots)\}_r$$

the deflection w_l inside the brace refers to the deflection w of the point to the left of the point r shown in Fig. 4. It is thus actually the deflection of point c of that figure. On the other hand, the deflection w_r in that quantity is the deflection of the point to the right of point r in Fig. 4, and that point is not indicated or named explicitly.

With this understanding the components of the general relaxation operator for any point c are

[13] Irregular stars, that is, stars for which the arms are not all of length a, will not be discussed here.

$$
\left.
\begin{aligned}
dR_c &= -8\,\{(w_r - w_l)^2 + (w_t - w_b)^2\}_c dw_c \\
dR_r &= \{3(w_r - w_l)^2 + (w_t - w_b)^2 \\
&\quad -(w_r - w_l)[6(w_r + w_l - 2w_c) + 2(w_t + w_b - 2w_c)] \\
&\qquad -(w_t - w_b)(w_{tr} - w_{tl} + w_{bl} - w_{br})\}_r dw_c \\
dR_l &= \{3(w_r - w_l)^2 + (w_t - w_b)^2 \\
&\quad +(w_r - w_l)[6(w_r + w_l - 2w_c) + 2(w_t + w_b - 2w_c)] \\
&\qquad + (w_t - w_b)(w_{tr} - w_{tl} + w_{bl} - w_{br})\}_l dw_c \\
dR_t &= \{3(w_t - w_b)^2 + (w_r - w_l)^2 \\
&\quad -(w_t - w_b)[6(w_t + w_b - 2w_c) + 2(w_r + w_l - 2w_c)] \\
&\qquad -(w_r - w_l)(w_{tr} - w_{tl} + w_{bl} - w_{br})\}_t dw_c \\
dR_b &= \{3(w_t - w_b)^2 + (w_r - w_l)^2 \\
&\quad + (w_t - w_b)[6(w_t + w_b - 2w_c) + 2(w_r + w_l - 2w_c)] \\
&\qquad + (w_r - w_l)(w_{tr} - w_{tl} + w_{bl} - w_{br})\}_b dw_c \\
dR_{tr} &= \{(w_r - w_l)(w_t - w_b)\}_{tr} dw_c \\
dR_{tl} &= -\{(w_r - w_l)(w_t - w_b)\}_{tl} dw_c \\
dR_{bl} &= \{(w_r - w_l)(w_t - w_b)\}_{bl} dw_c \\
dR_{br} &= -\{(w_r - w_l)(w_t - w_b)\}_{br} dw_c
\end{aligned}
\right\} \quad \ldots [36]
$$

With the double subscript scheme of mesh-point identification it is a simple matter to set out and corapute in tabular form all the quantities which make up this nonlinear relaxation operator for each and every mesh point in R.

To solve a problem the operator can be used in the manner indicated for the one-dimensional problems. In view of the complicated nature of the general relaxation operator it is advisable to obtain a solution for a coarse mesh first, so as to avoid having to deal with too many operators all of which are numerically different and all of which must be recomputed for each relaxation step. On obtaining the coarse mesh solution it can then be used as a basis from which to obtain a good starting approximation for a finer mesh solution, and in attempting to obtain the finer mesh solution the relaxation operators can be assumed to remain constant for several residual liquidation steps. Errors so introduced can be corrected by recomputing at frequent intervals the correct residuals by means of Equation [35]. In practice this process converges to a solution fairly rapidly.

Again it should be mentioned that for a singly or doubly symmetric region R the number of mesh spaces must be odd in one or both directions because of the $\partial w/\partial \xi$ or $\partial w/\partial \eta$ factor in Equation [20]. For such a region, on proceeding from a coarse to a finer mesh it is not allowable to use a mesh size of $(a/2)^m$, $m = 1, 2, \ldots$, as this would introduce an even number of mesh spaces. Further, if the finer mesh spacing was made to be $(a/3)^m$ it is likely that the number of mesh points so introduced would be unmanageably large. Accordingly it is suggested that the fine mesh spacing should not be taken to be a simple subdivision of the initial coarse mesh unless, perhaps, the coarse mesh be very coarse indeed.[14] In any case, initial values for the fine mesh points can be obtained from the coarse mesh solution by graphical cross-plotting or by interpolation.

17 For a two-dimensional "w-problem" example the region chosen was a rectangle of dimensions

$$0 \leq x \leq L, \quad 0 \leq y \leq 5L/7$$

or in nondimensional units

$$0 \leq \xi \leq 1, \quad 0 \leq \eta \leq 5/7$$

The mesh size chosen was $a = L/7$, that is, $n = 7$. The constant D of Equation [20] was chosen[15] as $D = 1000(11)$.[4]

For this problem the $w(\xi, \eta)$-displacements are symmetrical about the horizontal and vertical center lines of the rectangle. Hence, for numerical work, it was necessary to consider only one fourth of the region. The foregoing choice of mesh size thus resulted in six internal mesh points, Fig. 5(a and b). Using the relaxation technique, and with point relaxation only, a solution was obtained without difficulty. With w taken initially as zero everywhere the initial residual at each internal mesh point was[15] $4000(11/7)^4$. The solution obtained is presented in Fig. 6.

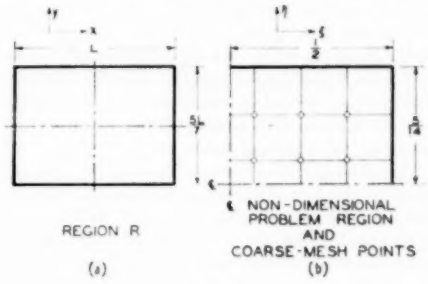

FIG. 5

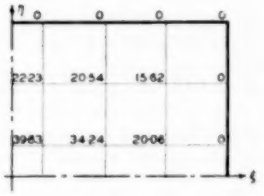

FIG. 6 SIMPLIFIED $w(\xi, \eta)$ SOLUTION FOR RECTANGULAR REGION PROBLEM

3 SOLUTION OF GENERAL u, v, w-PROBLEM

18 With the "simplified w-problem" solved it is easy to devise a technique for solving the general u, v, w-problem given by Equations [15]. Essentially, we use a combination of relaxation and iteration.

We commence with the w-solution just discussed. Here both u and v have been taken as zero everywhere. Then, with w taken as remaining constant, using finite differences and the relaxation process we solve the first of Equations [15]. During this step the v-displacements are still assumed zero everywhere, and the w-solution just obtained furnishes the initial residual pattern.

This u-problem is linear in the u-displacements, and so the relaxation operator is linear and independent of the mesh point considered. The relaxation procedure for this step is straightforward and well known.

Next, still with the w-values remaining unaltered, and now assuming the u-solution just obtained to remain temporarily unaltering also, the second or v-equation of Equations [15] is solved. This time both the u and the w-solutions contribute to make up the original residuals for this v-problem. Again, the relaxation procedure is simple and straightforward.

This completes one cycle of the process of solution.

For the second cycle we now have available approximate values of u, v, and w. The number D, of course, remains unaltered throughout and depends only on the initial choice. With the available u, v, w-values we can now recompute the residuals for the third or w-equation of Equations [15], and so the process can continue stepwise, during each step two of the three displacements being assumed to remain temporarily unalterable.

For the current w-step two alternatives are available. Referring to the third equation of Equations [15] we can regard all quantities on the right-hand side of that equation as being tem-

[14] In this case a fine mesh of size $a/3$ will not provide an unmanageable number of mesh points.

[15] Obviously it would have been better to have taken D as $1000(7)^4$. The number $1000(11)^4$ was a relic of some preliminary work.

porarily constant during this step of the second cycle, and form the relaxation operator from the left-hand side only. This would imply using the same w relaxation operator as that used in the foregoing simplified w-problem. Alternatively, a revised operator could be devised using all the w-terms in the third equation, it being assumed only that u and v remain temporarily constant during this step.

In the example to be discussed shortly both schemes were tried. Both schemes are satisfactory, but convergence of the process is much faster using the latter process, even though the relaxation operator for the latter is more complex than for the former.

With the second cycle of w-computation completed, the second cycle of u and of v can then be done, using the just obtained, revised, w-values to form initial residuals.

This relaxation-iteration process can be continued until all three sets of residuals are (simultaneously) sufficiently small to be neglected in comparison with the relaxation operators. Although tedious, the process involves no essential difficulties, and convergence seems rapid. About four cycles are necessary to obtain a solution.

It can be noted that, unlike the simplified w-problem, for the complete u, v, w-problem an even number of mesh subdivisions can be used, for although $w_{,\xi}$ and $w_{,\eta}$ are both zero at the center of a symmetric region (for a uniform load p), $w_{,\xi\xi}$ and $w_{,\eta\eta}$ are not, and the same is true for $u_{,\xi}$ and $v_{,\eta}$.

19 The residual and relaxation operators for the three Equations [15] can be derived in the manner already described. For the first of Equations [15], using the previous notation we have for any mesh point c the residual operator

$$(2/a^2)(u_r + u_l - 2u_c) + \{(1-\nu)/a^2\}(u_t + u_b - 2u_c)$$
$$+ \{(1+\nu)/4a^2\}(v_{tr} - v_{tl} + v_{bl} - v_{br}) + \{(1+\nu)/8a^3\}$$
$$(w_t - w_b)(w_{tr} - w_{tl} + w_{bl} - w_{br}) + (w_r - w_l)(w_r + w_l - 2w_c)$$
$$/a^3 + \{(1-\nu)/2a^3\}(w_r - w_l)(w_t + w_b - 2w_c) = (\text{residual})$$

that is

$$2u_r + 2u_l + (1-\nu)u_t + (1-\nu)u_b - (6-2\nu)u_c + K_e = R'_c \quad [37]$$

where

$$K_e = (1+\nu)(v_{tr} - v_{tl} + v_{bl} - v_{br})/4 + (1+\nu)(w_t - w_b)(w_{tr} - w_{tl} + w_{bl} - w_{br})/8a + (w_r - w_l)(w_r + w_l - 2w_c)/a + (1-\nu)(w_r - w_l)(w_t + w_b - 2w_c)/2a \quad [38]$$

For any one relaxation step in a cycle of the iteration process the quantity K_e is just a number. Although different at each mesh point it remains constant during the step, and so needs to be computed only at the commencement of the u-stage of each cycle.

From Equation [37] the u-relaxation operator is easily obtained for any mesh point c. It is

$$\left.\begin{aligned} dR'_r &= 2du_c = dR_l' \\ dR'_t &= (1-\nu)du_c = dR_b' \\ dR'_c &= -(6-2\nu)du_c \end{aligned}\right\} \quad [39]$$

This can be presented symbolically as in Fig. 7. As already mentioned the operator is the same, numerically, for all mesh points c. Its use is straightforward and simple.

The residual and relaxation operators for the second of Equations [15] are similar to those just derived. The residual operator is

$$(1-\nu)v_r + (1-\nu)v_l + 2v_t + 2v_b - (6-2\nu)v_c + J_c = R''_c \quad [40]$$

where

$$J_c = (1+\nu)(u_{tr} - u_{tl} + u_{bl} - u_{br})/4 + (1+\nu)(w_r - w_l)(w_{tr} - w_{tl} + w_{bl} - w_{br})/8a + (w_t - w_b)(w_t + w_b - 2w_c)/a + (1-\nu)(w_t - w_b)(w_r + w_l - 2w_c)/2a \quad [41]$$

As with K_e, for the v-stage of any one cycle of the iteration process, J_e is a constant which is different at each mesh point.

From Equations [44], for any mesh point c the relaxation operator is

$$\left.\begin{aligned} dR''_r &= (1-\nu)dv_c = dR''_l \\ dR''_t &= 2dv_c = dR''_b \\ dR''_c &= -(6-2\nu)dv_c \end{aligned}\right\} \quad [42]$$

It is presented diagrammatically in Fig. 8.

The operators for the third of Equations [15] are rather more complex. To derive them we rewrite that equation in the form

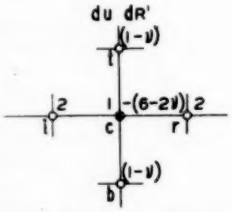

FIG. 7 $u(\xi, \eta)$ RELAXATION OPERATOR

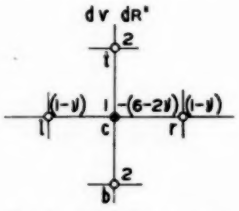

FIG. 8 $v(\xi, \eta)$ RELAXATION OPERATOR

$$\{w_{,\xi\xi}(3w_{,\eta}^2 + w_{,\xi}^2) + w_{,\eta\eta}(w_{,\xi}^2 + 3w_{,\eta}^2) + 4w_{,\xi}w_{,\eta}w_{,\xi\eta}\}$$
$$+ w_{,\xi}(E + \nu G) + w_{,\eta}(F + \nu H)$$
$$+ 2\{w_{,\xi\xi}L + (1-\nu)w_{,\xi\eta}M + w_{,\eta\eta}N\} = -D$$

where

$$E = 2u_{,\xi\xi} + u_{,\eta\eta} + v_{,\xi\eta}$$
$$F = 2v_{,\eta\eta} + v_{,\xi\xi} + u_{,\xi\eta}$$
$$G = v_{,\xi\eta} - u_{,\eta\eta}$$
$$H = u_{,\xi\eta} - v_{,\xi\xi}$$
$$L = u_{,\xi} + \nu v_{,\eta}$$
$$M = u_{,\eta} + v_{,\xi}$$
$$N = v_{,\eta} + \nu u_{,\xi}$$

We note that the functions in the first set of curly braces are identical with those already discussed in §§15, 16, while the remaining functions are linear in w. Also, the quantities $E, \ldots, N$ are all numbers which, although different from point to point, remain constant throughout any one w-relaxation step of an iteration cycle.

Finite-difference approximations to all the derivatives appearing in this equation have been discussed already. Using them, and also Equation [35], the residual operator for any mesh point c becomes

$$(w_r + w_l - 2w_c)\{3(w_r - w_l)^2 + (w_t - w_b)^2\}$$
$$+ (w_t + w_b - 2w_c)\{3(w_t - w_b)^2 + (w_r - w_l)^2\}$$
$$+ (w_r - w_l)(w_t - w_b)(w_{tr} - w_{tl} + w_{bl} - w_{br})$$
$$+ (w_r - w_l)2a(E_c + \nu G_c) + (w_t - w_b)2a(F_c + \nu H_c)$$
$$+ 2\{(w_r - w_l - 2w_c)2aL_c + (1-\nu)(w_{tr} - w_{tl} + w_{bl} - w_{br})aM_c/2$$
$$+ (w_t + w_b - 2w_c)2aN_c\} + 4a^4D = R_c \quad [43]$$

where the numbers $E_c, \ldots, N_c$ are given by

$$E_c = (2u_r + 2u_l + u_t + u_b - 6u_c) + (v_{tr} - v_{tl} + v_{bl} - v_{br})/4$$
$$F_c = (v_r + v_l + 2v_t + 2v_b - 6v_c) + (u_{tr} - u_{tl} + u_{bl} - u_{br})/4$$
$$G_c = (v_{tr} - v_{tl} + v_{bl} - v_{br})/4 - (u_t + u_b - 2u_c)$$
$$H_c = (u_{tr} - u_{tl} + u_{bl} - u_{br})/4 - (v_r + v_l - 2v_c)$$
$$L_c = (u_r - u_l) + \nu(v_t - v_b)$$
$$M_c = (u_t - u_b) + (v_r - v_l)$$
$$N_c = (v_t - v_b) + \nu(u_r - u_l)$$

and $a = 1/n$, n being the number of mesh spaces into which the representative length L of the problem region is subdivided.

Using Equations [36] and [43] the relaxation operator for a point c follows immediately. Its components are

$$\left.\begin{aligned}
dR_c &= -8\{(w_r - w_l)^2 + (w_t - w_b)^2 + a(L_c + N_c)\}_c dw_c \\
dR_r &= \{3(w_r - w_l)^2 + (w_t - w_b)^2 \\
&\quad - (w_r - w_l)[6(w_r + w_l - 2w_c) \\
&\quad + 2(w_t + w_b - 2w_c)] \\
&\quad - (w_t - w_b)(w_{tr} - w_{tl} + w_{bl} - w_{br}) \\
&\quad + 2a[2L_c - (E_c + \nu G_c)]\}_r dw_c \\
dR_l &= \{3(w_r - w_l)^2 + (w_t - w_b)^2 \\
&\quad + (w_r - w_l)[6(w_r + w_l - 2w_c) \\
&\quad + 2(w_t + w_b - 2w_c)] \\
&\quad + (w_t - w_b)(w_{tr} - w_{tl} + w_{bl} - w_{br}) \\
&\quad + 2a[2L_c + (E_c + \nu G_c)]\}_l dw_c \\
dR_t &= \{3(w_t - w_b)^2 + (w_r - w_l)^2 \\
&\quad - (w_t - w_b)[6(w_t + w_b - 2w_c) \\
&\quad + 2(w_r + w_l - 2w_c)] \\
&\quad - (w_r - w_l)(w_{tr} - w_{tl} + w_{bl} - w_{br}) \\
&\quad + 2a[2N_c - (F_c + \nu H_c)]\}_t dw_c \\
dR_b &= \{3(w_t - w_b)^2 + (w_r - w_l)^2 \\
&\quad + (w_t - w_b)[6(w_t + w_b - 2w_c) \\
&\quad + 2(w_r + w_l - 2w_c)] \\
&\quad + (w_r - w_l)(w_{tr} - w_{tl} + w_{bl} - w_{br}) \\
&\quad + 2a[2N_c + 2(F_c + \nu H_c)]\}_b dw_c \\
dR_{tr} &= \{(w_r - w_l)(w_t - w_b) + (1 - \nu)a\, M_c\}_{tr} dw_c \\
dR_{tl} &= -\{(w_r - w_l)(w_t - w_b) + (1 - \nu)a\, M_c\}_{tl} dw_c \\
dR_{bl} &= \{(w_r - w_l)(w_t - w_b) + (1 - \nu)a\, M_c\}_{bl} dw_c \\
dR_{br} &= -\{(w_r - w_l)(w_t - w_b) + (1 - \nu)a\, M_c\}_{br} dw_c
\end{aligned}\right\} \quad \ldots [44]$$

The terms which have been added to Equations [36] to produce Equations [44] are numbers which are independent of the current magnitudes of w but are computed from the current u and v-pattern. They remain constant throughout the w-stage of relaxation but must be computed afresh for each iteration cycle.

Rectangular Region

20 One problem was solved as an example of the application of the complete technique just discussed. It was the L by $5L/7$ rectangular membrane which formed the third example of the simplified w-problem, and for that example a solution was obtained on a mesh of size $a = 1/7$, Figs. 5.

For the current problem it was decided to obtain a solution on a mesh of one half the previous size, namely, one for which $a = 1/14$, and so, using the previously chosen value for D, for this problem

$$a^4D = 1000\,(11/14)^4$$

The problem was first solved completely on the coarse mesh, for which the initial values of $w(\xi, \eta)$ were already available. The mesh-point values of $w(\xi, \eta)$ taken as the starting approximation for the finer mesh were obtained from the previous coarse mesh solution by cross-plotting.

The complete $u(\xi, \eta)$, $v(\xi, \eta)$, $w(\xi, \eta)$-solution, obtained without difficulty in the manner already described, is presented in Figs. 9(a), 9(b), 9(c). For comparison the starting values of w (just mentioned) are also presented, enclosed in braces, in Fig. 9(c).

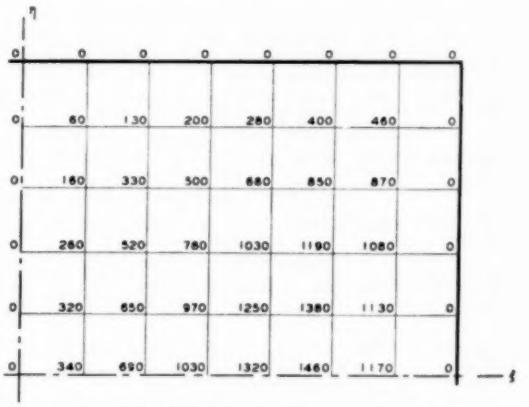

Fig. 9(a) Displacement Component $u(\xi, \eta)$

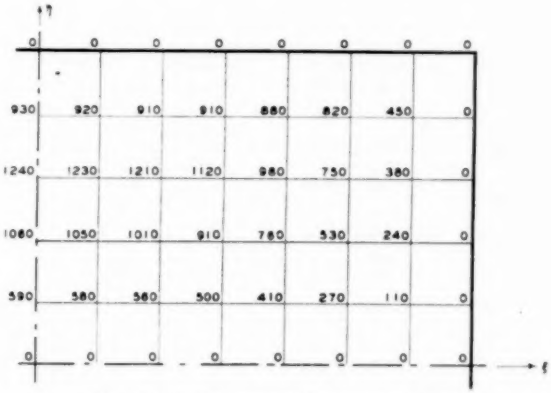

Fig. 9(b) Displacement Component $v(\xi, \eta)$

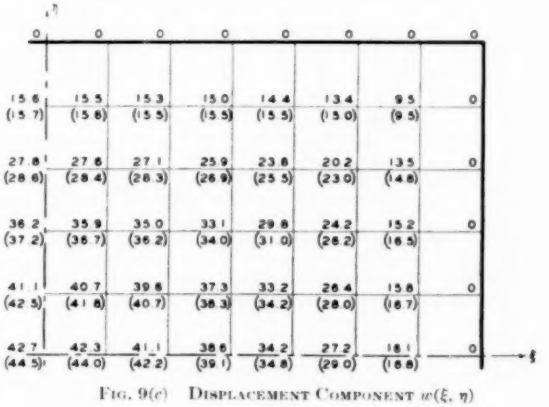

Fig. 9(c) Displacement Component $w(\xi, \eta)$

From this starting point four cycles of iteration were necessary to obtain the final solution. In the computations Poisson's ratio was taken to be $\nu = 0.3$.

To complete the problem, values and contours of the nondimensional stress components also were obtained. These are presented in Figs. 10, 11, and 12. These were computed by using Expressions [17] together with the appropriate finite-difference

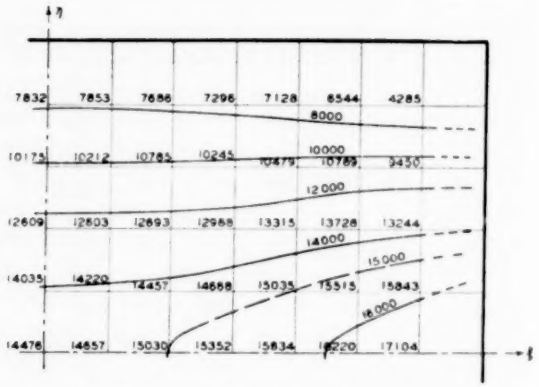

FIG. 10 VALUES AND CONTOURS OF NORMAL STRESS $\sigma_{\xi\xi}$

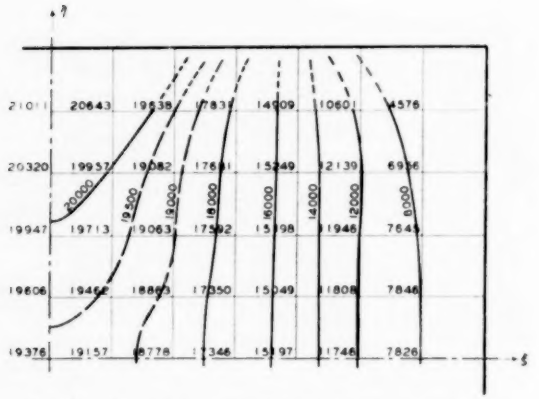

FIG. 11 VALUES AND CONTOURS OF NORMAL STRESS $\sigma_{\eta\eta}$

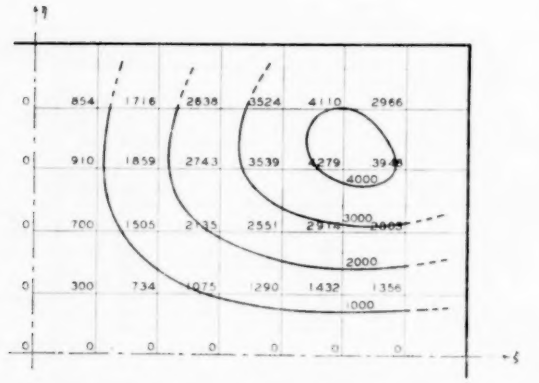

FIG. 12 VALUES AND CONTOURS OF SHEAR STRESS $(-)\sigma_{\xi\eta}$

approximations derived earlier. From these results the two principal stresses were computed using Equation [19], and values and contours are presented in Figs. 13 and 14.

In so far as the presented numerical values are concerned it must be mentioned that the stresses are not known to the accuracy the given numbers might indicate. The stresses are obtained by computation from the displacement solutions and, rather than round off figures to give an accuracy comparable to

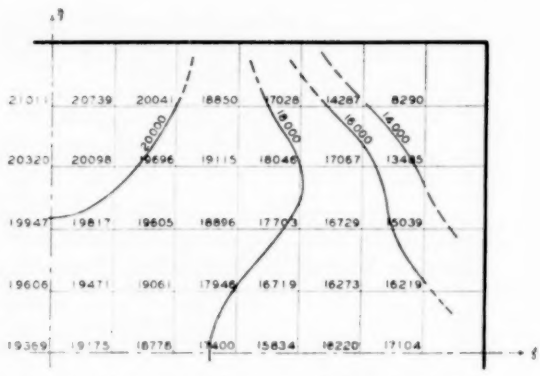

FIG. 13 VALUES AND CONTOURS OF PRINCIPAL STRESS σ_1

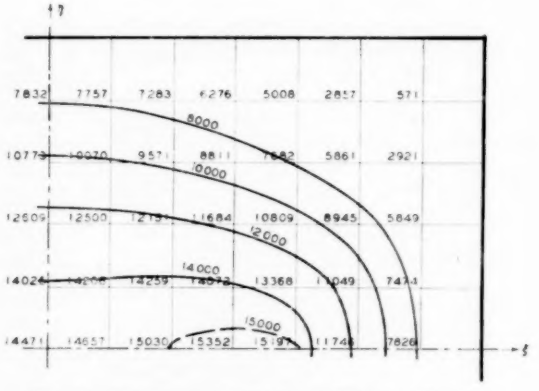

FIG. 14 VALUES AND CONTOURS OF PRINCIPAL STRESS σ_2

that with which the displacements are known, the full computational results have been retained.

Since the mesh used was still not very fine, and since end-point finite-difference expressions for derivatives are not as accurate as the corresponding center-point expressions, stress magnitudes were not computed at the boundary. Accordingly, the continuation of the various stress contour lines to the boundaries of the rectangular region has been indicated by broken lines.

These are intended as a guide only; for more accurate results in the region of the membrane edge a finer mesh should be used locally. This further refinement was not considered here.

INFINITE-STRIP REGION

21 Finally, we discuss briefly the complete membrane problem for the infinite-strip region. The corresponding simplified w-problem was treated earlier and, on investigation, it turns out that for the complete problem a simple exact analytical solution is readily obtainable for the case of a uniform load.[16] In fact, for this problem the solution is[17]

$$u(\xi) = -(2D^2/3)^{1/3}\,\xi(\xi + 1/2)(\xi - 1/2)$$

$$w(\xi) = -(3D/2)^{1/3}(\xi + 1/2)(\xi - 1/2), \quad (-1/2 \leq \xi \leq 1/2)$$

In virtue of the availability of this exact solution, at first sight

[16] Solutions for a variety of other load conditions are also easy to obtain. These will be discussed in a separate publication.

[17] See Appendix 4.

it might seem that it would be useful to solve this problem by relaxation methods also and so obtain a further indication of possible accuracy of the finite-difference solution. In this instance, however, this is not so, the reason being as follows:

In the foregoing, finite-difference approximations to various derivatives were derived in a very simple manner. The same expressions also can be derived more satisfactorily by considering a Taylor series expansion of u, and so on, about a mesh point. If this is done, it can be seen that the errors in those expressions involve the derivatives of the function considered which are higher than the derivative for which the finite-difference approximation has been obtained. In particular, for $du(\xi)/d\xi\ [=u'(\xi)]$ the error is of the form

$$\alpha u^{\mathrm{III}} + \beta u^{\mathrm{V}} + \ldots$$

and for $u''(\xi)$ is

$$\gamma u^{\mathrm{IV}} + \delta u^{\mathrm{VI}} + \ldots$$

However, reference to the foregoing exact solution shows that all derivatives of $u(\xi)$ higher than the third vanish, as also do all derivatives of $w(\xi)$ higher than the second. It follows, then, from the form of (*a*) and (*b*) of Appendix 4, that for this particular problem a finite-difference solution obtained by use of the operators developed earlier would, in fact, coincide with the exact solution at all mesh points, irrespective of the mesh size.

22 It should be obvious from the foregoing that the general technique does not depend for its success on the nature of the region treated or on the type of load distribution. Irregular-shaped regions could be handled equally as readily. To do so would require merely the consideration of "irregular star operators" (6, 7, 8) adjacent to the boundary.

BIBLIOGRAPHY

1 "Die Berechnung dünner rechteckiger Platten mit verschwindender Biegungsteifigkeit," by H. Hencky, ZAMM, vol. 1, 1921, p. 81.

2 "Theory of Plates and Shells," by S. Timoshenko, McGraw-Hill Book Company, Inc., New York, N. Y., 1940, p. 342.

3 "Vorlesungen über Technische Mechanik," by A. Föppl, B. G. Teubner, Leipzig, Germany, vol. 5, 1907, p. 132.

4 "Relaxation Methods Applied to Engineering Problems, VII A: Biharmonic Analysis as Applied to the Flexure and Extension of Flat Elastic Plates," by L. Fox and R. V. Southwell, Philosophical Transactions of the Royal Society, series C, vol. 1, 1941, pp. 15–56.

5 "The Edge Effect in Bending and Buckling With Large Deflections," by K. O. Friedrichs, Proceedings, Symposium, Applied Mathematics, American Mathematical Society, vol. 1, 1949, pp. 188–193.

6 "Numerical Methods of Analysis in Engineering," by L. E. Grinter, The Macmillan Company, New York, N. Y., 1949. (See chapter 3: "Numerical Solutions of Boundary Value Problems by Relaxation Methods," by F. S. Shaw.)

7 "Relaxation Methods in Theoretical Physics," by R. V. Southwell, Oxford University Press, New York, N. Y., 1946.

8 "An Introduction to Relaxation Methods," by F. S. Shaw, to be published by Dover Publications, New York, N. Y.

Appendix 1

Equation [21] to be solved is

$$(w^3{}_{,\xi})_{,\xi} = -D, \quad D = \text{const}$$

in the region $-1/2 \leq \xi \leq 1/2$, with terminal conditions

$$w(-1/2) = w(1/2) = 0$$

An integration yields

$$w^3{}_{,\xi} = C_1 - D\xi$$

or

$$w_{,\xi} = (C_1 - D\xi)^{1/3}$$

A second integration gives

$$w(\xi) = -(3/4D)(C_1 - D\xi)^{4/3} + C_2$$

Using the symmetry condition that

$$w_{,\xi} = 0 \text{ for } \xi = 0$$

it follows that

$$C_1 = 0$$

Hence, since $w(1/2) = 0$

$$C_2 = (3/4D)(D/2)^{4/3}$$

and so the solution is

$$w(\xi) = (3/4)D^{1/3}\{(1/2)^{4/3} - \xi^{4/3}\}$$

Appendix 2

Equation [20] is

$$w_{,xx}(3w^2{}_{,x} + w^2{}_{,y}) + w_{,yy}(w^2{}_{,x} + 3w^2{}_{,y}) + 4w_{,x}w_{,y}w_{,xy} = -2(1 - \nu^2)p/Eh$$

which can be rewritten as

$$\left(w_{,x}\frac{\partial}{\partial x} + w_{,y}\frac{\partial}{\partial y} + w_{,xx} + w_{,yy}\right)(w^2{}_{,x} + w^2{}_{,y}) = -2(1 - \nu^2)p/Eh$$

To transform this to (r, θ) co-ordinates we have the operators

$$\frac{\partial}{\partial x} = \cos\theta\,\frac{\partial}{\partial r} - \frac{\sin\theta}{r}\,\frac{\partial}{\partial\theta}$$

$$\frac{\partial}{\partial y} = \sin\theta\,\frac{\partial}{\partial r} + \frac{\cos\theta}{r}\,\frac{\partial}{\partial\theta}$$

from which we readily obtain the relations

$$w_{,xx} + w_{,yy} = w_{,rr} + w_{,r}/r + w_{,\theta\theta}/r^2$$

$$w^2{}_{,x} + w^2{}_{,y} = w^2{}_{,r} + w^2{}_{,\theta}/r^2$$

and

$$w_{,x}\frac{\partial}{\partial x} + w_{,y}\frac{\partial}{\partial y} = w_{,r}\frac{\partial}{\partial r} + (w_{,\theta}/r^2)\frac{\partial}{\partial\theta}$$

Using these the foregoing differential equation becomes

$$\left\{w_{,r}\frac{\partial}{\partial r} + (w_{,\theta}/r^2)\frac{\partial}{\partial\theta} + w_{,rr} + w_{,r}/r + w_{,\theta\theta}/r^2\right\}\{w^2{}_{,r} + w^2{}_{,\theta}/r^2\} = -2(1 - \nu^2)p/Eh$$

On expansion, recalling that the problem under discussion is independent of θ, this equation reduces to

$$3w^2{}_{,r}w_{,rr} + w^3{}_{,r}/r = -2(1 - \nu^2)p/Eh$$

or

$$\left(\frac{1}{r} + \frac{d}{dr}\right)\left(\frac{dw}{dr}\right)^3 = -2(1 - \nu^2)p/Eh$$

Appendix 3

The equation is

$$\left(\frac{1}{\xi} + \frac{d}{d\xi}\right)\left(\frac{dw}{d\xi}\right)^3 = -D; \quad w = w(\xi), \quad D = \text{const}$$

Put $(dw/d\xi)^3 = F$, and so obtain

$$F + \xi \frac{dF}{d\xi} = -D\xi$$

or

$$\frac{d}{d\xi}(F\xi) = -D\xi$$

An integration yields

$$F\xi = -D\xi^2/2 + C_1$$

and noting that $F = 0$ at $\xi = 0$ this reduces to

$$F = -D\xi/2$$

or

$$\frac{dw}{d\xi} = -(D\xi/2)^{1/3}$$

From this a second integration yields

$$w(\xi) = -(3/4)(D/2)^{1/3}\xi^{4/3} + C_2$$

and using the remaining boundary condition, namely

$$w = 0 \quad \text{for} \quad \xi = 1$$

the solution is

$$w(\xi) = (3/4)(D/2)^{1/3}(1 - \xi^{4/3})$$

Appendix 4

Equations [15] are

$$(u_{,\xi\xi} + u_{,\eta\eta}) + (u_{,\xi\xi} - \nu u_{,\eta\eta}) + (1 + \nu)v_{,\xi\eta}$$
$$= -\{(1 + \nu)w_{,\eta}w_{,\xi\eta} + 2w_{,\xi}w_{,\xi\xi} + (1 - \nu)w_{,\xi}w_{,\eta\eta}\}$$
$$(v_{,\xi\xi} + v_{,\eta\eta}) + (v_{,\eta\eta} - \nu v_{,\xi\xi}) + (1 + \nu)u_{,\xi\eta}$$
$$= -\{(1 + \nu)w_{,\xi}w_{,\xi\eta} + 2w_{,\eta}w_{,\eta\eta} + (1 - \nu)w_{,\eta}w_{,\xi\xi}\}$$
$$w_{,\xi\xi}(3w^2{}_{,\xi} + w^2{}_{,\eta}) + w_{,\eta\eta}(w^2{}_{,\xi} + 3w^2{}_{,\eta}) + 4w_{,\xi}w_{,\eta}w_{,\xi\eta} = -D$$
$$-\{w_{,\xi}(2u_{,\xi\xi} + u_{,\eta\eta} + v_{,\xi\eta}) + w_{,\eta}(2v_{,\eta\eta} + v_{,\xi\xi} + u_{,\xi\eta})$$
$$+ \nu w_{,\xi}(v_{,\xi\eta} - u_{,\eta\eta}) + \nu w_{,\eta}(u_{,\xi\eta} - v_{,\eta\eta})\}$$
$$-2\{w_{,\xi\xi}(u_{,\xi} + \nu v_{,\eta}) + (1 - \nu)w_{,\xi\eta}(u_{,\eta} + v_{,\xi}) + w_{,\eta\eta}(v_{,\eta} + \nu u_{,\xi})\}$$

For the infinite strip

$$-\frac{1}{2} \leq \xi \leq \frac{1}{2}, \quad -\infty \leq \eta \leq \infty$$

for an applied load independent of η it follows that

$$w = w(\xi) \text{ only}$$
$$u = u(\xi) \text{ only}$$
$$v = 0 \text{ everywhere}$$

With these restrictions Equations [15] simplify to

$$u_{,\xi\xi} = -w_{,\xi}w_{,\xi\xi} = -(w,^2{}_{\xi})_{,\xi}/2 \quad [a]$$

$$3w_{,\xi\xi}w,^2{}_{\xi} = -D - 2(w_{,\xi}u_{,\xi\xi} + u_{,\xi}w_{,\xi\xi}) \quad [b]$$

An integration of [a] yields

$$u_{,\xi} = -w,^2{}_{\xi}/2 + C_1 \quad [c]$$

and substituting this and Equation [a] in [b] yields

$$2C_1w_{,\xi\xi} = -D \quad [d]$$

which, on two integrations, becomes

$$2C_1w_{,\xi} = -D\xi + C_2 \quad [e]$$

$$2C_1w = -D\xi^2/2 + C_2\xi + C_3 \quad [f]$$

For a uniform applied load w is symmetrical and u antisymmetrical; thus the boundary conditions are

$$\left.\begin{array}{l} w = 0 \text{ for } \xi = 0.5 \\ w_{,\xi} = 0 \text{ for } \xi = 0 \end{array}\right\} \quad [g]$$

and

$$\left.\begin{array}{l} u = 0 \text{ for } \xi = 0.5 \\ u = 0 \text{ for } \xi = 0 \end{array}\right\} \quad [h]$$

From Equation [e] and the second Equation [g] it follows that

$$C_2 = 0$$

and from Equation [f] and the first Equation [g] we obtain

$$C_3 = D/8$$

so that

$$w_{,\xi} = -D\xi/2C_1 \quad [i]$$

$$w = -D(4\xi^2 - 1)/16C_1 \quad [j]$$

Returning to Equation [c] and substituting from Equation [i] we have

$$u_{,\xi} = \{C_1{}^3 - D^2\xi^2/8\}/C_1{}^2$$

From which one integration yields

$$u = \{C_1{}^3\xi - D^2\xi^3/24\}/C_1{}^2 + C_4 \quad [k]$$

From Equation [k] and the second Equation [h]

$$C_4 = 0, \quad C_1 \neq 0 \quad [l]$$

while the first Equation [h] yields

$$C_1 = (D^2/96)^{1/3} \quad [m]$$

Hence, finally, from Equations [j], [k], [l], and [m], the solution is

$$w(\xi) = -(3D/2)^{1/3}(\xi + 1/2)(\xi - 1/2)$$
$$u(\xi) = -(2D^2/3)^{1/3}\xi(\xi + 1/2)(\xi - 1/2)$$

Solutions to Equations [a] and [b] for loadings D which are not constant are also readily obtainable. These will be discussed in a separate publication.

Bending of Isotropic Thin Plates by Concentrated Edge Couples and Forces

By YI-YUAN YU,[1] ST. LOUIS, MO.

In this paper the complex variable method of Muschelišvili for solving the biharmonic equation is applied to problems of bending of isotropic thin plates by concentrated edge couples and forces. The results of the method as applied to plate problems by previous authors are presented first. Methods of handling concentrated edge couples and forces are developed. These are then applied to the circular plate as an example, for which exact solutions in closed forms are obtained. Worked out in detail are three particular problems; namely, those of circular plates subjected, respectively, to two bending couples, to two twisting couples, both applied at the ends of a diameter, and to four forces applied at the ends of two diameters perpendicular to each other. Numerical results are presented in the form of graphs.

Nomenclature

The following nomenclature is used in the paper:

x, y = rectangular co-ordinates
ρ, θ = curvilinear co-ordinates
ν, s = directions normal to and along boundary
$z = x + iy$, middle plane of plate
$\zeta = \rho e^{i\theta}$
$\sigma = e^{i\theta}$
α = angle between x and ρ-directions
$\alpha_i, \beta_i, \alpha_i', \beta_i'$ = real constants
$B_1 = 1/6$, one of Bernoulli's numbers
γ = unit circle
C = boundary of plate
E = Young's modulus
h = half-thickness of plate
ν = Poisson's ratio
D = flexural rigidity of plate
$n = -(3 + \nu)/(1 - \nu)$
R = radius of circular plate
w = deflection of plate
$\varphi_1(z), \psi_1(z), \chi_1(z)$ = analytic functions of z
$\omega(\zeta)$ = mapping function
$\varphi(\zeta), \psi(\zeta), \chi(\zeta)$; $\Phi(\zeta), \Psi(\zeta)$ = analytic functions of ζ
$f_1 + if_2$ = function of boundary loading
$m(s)$ = boundary moment as function of arc length
$p(s)$ = boundary shear resultant as function of arc length
M_x, M_y, H_{xy}; $M_\rho, M_\theta, H_{\rho\theta}$; $M_\nu, H_{\nu s}$ = bending and twisting moments per unit length with reference to the (x, y), (ρ, θ), (ν, s)-directions, respectively
$M_x(\nu), M_y(\nu)$ = x and y-components of resultant moment per unit of boundary arc length having exterior normal in the ν-direction
M_i^* = concentrated couple
M = magnitude of concentrated couple
Q_x, Q_y; Q_ρ, Q_θ; Q_ν = shearing force per unit length with reference to the (x, y), (ρ, θ), (ν, s)-directions, respectively
Q_i^* = concentrated force
P = magnitude of concentrated force
Re = real part of
$\bar{\ }$ = overbar, indicating conjugate complex quantity

Introduction

Lurie (1)[2] applied Muschelišvili's method (2) for solving the biharmonic equation to the discussion of several problems of the bending of circular plates It was mentioned in the same reference that the author had used the method in similar studies earlier in 1928; however, no reference of the earlier work was given. Lechnitzky (3) further extended the complex variable method to the study of bending of anisotropic plates. An English exposition of Lechnitzky's results is given in Sokolnikoff's notes (4). Using the method of Muschelišvili and Lechnitzky, Morkovin (5) further discussed in detail the bending of an anisotropic clamped elliptic plate. By means of the same method Friedmann (6) solved several problems relating to a large isotropic plate with a circular hole as well as a circular ring plate. Methods using complex variables have been applied to plate problems also by Stevenson (7) and Seth (8).

In the present paper the complex variable method of Muschelišvili is further applied to the study of bending of isotropic homogeneous thin plates, the boundaries of which are subjected to concentrated couples and forces. Problems of circular plates supported by concentrated edge forces have been discussed by Timoshenko in his book on plates (9). He also mentioned other plate problems, involving concentrated edge forces, which had been solved by Reissner (10), MacGregor (11), and Holl (12). Plate problems concerning concentrated edge couples have not received much attention. One such problem was discussed by Lechnitzky (3) in which a semi-infinite anisotropic plate is bent by a concentrated bending couple at its edge. The approach was different from that used in the present paper.

The present method reduces in a simple manner the problems of concentrated edge couples and forces to limiting cases of the first boundary-value problem of the plate theory in which the moment and shear resultant are prescribed along the plate boundary. From the derivation to be presented in this paper it may be seen that the present theory may as well be applied to the more real

---

[1] Assistant Professor, Department of Applied Mechanics, Washington University. Assoc. Mem. ASME.

Contributed by the Applied Mechanics Division and presented at the Annual Meeting, New York, N. Y., November 29–December 4, 1953, of The American Society of Mechanical Engineers.

Discussion of this paper should be addressed to the Secretary, ASME, 29 West 39th Street, New York, N. Y., and will be accepted until July 12, 1954, for publication at a later date. Discussion received after the closing date will be returned.

Note: Statements and opinions advanced in papers are to be understood as individual expressions of their authors and not those of the Society. Manuscript received by ASME Applied Mechanics Division, April 16, 1953. Paper No. 53—A-32.

[2] Numbers in parentheses refer to the Bibliography at the end of the paper.

and practical cases in which couples and forces actually are distributed over small but finite parts of the plate boundary instead of being concentrated at points on the boundary. The method also illustrates the similarity between the plate problems to be considered and their analogous ones in two-dimensional elasticity in which concentrated forces in the plane of a slice are applied at the boundary.

Small deflections will be assumed in the following discussion of bending of thin isotropic plates. We shall consider a free plate with concentrated external couples or forces acting at a finite number of points along its boundary. For convenience, concentrated couples and concentrated forces will be discussed separately. It may be seen that this does not restrict us from loading the plate with both couples and forces at the same time. The middle plane of the plate will be assumed to occupy a region which is bounded externally by a single closed curve and, in particular, by a circle. Other types and shapes of regions may be treated similarly; examples are expected to be worked out later.

Preliminary Results

When the middle plane of an isotropic homogeneous thin plate free from lateral load is assumed to be in the complex plane of $z = x + iy$ as shown in Fig. 1, the differential equation for its deflection w in a direction perpendicular to the plane has the form

$$\frac{\partial^4 w}{\partial x^4} + 2\frac{\partial^4 w}{\partial x^2 \partial y^2} + \frac{\partial^4 w}{\partial y^4} = 0$$

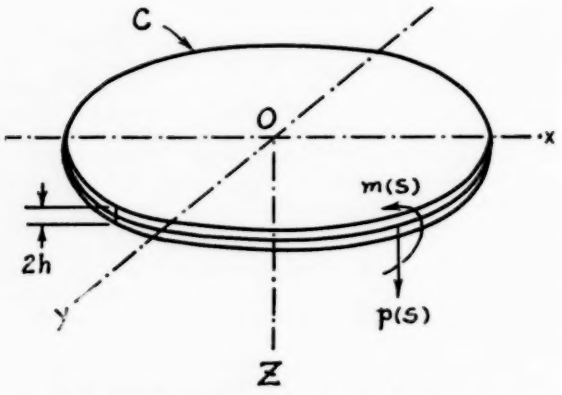

Fig. 1 Plate With Middle Plane in z-Plane

According to Muschelišvili, the solution of this biharmonic equation may be represented in terms of two analytic functions $\varphi_1(z)$ and $\psi_1(z)$ of the complex variable z

$$w = 2\mathrm{Re}[\bar{z}\,\varphi_1(z) + \chi_1(z)], \quad \chi_1(z) = \int \psi_1(z)\,dz \ldots\ldots [1]$$

We use bars to denote conjugate complex quantities.

The bending moments per unit length M_x, M_y, twisting moment per unit length H_{xy}, and the shearing forces per unit length Q_x, Q_y may conveniently be expressed in terms of $\varphi_1(z)$ and $\psi_1(z)$ as follows

$$\left.\begin{aligned} M_x + M_y &= -8D(1+\nu)\,\mathrm{Re}[\varphi_1'(z)] \\ M_y - M_x + 2iH_{xy} &= 4D(1-\nu)\,[\bar{z}\varphi_1''(z) + \psi_1'(z)] \\ Q_x - iQ_y &= -8D\varphi_1''(z) \end{aligned}\right\} \ldots\ldots [2]$$

in which $D = 2Eh^3/3(1-\nu^2)$ is the usual flexural rigidity of plate; E, ν, and h being, respectively, Young's modulus, Poisson's ratio, and the half-thickness of the plate. It is to be noted that H_{xy} has a sign opposite to that denoted by M_{xy} as used by Timoshenko.

As shown in Fig. 1, the moment and shear resultant per unit length along the boundary C of the plate will be given as functions of the arc length s along C

$$M_\nu = m(s), \quad Q_\nu + \frac{\partial H_{\nu s}}{\partial s} = p(s) \text{ (on } C) \ldots\ldots [3]$$

where ν denotes the exterior normal to C. The boundary condition can be shown to have the final form

$$n\varphi_1(z) + z\bar{\varphi}_1'(\bar{z}) + \bar{\psi}_1(\bar{z}) = f_1 + if_2 \text{ (on } C) \ldots\ldots [4]$$

in which

$$n = -\frac{3+\nu}{1-\nu}$$

and

$$f_1 + if_2 = \frac{1}{2D(1-\nu)} \int_0^s \left[m(s) + i \int_0^s p(s)ds \right] (dx + idy) \ldots [5]$$

The plate problem in which boundary moment and shear resultant are prescribed now becomes one of determining the two functions $\varphi_1(z)$ and $\psi_1(z)$ which satisfy the boundary condition, Equation [4]. Once these functions are determined, the deflection, moments, and shearing forces at any point in the plate may be computed by means of Equations [1] and [2].

The foregoing results are due to Lechnitzky and may be found in references (3), (4), and (6).

Conformal Mapping

Let the function

$$z = \omega(\zeta)$$

map the boundary C of the given region occupied by the middle plane of the plate in the z-plane into the unit circle γ in the ζ-plane. Curvilinear co-ordinates (ρ, θ) are thus introduced into the z-plane which are the maps of the polar co-ordinates in the ζ-plane given by $\zeta = \rho e^{i\theta}$.

Introducing the mapping function $\omega(\zeta)$ into Equation [1], we now have the deflection of the plate given by

$$w = 2\mathrm{Re}[\bar{\omega}(\bar{\zeta})\varphi(\zeta) + \chi(\zeta)] \ldots\ldots [6]$$

where

$$\varphi(\zeta) = \varphi_1[\omega(\zeta)] = \varphi_1(z), \quad \chi(\zeta) = \int \psi(\zeta)\omega'(\zeta)d\zeta$$

and

$$\psi(\zeta) = \psi_1[\omega(\zeta)] = \psi_1(z)$$

The moments and shearing forces at any point in the plate with reference to the new co-ordinates (ρ, θ) may be shown to be related to those with reference to the (x, y)-co-ordinates as follows

$$\begin{aligned} M_\rho + M_\theta &= M_x + M_y \\ M_\theta - M_\rho + 2iH_{\rho\theta} &= e^{2i\alpha}(M_y - M_x + 2iH_{xy}) \\ Q_\rho - iQ_\theta &= e^{i\alpha}(Q_x - iQ_y) \end{aligned}$$

in which α is the angle between the x and ρ-directions at the point. As was shown by Muschelišvili (2)

$$e^{i\alpha} = \frac{\omega'(\zeta)}{|\omega'(\zeta)|}\frac{\zeta}{\rho}, \quad e^{2i\alpha} = \frac{\omega'(\zeta)}{\bar{\omega}'(\bar{\zeta})}\frac{\zeta^2}{\rho^2}$$

therefore, Equations [2] lead to

$$\left.\begin{aligned} M_\rho + M_\theta &= -8D(1+\nu)\mathrm{Re}[\Phi(\zeta)] \\ M_\theta - M_\rho + 2iH_{\rho\theta} &= 4D(1-\nu)\frac{\bar\zeta^2}{\rho^2\bar\omega'(\bar\zeta)}[\bar\omega(\bar\zeta)\Phi'(\zeta) \\ &\quad + \omega'(\zeta)\Psi(\zeta)] \\ Q_\rho - iQ_\theta &= -8D\frac{\bar\zeta}{\rho|\omega'(\zeta)|}\Phi'(\zeta) \end{aligned}\right\} \ldots [7]$$

in which

$$\Phi(\zeta) = \frac{\varphi'(\zeta)}{\omega'(\zeta)}, \quad \Psi(\zeta) = \frac{\psi'(\zeta)}{\omega'(\zeta)}$$

The boundary Equation [4] is now transformed into

$$n\varphi(\sigma) + \frac{\omega(\sigma)}{\bar\omega'(\bar\sigma)}\bar\varphi'(\bar\sigma) + \bar\psi(\bar\sigma) = f_1 + if_2 \text{ (on } \gamma) \ldots [8]$$

in which $f_1 + if_2$ also has been transformed and is now a function of $\sigma = e^{i\theta}$; namely, the value of ζ on the boundary γ of the unit circle.

For a region bounded externally by a single closed curve and mapped onto the unit circle in the ζ-plane, each of the two analytic functions $\varphi(\zeta)$ and $\psi(\zeta)$ always can be represented by a power series consisting of only positive powers of ζ. Furthermore, because of the indeterminateness of the functions, we may write

$$\left.\begin{aligned} \varphi(\zeta) &= \alpha_1\zeta + (\alpha_2 + i\beta_2)\zeta^2 + (\alpha_3 + i\beta_3)\zeta^3 + \ldots \\ \psi(\zeta) &= \alpha_0' + i\beta_0' + (\alpha_1' + i\beta_1')\zeta \\ &\quad + (\alpha_2' + i\beta_2')\zeta^2 + \ldots \end{aligned}\right\} \ldots [9]$$

α and β being real constants.

General Solution for a Circular Plate

In the particular case of a circular region of radius R in the z-plane mapped onto the unit circle in the ζ-plane, the mapping function is

$$z = \omega(\zeta) = R\zeta$$

Equations [6], [7], and [8] reduce to

$$w = 2\mathrm{Re}[R\bar\zeta\varphi(\zeta) + \chi(\zeta)], \quad \chi(\zeta) = R\int\psi(\zeta)d\zeta \ldots [10]$$

$$\left.\begin{aligned} M_\rho + M_\theta &= -\frac{8D(1+\nu)}{R}\mathrm{Re}[\varphi'(\zeta)] \\ M_\theta - M_\rho + 2iH_{\rho\theta} &= \frac{4D(1-\nu)}{R}\sigma^2[\bar\zeta\varphi''(\zeta) + \psi'(\zeta)] \\ Q_\rho - iQ_\theta &= -\frac{8D}{R^2}\sigma\varphi''(\zeta) \end{aligned}\right\} \ldots [11]$$

$$n\varphi(\sigma) + \sigma\bar\varphi'(\bar\sigma) + \bar\psi(\bar\sigma) = f_1 + if_2 \text{ (on } \gamma) \ldots [12]$$

To solve for $\varphi(\zeta)$ and $\psi(\zeta)$ from the boundary Equation [12] for any arbitrary function $f_1 + if_2$, we multiply the equation and its conjugate throughout by

$$\frac{1}{2\pi i}\frac{d\sigma}{\sigma - \zeta}$$

and integrate around γ. The procedure is entirely the same as that used by Muschelišvili (13) in getting the general solution for a circular disk loaded in its plane. The following results for the plate problem may be obtained readily

$$\left.\begin{aligned} \varphi(\zeta) &= \frac{1}{n}\frac{1}{2\pi i}\int_\gamma\frac{f_1 + if_2}{\sigma - \zeta}d\sigma - \frac{\alpha_1\zeta}{n} \\ \psi(\zeta) &= \frac{1}{2\pi i}\int_\gamma\frac{f_1 - if_2}{\sigma - \zeta}d\sigma - \frac{\varphi'(\zeta)}{\zeta} + \frac{\alpha_1}{\zeta} \\ \alpha_1 &= \frac{1}{n+1}\left[\frac{d}{d\zeta}\left(\frac{1}{2\pi i}\int_\gamma\frac{f_1 + if_2}{\sigma - \zeta}d\sigma\right)\right]_{\zeta=0} \end{aligned}\right\} \ldots [13]$$

Plate Subjected to Concentrated Edge Couples

With the absence of the shearing force Q_ν, Equation [5] may be written

$$f_1 + if_2 = \frac{1}{2D(1-\nu)}\int_0^s [M_\nu + iH_{\nu s}](dx + idy) \ldots [14]$$

In Fig. 2 is shown part of the boundary of a plate between the

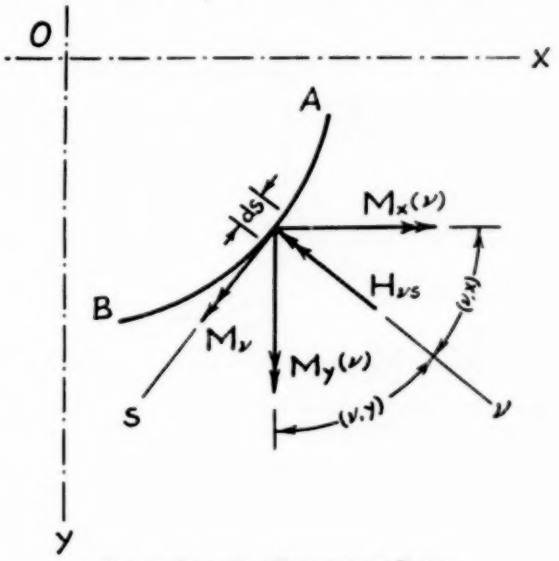

Fig. 2 Couples at Boundary of Plate

points A and B, of which ds is an element. All the moment vectors are shown in their positive directions as determined by the right-hand screw rule. The moments $M_x(\nu)$ and $M_y(\nu)$ represent the x and y-components of the resultant moment (per unit length) on ds, whose exterior normal is in the ν-direction. The relations between M_ν, $H_{\nu s}$ and $M_x(\nu)$, $M_y(\nu)$ may be established readily from the figure to be

$$M_\nu\cos(\nu, y) + H_{\nu s}\cos(\nu, x) = -M_x(\nu)$$

$$M_\nu\cos(\nu, x) - H_{\nu s}\cos(\nu, y) = M_y(\nu)$$

Multiplying the first equation by ds and the second by ids, adding the results, and remembering that

$$\cos(\nu, y)\,ds = -dx, \cos(\nu, x)\,ds = dy$$

we obtain

$$(M_\nu + iH_{\nu s})(dx + idy) = [M_x(\nu) + iM_y(\nu)]\,ds$$

Substituting this into the integrand in Equation [14] and applying the result to the finite length of arc between A and B, we write

$$[f_1 + if_2]_A^B = \frac{1}{2D(1-\nu)} \int_A^B [M_x(\nu) + iM_y(\nu)]ds \quad [15]$$

in which $[\ ]_A^B$ indicates the increase in the value of $f_1 + if_2$ as the boundary is described from A to B.

Consider now the case of a concentrated couple M^* (the star indicating that its dimension is not that of moment per unit length but simply that of moment) acting at a point P on the boundary and having components M_x^* and M_y^*. We enclose P with a small but finite circular arc A-C-B as shown in

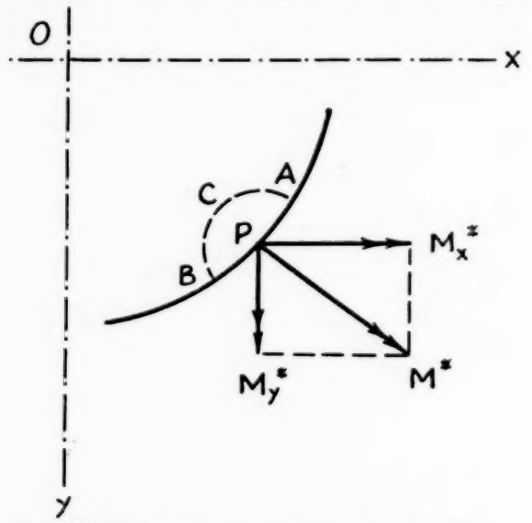

FIG. 3 CONCENTRATED COUPLE AT BOUNDARY OF PLATE

Fig. 3. Applying Equation [15] and letting A and B approach P, we have

$$[f_1 + if_2]_P = \frac{1}{2D(1-\nu)} [M_x^* + iM_y^*] = \frac{M^*}{2D(1-\nu)}$$

Observing the physical significance of the integral in Equation [15] we see that the limiting procedure adopted is justified. We conclude, therefore, that on passing the point P along the boundary in the positive direction, the function $f_1 + if_2$ gains a value equal to the concentrated couple applied at P divided by $2D(1-\nu)$. With the value of $f_1 + if_2$ assumed to be zero at an arbitrary starting point on a closed boundary, its value at any other point will be equal to the sum of the concentrated couples acting on the boundary between these points divided by $2D(1-\nu)$. It should be noted, however, that in going from the first point to the second, the positive direction of s is to be followed.

As an example we consider the problem of a circular plate having radius R subjected to an arbitrary number of, say r, concentrated couples $M_1^*, M_2^*, \ldots, M_r^*$ on its boundary at points corresponding to $\sigma_1 = e^{i\alpha_1}, \sigma_2 = e^{i\alpha_2}, \ldots, \sigma_r = e^{i\alpha_r}$, respectively, on the unit circle ($0 \leq \alpha_1 < \alpha_2 < \ldots < \alpha_r < 2\pi$). A similar problem in two-dimensional elasticity was discussed by Muschelišvili (13). It is evident that the couples must fulfill the equilibrium condition

$$\sum_{k=1}^{r} M_k^* = \sum_{k=1}^{r} (M_{kx}^* + iM_{ky}^*) = 0$$

According to this and the above conclusion we obtain Table 1 for the values of the function $f_1 + if_2$ on various arcs around the circumference of the plate, assuming its value to be zero on arc $\sigma_r\sigma_1$.

TABLE 1 VALUES OF FUNCTION $(f_1 + if_2)$

Arc	$2D(1-\nu)\ (f_1 + if_2)$
$\sigma_r\sigma_1$	0
$\sigma_1\sigma_2$	M_1^*
$\sigma_2\sigma_3$	$M_1^* + M_2^*$
...	...
$\sigma_{r-1}\sigma_r$	$M_1^* + M_2^* + \ldots + M_{r-1}^*$
$\sigma_r\sigma_1$	$M_1^* + M_2^* + \ldots + M_r^* = 0$

We have the following integrals

$$\frac{1}{2\pi i} \int_\gamma \frac{f_1 + if_2}{\sigma - \zeta}\, d\sigma = \frac{1}{2\pi i} \int_{\sigma_1} \frac{f_1 + if_2}{\sigma - \zeta}\, d\sigma + \frac{1}{2\pi i} \int_{\sigma_2}^{\sigma_1} \frac{f_1 + if_2}{\sigma - \zeta}\, d\sigma + \ldots + \frac{1}{2\pi i} \int_{\sigma_r}^{\sigma_1} \frac{f_1 + if_2}{\sigma - \zeta}\, d\sigma =$$

$$\frac{1}{2\pi i} \frac{1}{2D(1-\nu)} \left[M_1^* \log \frac{\sigma_2 - \zeta}{\sigma_1 - \zeta} + (M_1^* + M_2^*) \log \frac{\sigma_3 - \zeta}{\sigma_2 - \zeta} + \ldots + (M_1^* + M_2^* + \ldots + M_r^*) \log \frac{\sigma_1 - \zeta}{\sigma_r - \zeta} \right]$$

$$= \frac{i}{4\pi D(1-\nu)} \sum_{k=1}^{r} M_k^* \log (\sigma_k - \zeta)$$

$$\frac{1}{2\pi i} \int_\gamma \frac{f_1 - if_2}{\sigma - \zeta}\, d\sigma = \frac{i}{4\pi D(1-\nu)} \sum_{k=1}^{r} \bar{M}_k^* \log (\sigma_k - \zeta)$$

where

$$\bar{M}_k^* = M_{kx}^* - iM_{ky}^*$$

Substituting these results into Equations [13]

$$\alpha_1 = \frac{-i}{4\pi D(1-\nu)\,(n+1)} \sum_{k=1}^{r} \frac{M_k^*}{\sigma_k}$$

$$\left.\begin{aligned} \varphi(\zeta) &= \frac{i}{4\pi D(1-\nu)n} \sum_{k=1}^{r} M_k^* \log(\sigma_k - \zeta) + \frac{i\zeta}{4\pi D(1-\nu)\,(n+1)n} \sum_{k=1}^{r} \frac{M_k^*}{\sigma_k} \\ \psi(\zeta) &= \frac{i}{4\pi D(1-\nu)} \sum_{k=1}^{r} \bar{M}_k^* \log (\sigma_k - \zeta) + \frac{i}{4\pi D(1-\nu)n} \sum_{k=1}^{r} \frac{M_k^*}{\sigma_k (\sigma_k - \zeta)} \end{aligned}\right\} \quad [16]$$

These functions constitute the desired solution. Two particular problems will now be discussed, illustrating how the deflection, moments, and shearing forces may be determined.

CIRCULAR PLATE SUBJECTED TO TWO BENDING COUPLES

In the first problem the plate is subjected to two equal and opposite concentrated bending couples each of a magnitude M and acting at the ends of a diameter. As shown in Fig. 4, we are given

$$M_1^* = iM \text{ at } \sigma_1 = 1, \text{ and } M_2^* = -iM \text{ at } \sigma_2 = -1$$

Substituting these into Equations [16], we obtain the following analytic functions for the present problem

$$\varphi(\zeta) = -\frac{M}{4\pi D(1-\nu)n} \log \frac{1-\zeta}{1+\zeta} - \frac{M\zeta}{2\pi D(1-\nu)\,(n+1)n}$$

$$\psi(\zeta) = \frac{M}{4\pi D(1-\nu)} \log \frac{1-\zeta}{1+\zeta} - \frac{M}{2\pi D(1-\nu)n} \frac{\zeta}{1-\zeta^2}$$

from which

$$\varphi'(\zeta) = \frac{M}{2\pi D(1-\nu)n} \frac{1}{1-\zeta^2} - \frac{M}{2\pi D(1-\nu)(n+1)n}$$

$$\varphi''(\zeta) = \frac{M}{\pi D(1-\nu)n} \frac{\zeta}{(1-\zeta^2)^2}$$

$$\psi'(\zeta) = -\frac{M}{2\pi D(1-\nu)n} \frac{1+n+(1-n)\zeta^2}{(1-\zeta^2)^2}$$

$$\chi(\zeta) = R\int \psi(\zeta)d\zeta =$$

$$-\frac{RM}{4\pi D(1-\nu)}\left[\left(1-\frac{1}{n}\right)\log(1-\zeta^2) + \zeta \log\frac{1+\zeta}{1-\zeta}\right]$$

Constant terms have been freely added into these results, for the deflection, moments, and shearing forces to be calculated will not be affected. Calculations will be carried out for points along the radii $\theta = 0$ and $\theta = \pi/2$ as well as along the circumference $\rho = 1$ between the angles $\theta = 0$ and $\theta = \pi/2$. It can be seen that the foregoing functions would yield results symmetrical about both x and y-axes.

Along the radius $\theta = 0$, we have $\zeta = \rho$. Substituting the functions $\varphi(\zeta)$ and $\chi(\zeta)$ just obtained into Equation [10]

$$(w)_{\theta=0} = \frac{RM}{2\pi D(1-\nu)}\left[\left(\frac{1}{n}-1\right)(1-\rho)\log(1-\rho) + \left(\frac{1}{n}-1\right)(1+\rho)\log(1+\rho) - \frac{2\rho^2}{n(n+1)}\right] \quad [17]$$

from which

$$(w)_{\substack{\theta=0\\ \rho=0}} = 0, \quad (w)_{\substack{\theta=0\\ \rho=1}} = \frac{RM}{\pi D(1-\nu)n}\left[(1-n)\log 2 - \frac{1}{n+1}\right]$$

The difference between the last two values represents the maximum deflection of the plate in the present problem. Substituting $\varphi'(\zeta)$, $\varphi''(\zeta)$, and $\psi'(\zeta)$ into Equations [11] and solving

$$\left.\begin{aligned} (M_\theta)_{\theta=0} &= -\frac{M}{\pi nR}, \quad (M_\rho)_{\theta=0} = \frac{M}{\pi nR}\left(2\frac{1+n}{1-\rho^2} - 1\right) \\ (H_{\rho\theta})_{\theta=0} &= (Q_\theta)_{\theta=0} = 0, \quad (Q_\rho)_{\theta=0} = \\ &\quad -\frac{8M}{\pi R^2(1-\nu)n}\frac{\rho}{(1-\rho^2)^2} \end{aligned}\right\} \quad [18]$$

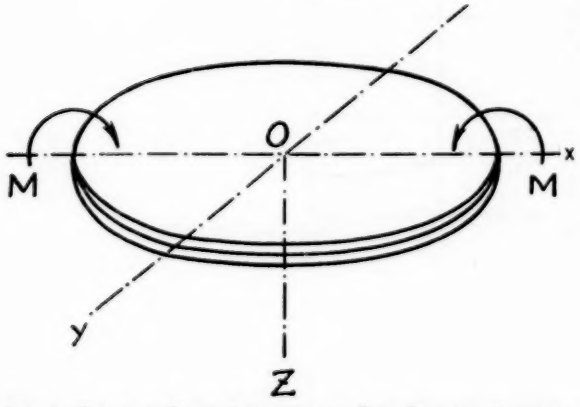

FIG. 4 CIRCULAR PLATE SUBJECTED TO TWO BENDING COUPLES

Similarly, along the radius $\theta = \pi/2$, we have $\zeta = i\rho$. And

$$\left.\begin{aligned} (w)_{\theta=\pi/2} &= \frac{RM}{2\pi D(1-\nu)}\left[2\left(\frac{1}{n}+1\right)\rho\tan^{-1}\rho + \left(\frac{1}{n}-1\right)\log(1+\rho^2) - \frac{2\rho^2}{n(n+1)}\right] \\ (M_\theta)_{\theta=\pi/2} &= \frac{M}{\pi nR}\frac{1+2n+2(n-2)\rho^2-\rho^4}{(1+\rho^2)^2} \\ (M_\rho)_{\theta=\pi/2} &= -\frac{M}{\pi nR}\left(\frac{1-\rho^2}{1+\rho^2}\right)^2 \\ (H_{\rho\theta})_{\theta=\pi/2} &= (Q_\theta)_{\theta=\pi/2} = 0, \\ (Q_\rho)_{\theta=\pi/2} &= \frac{8M}{\pi R^2(1-\nu)n}\frac{\rho}{(1+\rho^2)^2} \end{aligned}\right\} \quad [19]$$

Finally, along the circumference $\rho = 1$, we have $\zeta = \sigma$. And

$$\left.\begin{aligned} (w)_{\rho=1} &= \frac{RM}{2\pi D(1-\nu)}\left[\left(\frac{1}{n}-1\right)\cos^2\frac{\theta}{2}\log\left(\cos^2\frac{\theta}{2}\right) + \left(\frac{1}{n}-1\right)\sin^2\frac{\theta}{2}\log\left(\sin^2\frac{\theta}{2}\right) + \left(\frac{1}{n}+1\right)\frac{\pi}{2}\sin\theta + 2\left(\frac{1}{n}-1\right)\log 2 - \frac{2}{n(n+1)}\right] \\ (M_\theta)_{\rho=1} &= \frac{M}{\pi R}\frac{n-1}{n}, \quad (H_{\rho\theta})_{\rho=1} = \frac{M}{\pi R}\frac{1-n}{2n}\cot\theta \\ (M_\rho)_{\rho=1} &= (Q_\theta)_{\rho=1} = 0, \quad (Q_\rho)_{\rho=1} = \frac{2M}{\pi R^2(1-\nu)n}\frac{1}{\sin^2\theta} \end{aligned}\right\} \quad [20]$$

When Poisson's ratio is $\nu = 0.3$, the corresponding value of n is -4.714. Some of the more interesting quantities in Equations [17] to [20] have been computed numerically for these values of ν and n; the results are plotted in dimensionless forms as shown in Figs. 5 to 7. It is interesting to note the anticlastic form of the deflection surface.

CIRCULAR PLATE SUBJECTED TO TWO TWISTING COUPLES

This second problem can be worked out in the same manner as the first. We are given

$$M_1^* = M \text{ at } \sigma_1 = 1 \text{ and } M_2^* = -M \text{ at } \sigma_2 = -1$$

as shown in Fig. 8, M being the magnitude of each of the two twisting couples, which are applied at the ends of a diameter of the plate. By virtue of Equations [16]

$$\varphi(\zeta) = \frac{iM}{4\pi D(1-\nu)n}\log\frac{1-\zeta}{1+\zeta} + \frac{iM\zeta}{2\pi D(1-\nu)(n+1)n}$$

$$\psi(\zeta) = \frac{iM}{4\pi D(1-\nu)}\log\frac{1-\zeta}{1+\zeta} + \frac{iM}{2\pi D(1-\nu)n}\frac{\zeta}{1-\zeta^2}$$

Along the radius $\theta = 0$

$$\left.\begin{aligned} (w)_{\theta=0} &= (M_\theta)_{\theta=0} = (M_\rho)_{\theta=0} = (Q_\rho)_{\theta=0} = 0 \\ (H_{\rho\theta})_{\theta=0} &= \frac{M}{\pi nR}\frac{1-n}{1-\rho^2} \\ (Q_\theta)_{\theta=0} &= -\frac{8M}{\pi R^2(1-\nu)n}\frac{\rho}{(1-\rho^2)^2} \end{aligned}\right\} \quad [21]$$

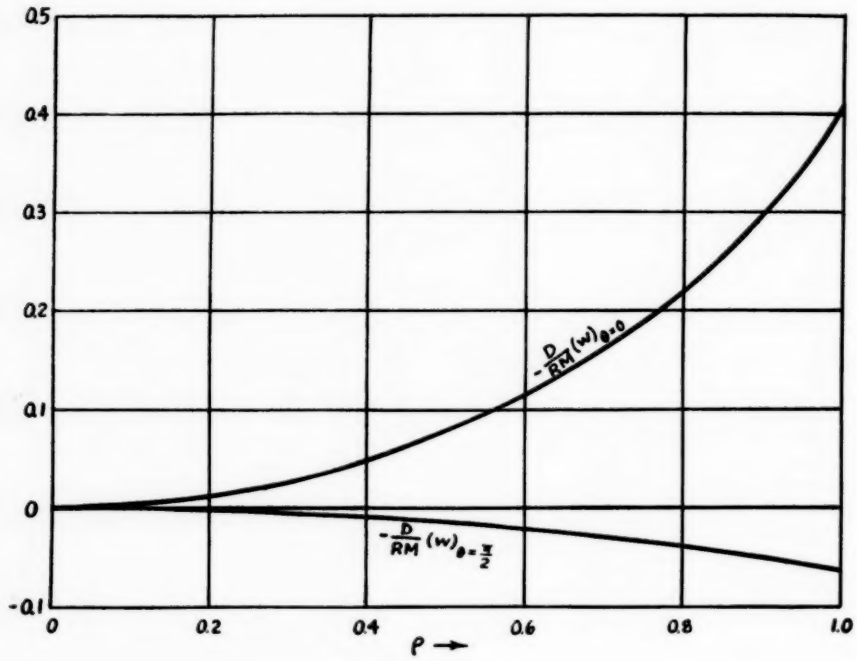

FIG. 5

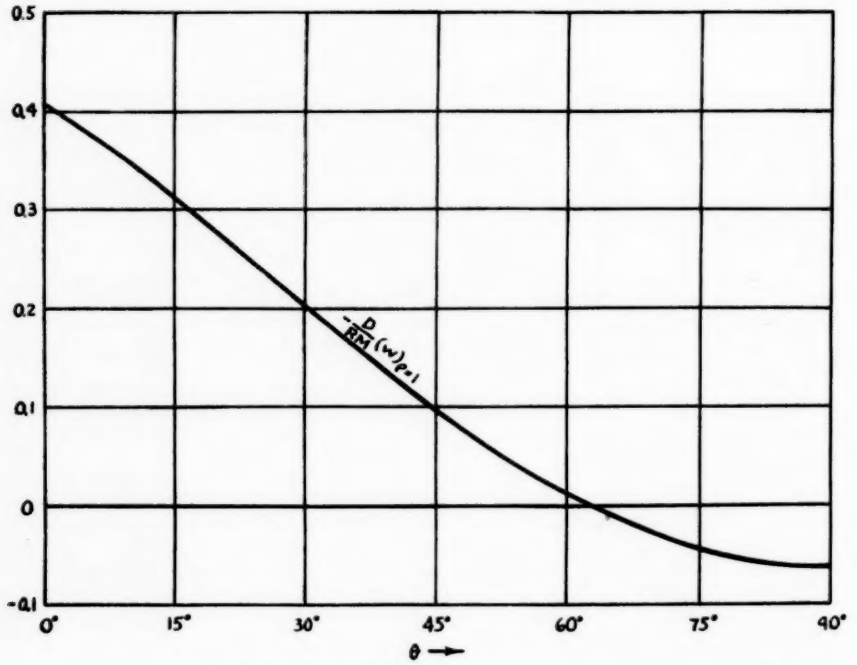

FIG. 6

FIGS. 5–7 RESULTS FOR PROBLEM OF TWO BENDING COUPLES

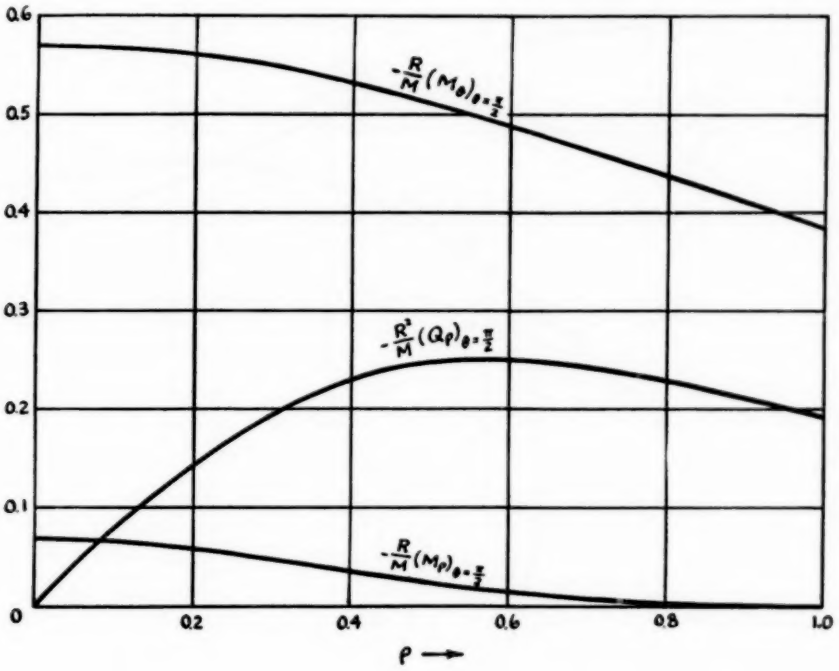

FIG. 7

Along the radius $\theta = \pi/2$

$$\left.\begin{aligned}(w)_{\theta=\pi/2} &= (M_\theta)_{\theta=\pi/2} = (M_\rho)_{\theta=\pi/2} \\ &= (Q_\rho)_{\theta=\pi/2} = 0 \\ (H_{\rho\theta})_{\theta=\pi/2} &= -\frac{M}{\pi nR}\frac{1-n-(3+n)\rho^2}{(1+\rho^2)^2} \\ (Q_\theta)_{\theta=0} &= \frac{8M}{\pi R^2(1-\nu)n}\frac{\rho}{(1+\rho^2)^2}\end{aligned}\right\} \quad \ldots [22]$$

Along the circumference $\rho = 1$, between $\theta = 0$ and $\theta = \pi/2$

$$(w)_{\rho=1} = \frac{RM}{2\pi D(1-\nu)}\left[\left(\frac{1}{n}-1\right)\sin\theta\log\left(\tan\frac{\theta}{2}\right)\right.$$

$$\left.+\left(\frac{1}{n}+1\right)\frac{\pi}{2}\cos\theta-\left(\frac{1}{n}+1\right)\left(\frac{\pi}{2}-\theta\right)\right]$$

$$(M_\theta)_{\rho=1} = \frac{M}{\pi R}\frac{1+n}{n}\cot\theta, \qquad (H_{\rho\theta})_{\rho=1} = \frac{M}{\pi R}\frac{1+n}{n}$$

$$(M_\rho)_{\rho=1} = (Q_\rho)_{\rho=1} = 0, \; (Q_\theta)_{\rho=1} = \frac{2M}{\pi R^2(1-\nu)n}\frac{1}{\sin^2\theta} \quad \ldots [23]$$

(cont.)

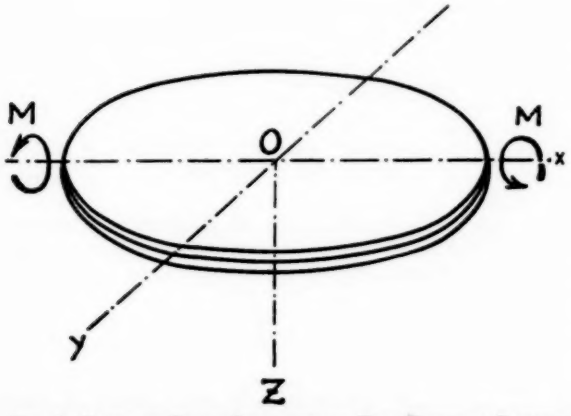

FIG. 8 CIRCULAR PLATE SUBJECTED TO TWO TWISTING COUPLES

Numerical values of some of the quantities in Equations [21] to [23] have been computed for the case in which $\nu = 0.3$ and are plotted as shown in Figs. 9 and 10.

It should be added here that the present case may find practical applications in the design of certain circular gates operated diametrically.

PLATE SUBJECTED TO CONCENTRATED EDGE FORCES

To obtain the function $f_1 + if_2$ for the case of concentrated forces applied at points along the boundary of a plate, we first put M_ν and $H_{\nu s}$ equal to zero in Equations [3]; thus

$$m(s) = 0, \quad p(s) = Q_\nu$$

Substituting these into Equation [5]

$$f_1 + if_2 = \frac{i}{2D(1-\nu)}\int_0^s\left[\int_0^s Q_\nu ds\right](dx + idy). \quad [24]$$

It was concluded in the case of concentrated couples that the value of $f_1 + if_2$ at any point on the boundary multiplied by $2D(1-\nu)$ is equal to the sum of the couples that are present between this point and another arbitrarily chosen point where $f_1 + if_2$ is assumed to have zero value. We therefore expect that the double integral in Equation [24] also represents some quantity of the nature of a moment. This will be shown to be true.

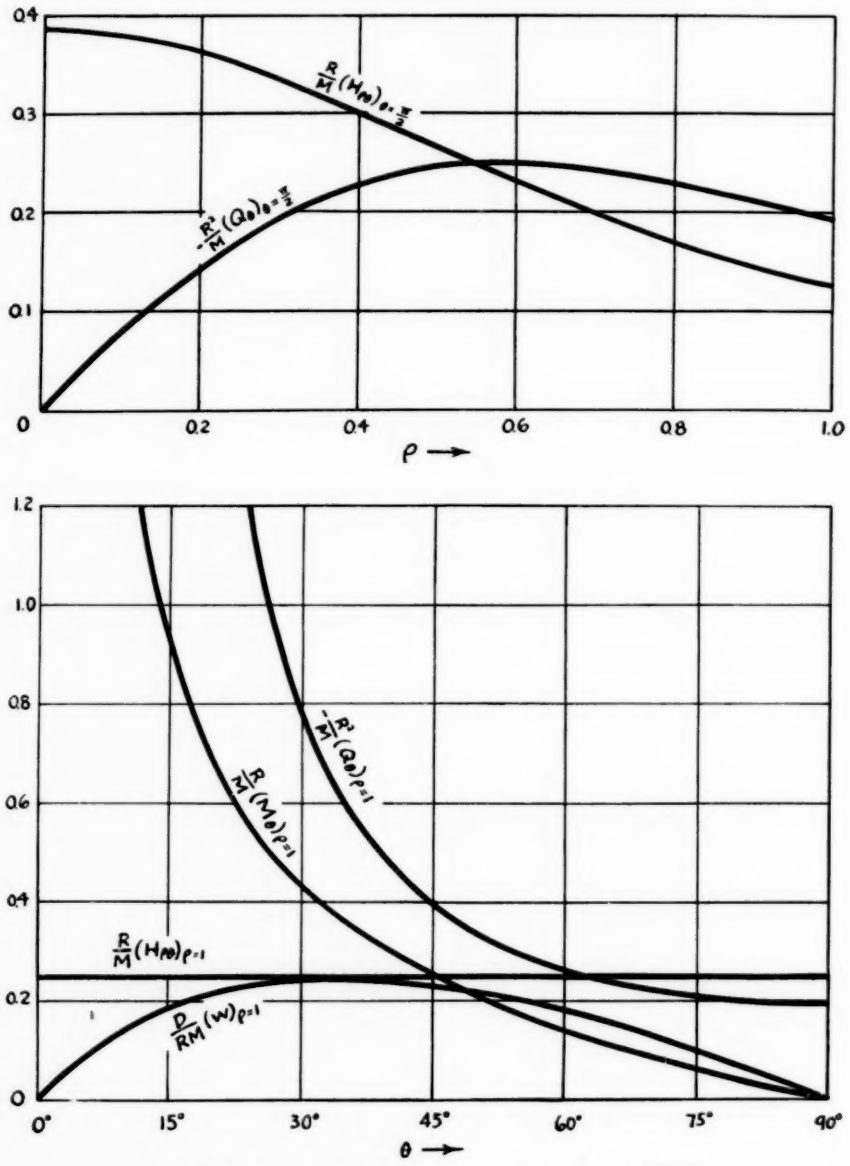

FIGS. 9–10 RESULTS FOR PROBLEM OF TWO TWISTING COUPLES

Consider first the case in which Q_ν represents some distributed shearing force varying along the boundary as shown in Fig. 11. The integral in Equation [24] may be considered as two integrals with x and y as the independent variables respectively; that is

$$f_1 + if_2 = \frac{i}{2D(1-\nu)}\left\{\int_0^s\left[\int_0^s Q_\nu ds\right]dx + i\int_0^s\left[\int_0^s Q_\nu ds\right]dy\right\} \quad [25]$$

For convenience we rewrite the first integral in Equation [25] in the form

$$\int_0^s\left[\int_0^s Q_\nu(s')ds'\right]dx'$$

As in Fig. 11, s and x refer to the end point P of some interval, and the same letters with primes refer to the varying point in that interval. Integrating by parts, we have

$$\int_0^s\left[\int_0^s Q_\nu(s')ds'\right]dx' = x\int_0^s Q_\nu(s')ds' - \int_0^s x'Q_\nu(s')ds' = \int_0^s (x-x')Q_\nu(s')ds' \quad [26]$$

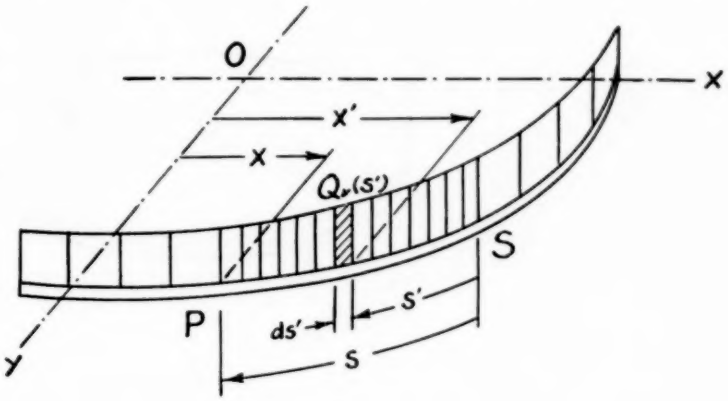

FIG. 11 SHEARING FORCE AT BOUNDARY OF PLATE

which may be seen easily from the same figure to represent the moment about a line through P and parallel to the y-axis of the distributed force between point S, where $f_1 + if_2$ is assumed to be zero, and point P, for which $f_1 + if_2$ is to be determined.

When there are concentrated forces Q_1^*, Q_2^*, . . . instead of distributed force between S and P, it may be shown by a similar limiting process as given in reference (14) that the last integral in Equation [26] is to be replaced by the following summation

$$\sum_i (x - x_i) Q_i^*$$

which is the sum of the moments of the forces Q_i^* between S and P about a line through P and parallel to the y-axis, x_i being the x-co-ordinate of the point of application of Q_i^*. The limiting procedure also may be justified from the physical significance of the integral and its corresponding summation.

Similarly, it may be seen that in the case of concentrated forces the second integral in Equation [25] takes the form of the summation

$$\sum_i (y - y_i) Q_i^*$$

which is the sum of the moments of the forces Q_i^* about a line through P parallel to the x-axis, y_i being the y-co-ordinate of the point of application of Q_i^*. The function $f_1 + if_2$ in Equation [24] finally takes the form

$$f_1 + if_2 = \frac{i}{2D(1-\nu)} \sum_i Q_i^*(z - z_i) \quad \ldots\ldots\ldots [27]$$

Consider now the example of a circular plate of radius R subjected to the concentrated forces $Q_1^*, Q_2^*, \ldots, Q_r^*$ on its boundary at points corresponding, respectively, to $\sigma_1 = e^{i\alpha_1}$, $\sigma_2 = e^{i\alpha_2}$, $\ldots$, $\sigma_r = e^{i\alpha_r}$ on the unit circle $(0 \leq \alpha_1 < \alpha_2 < \ldots < \alpha_r < 2\pi)$.

TABLE 2 VALUES OF $(f_1 + if_2)$

Arc	$2D(1-\nu)(f_1 + if_2)/iR$
$\sigma_1\sigma_1$	0
$\sigma_1\sigma_2$	$Q_1^*(\sigma - \sigma_1)$
$\sigma_2\sigma_2$	$Q_1^*(\sigma - \sigma_1) + Q_2^*(\sigma - \sigma_2)$
. . .	. . . . .
$\sigma_{r-1}\sigma_r$	$Q_1^*(\sigma - \sigma_1) + Q_2^*(\sigma - \sigma_2) + \ldots + Q_{r-1}^*(\sigma - \sigma_{r-1})$
$\sigma_r\sigma_1$	$Q_1^*(\sigma - \sigma_1) + Q_2^*(\sigma - \sigma_2) + \ldots + Q_r^*(\sigma - \sigma_r) = 0$

Table 2 listing values of $f_1 + if_2$ on various arcs may be obtained by means of Equation [27].

We compute the following integral

$$\frac{1}{2\pi i}\int_\gamma \frac{f_1 + if_2}{\sigma - \zeta}\,d\sigma = \frac{1}{2\pi i}\frac{iR}{2D(1-\nu)}\int_{\sigma_1} \frac{Q_1^*(\sigma - \sigma_1)}{\sigma - \zeta}\,d\sigma$$

$$+ \frac{1}{2\pi i}\frac{iR}{2D(1-\nu)}\int_{\sigma_2} \frac{Q_1^*(\sigma - \sigma_1) + Q_2^*(\sigma - \sigma_2)}{\sigma - \zeta}\,d\sigma + \ldots$$

$$+ \frac{1}{2\pi i}\frac{iR}{2D(1-\nu)}\int_{\sigma_r} \frac{Q_1^*(\sigma - \sigma_1) + \ldots + Q_r^*(\sigma - \sigma_r)}{\sigma - \zeta}\,d\sigma =$$

$$\frac{R(\sigma_1 - \zeta)}{4\pi D(1-\nu)}\sum_{k=1}^{r} Q_k^* - \frac{R[1 + \log(\sigma_1 - \zeta)]}{4\pi D(1-\nu)}\sum_{k=1}^{r} Q_k(\sigma_k - \zeta)$$

$$+ \frac{R}{4\pi D(1-\nu)}\sum_{k=1}^{r} Q_k^*(\sigma_k - \zeta)\log(\sigma_k - \zeta)$$

The first two summations in the result must vanish due to equilibrium requirements; therefore

$$\frac{1}{2\pi i}\int_\gamma \frac{f_1 + if_2}{\sigma - \zeta}\,d\sigma = \frac{R}{4\pi D(1-\nu)}\sum_{k=1}^{r} Q_k^*(\sigma_k - \zeta)\log(\sigma_k - \zeta)$$

Similarly

$$\frac{1}{2\pi i}\int_\gamma \frac{f_1 - if_2}{\sigma - \zeta}\,d\sigma = \frac{R}{4\pi D(1-\nu)}$$

$$\sum_{k=1}^{r} Q_k^*\left[\left(\frac{1}{\zeta} - \frac{1}{\sigma_k}\right)\log(\sigma_k - \zeta) - \frac{1}{\zeta}\log\sigma_k\right]$$

Substituting these results into Equations [13] yields the following solution of the problem

$$\alpha_1 = -\frac{R}{4\pi D(1-\nu)(n+1)}\sum_{k=1}^{r} Q_k^*\log\sigma_k$$

$$\varphi(\zeta) = \frac{R}{4\pi D(1-\nu)n}\sum_{k=1}^{r} Q_k^*(\sigma_k - \zeta)\log(\sigma_k - \zeta)$$

$$+ \frac{R\zeta}{4\pi D(1-\nu)(n+1)n}\sum_{k=1}^{r} Q_k^*\log\sigma_k \quad [28]$$

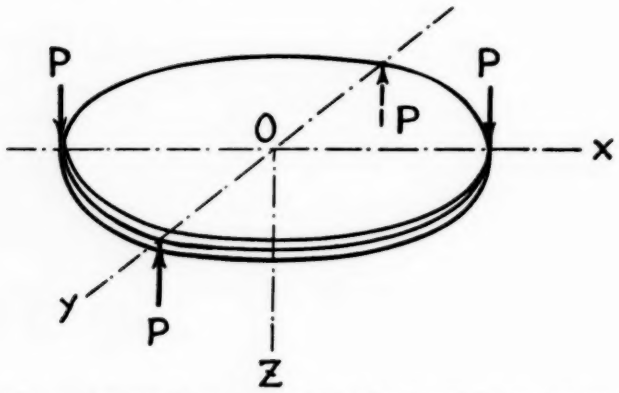

FIG. 12 CIRCULAR PLATE SUBJECTED TO FOUR CONCENTRATED FORCES

$$\psi(\zeta) = \frac{R(n+1)}{4\pi D(1-\nu)n}\frac{1}{\zeta}\sum_{k=1}^{r} Q_k^* \log\frac{\sigma_k - \zeta}{\sigma_k} - \frac{R}{4\pi D(1-\nu)}\sum_{k=1}^{r} Q_k^* \bar{\sigma}_k \log(\sigma_k - \zeta) \quad [29]$$

This general solution for concentrated forces acting on the boundary of a circular plate will be applied to the following particular problem.

CIRCULAR PLATE SUBJECTED TO FOUR CONCENTRATED FORCES

In this last problem we consider a circular plate subjected to four concentrated edge forces each of magnitude P. The forces are normal to the plate and are applied at the ends of two diameters perpendicular to each other, the pair at the ends of one diameter being opposite in direction to the other pair. The same problem was mentioned by Timoshenko (9).

As shown in Fig. 12, we have

$$\left.\begin{aligned} Q_1^* &= P \text{ at } \sigma_1 = 1, \quad Q_2^* = -P \text{ at } \sigma_2 = i \\ Q_3^* &= P \text{ at } \sigma_3 = -1, \quad Q_4^* = -P \text{ at } \sigma_4 = -i \end{aligned}\right\} \quad [30]$$

Substituting these into Equation [28], we note that the second term on the right side of the equation yields a term of the type $iC_1\zeta$ (C_1 being a real constant), which may be omitted without affecting either the deflection or the moments and shearing forces; therefore

$$\varphi(\zeta) = \frac{RP}{4\pi D(1-\nu)n}\left(\zeta \log\frac{\zeta^2+1}{\zeta^2-1} + \log\frac{\zeta-1}{\zeta+1} + i\log\frac{\zeta+i}{\zeta-i}\right)$$

By differentiation

$$\varphi'(\zeta) = \frac{RP}{4\pi D(1-\nu)n}\log\frac{\zeta^2+1}{\zeta^2-1},$$

$$\varphi''(\zeta) = \frac{RP}{\pi D(1-\nu)n}\frac{\zeta}{1-\zeta^4}$$

Substituting Equations [30] into [29]

$$\psi(\zeta) = \frac{RP(n+1)}{4\pi D(1-\nu)n}\frac{1}{\zeta}\log\frac{1-\zeta^2}{1+\zeta^2} - \frac{RP}{4\pi D(1-\nu)}\left(\log\frac{\zeta-1}{\zeta+1} + i\log\frac{\zeta-i}{\zeta+i}\right)$$

from which

$$\psi'(\zeta) = -\frac{RP(n+1)}{4\pi D(1-\nu)n}\frac{1}{\zeta^2}\log\frac{1-\zeta^2}{1+\zeta^2} - \frac{RP}{\pi D(1-\nu)n}\frac{1}{1-\zeta^4}$$

and

$$\chi(\zeta) = R\int\psi(\zeta)d\zeta = -\frac{R^2P(n+1)}{4\pi D(1-\nu)n}\left(\zeta^2 + \frac{\zeta^6}{9} + \frac{\zeta^{10}}{25} + \dots\right) - \frac{R^2P}{4\pi D(1-\nu)}\left(\log\frac{\zeta^2+1}{\zeta^2-1} + \zeta\log\frac{\zeta-1}{\zeta+1} + i\zeta\log\frac{\zeta-i}{\zeta+i}\right)$$

We have now obtained all that we need for calculating the deflection, moments, and shearing forces at any point in the plate through the use of Equations [10] and [11].

The deflection along the radius $\theta = 0$ may be obtained readily by substituting into Equation [10] the functions $\varphi(\zeta)$ and $\chi(\zeta)$ and putting $\zeta = \rho$; thus

$$(w)_{\theta=0} = \frac{R^2P}{2\pi D(1-\nu)n}\left[(\rho^2-n)\log\frac{1+\rho^2}{1-\rho^2} + (n-1)\rho\log\frac{1+\rho}{1-\rho} + 2(n+1)\rho\tan^{-1}\rho - (n+1)\left(\rho^2 + \frac{\rho^6}{9} + \frac{\rho^{10}}{25} + \dots\right)\right] \quad [31]$$

It is easy to see that $(w)_{\theta=0}$ is equal to zero at $\rho = 0$ and becomes maximum at $\rho = 1$, where the foregoing expression yields

$$(w)_{\substack{\theta=0\\ \rho=1}} = \frac{R^2P}{2\pi D(1-\nu)n}\left[(n-1)\log 2 + 2(n+1)\tan^{-1}1 - (n+1)\left(1 + \frac{1}{9} + \frac{1}{25} + \frac{1}{49} + \dots\right)\right] \quad [32]$$

The series in this result is observed to be related to one of Bernoulli's numbers (15)

$$B_1 = \frac{4}{3\pi^2}\left(1 + \frac{1}{3^2} + \frac{1}{5^2} + \frac{1}{7^2} + \dots\right)$$

Since B_1 is equal to $1/6$, we have

$$1 + \frac{1}{9} + \frac{1}{25} + \frac{1}{49} + \dots = 1.236$$

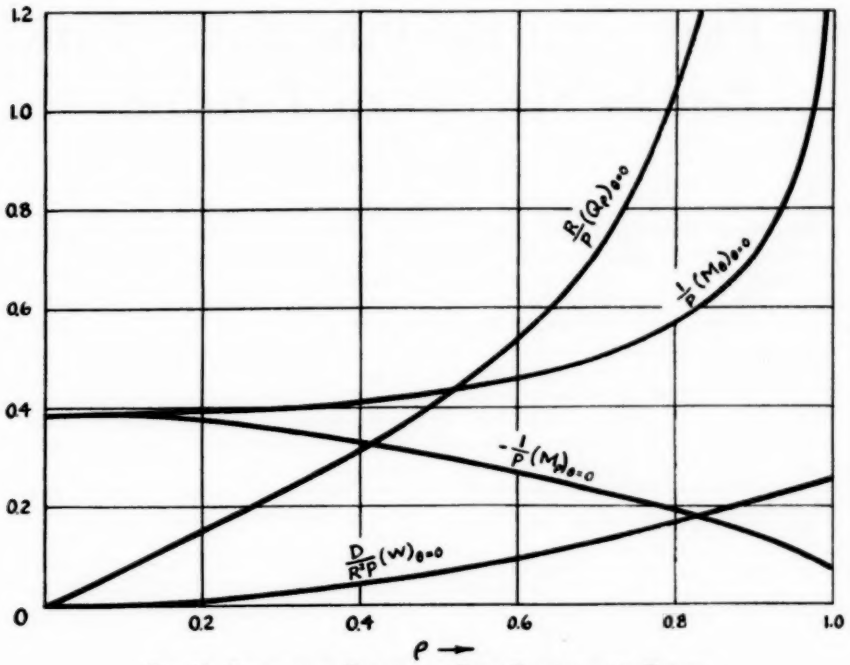

FIG. 13 RESULTS FOR PROBLEM OF FOUR CONCENTRATED FORCES

By means of Equations [11], we obtain the moments and shearing forces

$$\left.\begin{aligned}(M_\theta)_{\theta=0} &= \frac{P}{n\pi}\left[\frac{1+n}{2}\left(1+\frac{1}{\rho^2}\right)\log\frac{1+\rho^2}{1-\rho^2}-\frac{2}{1+\rho^2}\right]\\(M_\rho)_{\theta=0} &= \frac{P}{n\pi}\left[\frac{1+n}{2}\left(1-\frac{1}{\rho^2}\right)\log\frac{1+\rho^2}{1-\rho^2}+\frac{2}{1+\rho^2}\right]\\(Q_\rho)_{\theta=0} &= -\frac{8P}{\pi R(1-\nu)n}\frac{\rho}{1-\rho^4}\\(H_{\rho\theta})_{\theta=0} &= (Q_\theta)_{\theta=0}=0\end{aligned}\right\}\quad\ldots[33]$$

In the case in which $\nu = 0.3$, Equations [31] and [32] become

$$(w)_{\theta=0} = -\frac{R^2P}{D}\left[\frac{4.714+\rho^2}{20.8}\log\frac{1+\rho^2}{1-\rho^2}-0.275\,\rho\log\frac{1+\rho}{1-\rho}-0.357\,\rho\tan^{-1}\rho+0.1785\left(\rho^2+\frac{\rho^6}{9}+\frac{\rho^{10}}{25}+\ldots\right)\right]$$

$$(w)_{\substack{\theta=0\\ \rho=1}} = 0.252\,\frac{R^2P}{D}$$

These together with the numerical values of the quantities in Equations [33] calculated for the case $\nu = 0.3$ are plotted as shown in Fig. 13.

BIBLIOGRAPHY

1 "Problems Concerning the Bending of a Circular Plate," by A. I. Lurie, *Journal of Applied Mathematics and Mechanics*, vol. 4, 1940, pp. 93–102 (in Russian with English summary).

2 "Recherches sur les Problèmes aux Limites Relatifs à l'Équation Biharmonique et aux Équations de l'Élasticité à deux Dimensions," by N. Muschelišvili, *Mathematische Annalen*, vol. 107, 1932, pp. 282–312.

3 "Über Einige Fragen der Biegungstheorie der Dünnen Platten," by S. G. Lechnitzky, *Journal of Applied Mathematics and Mechanics*, vol. 2, 1938, pp. 181–210 (in Russian with German summary).

4 "Mathematical Theory of Elasticity," by I. S. Sokolnikoff, mimeographed lecture notes, Brown University, Providence, R. I., 1941, pp. 382–386.

5 "On the Deflection of Anisotropic Thin Plates," by V. Morkovin, *Quarterly of Applied Mathematics*, vol. 1, 1943, pp. 116–129.

6 "Über Einige Fragen der Theorie der Biegung von Dünnen Isotropen Platten," by M. M. Friedmann, *Journal of Applied Mathematics and Mechanics*, vol. 5, 1941, pp. 93–102 (in Russian with German summary).

7 "On the Equilibrium of Plates," by A. C. Stevenson, *Philosophical Magazine*, vol. 33, 1942, pp. 639–661.

"The Boundary Couples in Thin Plates," by A. C. Stevenson, *Philosophical Magazine*, vol. 34, 1943, pp. 105–114.

8 "Bending of Clamped Rectilinear Plates," by B. R. Seth, *Philosophical Magazine*, vol. 38, 1947, pp. 292–297.

9 "Theory of Plates and Shells," by S. Timoshenko, McGraw-Hill Book Company, Inc., New York, N. Y., 1940, pp. 270–272.

10 "Über die unsymmetrische Biegung dünner Kreisringplatten," by H. Reissner, *Ingenieur-Archiv*, vol. 1, 1929, pp. 72–83.

11 "Deflection of a Long Helical Gear Tooth," by C. W. MacGregor, *Mechanical Engineering*, vol. 57, 1935, pp. 225–227.

12 "Cantilever Plate With Concentrated Edge Load," by D. L. Holl, JOURNAL OF APPLIED MECHANICS, Trans. ASME, vol. 59, 1937, pp. A-8–A-10.

13 "Praktische Lösung der fundamentalen Randwertaufgaben der Elastizitätstheorie in der Ebene für Einige Berandungsformen," by N. Muschelišvili, *Zeitschrift für angewandte Mathematik und Mechanik*, vol. 13, 1933, pp. 264–282.

14 "Mathematical Methods in Engineering," by Th. von Kármán and M. A. Biot, McGraw-Hill Book Company, Inc., New York, N. Y., 1940, p. 262.

15 "A Short Table of Integrals," by B. O. Peirce, Ginn & Company, Boston, Mass., 1889, p. 90.

Plastic Flow in a Rectangularly Notched Bar Subjected to Tension[1]

By E. H. LEE,[2] PROVIDENCE, R. I.

A two-dimensional notched bar with rectangular root pulled in tension is considered. Large strains are analyzed so that plastic-rigid theory can be used. The initial motion based on the undeformed boundaries is considered, and also the subsequent flow including the deformation of the notch boundaries. In the absence of fracture, the solution can be continued until only line contact occurs at the notch root. The solution satisfies stress and velocity conditions for a St. Venant-Mises material in plastic flow at each stage of the deformation. The unsteady, large strain, motion can be analyzed, including the determination of the unknown free surface and the plastic-rigid boundary, due to a special property of the velocity solution and to the statical determinacy of the stress field in terms of the free-surface geometry.

Introduction

WE ARE concerned with the plastic flow in plane strain of a tension bar symmetrically notched with deep rectangular notches. This situation would occur experimentally in the test depicted in Fig. 1, if the width b of the bar is large compared with the thickness $2c$ at the notch root; for with a deep notch, plastic flow is localized to the vicinity of the notch root, and the parts remaining elastic prevent appreciable lateral contraction, thus leading to plastic flow in plane strain apart from free-surface effects near the lateral surfaces. We are concerned with large deformations, and the basic plastic-rigid theory already applied to a V-notched bar (1)[3] is adopted.

The present analysis is of interest in the interpretation of notched-bar tests, and also as a solution to an unsteady problem of plastic flow in plane strain with a deforming free surface. Previous large strain solutions have been steady state, or quasisteady in which the configuration maintains geometrical similarity (for example, the indentation of a rigid wedge into a plastic body having a plane surface, reference 2), or unsteady but in which the free surfaces of the body are parts of rigid regions (for example, the compression of a slab between rigid plates, reference 3). In the present problem it has been found possible to determine the motion of the deforming free boundary even though the form of the slip-line field changes, thus representing a somewhat more general type of solution than has been presented previously.

The solution is based on the theory of plasticity, which can be applied quite independently of fracture considerations. Thus the development of plastic flow can be evaluated until the notch root reduces to line contact between the two heads of the specimen, after which they separate. In practice, for most materials this development would be modified at some stage by the occurrence of fracture cracks which would change the plastic-flow pattern. The present solution may be of some value in assessing the onset of such fracture cracks.

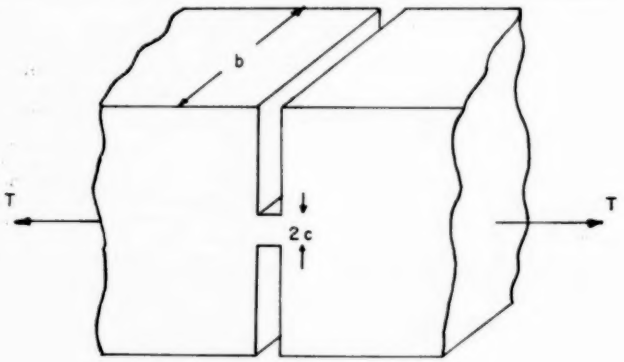

Fig. 1

Since strains of the order unity are considered, it is permissible to neglect elastic strains, of order 10^{-3}, and adopt a plastic-rigid theory. We shall apply the so-called St. Venant-Mises theory which considers ideally plastic flow at a constant value of the von Mises quadratic stress invariant. In plane strain this leads to plastic flow at a constant value of the maximum shear stress. Rigid body motion occurs when the maximum shear stress falls below this value. The resulting basic theory has been discussed fully in the recent literature (4, 5, 6), and solutions based on this theory have been shown to have a definite significance in elastic-plastic theory (7, 8). Since the basic theory is readily available in the literature, a brief statement of the main equations only will be given.

[1] This work was carried out under Contract ORDEB 52-988 under the supervision of Watertown Arsenal Laboratory, and was presented at the Eighth International Congress on Theoretical and Applied Mechanics, August, 1952.

[2] Professor of Applied Mathematics, Graduate Division of Applied Mathematics, Brown University. Mem. ASME.

Contributed by the Applied Mechanics Division and presented at the Annual Meeting, New York, N. Y., November 29–December 4, 1953, of The American Society of Mechanical Engineers.

Discussion of this paper should be addressed to the Secretary, ASME, 29 West 39th Street, New York, N. Y., and will be accepted until July 12, 1954, for publication at a later date. Discussion received after the closing date will be returned.

Note: Statements and opinions advanced in papers are to be understood as individual expressions of their authors and not those of the Society. Manuscript received by ASME Applied Mechanics Division, September 12, 1952. Paper No. 53—A-29.

[3] Numbers in parentheses refer to Bibliography at end of paper.

In general, plastic-flow problems involve mixed boundary conditions with tractions prescribed on certain parts of the boundaries, and velocities prescribed elsewhere, or certain components of traction and velocity prescribed together. Since large strains can occur, the deformation of the boundaries due to the plastic flow must be taken into account. In general, a body will be partly plastic and partly rigid, so that the analysis involves the determination of the plastic-rigid boundaries and the domains in which corresponding conditions must be satisfied. In the plastic regions the stress must satisfy the yield condition and the equilibrium equations, since in the present type of quasistatic theory inertia forces are neglected. These conditions lead to a pair of first-order hyperbolic equations which, following Hencky (9), can be expressed most readily in terms of the geometry of the trajectories directed along the planes of maximum shear stress, or slip lines. The relevant variables are indicated in Fig. 2 in which k is the maximum shear stress and p the associated normal stress. In terms of these the stress equations take the form

$$\left.\begin{aligned} p + 2k\varphi &\text{ is constant along an } \alpha\text{-line} \\ p - 2k\varphi &\text{ is constant along a } \beta\text{-line} \end{aligned}\right\} \quad \ldots\ldots [1]$$

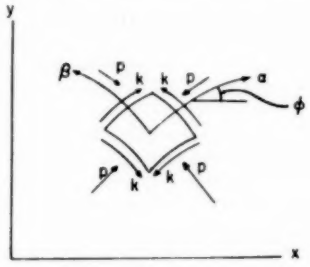

Fig. 2

The velocity field in the plastic regions must determine incompressible flow with strain rates associated with the stress field according to the Mises flow condition. In terms of the velocity components u and v along the slip-line directions α and β, respectively, these conditions reduce to

$$\left.\begin{aligned} du - vd\varphi &= 0 \text{ along an } \alpha\text{-line} \\ dv + ud\varphi &= 0 \text{ along a } \beta\text{-line} \end{aligned}\right\} \quad \ldots\ldots [2]$$

as first developed by Geiringer (10).

In the rigid regions it must be possible to satisfy the equilibrium equations without violating the yield condition, and the rigid-body motion must be compatible with the adjacent plastic-flow field. This latter condition demands that plastic-rigid boundaries must be slip lines of the plastic field.

The conditions given in the foregoing determine what is called in the literature "a complete solution" in contrast to solutions of the stress equations of plasticity only. A complete solution is necessary for a satisfactory analysis of a physical problem, and such is our concern in the present paper.

The Initial Motion Solution

The initial motion solution of the present problem which applies before appreciable boundary motion has occurred was first given by Hill (11), and the corresponding slip-line field is shown in Fig. 3. *A-C-D-F* is the notch surface which is free from traction, thus demanding straight slip lines in triangles *B-G-C* and *C-L-D* with slip lines at 45 deg to the free surfaces. This follows from developments based on Equations [1]. The slip lines in *G-C-H* and *K-C-L* consist of circles with center *C* together with their radii, as determined by the straight slip lines *G-C* and *C-L* and the singularity at *C*. These domains must be joined by a rectangular region of straight slip lines, *J-H-C-K*, with sides parallel to the center lines of the system. This is required to determine a consistent value of p, according to Equations [1], starting with conditions at either of the free surfaces *B-C* and *C-D*, and with $p = -k$

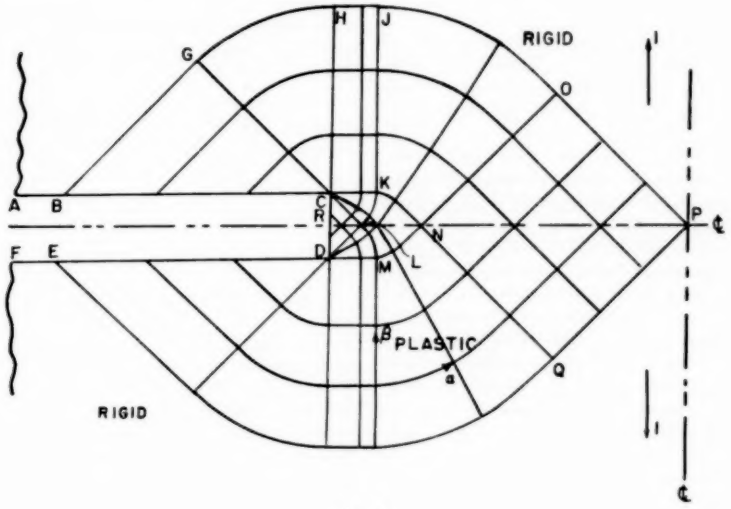

Fig. 3

along both these boundaries. The circular slip lines *K-L* and *L-M* determine the field *K-L-M-N* which can be expressed in terms of Bessel functions as shown by Carathéodory and Schmidt (12). Numerical values for the points of intersection of such a slip line net have been given by Hill.[4] The straight slip line *K-J* determines the slip-line domain *J-K-N-O* to be formed by normals to the curve *K-N* and their orthogonal trajectories. The straight slip lines *O-N* and *N-Q* determine a region of straight slip lines *O-N-Q-P* extending to the center of the notched bar at *P*. The

[4] Reference (4), p. 350.

right-hand half of the field, not shown in Fig. 3, is of course given by symmetry about the center line.

The slip-line field could be extended beyond the boundary *B-G-H-J-O-P*, but as in the case of the V-notched bar (1), such an extension of the region of appreciable plastic flow would lead to the expenditure of more work for a given extension, and would thus not be expected to occur in practice. This conclusion applies even though the uniqueness theorem of Hill (13) shows that the stresses beyond this boundary reach the yield limit, since an alternative velocity solution can be found giving nonzero strain rate there. We therefore consider this boundary to limit the region of appreciable plastic flow. To obtain a complete solution it is strictly necessary to check that the boundary tractions on *B-G-H-J-O-P* can be transmitted through the shanks of the notched bar without violating the yield condition. We shall assume that this is possible for a sufficiently wide shank. At present no technique is available for checking this point rigorously, although there are reasons suggesting that a rigid region bounded in this way is satisfactory. For example, the slip-line field in Fig. 3 can be extended with a free-surface condition satisfied on the notch surfaces or within the bar material, and difficulty due to occurrence of a limit line only occurs in a region far removed from the notch root. It would seem that difficulty in this region could be avoided by spreading the stress field with a reduced maximum shear stress between this point and the notch root, and thus generating a satisfactory stress field in the rigid region.

From the slip-line field of Fig. 3 the stresses and total tensile force can be determined readily using Equations [1] and $p = -k$ along the free surfaces. In publications following (11), Hill has cast some doubt on the solution depicted in Fig. 3.[5] However, the stress uniqueness theorem (13) shows this field to be determined uniquely by the boundary conditions just as is that for a circular rooted notch. It seems, therefore, that the doubts expressed are without foundation. In fact, extension of the theorems to an elastic-plastic body (8) shows this same stress distribution also to be determined uniquely in this case when unconstrained flow sets in.

To study the velocity field of flow we consider the rigid shanks of the notched bar each to have unit velocity as shown in Fig. 3. It is convenient to bring the lower shank to rest by superposing a unit vertical velocity on the whole system. Particles on the center line *L-N-P* then have a unit vertical velocity component. Since the β-lines in the region below *E-D-M-N-O* are all straight, the second of Equations [2] implies that v has a constant value along each of them. Continuity with the static rigid region across *E-Q-P* determines this constant value to be zero for all such β-lines. The first of Equations [2] then determines u to be constant along each α-line below *E-D-M-N-O*, and the need for a unit vertical component of velocity along *N-P* requires this constant value to be $\sqrt{2}$. Thus particles of the free surface *E-D* move as a rigid body without rotation.

From the foregoing discussion the particles on *D-M* have zero vertical component of velocity. Since the region *D-L-M* has one set of straight slip lines, it follows from Equations [2] that the velocity component normal to *D-L* for particles on *D-L* is uniform. For in this region u is a function of φ only, since the α-lines are straight, and integration of the second of Equations [2] implies a uniform value of v along each straight slip line. Similarly, the values of u along *C-L* are constant, and the straight-line slip-line field in *C-L-D* implies that the particles of the free surface *C-D* move as a rigid body without rotation. Thus, although a complex velocity distribution occurs in the region *K-L-M-N*, the free-boundary velocities take on a very simple form. In the next section it is shown that this simple form of boundary motion enables the large strain solution to be determined readily.

[5] Reference (14), p. 51; reference (4), p. 250.

Solution for Finite Strain

Let us consider the initial boundary deformation when plastic flow commences as determined by the initial-motion solution presented in the previous section. We will consider the symmetrical flow pattern with the rigid shanks separating each with unit velocity as shown in Fig. 3. The boundary *A-B* moves, remaining parallel to itself, with the unit velocity upward of the top rigid region. The analysis of the previous section shows that the boundary *B-C* also moves without rotation, having an upward velocity of magnitude 2. *D-C* moves horizontally reducing the notch root semiwidth *R-P*. The motion of the rest of the notch boundaries is determined by symmetry. Thus the notch boundaries of the plastic region remain straight lines parallel to their original directions. Owing to the change in the component of velocity normal to the boundary at *B*, a boundary disturbance occurs there just as in the case of the V-notch (1). However, because of the reduction of notch width *R-P*, the solution for subsequent plastic flow will require a plastic region extending only to the undeformed regions of the boundary *A-C*, and the deformation of the boundary will not affect the slip-line field. This deformation, in fact, will produce a strengthening of the rigid region.

Thus a solution of the continued plastic flow of the notched bar pulled in tension can be found with the notch root maintaining its rectangular form. With this configuration the analysis of the complete boundary motion follows easily, and is developed in the next section. A difficulty arises because of the fact that although the motion of all particles of the boundary is determined by the simple velocity field detailed in the foregoing, the subsequent boundary geometry is not determined uniquely. The singularity at the vertex *C*, and at the three other points similarly situated, offers the possibility of other configurations. This situation is illustrated by the displacement vectors shown in Fig. 4 which are calculated

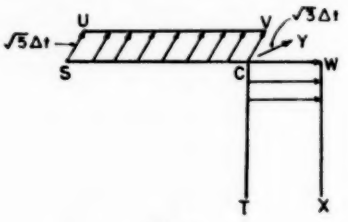

Fig. 4

on the assumption that the particle velocities determined by the initial motion are maintained for a time increment Δt. The part *S-C* of the boundary *B-C* moves to *U-V* with unit horizontal component of velocity, and the vertical component of magnitude 2. The part *C-T* of the boundary *C-R* moves horizontally to *W-X* with a velocity of magnitude RN/CR, as developed in the next section. Thus material particles forming the original surface leave a gap between *V* and *W* which must be bridged by material originally below the surface. The arrow *Y* indicates the motion of a particle initially adjacent to *C* but in the domain *H-C-K-J* of Fig. 3, with the same assumption that it retains its initial velocity for a time Δt. It is seen that if such particles retained their initial velocity the corner would be rounded out. However, the assumption that the new boundary consists of *U-V* and *X-W* extended to their intersection is kinematically satisfactory, since as soon as an interior point comes to the surface at the apex it becomes part of either straight boundary and moves with it.

This particular solution is determined by a particular trajectory of the singularity at *C* through the material, which opens up new surface material to supply the linear extension of the existing

boundaries. The situation is similar to that existing at the notch root in the V-notch solution (1). The question of choice between the various possibilities for the boundary configuration which develops from the initial singularity at C is discussed in the final section. It is shown there that a stability argument suggests the extension to intersection of the straight boundaries U-V and X-W.

Thus, as the extension proceeds, the notch surfaces in the plastic region retain their rectangular form. R-P in Fig. 3 decreases in magnitude, while C-D increases. This change in the geometry of the notch, prescribed by the increasing ratio CD/RP, changes the form of the slip-line field. R-N, which is directly proportional to C-D, increases, and combined with the decrease in R-P, causes a more marked decrease in N-P. The constant length of the normals between their orthogonal trajectories G-H-J-O and C-K-N demands the equality of N-O and C-G, which implies the equality of B-C and N-P. Thus, as plastic flow continues, B approaches C, and at some stage in the extension they will coalesce. The form of the solution then changes. The horizontal notch boundary A-C is then part of the rigid region, and the configuration shown in Fig. 5 occurs. Immediately following the disappearance of the plastic boundary B-C in Fig. 3, C-K in Fig. 5 is horizontal, but as R-P decreases as a result of the subsequent plastic flow, a smaller value of $\sphericalangle K$-C-L is required to extend the plastic region to the center of the notch.

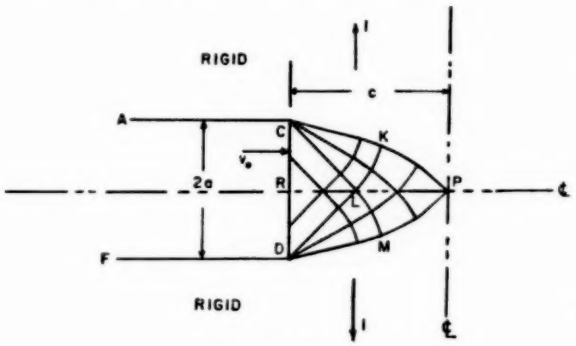

Fig. 5

Again, the stability considerations of the final section suggest the continued existence of the right-angled vertex at C, and the boundary C-D moves horizontally as a rigid body according to a development similar to that used in the case of the configuration in Fig. 3. C-D increases, and R-P decreases until L and P coalesce, the angle K-C-L having been reduced to zero, and the configuration again changes. The further development is shown in Fig. 6, and in this case the stability discussion does not suggest retention of the right-angled vertex at C.

In Fig. 6 the plastic field consists of the uniform tensile stress slip-line field C-D-P. C-D moves horizontally with velocity unity, while the plastic rigid boundaries C-P and P-D remain fixed in space. The initial position C_0 of C when this configuration first obtains determines a bend in the rigid boundary, and the newly developed boundary is the straight line C_0-C. This part of the solution is the reverse flow of the pressing together of two wedges, or a wedge against a smooth flat surface, as given by Hill (15). This configuration applies until C, D, and P coincide at P and the two flanks of the notched bar separate.

Thus the entire motion can be developed using the slip-line configurations shown in Figs. 3, 5, and 6, and the development through these stages from the initial geometry determines the changing form of the notch. Some details of the velocity solution

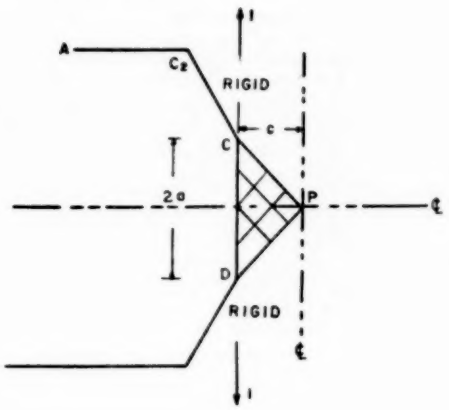

Fig. 6

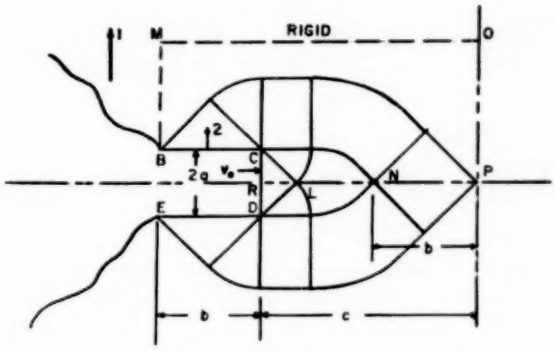

Fig. 7

are given in the next section, and a particular solution is discussed in the following section.

Boundary Motion

The motion of the horizontal boundaries A-C and F-D has been derived in the foregoing. The uniform velocity of the remaining part of the notch boundary C-D can be determined simply by expressing the condition for incompressible flow in terms of boundary motion. Fig. 7 repeats the configuration of Fig. 3 in order to discuss this aspect. We consider the total out-flow across the boundary B-M-O-P-R-C, which must be zero for an incompressible material. There is no flow across the boundaries B-M, R-P, and O-P and the rest give the relation

$$1 \times MO = 2BC + v_0 \times CR.$$

Expressing this in terms of the dimensions a, b, and c, shown in Fig. 7, we have

$$v_0 = \frac{c - b}{a} = \frac{RN}{CR} \qquad [3]$$

Now the configuration C-R-D-N remains geometrically similar throughout the flow until B and C coincide, and the Ratio [3] retains the value[4] 3.64. Thus, while the configuration of Fig. 3 applies, the boundary C-D moves with constant velocity.

The changing geometry of the notch root can now be evaluated simply. While the configuration of Fig. 3 applies

$$b = c - RN = c - 3.64a$$

$\dot{a} = 2$, $\dot{c} = -3.64$, therefore $\dot{b} = -10.92$.

These velocities determine the velocities of all boundary points shown in Fig. 3. For example, B_0, the initial position of the point B, subsequently remains in the upper rigid region, and moves vertically with unit velocity. Since the center line of the notched bar is fixed in space, the configuration point B (to be distinguished from the material particle velocity there) has the horizontal component of velocity $-(\dot{b} + \dot{c}) = 14.56$, and vertical component $\dot{a} = 2$. In this way the motion of all boundary points can be evaluated, and successive positions of the boundary determined.

After N and P coalesce, geometrical similarity of the field C-K-P-M-D-R in Fig. 5 no longer obtains. The incompressible flow discussion carries through, however, and since $\dot{b} = 0$, Ratio [3] becomes

$$v_0 = \frac{c}{a} \qquad [4]$$

but this ratio no longer remains constant as for the previous configuration. Since the vertex c is now bounded above by the rigid region, $\dot{a} = 1$, and $a = a_1 + t_1$, where a_1 is the value of a when this configuration is initiated, and t_1 is the time measured from this instant. Ratio [4] therefore gives the differential equation

$$\dot{c} = -\frac{c}{a_1 + t_1} \qquad [5]$$

with the solution

$$c = \frac{a_1 c_1}{a_1 + t_1} = \frac{a_1 c_1}{a} \qquad [6]$$

Now (a, c) are the Cartesian co-ordinates of the vertex C, so that throughout motion according to the configuration of Fig. 5, C lies on the rectangular hyperbola $ac = a_1 c_1$. Since the entire upper boundary to the left of C moves with unit velocity as part of the upper rigid region, the boundary configuration corresponding to any position of C is simply determined. This type of motion continues until a and c attain equal values $a_2 = \sqrt{a_1 c_1}$ when the configuration of the type shown in Fig. 6 is initiated.

For this geometry $a = c$, and application of Ratio [4] gives $v_0 = 1$. Thus $\dot{c} = \dot{a} = -1$, and $a = a_2 - t_2$, where a_2 is the value of a when this configuration is initiated, and t_2 is the time measured from this instant. The part of the boundary AC_2C moves with the unit vertical velocity of the rigid region, so that its successive positions can be determined readily.

The two halves of the notched bar part when $a = a_2 - t_2 = 0$, thus $t_2 = a_2$ added to the time during which the previous configurations obtain gives the total time of extension, and thus the total motion of the rigid shanks.

A Particular Case

The boundary motion has been worked out in detail for a particular case, with an initial ratio c/a of 10. The changing geometry of the notch boundary is shown in Fig. 9. C_0 is the initial position of the vertex C, and the configuration of Fig. 3 applies. This changes to Fig. 5 at C_1 and to Fig. 6 at C_2.

Initially $b_0 = 10\,a_0 - 3.64\,a_0 = 6.36\,a_0$, and with $\dot{b} = -10.92$ as detailed in the previous section, b is reduced to zero with a consequent change in configuration at $t = 0.582\,a_0$. At this time $a = a_1 = 2.164\,a_0$, $c_1 = 3.64\,a_1 = 7.88\,a_0$.

These values of a_1 and c_1 determine the hyperbolic locus of C, Equation [6], during the configuration corresponding to Fig. 5, which ceases when $a_2 = c_2 = \sqrt{a_1 c_1} = 4.13\,a_0$. The corresponding value of t_1, Equation [6], is $0.909\,a_1 = 1.967\,a_0$, giving the total time to this instant $2.549\,a_0$.

The final configuration corresponding to Fig. 6 continues to a time $t_2 = a_2 = 4.13\,a_0$, so that the total time of extension before separation is $6.679\,a_0$. The relative separation between the flanks is therefore $13.358\,a_0$ since their relative velocity of separation is 2 throughout.

Any other rectangular rooted notched bar can be handled in a similar way. If the initial ratio $c/a > 3.64$ all three configurations occur, if $3.64 > c/a > 1$ only the latter two, and if $c/a < 1$ initially, an unstable situation similar to necking in a cylindrical tensile specimen arises and the subsequent motion is not uniquely determined, although the present theory indicates that only the vertical notch boundaries will deform appreciably.

It is interesting to note that essentially the same type of solution will go through if the upper and lower notch boundaries are equally inclined to the horizontal at some angle other than zero to form a V-notch with a vertical root.

Stability of the Vertexes

It was shown in the section, Solution for Finite Strain, that the initial motion solution determines uniform velocities for the individual linear segments of the notch boundary adjacent to the plastic region. However, because of the singularity at the vertex C in Fig. 3, it is shown in Fig. 4 that the uniformity of the velocity of segments of the boundary does not necessarily imply that the boundaries simply remain straight lines intersecting at right angles. The points V and W in Fig. 4 must be connected by a surface consisting of material which initially lay below the surface of the notch. The determination of the detailed motion in this region depends on whether or not the vertex continues to exist, and if it does, how it moves relative to the material. This situation could be investigated thoroughly by considering a small rounding off of the vertex, which would remove the singularity, and studying the motion of this system. Such an investigation is not carried out in the present paper. However, the stability criterion of investigating the force required to produce various kinematically admissible solutions, and considering the one requiring the least force at each extension value to be that occurring in practice, offers an alternative approach.

It is shown in the same section that the free boundaries of the plastic region maintaining their form of straight lines intersecting in right angles constitute a kinematically admissible solution. The displacement diagram, Fig. 4, indicates the tendency toward rounding out of the vertexes. It can be shown that such a rounding out increases the total tensile force, thus implying the stability and physical occurrence of the solution analyzed in this paper. That the additional material does not decrease the tensile force has been stated by Drucker, Prager, and Greenberg (16). However, this work can be extended readily to show that the force is, in fact, increased. With rounded-out corners, a slip-line field as depicted by the full lines in Fig. 8 arises. Let this stress field be given by the distribution σ_{ij}, and correspond with the tensile force T. Now consider the stress distribution $\sigma_{ij}{}^V$, given by the broken slip lines for the notch with vertexes, and corresponding force T^V. Let us consider the boundary with the rounded corners, consider $\sigma_{ij}{}^V$ to be zero in the added material, and make use of the velocity field u_i and the strain-rate field $\dot{\epsilon}_{ij}$ associated with σ_{ij}. Then the equation of virtual work can be written

$$2(T - T^V) = \int (\sigma_{ij} - \sigma_{ij}{}^V)\,\dot{\epsilon}_{ij}\,dV + \int (k - \tau^V)|u|dS_D$$

where the first integral is taken over the volume of the bar, and the second over discontinuity surfaces of the velocities u_i (for details of this type of relation written in the foregoing form see Hill, reference 13). Now, since $\sigma_{ij}{}^V$ does not violate the yield condition, and from Fig. 8 is clearly not identically equal to σ_{ij}

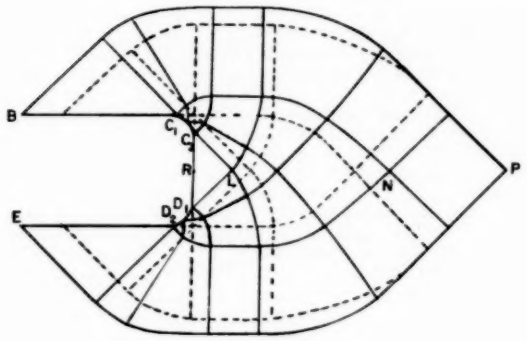

FIG. 8

In the stability discussion we have considered only the possibility of the vertex rounding out, as suggested by the displacement field in Fig. 4. Is it possible for the vertex to sharpen and indent below the line of the initial boundaries and give flow with a still smaller force? This possibility is discounted in the present analysis since the maintenance of the vertex is determined by the boundary motions, and it does not seem plausible that it would penetrate with a velocity greater than that of the boundaries and subsurface material. It seems that an indenter at the vertex would be necessary to make the singularity move in this way relative to the material motion. Presumably this difficulty also could be analyzed rigorously by rounding out the initial vertex and evaluating the resulting motion.

This discussion has indicated that the solution presented satisfies stability conditions, which imply development of plastic flow

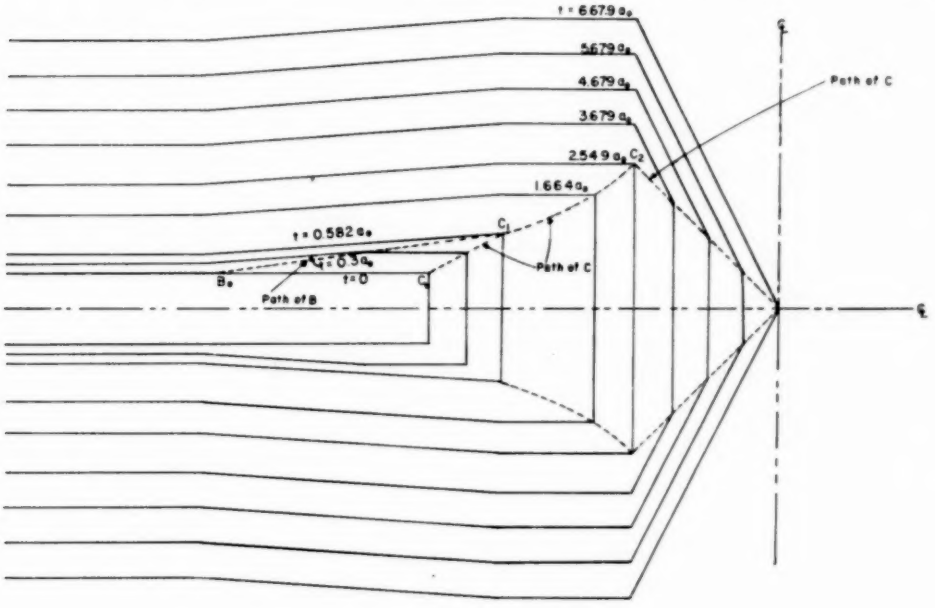

FIG. 9

throughout the region of plastic flow, $\dot{\epsilon}_{ij} \neq 0$, the integrals on the right-hand side are positive and $T > T^v$. Although this argument proves the inequality, the magnitude of the force difference is not demonstrated. This can be obtained by studying particular examples, and for example, Hill (11) has shown that a fully rounded-out notch having a semicircular root demands an appreciable increase in force. The force comparison should be strictly made at the same extension, and for rounded-out vertexes, incompressibility would imply a slightly narrower notch root width and thus a slight reduction in the force on this account. This will be a small effect, and a check in the case of the semicircular bar shows it to have an appreciably smaller effect than the increase in force discussed in the foregoing.

The same argument carries through for the configuration of Fig. 5. In the case of Fig. 6, an increase in length of the vertical boundary *C-D* does not reduce the tensile force to produce plastic flow, since no more favorable distribution than uniform stress at the root can be attained. Thus, in this case the initially right-angled vertex fills out to give the boundary AC_2C, to make full use of the force reduction associated with the maximum reduction in notch width mentioned previously.

as evaluated in this paper during continued extension of the notched bar.

BIBLIOGRAPHY

1 "Plastic Flow in a V-Notched Bar Pulled in Tension," by E. H. Lee, JOURNAL OF APPLIED MECHANICS, Trans. ASME, vol. 74, 1952, pp. 331–336.

2 "The Theory of Wedge Indentation of Ductile Materials," by R. Hill, E. H. Lee, and S. J. Tupper, Proceedings of the Royal Society, London, England, series A, vol. 188, 1947, pp. 273–289.

3 "A Method of Numerical Analysis of Plastic Flow in Plane Strain and Its Application to the Compression of a Ductile Material Between Rough Plates," by R. Hill, E. H. Lee, and S. J. Tupper, JOURNAL OF APPLIED MECHANICS, Trans. ASME, vol. 73, 1951, pp. 46–62.

4 "The Mathematical Theory of Plasticity," by R. Hill, Oxford, England, 1950.

5 "Theory of Perfectly Plastic Solids," by W. Prager and P. G. Hodge, Jr., John Wiley & Sons, Inc., New York, N. Y., 1951.

6 "The Theoretical Analysis of Metal-Forming Problems in Plane Strain," by E. H. Lee, JOURNAL OF APPLIED MECHANICS, Trans. ASME, vol. 74, 1952, pp. 97–103.

7 "On Plastic-Rigid Solutions and Limit Design Theorems for Elastic-Plastic Bodies," by D. C. Drucker, H. J. Greenberg, E. H.

Lee, and W. Prager, Proceedings of the First U. S. National Congress of Applied Mechanics, pp. 533–538.

8 "On the Significance of the Limit Load Theorems for an Elastic-Plastic Body," by E. H. Lee, *Philosophical Magazine*, series 7, vol. 43, May 1952, pp. 549–560.

9 "Über einige statische bestimmte Faelle des Gleichgewichts in Plastischen Körpern," by H. Hencky, *Zeitschrift für angewandte Mathematik und Mechanik*, vol. 3, 1923, pp. 241–251.

10 "Beitrag zum volstaendigen ebenen Plastizitaetsproblem," by H. Polaczek-Geiringer, Proceedings of the Third International Congress of Applied Mechanics, vol. 2, 1930, pp. 185–190.

11 "The Two-Dimensional Theory of Plastic Yielding of Deeply-Notched Bars in Tension," by R. Hill, Arm. Research Department, Theoretical Research Report 9/46, Ministry of Supply, U. K., 1946.

12 "Über die Hencky-Prandtlschen Kurven," by C. Carathéodory and E. Schmidt, *Zeitschrift für angewandte Mathematik und Mechanik*, vol. 3, 1923, pp. 468–475.

13 "On the State of Stress in a Plastic-Rigid Body at the Yield Point," by R. Hill, *Philosophical Magazine*, vol. 42, 1951, pp. 868–875.

14 "The Plastic Yielding of Notched Bars Under Tension," by R. Hill, *Quarterly Journal of Mechanics and Applied Mathematics*, vol. 2, 1949, pp. 40–52.

15 "Some Special Problems of Indentation and Compression in Plasticity," by R. Hill, Proceedings of the Seventh International Congress of Applied Mechanics, vol. 1, 1948, pp. 365–377.

16 "Extended Limit Design Theorems for Continuous Media," by D. C. Drucker, W. Prager, and H. J. Greenberg, *Quarterly of Applied Mathematics*, vol. 9, January, 1952, p. 4.

Transmission of Tension From a Bar to a Plate[1]

By J. N. GOODIER[2] and C. S. HSU[3]

When a bar or strip is lap-jointed to a plate, and transmits tension to it, the transmission is not effected only by a smooth distribution of force along the lap joint; there is also a highly concentrated force, a considerable fraction of the total tension, where the bar meets the plate, and a second force at the end of the bar. These forces are investigated by strain-gage measurements for various lengths of lap, and by a plane-stress calculation, with fair agreement. The results suggest that the fatigue strength of such joints will depend on the detailed local character of the joint where the bar meets the plate, rather than on the length of the joint.

Transmission of a Force in Lapped Plates

THE main object of investigation is the manner in which tension is communicated from a bar or strip to a semi-infinite plate (as in Fig. 4*a*). For this we require the theoretical results obtained in this section for the more general problem indicated by Fig. 1. A thin flat plate D_1 overlaps another

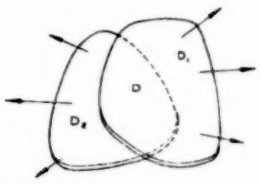

Fig. 1 Lap-Jointed Thin Plates

thin flate plate D_2, the two being bonded together over the whole of the common surface D. The assemblage is in equilibrium under some set of in-plane forces applied to the nonoverlapping parts of D_1 and D_2. A complete analysis necessarily would include bending of the plates as well as the deformation in their planes (plane stress). Here bending is excluded. D_2, although represented as a single plate for simplicity, may actually consist of two equal plates, one on each side of D_1, as in the test specimen to which the theoretical results are to be applied.

If the Poisson's ratios ν_1, ν_2, of D_1 and D_2 are the same, the force transmitted by the bond at the common surface D is a line distribution confined to the periphery of D. No force is transmitted by the bond in the interior of D. The (uniform) thicknesses of the plates, and their Young's moduli, need not be identical.

To prove this we observe that the differential equations for elastic displacement u, v in a thin plate in plane stress are two of the type[4]

$$\frac{\partial^2 u}{\partial x^2} + \frac{\partial^2 u}{\partial y^2} + \frac{1+\nu}{1-\nu}\frac{\partial}{\partial x}\left(\frac{\partial u}{\partial x} + \frac{\partial v}{\partial y}\right) + \frac{X}{hG} = 0$$

with X meaning body force per unit area, ν Poisson's ratio, h the thickness, and G the shear modulus. If a finite, simply connected plate has prescribed displacements all around its edge, the solution of the boundary-value problem determines the displacements throughout the interior. The displacements are effected by a line distribution of force around the edge, as well as the body force.

The part D of the plate D_1 and the part D of the plate D_2 present two such problems. Their displacements are the same throughout, because they are bonded together. The body (bond) forces are equal and opposite. Using subscripts 1 and 2 for D_1 and D_2 we may write

$$\frac{\partial^2 u}{\partial x^2} + \frac{\partial^2 u}{\partial y^2} + \frac{1+\nu_1}{1-\nu_1}\frac{\partial}{\partial x}\left(\frac{\partial u}{\partial x} + \frac{\partial v}{\partial y}\right) + \frac{X}{h_1 G_1} = 0$$

and a companion equation, for D_1, and

$$\frac{\partial^2 u}{\partial x^2} + \frac{\partial^2 u}{\partial y^2} + \frac{1+\nu_2}{1-\nu_2}\frac{\partial}{\partial x}\left(\frac{\partial u}{\partial x} + \frac{\partial v}{\partial y}\right) - \frac{X}{h_2 G_2} = 0$$

and a companion equation, for D_2. Subtraction[5] shows at once that $X = 0$ provided $\nu_1 = \nu_2$. It is not necessary that the shear or Young's moduli be the same, nor that the thicknesses be the same.

When the Poisson's ratios are different, the body (bond) force will not, in general, vanish. We may expect that the force is transmitted by this distributed bond force over D together with a line distribution round the periphery.

In any case it is possible to deduce the line distribution of force around the periphery of D, and the stress in the overlapping plates just inside the periphery, when the stress is known in D_1 or (D_2) just outside the periphery. The relations involve only local values at a point of the periphery. If, for instance, the plates are welded around the periphery of D, measurement of the strain at a point just outside will suffice for the evaluation of the force per unit length transmitted by the weld at that point.

Fig. 2(*a*) indicates the region D of the plate D_1 and also a small rectangular element of D_1 through which the periphery passes. This element is also shown in Fig. 2(*b*) with stress components σ'_{sl}, σ'_{sl}, τ'_{sn} on the "outside," σ_{sl}, σ_{sl}, τ_{sn} on the inside, and line forces $F_s ds$ and $F_n ds$ along and normal to the periphery.

---

[1] The results reported in this paper were obtained in the course of research carried out under a contract between the Office of Naval Research and Stanford University (N6 ONR 251 TO 12).

[2] Professor of Engineering Mechanics; Stanford University, Stanford, Calif. Mem. ASME.

[3] Research Engineer, International Business Machines Corporation, Poughkeepsie, N. Y.

Contributed by the Applied Mechanics Division and presented at the Annual Meeting, New York, N. Y., November 29–December 4, 1953, of The American Society of Mechanical Engineers.

Discussion of this paper should be addressed to the Secretary, ASME, 29 West 39th Street, New York, N. Y., and will be accepted until July 12, 1954, for publication at a later date. Discussion received after the closing date will be returned.

Note: Statements and opinions advanced in papers are to be understood as individual expressions of their authors and not those of the Society. Manuscript received by ASME Applied Mechanics Division, May 25, 1953. Paper No. 53—A-41

[4] See, for instance, "Theory of Elasticity," by S. Timoshenko and J. N. Goodier, McGraw-Hill Book Company, Inc., New York, N. Y., 1951, problem 7, p. 28.

[5] The authors are indebted here to Dr. E. Sternberg for an improvement on the original argument.

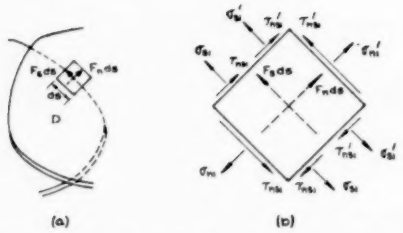

FIG. 2 RECTANGULAR ELEMENT COVERING ELEMENT ds OF BOND PERIPHERY

Taking the ratio of the sides of the element dn/ds to zero limit, equilibrium requires

$$t_1(\sigma_{n1} - \sigma'_{n1}) = F_n, \quad t_1(\tau_{ns1} - \tau'_{ns1}) = F_s \ldots [1]$$

where t_1 is the thickness of the plate D_1.

The underlying element of D_2 is indicated in Fig. 3, with stresses

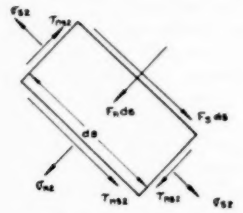

FIG. 3 RECTANGULAR ELEMENT OF LOWER PLATE AT PERIPHERY

σ_{s2}, σ_{n2}, τ_{ns2}, and forces $F_s ds$, $F_n ds$ as edge forces. Equilibrium yields

$$t_2\sigma_{n2} = -F_n, \quad t_2\tau_{ns2} = -F_s \ldots [2]$$

where t_2 is the thickness of the plate D_2.

Since complete correspondence of displacements in the D-region in the two plates is preserved (by the bond over D when the Poisson's ratios differ), the strains (in the plane) are the same for the two plates throughout D. The extensional strain ϵ_{s1} along, and just inside, the periphery, is the same as the value just outside in D_1, denoted by ϵ'_{s1}. We have, therefore, with γ for shear strain

$$\epsilon_{s1} = \epsilon'_{s1}; \quad \epsilon_{s2} = \epsilon_{s1}; \quad \epsilon_{n2} = \epsilon_{n1}; \quad \gamma_{ns2} = \gamma_{ns1} \ldots [3, 4, 5, 6]$$

Elimination of F_n, F_s between Equations [1] and [2] yields the two equations

$$t_1\sigma_{n1} + t_2\sigma_{n2} = t_1\sigma'_{n1}; \quad t_1\tau_{ns1} + t_2\tau_{ns2} = t_1\tau'_{ns1} \ldots [7]$$

When the stresses are expressed in terms of the strains by the plane stress-strain relations

$$E\epsilon_n = \sigma_n - \nu\sigma_s, \; E\epsilon_s = \sigma_s - \nu\sigma_n, \; G\gamma_{ns} = \tau_{ns} \ldots [8]$$

the Equations [7] become (G denoting shear modulus)

$$[t_1E_1/(1-\nu_1^2)](\epsilon_{n1} + \nu_1\epsilon_{s1}) + [t_2E_2/(1-\nu_2^2)](\epsilon_{n2} + \nu_2\epsilon_{s2}) = [t_1E_1/(1-\nu_1^2)](\epsilon'_{n1} + \nu_1\epsilon'_{s1}) \ldots [9]$$

$$t_1G_1\gamma_{ns1} + t_2G_2\gamma_{ns2} = t_1G_1\gamma'_{ns1} \ldots [10]$$

We now write in accordance with Equations [3, 4, 5, 6]

$$\epsilon_s = \epsilon_{s1} = \epsilon_{s2} = \epsilon'_{s1}; \; \epsilon_n = \epsilon_{n1} = \epsilon_{n2}; \; \gamma_{ns} = \gamma_{ns1} = \gamma_{ns2} \ldots [11]$$

regarding ϵ_s, ϵ_n, γ_{ns} as quantities to be found in terms of the outside values ϵ'_{s1}, ϵ'_{n1}, γ'_{ns1}. Equation [10] becomes an equation for γ_{ns}, and Equation [9] an equation for ϵ_n, giving

$$[1 + (t_2G_2/t_1G_1)]\gamma_{ns} = \gamma'_{ns1} \ldots [12]$$

$$\left[1 + \frac{t_2E_2(1-\nu_1^2)}{t_1E_1(1-\nu_2^2)}\right]\epsilon_n = \epsilon'_{n1} - \frac{t_2E_2(1-\nu_1^2)}{t_1E_1(1-\nu_2^2)}\nu_2\epsilon'_{s1} \ldots [13]$$

With these and the first of Equations [11] the strain in the two plates just within D is completely expressed in terms of the strain just outside. To calculate the line force F_n, F_s per unit run, we may substitute in Equation [2] the stresses σ_{n2}, τ_{ns2} deduced from ϵ_s, ϵ_n, γ_{ns} by means of the stress-strain relations of the type [8]. Then

$$F_n = -\frac{E_2t_2}{1-\nu_2^2}(\epsilon_n + \nu_2\epsilon_s); \; F_s = -t_2G_2\gamma_{ns} \ldots [14]$$

and by use of Equations [12] and [13], with [11], we find

$$F_n = -t_1\frac{(1-\nu_1\nu_2)\sigma'_{n1} - (\nu_1 - \nu_2)\sigma'_{s1}}{1 - \nu_1^2 + (1-\nu_2^2)\dfrac{E_1t_1}{E_2t_2}} \ldots [15]$$

$$F_s = -\frac{t_1\tau'_{ns1}}{1 + \dfrac{t_1G_1}{t_2G_2}} \ldots [16]$$

When $\nu_1 = \nu_2$, and consequently the bond force consists of the line force only, these become

$$F_n = -\frac{t_1\sigma'_{n1}}{1 + \dfrac{E_1t_1}{E_2t_2}}, \quad F_s = -\frac{t_1\tau'_{ns1}}{1 + \dfrac{G_1t_1}{G_2t_2}} \ldots [17]$$

and when $t_1 = t_2$, $E_1 = E_2$, $\nu_1 = \nu_2$

$$F_n = -\frac{1}{2}t_1\sigma'_{n1}, \quad F_s = -\frac{1}{2}t_1\tau'_{ns1} \ldots [18]$$

indicating that one half of each type of load in D_1—normal and tangential—is immediately communicated to D_2. This may be regarded as immediately apparent in this simple case, since D_1 may be considered to "fork" into two equal layers of the half-thickness.

TRANSMISSION OF TENSION FROM A STRIP TO A PLATE

Fig. 4 shows a "bar" consisting of two equal strips D_2, attached, one on each side, to a semi-infinite plate D_1. The thickness of

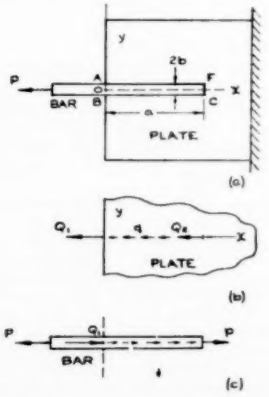

FIG. 4 BAR TRANSMITTING TENSION TO PLATE

each strip is one half that of the plate. The materials being the same, we have the case covered by Equations [18], and these indicate that half of the tension in the strips is immediately communicated to the plate. This implies an abrupt 50 per cent drop of the tension in the strips where they meet the edge of the plate. At the ends of the strips, on the plates, line load on the bond periphery is also to be expected; that is, the tension in the strip will not fall smoothly to zero toward the end, but to some non-zero value, with an abrupt fall to zero right at the end.

These expectations are borne out by wire resistance strain-gage measurements made on a monolithic model machined from a solid steel plate. Fig. 5 shows the axial tensile strain of the strips

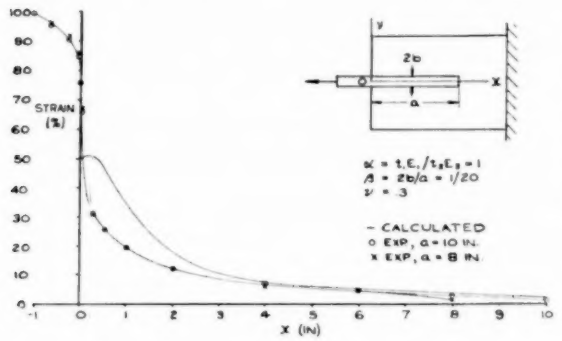

FIG. 5 DISTRIBUTION OF STRAIN ALONG BAR

of length until the length was down from 10 in. to 3 in. The 3-in. curve is shown in Fig. 6, followed by Figs. 7, 8, 9, 10 for lengths 2, 1, $^1/_2$, $^1/_4$ in., respectively. The sudden drop to zero tension at the inboard end is now apparent.

The gages used were $^1/_8$ in. and $^1/_{16}$ in., the latter in the region of rapid variation of strain where the strips enter the plate. The points to the left of the origin, corresponding to measurements in the free parts of the strips, were obtained from gages on each side of each strip, to eliminate bending. The gages on each side of the attached parts also were paired to eliminate bending.

THE THEORETICAL PROBLEM

The problem of a bar or strip attached to a plate and transmitting force to it has a natural formulation in terms of integral equations, as in the papers of Reissner (1)[6] and Benscoter (2). With the exception of Glover (3), who arrives at the abrupt changes of tension in the bar through the singularity of the kernel of the integral equation, the significance of the line loads around the bond has not been recognized. Here we derive the calculated curve in Fig. 5, taking advantage of the results of the first section as to the line loads and the abrupt changes of tension, the integral equation being required only for the determination of the smooth curve within the attached length of the strip.

In the papers referred to, and also in the calculations of Monge (4), the bar is regarded as indefinitely slender and so as applying a line load to the plate, Fig. 4(*b*). The results of the first section show that the strip, regarded as a narrow rectangular plate, will communicate load as a line load all around the periphery of the

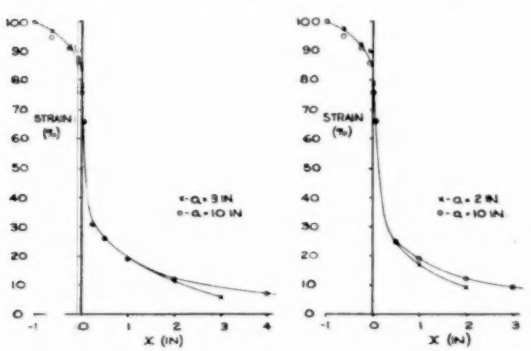

FIG. 6

FIG. 7

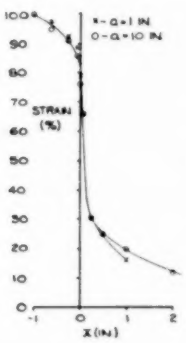

FIG. 8

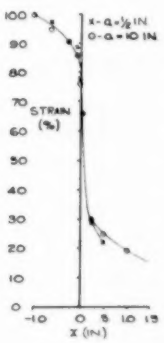

FIG. 9

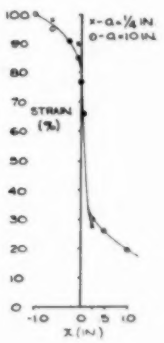

FIG. 10

DISTRIBUTION OF STRAIN ALONG BAR

along the middle line, the length of the latter bonded to the plate being 10 in. Points (crosses) for an 8-in. length also are shown. The calculated curve in Fig. 8 was derived by a method to be explained. It will be observed that the sharp drop of tension at entry to the plate appears to exceed somewhat the predicted 50 per cent, but there is of course no abrupt discontinuity on account of the finite thickness of the strip, interposed between gage and bond, and also of inevitable departure from a strictly plane state of stress. The points to the left of the origin represent measurements in the free part of the strips. The simple tension value is not reached immediately because the plate imposes a lateral restraint on the strips which is felt to a distance of about one strip width away from the edge of the plate. The drop of tension to zero at the inboard end of the strips appears as very small.

The measurements were repeated for shorter lengths of strip—by machining off the end parts. The curves for the remaining length of strip remained essentially unaffected by these reductions

bond. Therefore it will apply two line loads along its two longitudinal edges, in addition to the end loads. But if the strip is regarded as a narrow rectangular plate, rather than as a bar acting in uniaxial tension only, it is affected by lateral stress induced by the attachment to the plate. Taking this into account would lead to excessive computation. The present work was limited to a calculation in terms of a single line load, on the axis of the strip, in order to see how well theory of this type can predict the observed results.

The Integral Equation. As in Fig. 4(*b*), the semi-infinite plate ($x > 0$) is stressed by a concentrated force Q_1 at $x = 0$, a concentrated force Q_2 at $x = a$ (the end of the strip), and a distributed load $q(x)$ per unit length in $0 < x < a$.

The strain at $(x, 0)$ in the x-direction, due to a force F, Fig. 11, acting at $(\xi, 0)$ in the negative x-direction, is (5)

[6] Numbers in parentheses refer to the Bibliography at the end of the paper.

$$\frac{F}{\pi t_2 E_2} K(x, \xi) \text{ where } 4K(x, \xi) = \frac{(3 - \nu)(1 + \nu)}{x - \xi}$$

$$+ \frac{5 - 2\nu + \nu^2}{x + \xi} + 2(1 + \nu)^2 \frac{\xi(x - \xi)}{(x + \xi)^3} \quad \ldots\ldots [19]$$

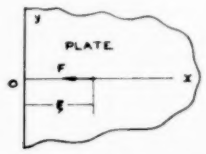

FIG. 11 MELAN'S PROBLEM

and therefore the strain $\epsilon_x(x, 0)$ due to the loading Q_1, Q_2, and $q(x)$ is

$$\epsilon_x(x, 0) = \frac{1}{\pi t_2 E_2}\left[Q_1 K(x, 0) + Q_2 K(x, a) + \int_0^a K(x, \xi) q(\xi) d\xi\right] \quad \ldots\ldots [20]$$

Writing $p(x)$ for the tension in the strip, we have a tensile strain $p(x)/(2bt_1E_1)$ which must be identical with the strain [20] in the plate. We have also

$$q(\xi) = -\frac{d}{d\xi} p(\xi) \quad \ldots\ldots [21]$$

and therefore

$$p(x) = \frac{2bt_1E_1}{\pi t_2 E_2}\left[Q_1 K(x, 0) + Q_2 K(x, a) - \int_0^a K(x, \xi) \frac{d}{d\xi} p(\xi) d\xi\right] \quad \ldots\ldots [22]$$

as an integral equation for $p(x)$. By Equations [17] the value of Q_1 is, in terms of the tension P applied to the strip

$$P/\left(1 + \frac{E_1 t_1}{E_2 t_2}\right)$$

and we have also $Q_2 = p(a)$.

The solution of Equation [22] for the specimen tested was carried out numerically by reducing Equation [22] to eight simultaneous algebraic equations for eight values $p_1, p_2 \ldots, p_8$ of $p(x)$ at eight selected points in the interval $0 < x < a$. The kernel $K(x, \xi)$ has a singularity at $x = \xi$, arising from the first term in Equation [19]. The integral in Equation [22] is thus an improper one, and the physical situation requires the Cauchy principal value. For the calculation, the integral was replaced by an ordinary integral by the following treatment of the part due to the singular term

$$\int_0^a \frac{1}{x - \xi} p'(\xi) d\xi = -\int_0^a \frac{p'(x) - p'(\xi)}{x - \xi} d\xi + p'(x) \int_0^a \frac{d\xi}{x - \xi}$$

with

$$\int_0^a \frac{d\xi}{x - \xi} = \log \frac{x}{a - x}$$

Here $p'(\xi)$ means $dp(\xi)/d\xi$ and $p'(x)$ means $dp(x)/dx$. The first integral on the right is ordinary since $p'(x)$ has a derivative at any point between $x = 0$ and $x = a$. The points used were $x/a = 0.05, 0.1, 0.2, 0.3, 0.4, 0.5, 0.7, 0.9$, and it was assumed that $p(a) = p(0.9a)$. Simpson's rule was used for the integral.

The curve obtained is shown in Fig. 5, with the designation "calculated." The agreement with the measurements is only fair.

However, in view of the abrupt communication of half the tension P to the plate at its edge where the strip enters, the fatigue strength of an attachment of this kind will depend on the detail in this region rather than on the exact form of the q curve.

Fig. 12 shows a second calculated curve for case $2b/a = 1/10$, as when the strip is twice as wide as in first case $2b/a = 1/20$.

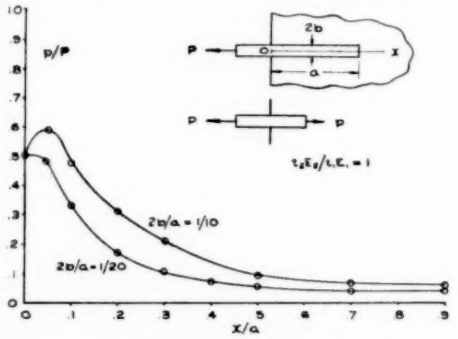

FIG. 12 CALCULATED DISTRIBUTION OF STRAIN ALONG BAR

BIBLIOGRAPHY

1 "Note on the Problem of the Distribution of Stress in a Thin Stiffened Elastic Sheet," by E. Reissner, Proceedings of the National Academy of Sciences, vol. 26, April, 1940, pp. 300–305.

2 "Analysis of a Single Stiffener on an Infinite Sheet," by S. U. Benscoter, JOURNAL OF APPLIED MECHANICS, Trans. ASME, vol. 71, 1949, pp. 242–246.

3 Discussion of Reference (2), by R. E. Glover, JOURNAL OF APPLIED MECHANICS, Trans. ASME, vol. 72, 1950, p. 218.

4 "Estudio de Barra Sometida a Esfuerzo Axial Soldada a una Placa Semiindefinida," by F. C. Monge, Instituto Tecnico de la Construccion y Edificacion, Publication No. 59.

5 "Der Spannungszustand der durch eine Einzelkraft im Innern beanspruchten Halbscheibe," by E. Melan, *Zeitschrift für angewandte Mathematik und Mechanik*, vol. 12, 1932, p. 343.

The Stresses in a Flat Curved Bar Resulting From Concentrated Tangential Boundary Loads[1]

By NING-GAU WU[2] AND C. W. NELSON[3]

The Fourier integral method is applied to plane-stress problems of a curved bar bounded by two concentric circles and loaded by concentrated tangential boundary loads. The solutions presented may be combined with results given in previous papers (1, 2)[4] dealing with radial boundary loads so as to obtain the stresses in a curved bar loaded by any combination of concentrated boundary loads inclined at any angle to the radial direction.

Introduction

IN previous papers (1, 2), Fourier integral solutions were presented for the stresses in flat curved bars loaded by radial loads on the circular boundaries. In this paper a Fourier integral solution is developed for the problem of a flat curved bar loaded by concentrated tangential boundary loads as shown in Figs. 1 (*a*) and (*b*). A plane-stress condition is assumed throughout this paper.

Since it is apparently impossible to apply pure tangential forces to the surface of an elastic body, it should be pointed out that the results for Figs. 1 (*a*) and (*b*) may be combined with previously published results (1, 2) for concentrated radial boundary loads. By such superposition, the stresses in a curved bar loaded by any combination of inclined boundary loads may be obtained. In addition, there are many possibilities for the application or extension of the results of this paper to other elasticity problems. Examples of such problems are a curved bar loaded by internal forces; the plane-stress approximation of a spoked wheel; the plane-stress approximation of the transmission of torque between a wheel and axle; and, for the special case of a straight beam, the plane-stress approximation of the press-fit problem.

This paper deals with open rings while some of the examples just listed are closed-ring problems. This apparent inconsistency disappears if it is recognized that a Fourier series solution for a closed ring can be replaced by a Fourier integral approximation, usually with extremely good accuracy if care is taken to remove any dislocations introduced by the process. For ratios of *a*(inner radius)/*b*(outer radius) approaching unity, the Fourier integral solution would presumably be more convenient to evaluate than the slowly convergent $\left(\text{for } \frac{a}{b} \to 1\right)$ series solution.

The authors recognize that, for ordinary design purposes, most of the problems listed in the foregoing paragraph should be handled by approximate methods. For example, some of them should be treated by an approximate theory for the bending of curved beams. On the other hand, there are many problems where stresses are affected by the proximity of loads and there are at least a few cases where methods such as used in this paper make it possible to estimate such effects (see, for example, Table 4 of reference 2). The solutions given in this paper, like any elasticity solutions for problems involving concentrated loads, should not be applied in the immediate neighborhood of the points of application of the concentrated loads. In practical applications, all loads are distributed. In some cases the curves presented in this paper can be used as influence lines in dealing with distributed loads.

Throughout this paper the thicknesses of the bodies perpendicular to the plane of the paper are assumed to be unity so that the load P in Fig. 1(*a*), for example, represents force per unit thickness. In Figs. 1 (*a*) and (*b*) the wall at the left end of each beam is shown only to indicate which end of the beam is supported and the solutions which are presented do not hold in the immediate vicinity of the wall.

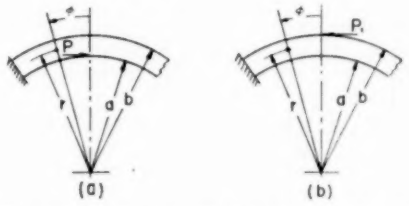

FIG. 1

The problems illustrated in Figs. 1 (*a*) and (*b*) will be solved by determining Airy's stress function which will be denoted by ψ. This stress function must satisfy the biharmonic equation

$$\nabla^2\nabla^2\psi = 0 \qquad [1]$$

where ∇^2 stands for the Laplace operator which, in polar coordinates (r, ϕ), is

$$\nabla^2 = \frac{\partial^2}{\partial r^2} + \frac{1}{r}\frac{\partial}{\partial r} + \frac{1}{r^2}\frac{\partial^2}{\partial \phi^2}$$

The stresses must be determined from the stress function by the equations

$$\sigma_r = \frac{1}{r}\frac{\partial \psi}{\partial r} + \frac{1}{r^2}\frac{\partial^2 \psi}{\partial \phi^2} \qquad [2]$$

$$\sigma_\phi = \frac{\partial^2 \psi}{\partial r^2} \qquad [3]$$

$$\tau_{r\phi} = -\frac{\partial}{\partial r}\left(\frac{1}{r}\frac{\partial \psi}{\partial \phi}\right) \qquad [4]$$

[1] Some of the material presented in this paper was taken from a thesis submitted by Ning-Gau Wu at the University of California in partial fulfillment of the requirements for the degree of Doctor of Philosophy, 1952.

[2] Chief Design Engineer, Jacuzzi Brothers, Inc., Richmond, Calif. Assoc. Mem. ASME.

[3] Associate Professor of Engineering Design, University of California, Berkeley, Calif. Mem. ASME.

[4] Numbers in parentheses refer to Bibliography at end of paper.

Contributed by the Applied Mechanics Division and presented at the Annual Meeting, New York, N. Y., November 29–December 4, 1953, of THE AMERICAN SOCIETY OF MECHANICAL ENGINEERS.

Discussion of this paper should be addressed to the Secretary, ASME, 29 West 39th Street, New York, N. Y., and will be accepted until July 12, 1954, for publication at a later date. Discussion received after the closing date will be returned.

NOTE: Statements and opinions advanced in papers are to be understood as individual expressions of their authors and not those of the Society. Manuscript received by ASME Applied Mechanics Division, November 24, 1952. Paper No. 53—A-47.

Stresses determined by Equations [2], [3], [4] will satisfy equilibrium and compatibility requirements. In each of the problems considered, a proper combination of solutions of Equation [1] must be formed so that boundary conditions will be satisfied.

Antisymmetrical Bending With Load on Inner Circular Boundary

The solution for Fig. 1(a) will be obtained by superposition of two solutions one of which will be derived in the following section.

Fig. 2(a) shows a portion of a circular ring with circular boundaries $r = a$ and $r = b$ and radial boundaries which, for convenience, are shown at $\phi = \pi/2$ and $\phi = -\pi/2$ radians. Radial boundaries at $\phi = \pm m\pi/2$ ($m = 5$, 9, and so on) would be more appropriate to the method of solution and should be regarded as being physically possible since the problem is one of plane stress and the thickness of the ring may be very small so that the ends may slip past each other like the coils of a flat spiral spring. The ring is loaded by shear stresses p, uniformly distributed from $\phi = -\beta$ to $\phi = \beta$ on the inner boundary $r = a$. The magnitude and sense of these shear stresses are such that their force resultant has the magnitude P and acts toward the right. Assuming the internal stresses in the curved bar to be antisymmetrical with respect to the cross section $\phi = 0$, the resultant force P will be balanced by two shearing forces $P/2$ acting toward the left, one at the cross section $\phi = \pi/2$ and one at the cross section $\phi = -\pi/2$, and by two moments $M/2$ acting as shown.

After the stress function for Fig. 2(a) has been derived, the stress function for Fig. 2(b) will be obtained by letting β approach zero in the solution for Fig. 2(a), at the same time specifying that the resultant tangential force on the inner boundary shall remain finite and of magnitude P. It should be noted that the assumption of uniformly distributed shear stress on the inner boundary from $\phi = -\beta$ to $\phi = \beta$ as in Fig. 2(a) is not essential in order to arrive at a solution for the problem of Fig. 2(b). Any other configuration of distributed load may be assumed in Fig. 2(a) provided it gives a concentrated load P at $\phi = 0$ when the limit process is applied.

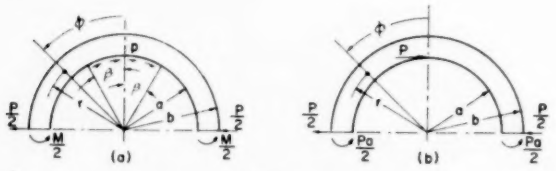

Fig. 2

Because of the antisymmetrical system of loads in Fig. 2(a), a solution for that problem can be obtained in integral form by taking the limit of the sum of many particular solutions of Equation [1], each particular solution having the form

$$\psi_n = (c_n r^n + d_n r^{n+2} + c'_n r^{-n} + d^{n'} r^{-n+2}) \sin n\phi \quad [5]$$

where n is not necessarily an integer.

The boundary stress conditions for Fig. 2(a) are

$$(\tau_{r\phi})_{r=a} = F_1(\phi) \quad [6]$$

$$(\tau_{r\phi})_{r=b} = 0 \quad [7]$$

$$(\sigma_r)_{r=a} = 0 \quad [8]$$

$$(\sigma_r)_{r=b} = 0 \quad [9]$$

Although ψ, σ_ϕ, σ_r are odd functions of ϕ, it is clear that $\tau_{r\phi}$ and $F_1(\phi)$ are even functions of ϕ. $F_1(\phi)$ may be defined in the interval $-\infty < \phi < \infty$ as follows

$$F_1(\phi) = 0 \text{ for } -\infty < \phi < -\beta$$

$$F_1(\phi) = p \text{ for } -\beta < \phi < \beta$$

$$F_1(\phi) = 0 \text{ for } \beta < \phi < \infty$$

From the formula

$$F_1(\phi) = \frac{2}{\pi} \int_0^\infty d\eta \int_0^\infty F_1(\lambda) \cos n\phi \cos n\lambda \, d\lambda \quad [10]$$

which expresses an even function of ϕ as a Fourier cosine integral, it can be shown that

$$F_1(\phi) = \frac{2}{\pi} \int_0^\infty \frac{p}{n} \sin n\beta \cos n\phi \, dn \quad [11]$$

For the limiting case when β approaches zero but the total load on the inner boundary remains finite and equal to P, Equation [11] reduces to

$$\lim_{\beta \to 0} F_1(\phi) = \frac{2}{\pi} \int_0^\infty \frac{P}{2a} \cos n\phi \, dn \quad [12]$$

Equation [12] is applicable to Fig. 2(b).

One step in the solution of the problem of Fig. 2(b) will be to form a sum of many stress functions ψ_n such as given by Equation [5]. Boundary conditions [7], [8], and [9] can be satisfied separately by each ψ_n. Application of these three boundary conditions results in the elimination of three of the four constants c_n, d_n, c_n', d_n' so that Equation [5] takes the form

$$\psi_n = \frac{-a^{n+1} c_n' \, g(r, n) \sin n\phi}{(n-1)[n^2 a^{2n}(b^2 - a^2) - (n+2)a^2(b^{2n} - a^{2n})]} \quad [13]$$

where

$$g(r,n) = \left\{ \begin{array}{l} n^2 \left(\frac{b}{a} - \frac{a}{b}\right)\left[\frac{n(b^2 - r^2)}{b}\left(\frac{r^n}{a^n} - \frac{a^n}{r^n}\right) + \frac{(b^2 - r^2)}{b}\left(\frac{r^n}{a^n} + \frac{a^n}{r^n}\right)\right] \\ -n\left(\frac{b^n}{a^n} - \frac{a^n}{b^n}\right)\left[\frac{n(r^2 - a^2)}{a}\left(\frac{b^n}{r^n} - \frac{r^n}{b^n}\right) + \frac{(r^2 - a^2)}{a}\left(\frac{b^n}{r^n} + \frac{r^n}{b^n}\right)\right] \\ +2n\left(\frac{b}{a} - \frac{a}{b}\right)\frac{r^2}{b}\left(\frac{r^n}{a^n} - \frac{a^n}{r^n}\right) \\ -2\left(\frac{b^n}{a^n} - \frac{a^n}{b^n}\right) a \left(\frac{b^n}{r^n} - \frac{r^n}{b^n}\right) \end{array} \right\} \quad [14]$$

The algebra required in order to arrive at Equation [13] has been omitted. The details of this derivation are given in reference (4).

The stress function

$$\sum_{n=0,\,\Delta n,\,2\Delta n,\ldots}^{\infty} \psi_n \, \Delta n$$

obtained by forming an infinite series of stress functions of the type given in Equation [13] each multiplied by Δn will still satisfy boundary conditions [7], [8], and [9]. As Δn approaches zero, the limit of this infinite series becomes

$$\psi = \int_0^\infty \psi_n \, dn \qquad [15]$$

Application of Equation [4] to the stress function of Equation [15] gives

$$\tau_{r\phi} = \int_0^\infty \left[-\frac{\partial}{\partial r}\left(\frac{1}{r}\frac{\partial \psi_n}{\partial \phi}\right)\right] dn \qquad [16]$$

The remaining boundary condition [6] when considered in conjunction with Equation [16] requires that

$$F_1(\phi) = \int_0^\infty \left[-\frac{\partial}{\partial r}\left(\frac{1}{r}\frac{\partial \psi_n}{\partial \phi}\right)\right]_{r=a} dn \qquad [17]$$

Comparing Equations [12] and [17], it may be seen that

$$\int_0^\infty \left\{ \left[\frac{\partial}{\partial r}\left(\frac{1}{r}\frac{\partial \psi_n}{\partial \phi}\right)\right]_{r=a} + \frac{P}{\pi a}\cos n\phi \right\} dn = 0 \qquad [18]$$

or

$$\int_0^\infty \left\{ \frac{2n(n+1)a^n b^n \left[\left(\frac{b^n}{a^n} - \frac{a^n}{b^n}\right)^2 - n^2\left(\frac{b}{a} - \frac{a}{b}\right)^2\right]}{b^n[n^2a^{2n}(b^2 - a^2) - (n+2)a^2(b^{2n} - a^{2n})]} c_n' + \frac{P}{\pi a}\right\} \cos n\phi \, dn = 0 \qquad [19]$$

Equation [19] must hold for all the values of ϕ and this requires that the integrand in the left member of the equation must be zero, from which

$$c_n' = -\frac{P}{2\pi} \frac{[n^2a^{2n}(b^2 - a^2) - (n+2)a^2(b^{2n} - a^{2n})]}{n(n+1)a^{n+1}\left[\left(\frac{b^n}{a^n} - \frac{a^n}{b^n}\right)^2 - n^2\left(\frac{b}{a} - \frac{a}{b}\right)^2\right]} \qquad [20]$$

Therefore the stress function for Fig. 2(*b*) is

$$\psi_1 = \frac{P}{2\pi}\int_0^\infty \frac{g(r, n)\sin n\phi \, dn}{n(n^2 - 1)\left[\left(\frac{b^n}{a^n} - \frac{a^n}{b^n}\right)^2 - n^2\left(\frac{b}{a} - \frac{a}{b}\right)^2\right]} \qquad [21]$$

where $g(r, n)$ is given by Equation [14] and the subscript 1 has been added on ψ to distinguish this stress function from others used in this paper.

By introducing the new symbols

$$z = n \ln \frac{1}{\alpha} \qquad [22]$$

where

$$\alpha = \frac{a}{b}$$

and

$$\left.\begin{aligned} \Phi &= \frac{\phi}{\ln \frac{1}{\alpha}}, \quad A = \frac{\ln \frac{r}{a}}{\ln \frac{1}{\alpha}}, \quad B = \frac{\ln \frac{b}{r}}{\ln \frac{1}{\alpha}} \\ X &= \frac{\sinh \ln \frac{1}{\alpha}}{\ln \frac{1}{\alpha}} = \frac{1 - \alpha^2}{2\alpha \ln \frac{1}{\alpha}} \end{aligned}\right\} \qquad [23]$$

Equation [21] can be put in the form

$$\psi_1 = \frac{P}{2\pi}\int_0^\infty \left\{ \begin{aligned} &\frac{Xz^2}{\ln \frac{1}{\alpha}}\left[\frac{(b^2 - r^2)}{b \ln \frac{1}{\alpha}} z \sinh Az + \frac{(b^2 - r^2)}{b}\cosh Az\right] \\ &- \frac{z \sinh z}{\ln \frac{1}{\alpha}}\left[\frac{(r^2 - a^2)}{a \ln \frac{1}{\alpha}} z \sinh Bz + \frac{(r^2 - a^2)}{a}\cosh Bz\right] \\ &+ \frac{2r^2}{b} Xz \sinh Az \\ &\frac{-2a \sinh z \sinh Bz}{z\left[\left(\frac{z}{\ln \frac{1}{\alpha}}\right)^2 - 1\right](\sinh^2 z - X^2z^2)} \end{aligned} \right\} \sin \Phi z \, dz \qquad [24]$$

Since the stress function is only a tool to be used in evaluating the stresses, it is not of much value to be able to evaluate the stress function at various points (r, ϕ) unless such evaluation makes it easier to find the derivatives of ψ required in Equations [2], [3], [4]. The only real positive root of the factor

$$\left[\left(\frac{z}{\ln \frac{1}{\alpha}}\right)^2 - 1\right]$$

in the denominator of the integrand in Equation [24] is $z = \ln(1/\alpha)$, i.e., $n = 1$. The only real positive root of the factor $(\sinh^2 z - X^2z^2)$ in the same denominator is also $z = \ln(1/\alpha)$. Thus the integrand appears to contain the factor $[z - \ln(1/\alpha)]^3$ in the denominator. However, it can be shown that the numerator

of the integrand also contains the factor $[z - \ln(1/\alpha)]$. This can be shown by substituting $z = \ln(1/\alpha)$ and $\sinh z = Xz = X \ln 1/\alpha$ into the numerator which then reduces to zero. This explains why the stress function of Equation [24] can be integrated to obtain a finite value for a general point (r, ϕ). The stress function of Equation [24] is an improper integral but is quite usable and has a value, and only one, for each point (r, ϕ).

Two Problems Involving Symmetrical Bending

Fig. 3(*a*) shows a portion of a circular ring subjected to pure bending by end moments of magnitude $Pa/2$ having the sense indicated in the figure. Fig. 3(*b*) shows a half circular ring subjected to end forces $P/2$ acting as shown in the figure. The solutions for these two cases were obtained first by H. Golovin. The stress functions for Figs. 3(*a*) and (*b*) will be denoted by ψ_2 and ψ_3, respectively. The expression for ψ_2 is (3*a*)

$$\psi_2 = \frac{Pa\left\{\begin{array}{l}4a^2b^2 \ln(b/a) \ln r + 2(b^2 - a^2)r^2 \ln r \\ -[b^2 - a^2 + 2(b^2 \ln b - a^2 \ln a)]r^2\end{array}\right\}}{2\left[(b^2 - a^2)^2 - 4a^2b^2\left(\ln \frac{b}{a}\right)^2\right]} \quad \ldots [25]$$

The expression for ψ_3 is (3*b*)

$$\psi_3 = \frac{P\left[r^3 - \frac{a^2b^2}{r} - 2(b^2 + a^2)r \ln r\right]}{4\left[(b^2 - a^2) - (b^2 + a^2)\ln \frac{b}{a}\right]} \cos\phi \quad \ldots [26]$$

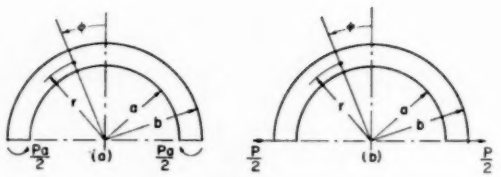

Fig. 3

Cantilever Curved Bar With Single Tangential Load on Inner Curved Boundary

The stress function for the problem shown in Fig. 1(*a*) will be denoted by ψ_1 and, by the principle of superposition, it may be expressed as

$$\psi_1 = \psi_1(a,b,r,\phi,P) = \psi_1 + \psi_2 + \psi_3 \quad \ldots [27]$$

Cantilever Curved Bar With Single Tangential Load on Outer Curved Boundary

The stress function for a cantilever curved bar with a single tangential load P_1 on the outer curved boundary as shown in Fig. 1(*b*), will be denoted by ψ_{II}. It may be derived by the procedure used in obtaining ψ_I and the result is

$$\psi_{II} = \psi_1(b,a,r,\phi,P_1) \quad \ldots [28]$$

Determination of Stresses From Stress Functions

When the operations indicated by Equations [2] to [4] are performed on the stress function given by Equation [27], the stresses for the problem of Fig. 1(*a*) are found to be

$$\sigma_{r1} = \sigma_{r1}(a,b,r,\phi,P)$$

$$= \frac{2Pa\left[\frac{a^2b^2}{r^2}\ln\frac{b}{a} + b^2 \ln\frac{r}{b} + a^2 \ln\frac{a}{r}\right]}{(b^2 - a^2)^2 - 4a^2b^2\left(\ln\frac{b}{a}\right)^2}$$

$$+ \frac{P\left[r + \frac{a^2b^2}{r^2} - \frac{b^2 + a^2}{r}\right]}{2\left[b^2 - a^2 - (b^2 + a^2)\ln\frac{b}{a}\right]}\cos\phi$$

$$- \frac{P}{2\pi\left(\ln\frac{1}{\alpha}\right)^2}\left[\begin{array}{l}\frac{4X\left(\ln\frac{1}{\alpha}\right)^2}{b}\int_0^\infty \frac{\sinh Az \sin \Phi z}{\sinh^2 z - X^2z^2}\,dz \\ + \frac{X\left(\frac{b^2}{r^2} - 1\right)}{b}\int_0^\infty \frac{z^2 \sinh Az \sin \Phi z}{\sinh^2 z - X^2z^2}\,dz \\ - \frac{\left(1 - \frac{a^2}{r^2}\right)}{a}\int_0^\infty \frac{z \sinh z \sinh Bz \sin \Phi z}{\sinh^2 z - X^2z^2}\,dz \\ - \frac{2\ln\frac{1}{\alpha}\left(1 - \frac{a^2}{r^2}\right)}{a}\int_0^\infty \frac{\sinh z \cosh Bz \sin \Phi z}{\sinh^2 z - X^2z^2}\,dz\end{array}\right] \quad \ldots [29]$$

$$\sigma_{\phi 1} = \sigma_{\phi 1}(a,b,r,\phi,P) = \frac{2Pa\left[b^2 - a^2 - \frac{a^2b^2}{r^2}\ln\frac{b}{a} + b^2\ln\frac{r}{b} + a^2\ln\frac{a}{r}\right]}{(b^2-a^2)^2 - 4a^2b^2\left(\ln\frac{b}{a}\right)^2} + \frac{P\left[3r - \frac{a^2b^2}{r^3} - \frac{b^2+a^2}{r}\right]}{2\left[b^2 - a^2 - (b^2+a^2)\ln\frac{b}{a}\right]}\cos\phi$$

$$- \frac{P}{2\pi\left(\ln\frac{1}{\alpha}\right)^2}\left[\begin{array}{l} \frac{4X\left(\ln\frac{1}{\alpha}\right)^2}{b}\int_0^\infty \frac{\sinh Az\sin\Phi z}{\sinh^2 z - X^2z^2}\,dz \\ -\frac{X\left(\frac{b^2}{r^2}-1\right)}{b}\int_0^\infty \frac{z^2\sinh Az\sin\Phi z}{\sinh^2 z - X^2z^2}\,dz \\ +\frac{4X\ln\frac{1}{\alpha}}{b}\int_0^\infty \frac{z\cosh Az\sin\Phi z}{\sinh^2 z - X^2z^2}\,dz \\ +\frac{\left(1-\frac{a^2}{r^2}\right)}{a}\int_0^\infty \frac{z\sinh z\sinh Bz\sin\Phi z}{\sinh^2 z - X^2z^2}\,dz \\ -\frac{2\left(\ln\frac{1}{\alpha}\right)\left(1+\frac{a^2}{r^2}\right)}{a}\int_0^\infty \frac{\sinh z\cosh Bz\sin\Phi z}{\sinh^2 z - X^2z^2}\,dz \end{array}\right] \quad \ldots [30]$$

$$\tau_{r\phi 1} = \tau_{r\phi 1}(a,b,r,\phi,P) = \frac{P\left[r + \frac{a^2b^2}{r^3} - \frac{(b^2+a^2)}{r}\right]}{2\left[b^2 - a^2 - (b^2+a^2)\ln\frac{b}{a}\right]}\sin\phi$$

$$+ \frac{P}{2\pi\left(\ln\frac{1}{\alpha}\right)^2}\left[\begin{array}{l} \frac{2X\ln\frac{1}{\alpha}}{b}\int_0^\infty \frac{z\sinh Az\cos\Phi z}{\sinh^2 z - X^2z^2}\,dz \\ -\frac{X\left(\frac{b^2}{r^2}-1\right)}{b}\int_0^\infty \frac{z^2\cosh Az\cos\Phi z}{\sinh^2 z - X^2z^2}\,dz \\ +2\left(\ln\frac{1}{\alpha}\right)\frac{a}{r^2}\int_0^\infty \frac{\sinh z\sinh Bz\cos\Phi z}{\sinh^2 z - X^2z^2}\,dz \\ -\frac{\left(1-\frac{a^2}{r^2}\right)}{a}\int_0^\infty \frac{z\sinh z\cosh Bz\cos\Phi z}{\sinh^2 z - X^2z^2}\,dz \end{array}\right] \quad \ldots [31]$$

From the stress function given by Equation [28], the stresses for the problem of Fig. 1(*b*) are found to be

$$\sigma_{r\text{II}} = \sigma_{r1}(b,a,r,\phi,P_1) \quad \ldots [32]$$

$$\sigma_{\phi\text{II}} = \sigma_{\phi 1}(b,a,r,\phi,P_1) \quad \ldots [33]$$

$$\tau_{r\phi\text{II}} = \tau_{r\phi 1}(b,a,r,\phi,P_1) \quad \ldots [34]$$

Following a line of reasoning identical with that used in an earlier paper (2), it is possible to predict the results that will be obtained by evaluating the integrals in Equations [29] to [34] for absolute values of Φ greater than about 2. By Saint Venant's principle, the stresses at one or two beam depths to the right of the loads in Figs. 1(*a*) and (*b*) must be very small. Therefore, considering Equation [30], for example, it is to be expected that for absolute values of Φ greater than about 2, the portion of the expression for $\sigma_{\phi 1}$ containing the integrals (an odd function of ϕ) contributes about the same magnitude of stress as the remaining terms (an even function of ϕ). This must be true if $\sigma_{\phi 1}$ is to approach zero as required, when Φ varies through negative values of increasing magnitude. Furthermore, if the odd function of ϕ and the even function of ϕ in the expression for $\sigma_{\phi 1}$ approximately cancel each other for $\Phi < -2$, it follows that, for $\Phi > 2$, an approximate expression for $\sigma_{\phi 1}$ is

$$(\sigma_{\phi 1})_{\Phi>2} \approx \frac{4Pa\left[b^2 - a^2 - \frac{a^2b^2}{r^2}\ln\frac{b}{a} + b^2\ln\frac{r}{b} + a^2\ln\frac{a}{r}\right]}{(b^2-a^2)^2 - 4a^2b^2\left(\ln\frac{b}{a}\right)^2} + \frac{P\left[3r - \frac{a^2b^2}{r^3} - \frac{b^2+a^2}{r}\right]}{\left[b^2 - a^2 - (b^2+a^2)\ln\frac{b}{a}\right]}\cos\phi \quad \ldots [35]$$

To learn much more about the stresses, it is necessary to evaluate the integrals in Equations [29] to [34].

Evaluation of Stresses

Two different methods have been used for the evaluation of the various integrals required in this paper. These methods, a series method for values of Φ less than unity and the contour integral method for Φ greater than about 0.5 or 1.0, have been discussed at length in previous papers (1, 2). Details of the application of both methods to the integrals occurring in the present paper are given in reference (4). Reference (5) contains tables of values of

$$\frac{1}{2\pi}\int_0^\infty \frac{z\cos \Phi z\, dz}{\sinh z \pm Xz}$$

while values of

$$\frac{1}{2\pi}\int_0^\infty \frac{\cosh z \sin \Phi z\, dz}{\sinh z \pm Xz}$$

i.e., $\lim_{B\to(1^-)} \left\{\frac{1}{2\pi}\int_0^\infty \frac{\cosh Bz \sin \Phi z\, dz}{\sinh z \pm Xz}\right\}$

$$\frac{1}{2\pi}\int_0^\infty \frac{\sin \Phi z\, dz}{\sinh z \pm Xz}$$

$$\frac{1}{2\pi}\int_0^\infty \frac{\sinh Az\, dz}{\sinh z \pm Xz}$$

$$\frac{1}{2\pi}\int_0^\infty \frac{z\cosh Az\, dz}{\sinh z \pm Xz}$$

are tabulated in Appendix 1 of reference (4).

Using the tables of integrals just referred to, the numerical values of stresses for the problems of Figs. 1(a) and (b) may be obtained. The stresses for the problem of Fig. 1(a) will be considered first.

The circumferential normal stress on the inner boundary of Fig. 1(a), obtained by substituting $r = a$ into Equation [30], is

$$(\sigma_{\phi 1})_{r=a} = \frac{P}{b-a}\left\{\frac{2X(\alpha X-1)}{(1+\alpha)(X^2-1)} + \frac{2X(1-\alpha)}{1+\alpha^2-2\alpha X}\cos\phi + \frac{2X}{\pi(1+\alpha)}\left[\int_0^\infty \frac{\cosh z \sin \Phi z\, dz}{\sinh z - Xz} + \int_0^\infty \frac{\cosh z \sin \Phi z\, dz}{\sinh z + Xz} - \alpha\int_0^\infty \frac{\sin \Phi z\, dz}{\sinh z - Xz} + \alpha\int_0^\infty \frac{\sin \Phi z\, dz}{\sinh z + Xz}\right]\right\} \quad [36]$$

On the outer boundary of Fig. 1(a) the circumferential stress is

$$(\sigma_{\phi 1})_{r=b} = \frac{P}{b-a}\left\{\frac{2\alpha X(X-\alpha)}{(1+\alpha)(X^2-1)} - \frac{2\alpha X(1-\alpha)}{1+\alpha^2-2\alpha X}\cos\phi + \frac{2\alpha X}{\pi(1+\alpha)}\left[\alpha\int_0^\infty \frac{\sin \Phi z\, dz}{\sinh z - Xz} + \alpha\int_0^\infty \frac{\sin \Phi z\, dz}{\sinh z + Xz} - \int_0^\infty \frac{\cosh z \sin \Phi z\, dz}{\sinh z - Xz} + \int_0^\infty \frac{\cosh z \sin \Phi z\, dz}{\sinh z + Xz}\right]\right\} \quad [37]$$

It can be shown that, when X approaches unity, i.e., when $\alpha \to 1$, the limiting forms of Equations [36] and [37] agree with the known results for the straight-beam problem (6) corresponding to Fig. 1(a). The demonstration of such agreement depends in part on the fact that

$$\operatorname{Lim}_{X\to(1^+)} \int_0^\infty \frac{\cosh z \sin \Phi z\, dz}{\sinh z - Xz} = \int_0^\infty \left[\frac{\cosh z \sin \Phi z}{\sinh z - z} - \frac{6\Phi}{z^2}\right] dz \quad [38]$$

Values of $(\sigma_{\phi 1})_{r=a}$ for the problem of Fig. 1(a) are plotted in Fig. 4 for four values of α, i.e., for four ratios of inner radius to outer radius of the curved bar. It may be seen that there is an infinite discontinuity in the curves at $\Phi = 0$. This is to be expected because, for the concentration loading of Fig. 1(a), an infinite compressive stress in the circumferential direction is to be anticipated immediately to the right of the load with an infinite tensile stress immediately to the left of the load.

Values of $(\sigma_{\phi 1})_{r=b}$ for four values of α, for the problem of Fig. 1(a), are plotted in Fig. 5.

Although the scales used in Figs. 4 and 5 do not permit this to be shown, the calculations for Figs. 4 and 5 (4) disclose that, for $\Phi = -1$ or approximately one beam depth to the right of the load in Fig. 1(a), the value of $\sigma_{\phi 1}$ on either curved boundary has already decreased to about 2 per cent of $P/(b-a)$ for any value of α between $\alpha = 0.7$ and $\alpha = 1.0$. According to the discussion following Equation [34], the error due to applying Equation [35] to obtain $\sigma_{\phi 1}$ on either boundary at $\Phi = +1$ will also be only about 2 per cent of $P/(b-a)$.

In each of Figs. 4 and 5 one of the cases considered is the case of a straight beam ($\alpha = 1$) which is included for the sake of comparison with the cases of curved bars having $\alpha = 0.9$, $\alpha = 0.8$, and $\alpha = 0.7$. It should be noted that, for a straight beam, letting $x = r\sin\phi$ in Figs. 1(a) and (b)

$$\lim_{\alpha\to 1} \Phi = \lim_{\alpha\to 1} \frac{\phi}{\ln\frac{1}{\alpha}} = \frac{x}{b-a} \quad [39]$$

For a curved bar, Φ is approximately the distance in beam depths measured from $\phi = 0$ along the circle $r = \sqrt{ab}$. The curves in the inserts of Figs. 4 and 5 have been carried to comparatively large values of Φ and this helps in interpreting Φ in terms of an angle ϕ measured in degrees or radians. For example, the point at which the curve for $\alpha = 0.7$ reaches its first extremal value (at $\Phi = 8.808$) in Fig. 4 corresponds to an angle $\phi = 180$ deg for $\alpha = 0.7$. Similarly, $\Phi = 14.079$ corresponds to an angle $\phi = 180$ deg for $\alpha = 0.8$, and $\Phi = 29.818$ corresponds to an angle $\phi = 180$ deg for $\alpha = 0.9$.

So far, only the stresses along the curved boundaries of Fig. 1(a) have been considered. For the same loading, the stresses at the cross section $\Phi = 0$ are

$$(\sigma_{r1})_{\Phi=0} = \frac{-P}{b-a}\frac{X\left[\alpha^2\left(A-\frac{b^2}{r^2}\right)+B\right]}{(1+\alpha)(X^2-1)} + \frac{P}{b-a}\frac{\alpha X\left[(1+\alpha^2)\frac{b}{r} - \alpha^2\frac{b^3}{r^3} - \frac{r}{b}\right]}{(1+\alpha)(1+\alpha^2-2\alpha X)} \quad [40]$$

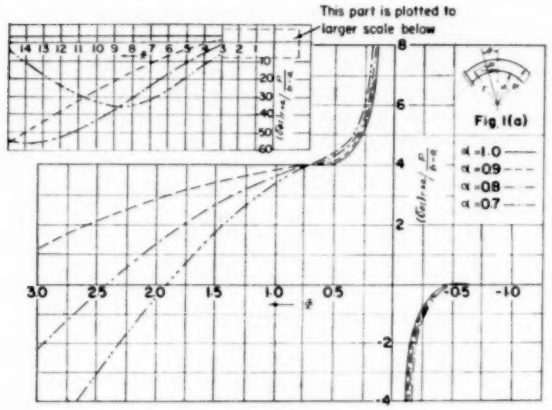

FIG. 4 CIRCUMFERENTIAL NORMAL STRESS, $\sigma_{\phi 1}$, AT INNER BOUNDARY FOR LOADING SHOWN IN FIG. 1(a)

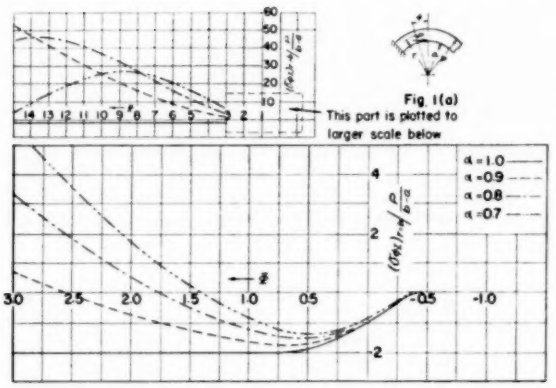

FIG. 5 CIRCUMFERENTIAL NORMAL STRESS, $\sigma_{\phi 1}$, AT OUTER BOUNDARY FOR LOADING SHOWN IN FIG. 1(a)

$$(\sigma_{\phi 1})_{\phi=0} = \frac{-P}{b-a}\,\frac{X\left[\alpha^2\left(A+\frac{b^2}{r^2}\right)+B-2\alpha X\right]}{(1+\alpha)(X^2-1)} + \frac{P}{b-a}\,\frac{\alpha X\left[(1+\alpha^2)\frac{b}{r}+\alpha^2\frac{b^3}{r^3}-3\frac{r}{b}\right]}{(1+\alpha)(1+\alpha^2-2\alpha X)} \quad [41]$$

$$(\tau_{r\phi 1})_{\phi=0} = \frac{P}{b-a}\,\frac{2\alpha X^2}{\pi(1+\alpha)}\left[\int_0^\infty \frac{z\sinh Az}{\sinh^2 z - X^2z^2}\,dz - \frac{\alpha X}{(1-\alpha^2)}\left(\frac{b^2}{r^2}-1\right)\int_0^\infty \frac{z^2\cosh Az}{\sinh^2 z - X^2z^2}\,dz + \frac{\alpha}{X}\,\frac{b^2}{r^2}\int_0^\infty \frac{\sinh z\sinh Bz}{\sinh^2 z - X^2z^2}\,dz - \frac{1}{(1-\alpha^2)}\left(1-\frac{a^2}{r^2}\right)\int_0^\infty \frac{z\sinh z\cosh Bz}{\sinh^2 z - X^2z^2}\,dz\right] \quad [42]$$

Results calculated from Equations [40], [41], and [42] are shown, respectively, in Figs. 6, 7, and 8. The stresses are plotted against $(r-a)/(b-a)$ rather than A because A does not vary linearly with r but instead is related to r by one of Equations [23].

From Fig. 7 it may be seen that the curves of $(\sigma_{\phi 1})_{\phi=0}$ versus $(r-a)/(b-a)$ for $\alpha = 0.7$ to $\alpha = 1.0$ are rather close together. It should be noted that the scale for $(\sigma_{r1})_{\phi=0}$ in Fig. 6 is much larger than the scale for $(\sigma_{\phi 1})_{\phi=0}$ in Fig. 7. Taking this into account, the stresses in Fig. 6 are small compared to those in Fig. 7 and it may be concluded that the stress condition very near to the load in Fig. 1(a) is not a great deal different from that for a straight beam.

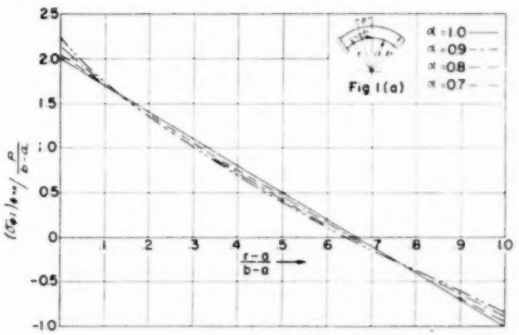

FIG. 7 CIRCUMFERENTIAL NORMAL STRESS, $\sigma_{\phi 1}$, AT SECTION $\Phi = 0$ FOR LOADING SHOWN IN FIG. 1(a)

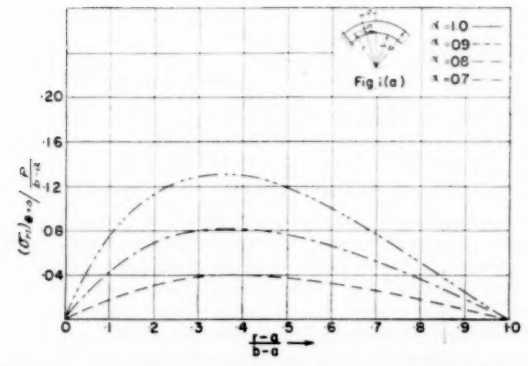

FIG. 6 RADIAL STRESS, σ_{r1}, AT SECTION $\Phi = 0$ FOR LOADING SHOWN IN FIG. 1(a)

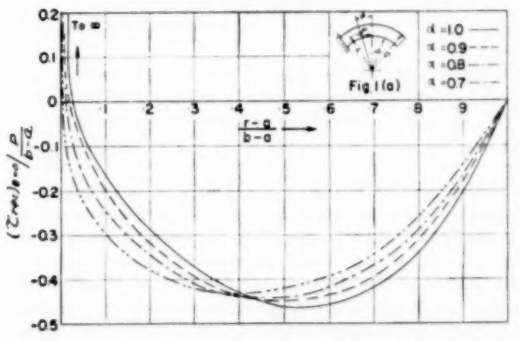

FIG. 8 SHEAR STRESS, $\tau_{r\phi 1}$, AT SECTION $\Phi = 0$ FOR LOADING SHOWN IN FIG. 1(a)

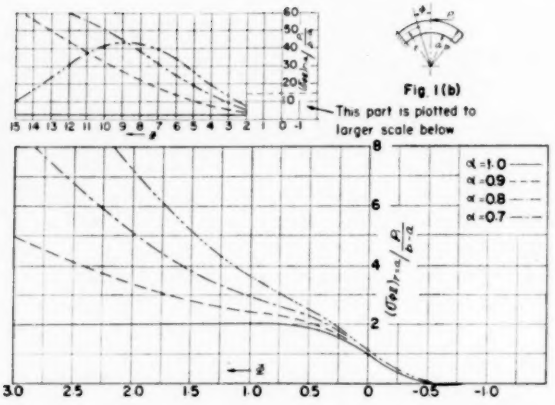

FIG. 9 CIRCUMFERENTIAL NORMAL STRESS, $\sigma_{\phi II}$, AT INNER BOUNDARY FOR LOADING SHOWN IN FIG. 1(*b*)

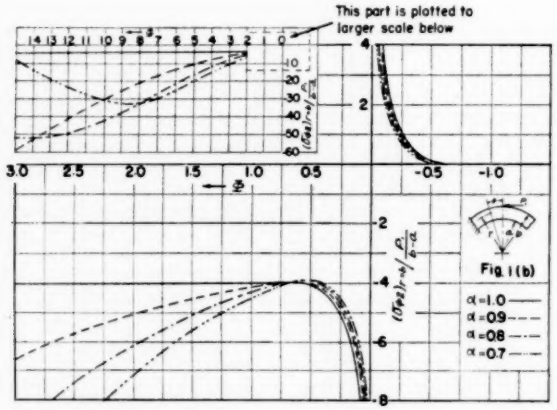

FIG. 10 CIRCUMFERENTIAL NORMAL STRESS, $\sigma_{\phi II}$, AT OUTER BOUNDARY FOR LOADING SHOWN IN FIG. 1(*b*)

The curves of $(\tau_{r\phi I})_{\Phi=0}$ versus $(r-a)/(b-a)$ in Fig. 8 are exactly the same as the corresponding curves would be for a curved bar loaded as in Fig. 2(*b*) because there is zero shear stress on the plane $\Phi = 0$ due to the stress functions ψ_2 and ψ_3 corresponding to Figs. 3(*a*) and (*b*).

Since the stresses have been discussed only for the cross section $\Phi = 0$, it should be pointed out that the stresses at a cross section $\Phi = 0.01$, for example, are much different than the stresses at $\Phi = 0$.

The stresses for the problem of Fig. 1(*b*) are calculated in a manner similar to that used for the problem of Fig. 1(*a*). Figs. 9, 10, 11, 12, and 13 show, respectively, the values of $(\sigma_{\phi II})_{r=a}$, $(\sigma_{\phi II})_{r=b}$, $(\sigma_{rII})_{\Phi=0}$, $(\sigma_{\phi II})_{\Phi=0}$, and $(\tau_{r\phi II})_{\Phi=0}$ again for four values of α.

The graphs of the stresses given in Figs. 4 to 13 appear to be adequate to show the significant features of the stress distributions considered and these graphs probably can be read with sufficient accuracy to permit their use in any machine design problem where correction of stress calculations obtained by approximate formulas commonly used for curved bars appears to be justified. However, if for any reason greater accuracy is desired, tabulated values of the stresses from which the graphs were prepared are available in reference (4).

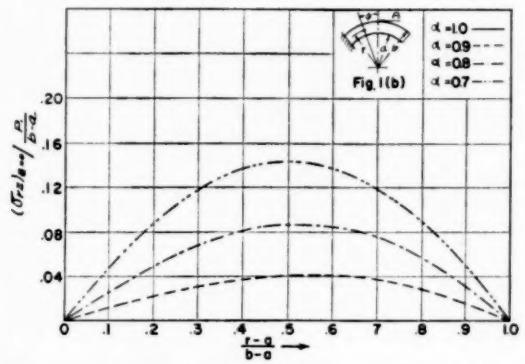

FIG. 11 RADIAL STRESS, σ_{rII}, AT SECTION $\Phi = 0$ FOR LOADING SHOWN IN FIG. 1(*b*)

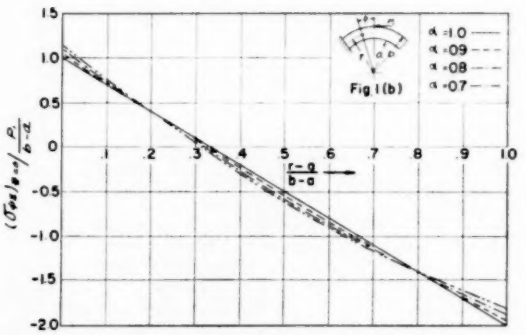

FIG. 12 CIRCUMFERENTIAL NORMAL STRESS, $\sigma_{\phi II}$, AT SECTION $\Phi = 0$ FOR LOADING SHOWN IN FIG. 1(*b*)

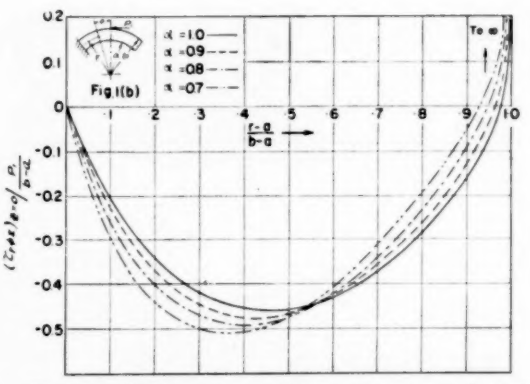

FIG. 13 SHEAR STRESS, $\tau_{r\phi II}$, AT SECTION $\Phi = 0$ FOR LOADING SHOWN IN FIG. 1(*b*)

CONCLUSIONS

The Fourier integral method can be applied to the plane-stress problem of a curved bar loaded by tangential loads on the circular boundaries. By superposition of the solutions presented in this paper and the solutions for a flat curved bar with radial boundary loads (1, 2), the stresses for any concentrated boundary load or any combination of concentrated boundary loads may be obtained. Problems involving distributed shear loads on the circular boundaries of a curved flat bar also may be treated by the procedure used in this paper.

Solutions of idealized problems of the type considered in this paper probably have their greatest value in furnishing a means of checking the adequacy of approximate formulas or in providing correction factors to be applied to approximate formulas. Comparisons with approximate formulas have not been attempted in this paper because it would only be practical to select an example or two from numerous possibilities. Moreover, the demonstration that the formulas derived in this paper reduce approximately to previously known simpler formulas at all cross sections more than one or two beam depths from the loads accomplishes in part the same purpose that would be served by a comparison with approximate formulas.

BIBLIOGRAPHY

1 "A Fourier Integral Solution for the Plane-Stress Problem of a Circular Ring With Concentrated Radial Loads," by C. W. Nelson, JOURNAL OF APPLIED MECHANICS, Trans. ASME, vol. 73, 1951, pp. 173–182.

2 "The Stresses in a Flat Curved Bar Due to Concentrated Radial Loads," by C. W. Nelson, C. J. Ancker, Jr., and Ning-Gau Wu, JOURNAL OF APPLIED MECHANICS, Trans. ASME, vol. 74, 1952, pp. 529–536.

3 "Theory of Elasticity," by S. Timoshenko and J. N. Goodier, McGraw-Hill Book Company, Inc., New York, N. Y., 1951, (*a*) chapter 4, pp. 61–65; (*b*) chapter 4, pp. 73–78.

4 "Stresses in a Flat Curved Bar With Concentrated Boundary Loads," by Ning-Gau Wu, PhD thesis, University of California, Berkeley, Calif., 1952.

5 "Evaluation of Definite Integrals Encountered in Elasticity Problems Involving Curved Flat Bars, I," by C. W. Nelson, Ning-Gau Wu, and C. J. Ancker, Jr., University of California Institute of Engineering Research Report, Series No. 53, Issue No. 1, March, 1952.

6 "On an Approximate Solution for the Bending of a Beam of Rectangular Cross Section Under Any System of Load, With Special Reference to Points of Concentrated or Discontinuous Loading," by L.N.G. Filon, Philosophical Transactions of the Royal Society of London, England, series A, vol. 201, 1903, pp. 63–155.

On the Equations of Motion of Cylindrical Shells[1]

By P. M. NAGHDI[2] AND J. G. BERRY,[3] ANN ARBOR, MICH.

From the basic equations of thin cylindrical shells consistent with Love's first approximation, three uncoupled displacement equations of motion are deduced, the effect of rotary inertia being neglected. Comparison is made with the works of other authors who have used a variety of approximations in arriving at the equations of motion of cylindrical shells. Thus, in a qualitative manner, further insight is gained as to the effectiveness and practicality of these approximations in the solutions of problems of cylindrical shells.

Introduction

THE formulation of the classical theory of thin elastic shells and, in particular, cylindrical shells, has received repeated attention in literature.[4] The basic assumptions used in the classical theory consistent with the conventional assumptions for displacements[5] are: (*a*) the thickness h of the shell is small compared with the least radius of curvature R of the middle surface; (*b*) the strains and displacements are sufficiently small so that quantities of the second and higher orders may be neglected in the components of strain; (*c*) the component of stress normal to the middle surface is small compared with other components of normal stress and may be neglected in the stress-strain relations; and (*d*) the normals to the undeformed middle surface remain normal to the deformed middle surface and suffer no extension. The last two assumptions imply neglect of the transverse normal stress and shear deformation, respectively.

The classical theory of shells in the sense of Love's first approximation (2) is based on the four assumptions mentioned, with a further stipulation that the ratio z/R, Fig. 1, is neglected in comparison with unity in the expressions of both stress-resultants and strain-displacement relations.[6]

A number of writers have modified Love's first approximation by retaining terms involving $(z/R)^2$ in the stress resultants and the strain displacement relations,[7] while others have partially

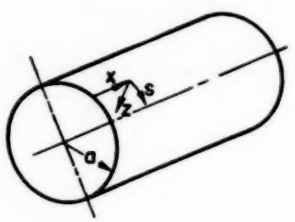

FIG. 1 CO-ORDINATE SYSTEM FOR A CIRCULAR CYLINDRICAL SHELL

or completely abandoned assumptions (*c*) and (*d*) thus accounting wholly or in part for the effect of transverse normal stress and shear deformation.[8]

In the present paper a set of uncoupled displacement equations of motion is obtained for circular cylindrical shells which is consistent with Love's first approximation, the effect of rotary inertia being neglected. Comparison is then made between the resulting characteristic equation and the works of other authors who have employed a variety of approximations in arriving at the coupled equations of motion.

The Co-Ordinate System

The co-ordinate system for a circular cylindrical shell is shown in Fig. 1; the x-axis is directed along the generator of the cylinder, s is measured clockwise in the circumferential direction, and the z-axis is directed inward along the positive normal to the middle surface of the shell. The co-ordinate curves x and s, as lines of curvature, specify position of a point on the middle surface and the square of a linear element for the triply orthogonal co-ordinate system (x, s, z) may be shown to be

$$(ds)^2 = dx^2 + \left(1 - \frac{z}{a}\right)^2 ds^2 + dz^2 \quad \ldots\ldots\ldots [1]$$

where a is the radius of the circular cylinder.

Basic Equations of Thin Circular Cylindrical Shells

In order to make our discussion self-contained, we record here the basic equations for circular cylindrical shells in accordance with the classical theory where the effects of transverse shear deformation and normal stress are neglected. From these, there will be deduced the basic equations commonly known as Love's first approximation.

The stress-resultant and the stress-couple differential equations of equilibrium, which may be obtained from Fig. 2, are

---

[1] The subject matter of this paper was sponsored by the U. S. Naval Ordnance Test Station, Inyokern, China Lake, Calif., and supported by the U. S. Navy Bureau of Ordnance, task assignment NOTS-Re6a-268-11-52.

[2] Associate Professor of Engineering Mechanics, University of Michigan. Assoc. Mem. ASME.

[3] Instructor in Engineering Mechanics, University of Michigan. Assoc. Mem. ASME.

[4] The complete bibliography of the subject is beyond the scope of this paper. For an exposition of the general theory of shells, see reference (1). Numbers in parentheses refer to the Bibliography at the end of the paper.

[5] These are U, V, and W along the x, s, and z-directions, respectively (see Fig. 1): $U(x, s, z) = u(x, s) + zu'(x, s)$, $V(x, s, z) = v(x, s) + zv'(x, s)$, $W(x, s, z) = w(x, s)$ where $u' = -\partial w/\partial x$ and $v' = -(\partial w/\partial s + v/R)$ are consequences of the assumption (*d*).

[6] See Equations [4] and [6] of this paper.

Contributed by the Applied Mechanics Division and presented at the Annual Meeting, New York, N. Y., November 29–December 4, 1953, of THE AMERICAN SOCIETY OF MECHANICAL ENGINEERS.

Discussion of this paper should be addressed to the Secretary, ASME, 29 West 39th Street, New York, N. Y., and will be accepted until July 12, 1954, for publication at a later date. Discussion received after the closing date will be returned.

NOTE: Statements and opinions advanced in papers are to be understood as individual expressions of their authors and not those of the Society. Manuscript received by ASME Applied Mechanics Division April 2, 1953. Paper No. 53—A-34.

[7] References (6) and (7).

[8] References (1), (3), (10), (11), and (12). Reference (1) contains a consistent theory of shells where the effects of both transverse normal stress and shear deformation have been accounted for; also see reference (3).

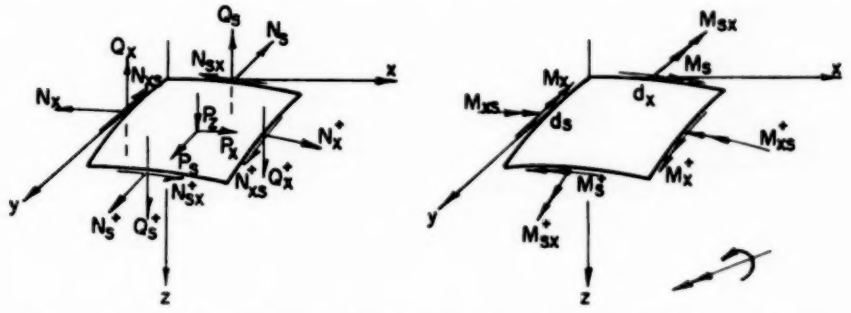

FIG. 2 AN ELEMENT OF CYLINDRICAL SHELL SHOWING STRESS RESULTANTS AND STRESS COUPLES; $N_x^* \equiv N_x + \frac{\partial N_x}{\partial x}\,dx$, $N_s^* \equiv N_s + \frac{\partial N_s}{\partial s}\,ds$, AND SO ON

$$\left.\begin{aligned} \frac{\partial N_x}{\partial x} + \frac{\partial N_{xs}}{\partial s} + p_x &= 0 \\ \frac{\partial N_{xs}}{\partial x} + \frac{\partial N_s}{\partial s} - \frac{Q_s}{a} + p_s &= 0 \\ \frac{\partial Q_x}{\partial x} + \frac{\partial Q_s}{\partial s} + \frac{N_s}{a} + p_z &= 0 \end{aligned}\right\} \quad \ldots\ldots\ldots\ldots [2]$$

and

$$\left.\begin{aligned} \frac{\partial M_x}{\partial x} + \frac{\partial M_{xs}}{\partial S} - Q_x &= 0 \\ \frac{\partial M_{xs}}{\partial x} + \frac{\partial M_s}{\partial s} - Q_s &= 0 \\ N_{xs} - N_{sx} + \frac{M_{xs}}{a} &= 0 \end{aligned}\right\} \quad \ldots\ldots\ldots\ldots [3]$$

where the stress resultants and couples are defined by

$$\left.\begin{aligned} N_x &= \int_{-h/2}^{+h/2} \sigma_x \left(1 - \frac{z}{a}\right) dz, \quad N_s = \int_{-h/2}^{+h/2} \sigma_s\, dz \\ N_{xs} &= \int_{-h/2}^{+h/2} \sigma_{xs} \left(1 - \frac{z}{a}\right) dz, \quad N_{sx} = \int_{-h/2}^{+h/2} \sigma_{sx}\, dz \end{aligned}\right\} \quad [4a]$$

$$Q_x = \int_{-h/2}^{+h/2} \sigma_{xz} \left(1 - \frac{z}{a}\right) dz, \quad Q_s = \int_{-h/2}^{+h/2} \sigma_{sz}\, dz \ldots [4b]$$

$$\left.\begin{aligned} M_x &= \int_{-h/2}^{+h/2} \sigma_x \left(1 - \frac{z}{a}\right) z dz, \quad M_s = \int_{-h/2}^{+h/2} \sigma_s\, z dz \\ M_{xs} &= \int_{-h/2}^{+h/2} \sigma_{xs} \left(1 - \frac{z}{a}\right) z dz, \quad M_{sx} = \int_{-h/2}^{+h/2} \sigma_{sx}\, z dz \end{aligned}\right\} \quad \ldots\ldots\ldots [4c]$$

and p_x, p_s, p_z represent the effective external as well as body forces per unit area of the middle surface of the shell. These may be written as

$$\left.\begin{aligned} p_x &= -\rho h \frac{\partial^2 u}{\partial t^2} + \bar{p}_x \\ p_s &= -\rho h \frac{\partial^2 v}{\partial t^2} + \bar{p}_s \\ p_z &= -\rho h \frac{\partial^2 w}{\partial t^2} + \bar{p}_z \end{aligned}\right\} \quad \ldots\ldots\ldots\ldots [5]$$

where $\bar{p}_x$, $\bar{p}_s$, $\bar{p}_z$ do not involve the displacements u, v, and w and ρ denotes the density.

It may be mentioned that the last equilibrium equation in Equations [3] is merely an identity, and that in the first two of Equations [3] the effect of rotary inertia has been neglected.

The pertinent strain-displacement relations are

$$\left.\begin{aligned} \epsilon_x &= \frac{\partial u}{\partial x} - z \frac{\partial^2 w}{\partial x^2} \\ \epsilon_s &= \frac{1}{\left(1 - \frac{z}{a}\right)} \left[\left(\frac{\partial v}{\partial s} - \frac{w}{a}\right) - z\left(\frac{\partial^2 w}{\partial s^2} + \frac{1}{a}\frac{\partial v}{\partial s}\right)\right] \\ \epsilon_{xs} &= \frac{1}{\left(1 - \frac{z}{a}\right)} \left\{\left(1 - \frac{z}{a}\right)\left[\frac{\partial v}{\partial x}\right.\right. \\ &\quad \left.\left. - z\left(\frac{\partial^2 w}{\partial x \partial s} + \frac{1}{a}\frac{\partial v}{\partial x}\right)\right] + \left[\frac{\partial u}{\partial s} - z\frac{\partial^2 w}{\partial s \partial x}\right]\right\} \end{aligned}\right\} \quad \ldots [6]$$

and the corresponding stress-strain relations are given by

$$\left.\begin{aligned} \sigma_x &= \frac{E}{1 - \nu^2}(\epsilon_x + \nu\epsilon_s) \\ \sigma_s &= \frac{E}{1 - \nu^2}(\epsilon_s + \nu\epsilon_x) \\ \sigma_{xs} &= \frac{E}{2(1 + \nu)}\epsilon_{xs} \end{aligned}\right\} \quad \ldots\ldots\ldots\ldots [7]$$

where E is Young's modulus and ν is Poisson's ratio.

The basic equations of the theory of thin shells in the sense of Love's first approximation may now be deduced if the ratio z/a is neglected in comparison with unity in Equations [1] [4], and [6]. Thus, this approximation affects the stress resultants and stress couples, as well as the components of strain given by Equations [6].

If we write the components of strain in the form

$$\epsilon_x = e_x + z\vartheta_x, \quad \epsilon_s = e_s + z\vartheta_s, \quad \epsilon_{xs} = e_{xs} + z\vartheta_{xs} \ldots [8]$$

then from Equations [6] the membrane strains or components of strain at the middle surface ($z = 0$) are

$$e_x = \frac{\partial u}{\partial x}, \quad e_s = \frac{\partial v}{\partial s} - \frac{w}{a}, \quad e_{xs} = \frac{\partial v}{\partial x} + \frac{\partial u}{\partial s} \ldots\ldots [9]$$

and the expressions for the change of curvatures are given by[9]

$$\vartheta_x = -\frac{\partial^2 w}{\partial x^2}, \quad \vartheta_s = -\frac{1}{a}\frac{\partial v}{\partial s} - \frac{\partial^2 w}{\partial s^2},$$

$$\vartheta_{xs} = -\frac{1}{a}\frac{\partial v}{\partial x} - 2\frac{\partial^2 w}{\partial x \partial s} \quad \ldots\ldots [10]$$

Introducing Relations [7] into the stress resultants, Equations [4a] and the stress couples, Equations [4c], with the appropriate neglect of z/a-terms, performing the required integration, and making use of Relations [8], there results the following stress-strain relations

$$\left.\begin{aligned} N_x &= \frac{Eh}{1-\nu^2}(e_x + \nu e_s) \\ N_s &= \frac{Eh}{1-\nu^2}(e_s + \nu e_x) \\ N_{xs} = N_{sx} &= \frac{Eh}{2(1+\nu)}\, e_{xs} \end{aligned}\right\} \quad \ldots\ldots [11a]$$

$$\left.\begin{aligned} M_x &= D(\vartheta_x + \nu\vartheta_s) \\ M_s &= D(\vartheta_s + \nu\vartheta_x) \\ M_{xs} &= \frac{D(1-\nu)}{2}\,\vartheta_{xs} \end{aligned}\right\} \quad \ldots\ldots [11b]$$

where

$$D = \frac{Eh^3}{12(1-\nu^2)}$$

By Equations [8], [7], and [11], the pertinent components of the stress tensor are given by

$$\left.\begin{aligned} \sigma_x &= \frac{N_x}{h} + \frac{12z}{h^3} M_x \\ \sigma_s &= \frac{N_s}{h} + \frac{12z}{h^3} M_s \\ \sigma_{xs} &= \frac{N_{xs}}{h} + \frac{12z}{h^3} M_{xs} \end{aligned}\right\} \quad \ldots\ldots [12]$$

It should be noted that Q_x and Q_s cannot be obtained from Expressions [4b] since, by virtue of assumption (*d*), σ_{xz} and σ_{sz} have been neglected. However, if Equations [10] are substituted into the first two of Equations [3], the expressions for Q_x and Q_s will result.

The five independent differential equations of equilibrium, namely, Equations [2] and the first two of Equations [3], remain unaltered in the present approximation. However, it is noted that in view of the last of Equations [11a], the identity $N_{xs} - N_{sx} = -M_{sx}/a$ of the last of moment equilibrium, Equations [3], is not satisfied. This discrepancy is due to the approximation introduced and it is difficult to see how this can affect the solution of a specific problem appreciably.

Equations [9], [10], [11], [2], and the first two of Equations [3] constitute 17 equations in the 17 unknowns M_x, M_s, M_{xs}; N_x, N_s, N_{xs}; Q_x, Q_s; e_x, e_s, e_{xs}; ϑ_x, ϑ_s, ϑ_{xs}; and u, v, and w. These equations describe completely the state of stress and deformation of a thin circular cylindrical shell, within the scope of Love's first approximation.

Reduction to Three Partial Differential Equations

We now reduce the 17 equations of the preceding section to three displacement equations of motion as follows: Eliminate Q_x and Q_s from Equations [2] by Equations [3], and using Relations [11], [9], and [10], we arrive at three coupled independent equations involving u, v, and w[10]

$$\frac{\partial^2 u}{\partial x^2} + \frac{(1-\nu)}{2}\frac{\partial^2 u}{\partial s^2} + \frac{(1+\nu)}{2}\frac{\partial^2 v}{\partial x \partial s} - \frac{\nu}{a}\frac{\partial w}{\partial x} + \frac{(1-\nu^2)}{Eh}\, p_x = 0 \quad \ldots\ldots [13a]$$

$$\frac{(1+\nu)}{2}\frac{\partial^2 u}{\partial x \partial s} + \frac{(1-\nu)}{2}(1+k)\frac{\partial^2 v}{\partial x^2} + (1+k)\frac{\partial^2 v}{\partial s^2} - \frac{1}{a}\frac{\partial w}{\partial s} + ka\frac{\partial^3 w}{\partial x^2 \partial s} + ka\frac{\partial^3 w}{\partial s^3} + \frac{(1-\nu^2)}{Eh}\, p_s = 0 \quad \ldots\ldots [13b]$$

$$\frac{\nu}{a}\frac{\partial u}{\partial x} - ka\frac{\partial^3 v}{\partial x^2 \partial s} - ka\frac{\partial^3 v}{\partial s^3} + \frac{1}{a}\frac{\partial v}{\partial s} - ka^2\frac{\partial^4 w}{\partial x^4} - 2ka^2\frac{\partial^4 w}{\partial x^2 \partial s^2} - ka^2\frac{\partial^4 w}{\partial s^4} - \frac{w}{a^2} + \frac{(1-\nu^2)}{Eh}\, p_z = 0 \quad \ldots [13c]$$

where $k = \dfrac{h^2}{12a^2}$.

We shall now uncouple Equations [13] and obtain three equations, one involving u and w, and one v and w, and a single differential equation involving w alone. This may be carried out as follows:

1 Apply the operators $\partial^2/\partial x^2$ and $\partial^2/\partial s^2$ to Equation [13a] independently of one another, and in each case solve for terms containing v.

2 Apply the operator $\partial^2/(\partial x \partial s)$ to Equation [13b] and using the results of the previous step after some combination, the resulting equation becomes

$$\left.\begin{aligned} &(1+k)\nabla^4 u + \frac{(1+\nu)^2}{2(1-\nu)}k\frac{\partial^4 u}{\partial x^2 \partial s^2} - \frac{\nu}{a}\frac{\partial^3 w}{\partial x^3} + \frac{1}{a}\frac{\partial^3 w}{\partial x \partial s^2} \\ &- \frac{k}{a}\left[\nu\frac{\partial^3 w}{\partial x^3} + \frac{2\nu}{(1-\nu)}\frac{\partial^3 w}{\partial x \partial s^2}\right] - \frac{(1+\nu)}{(1-\nu)}ka\left[\frac{\partial^5 w}{\partial x^3 \partial s^2} + \frac{\partial^5 w}{\partial x \partial s^4}\right] \\ &+ \frac{(1+\nu)}{Eh}(1+k)\left[2\frac{\partial^2 p_x}{\partial s^2} + (1-\nu)\frac{\partial^2 p_s}{\partial x^2}\right] - \frac{(1+\nu)^2}{Eh}\frac{\partial^2 p_s}{\partial x \partial s} = 0 \end{aligned}\right\} \quad [14a]$$

[9] It appears that there is no uniformity in literature for the expression of twist ϑ_{xs}. Love (2), Timoshenko (4), and others write $\left[-\frac{2}{a}\frac{\partial v}{\partial x} - 2\frac{\partial^2 w}{\partial x \partial s}\right]$ for the twist when conformed to our notation, while ϑ_{xs} of this paper is in accord with that of reference (1). In the spirit of Love's first approximation, if "the neglect of z/a in comparison with unity" is introduced in both Equations [6] and [4] before deriving Equations [11], then ϑ_{xs} is given by Equation [10]. However, if this approximation is introduced following the substitution of [6] into Equations [4], then ϑ_{xs} would have the form given by Love and Timoshenko; in this connection, see reference (5).

[10] It appears reasonable to neglect $k = h^2/12a^2$ in comparison with unity in Equations [13], but to do so at the present will result in the loss of a number of terms in the uncoupled equations of motion, Equations [15].

where

$$\nabla^4 \equiv \frac{\partial^4}{\partial x^4} + 2\frac{\partial^4}{\partial x^2 \partial s^2} + \frac{\partial^4}{\partial s^4}$$

In an analogous manner and application of the same operators as before to Equations [13*b*] and [13*a*], we arrive at

$$(1+k)\nabla^4 v + \frac{(1+\nu)^2}{2(1-\nu)} k \frac{\partial^4 v}{\partial x^2 \partial s^2} - \frac{(2+\nu)}{a}\frac{\partial^3 w}{\partial x^2 \partial s} - \frac{1}{a}\frac{\partial^3 w}{\partial s^3} + ka\left[\frac{2}{(1-\nu)}\frac{\partial^4 w}{\partial x^4 \partial s} + \frac{(3-\nu)}{(1-\nu)}\frac{\partial^4 w}{\partial x^2 \partial s^3} + \frac{\partial^4 w}{\partial s^5}\right] + \frac{(1+\nu)}{Eh}\left[2\frac{\partial^2 p_s}{\partial x^2} + (1-\nu)\frac{\partial^2 p_s}{\partial s^2}\right] - \frac{(1+\nu)^2}{Eh}\frac{\partial^2 p_x}{\partial x \partial s} = 0 \quad \ldots\ldots [14b]$$

Similarly, by operating on Equation [14*a*] with $\partial/\partial x$ and on Equation [14*b*] with $\partial/\partial s$ and combining these results with that obtained from the application of ∇^4 to Equation [13*c*], there follows

$$\left.\begin{aligned}
&\nabla^8 w + \frac{1}{ka^4}\nabla^4 w - \frac{1}{a^4 k(1+k)}\left\{\nabla^4 w - (1-\nu^2)\frac{\partial^4 w}{\partial x^4}\right. \\
&+ \nu^2 k\left[\frac{\partial^4 w}{\partial x^4} + \frac{2}{(1-\nu)}\frac{\partial^4 w}{\partial x^2 \partial s^2}\right] - ka^2\left[(2+\nu)\frac{\partial^6 w}{\partial x^4 \partial s^2} + (3+\nu)\frac{\partial^6 w}{\partial x^2 \partial s^4}\right. \\
&\left.\left.+ \frac{\partial^8 w}{\partial s^6}\right] - \frac{(1+\nu)^2}{2(1-\nu)} ka\left[\nu\frac{\partial^5 u}{\partial x^2 \partial s^3} + \frac{\partial^5 v}{\partial x^2 \partial s^3}\right]\right\} + \frac{1}{a}\nabla^4\left[\frac{\partial^3 v}{\partial x^2 \partial s} + \frac{\partial^3 v}{\partial s^3}\right] \\
&+ \frac{\nu}{1-\nu}\frac{1}{aD}\left[2\frac{\partial^3 p_x}{\partial x \partial s^2} + (1-\nu)\frac{\partial^3 p_s}{\partial x^3}\right] - \frac{(1+\nu)}{(1-\nu)}\frac{\nu}{aD}\frac{1}{(1+k)}\frac{\partial^3 p_s}{\partial x^2 \partial s} \\
&+ \frac{1}{(1-\nu)}\frac{2}{aD}\frac{1}{(1+k)}\left[\frac{\partial^3 p_s}{\partial x^2 \partial s} + \frac{(1-\nu)}{2}\frac{\partial^3 p_s}{\partial s^3}\right] - \frac{1}{aD}\frac{1}{(1+k)}\frac{(1+\nu)}{(1-\nu)}\frac{\partial^3 p_x}{\partial x \partial s^2} \\
&- \frac{1}{D}\nabla^4 p_s = 0
\end{aligned}\right\} \quad [14c]$$

If we now introduce Equations [5] into Equations [14], we observe that the latter are not as yet uncoupled. The terms containing v and u in Equations [14*a*] and [14*b*], respectively, may be eliminated as follows:

1 Operate on both Equations [13*a*] and [13*b*] with

$$2(1+\nu)\frac{\rho}{E}\frac{\partial^2}{\partial t^2}$$

2 Subtract the results in each case from Equations [14*a*] and [14*b*], respectively, to arrive at Equations [15*a*] and [15*b*].

In Equation [14*c*] the terms involving u and v are

$$\frac{(1+\nu)^2}{2(1-\nu)}\frac{1}{a^3(1+k)}\frac{\partial^4}{\partial x^2 \partial s^2}\left[\nu\frac{\partial u}{\partial x} + \frac{\partial v}{\partial s}\right] + \frac{1}{a}\frac{\partial}{\partial s}(\nabla^6 v) - \frac{\nu}{1-\nu}\frac{\rho h}{aD}\frac{\partial^2}{\partial t^2}\left[2\frac{\partial^3 u}{\partial x \partial s^2} + (1-\nu)\frac{\partial^3 u}{\partial x^3}\right] + \frac{(1+\nu)}{(1-\nu)}\frac{\nu\rho h}{aD}\frac{1}{(1+k)}\frac{\partial^2}{\partial t^2}\left(\frac{\partial^3 v}{\partial x^2 \partial s}\right) - \frac{1}{(1-\nu)}\frac{\rho h}{aD}\frac{1}{(1+k)}\frac{\partial^2}{\partial t^2}\left[2\frac{\partial^3 v}{\partial x^2 \partial s} + (1-\nu)\frac{\partial^3 v}{\partial s^3}\right] + \frac{(1+\nu)}{(1-\nu)}\frac{\rho h}{aD}\frac{1}{(1+k)}\frac{\partial^2}{\partial t^2}\left(\frac{\partial^3 u}{\partial x \partial s^2}\right)$$

and the elimination of these from Equation [14*c*] is accomplished in the following manner:

1 Apply the operator

$$\frac{\nu}{k(1+k)a^3}\frac{\partial}{\partial x}$$

to Equation [14*a*].

2 Apply the operator

$$\frac{1}{k(1+k)a^3}\frac{\partial}{\partial s}$$

to Equation [14*b*].

3 Add the results of steps 1 and 2.

4 Apply the operator

$$\frac{1}{ka^4}\nabla^4$$

to Equation [13*c*] and subtract the result from that of step 3.

5 Subtract the result of step 4 from Equation [14*c*] to obtain Equation [15*c*].

The differential Equations [15] are the uncoupled equations of motion of circular cylindrical shells in the unknowns u, v, and w.[11]

It is clear from the differential Equations [15] that the order of the primitive Equations [13] has been raised from an eighth-order to a sixteenth-order set of partial differential equations. But, since the homogeneous differential equations in u and v associated with Equations [15*a*, *b*] do not yield independent solutions, the result is mathematically consistent with the existence of four boundary conditions at each edge of the cylindrical shell.

[11] Since $k = h^2/(12a^2) << 1$, it now is reasonable to simplify these equations by replacing the quantities $(1+k)$ by unity.

$$(1+k)\nabla^4 u + \frac{(1+\nu)^2}{2(1-\nu)}\, k\, \frac{\partial^4 u}{\partial x^2 \partial s^2} - \frac{(1+\nu)}{E}\rho\frac{\partial^2}{\partial t^2}\left\{(1+k)\left[2\frac{\partial^2 u}{\partial s^2} + (1-\nu)\frac{\partial^2 u}{\partial x^2}\right] + 2\frac{\partial^2 u}{\partial x^2} + (1-\nu)\frac{\partial^2 u}{\partial s^2} - 2\frac{(1-\nu^2)}{E}\rho\frac{\partial^2 u}{\partial t^2}\right\} - \frac{\nu}{a}(1+k)\frac{\partial^3 w}{\partial x^3} + \frac{1}{a}\left(1 - \frac{2\nu}{1-\nu}k\right)\frac{\partial^3 w}{\partial x \partial s^2} - \frac{1+\nu}{1-\nu}ka\left[\frac{\partial^3 w}{\partial x^3 \partial s^2} + \frac{\partial^3 w}{\partial x \partial s^4}\right] + \frac{1+\nu}{E}\rho\frac{\partial^2}{\partial t^2}\left(2\frac{\nu}{a}\frac{\partial w}{\partial x}\right) + \frac{1+\nu}{Eh}(1+k)\left[2\frac{\partial^2 p_s}{\partial s^2} + (1-\nu)\frac{\partial^2 p_x}{\partial x^2}\right] - \frac{(1+\nu)^2}{Eh}\frac{\partial^2 p_s}{\partial x \partial s} - 2\frac{(1+\nu)(1-\nu^2)}{E^2 h}\rho\frac{\partial^2 p_s}{\partial t^2} = 0 \quad \ldots\ldots [15a]$$

$$(1+k)\nabla^4 v + \frac{(1+\nu)^2}{2(1-\nu)}\, k\, \frac{\partial^4 v}{\partial x^2 \partial s^2} - \frac{(1+\nu)}{E}\rho\frac{\partial^2}{\partial t^2}\left\{(1+k)\left[2\frac{\partial^2 v}{\partial s^2} + (1-\nu)\frac{\partial^2 v}{\partial x^2}\right] + 2\frac{\partial^2 v}{\partial x^2} + (1-\nu)\frac{\partial^2 v}{\partial s^2} - 2\frac{(1-\nu^2)}{E}\rho\frac{\partial^2 v}{\partial t^2}\right\} - \frac{1}{a}\frac{\partial^3 w}{\partial s^3} - \frac{2+\nu}{a}\frac{\partial^3 w}{\partial x^2 \partial s} + ka\left[\frac{2}{1-\nu}\frac{\partial^3 w}{\partial x^4 \partial s} + \frac{3-\nu}{1-\nu}\frac{\partial^5 w}{\partial x^2 \partial s^3} + \frac{\partial^5 w}{\partial s^5}\right] - \frac{(1+\nu)}{E}\rho\frac{\partial^2}{\partial t^2}\left[-\frac{2}{a}\frac{\partial w}{\partial s} + 2ka\frac{\partial^3 w}{\partial x^2 \partial s} + 2k\frac{\partial^3 w}{\partial s^3}\right] + \frac{1+\nu}{Eh}\left[2\frac{\partial^2 p_s}{\partial x^2} + (1-\nu)\frac{\partial^2 p_s}{\partial s^2} - (1+\nu)\frac{\partial^2 p_x}{\partial x \partial s}\right] - \frac{2(1+\nu)(1-\nu^2)}{E^2 h}\rho\frac{\partial^2 p_s}{\partial t^2} = 0 \quad \ldots\ldots [15b]$$

$$\nabla^8 w + \frac{1}{a^4}\nabla^4 w + \frac{12(1-\nu^2)}{a^2 h^2}\frac{\partial^4 w}{\partial x^4} - \frac{\nu^2}{a^4}\frac{\partial^4 w}{\partial x^4} + \frac{1+2\nu-3\nu^2}{2(1-\nu)a^4}\frac{\partial^4 w}{\partial x^2 \partial s^2} + \frac{2}{a^2}\left[(2+\nu)\frac{\partial^6 w}{\partial x^4 \partial s^2} + (3+\nu)\frac{\partial^6 w}{\partial x^2 \partial s^4} + \frac{\partial^6 w}{\partial s^6}\right] - k\left[\frac{2}{(1-\nu)}\frac{\partial^6}{\partial x^4 \partial s^2}(\nabla^2 w) + \frac{3-\nu}{1-\nu}\frac{\partial^6}{\partial x^2 \partial s^4}(\nabla^2 w) + \frac{\partial^6}{\partial s^6}(\nabla^2 w) - \frac{(1+\nu)^2}{2(1-\nu)}\frac{\partial^4}{\partial x^2 \partial s^2}(\nabla^4 w)\right] + \frac{\rho h}{aD}\frac{\partial^2}{\partial t^2}\left\{a\nabla^4 w + \frac{ka}{2}\frac{(1+\nu)^2}{(1-\nu)}\frac{\partial^4 w}{\partial x^2 \partial s^2} + k^2 a^3\frac{(1+\nu)^2}{(1-\nu)}\frac{\partial^2}{\partial x^2}(\nabla^4 w) + \frac{k(1+\nu)}{a(1-\nu)}\frac{\partial^2 w}{\partial x^2} - \frac{4ka}{(1-\nu)}\frac{\partial^2}{\partial s^2}(\nabla^2 w) + \frac{2k^2 a^3}{(1-\nu)}\frac{\partial^2}{\partial s^2}(\nabla^4 w) - \frac{(3-\nu+2k)}{a(1-\nu)}(\nabla^2 w) - \frac{ka^3(3-\nu+2k)}{(1-\nu)}(\nabla^6 w) + \frac{2\nu^2}{a(1-\nu)}\frac{\partial^2 w}{\partial x^2} + \frac{2}{a(1-\nu)}\frac{\partial^2 w}{\partial s^2} + ka(1+\nu)^2\frac{\rho}{E}\frac{\partial^2}{\partial x^2}\left(\frac{\partial^2 w}{\partial t^2}\right) - a(1+\nu)(3-\nu+2k)\frac{\rho}{E}\nabla^2\left(\frac{\partial^2 w}{\partial t^2}\right) + 2ka^3(1+\nu)\frac{\rho}{E}\nabla^4\left(\frac{\partial^2 w}{\partial t^2}\right) + \frac{2(1+\nu)}{a}\frac{\rho}{E}\frac{\partial^2 w}{\partial t^2} + 2a(1+\nu)(1-\nu^2)\left(\frac{\rho}{E}\right)^2\frac{\partial^4 w}{\partial t^4} - \frac{ka(1+\nu)^2}{Eh}\frac{\partial^2 p_s}{\partial x^2} + \frac{2ka^2(1+\nu)}{Eh}\frac{\partial}{\partial s}(\nabla^2 p_s) + \frac{a(1+\nu)(3-\nu+2k)}{Eh}\nabla^2 p_z - \frac{2a(1+\nu)(1-\nu^2)}{Eh}\left(\frac{\rho}{E}\right)\frac{\partial^2 p_z}{\partial t^2} - \frac{2(1+\nu)}{Eh}\left(\nu\frac{\partial p_z}{\partial x} + \frac{\partial p_s}{\partial s}\right)\right\} + \frac{1}{aD}\left\{-\frac{\partial^3 p_z}{\partial x \partial s^2} + \nu\frac{\partial^3 p_z}{\partial x^3} + (2-\nu)\frac{\partial^3 p_s}{\partial x^2 \partial s} + \frac{\partial^3 p_s}{\partial s^3} - a\nabla^4 p_s\right\} + \frac{1}{aEh}\left\{-2(1+\nu)\frac{\partial^3}{\partial x^2 \partial s}(\nabla^2 p_s) + (1-\nu^2)\frac{\partial^3}{\partial s^3}(\nabla^2 p_s) - \frac{2(1+\nu)^3}{a}\frac{\partial^4 p_z}{\partial x^2 \partial s^2}\right\} = 0 \quad \ldots\ldots [15c]$$

Discussion and Comparison With Works of Other Authors

In order to verify, at least partially, the results of Equations [15], let the displacements u, v, and w be of the form

$$\left.\begin{aligned} u &= \sum_{n=0}^{\infty} A_n e^{\lambda x/a}\cos\frac{ns}{a}e^{ipt} \\ v &= \sum_{n=1}^{\infty} B_n e^{\lambda x/a}\sin\frac{ns}{a}e^{ipt} \\ w &= \sum_{n=0}^{\infty} C_n e^{\lambda x/a}\cos\frac{ns}{a}e^{ipt} \end{aligned}\right\} \quad \ldots\ldots [16]$$

Substitution of Equations [16] into the primitive differential Equations [13], in the absence of quantities denoted by p_x, p_s, and p_z, yields three equations in the coefficients A_n, B_n, and C_n. The characteristic equation obtained by setting the determinant of these coefficients equal to zero is identical with the characteristic equation which may be obtained directly from Equation [15c]. If, in the characteristic equation, the quantities $(1+k)$ are replaced by unity, then there results

$$\lambda^8 - \left[4n^2 - \frac{(3-\nu)}{(1-\nu)}\gamma p^2\right]\lambda^6 + \left[6n^4 - 2(2+\nu)n^2 + \frac{1-\nu^2}{k} - \gamma p^2\left(\frac{3(3-\nu)}{1-\nu}n^2 + \frac{1}{k}\right) + \frac{2}{1-\nu}\gamma^2 p^4\right]\lambda^4 - \left[4n^6 - 2(3+\nu)n^4 + \frac{5+3\nu}{2}n^2 - \gamma p^2\left(\frac{3(3-\nu)}{1-\nu}n^4 + \frac{2n^2}{k} + \frac{3+2\nu}{k}\right) + \gamma^2 p^4\left(\frac{3-\nu}{1-\nu}\frac{1}{k} + \frac{4}{1-\nu}n^2\right)\right]\lambda^2 + \left[n^8 - 2n^6 + n^4 - \gamma p^2\left(\frac{3-\nu}{1-\nu}n^6 + \frac{n^4}{k} + \frac{n^2}{k}\right) + \gamma^2 p^4\left(\frac{3-\nu}{1-\nu}\frac{n^2}{k} + \frac{2}{1-\nu}n^4 + \frac{2}{(1-\nu)k}\right) - \frac{2}{(1-\nu)k}\right]\gamma^2 p^6 = 0 \quad [17]$$

where

$$\gamma = \frac{(1-\nu^2)}{E}\rho a^2$$

The characteristic equation associated with the differential Equations [15] when the displacements are independent of time may be obtained from Equation [17] by putting the terms involving p^2 equal to zero. Thus

$$\lambda^8 - 4n^2\lambda^6 + \left[\frac{1-\nu^2}{k} + 6n^4 - 2(2+\nu)n^2\right]\lambda^4 + \left[-4n^6 + 2(3+\nu)n^4 - \frac{5+3\nu}{2}n^2\right]\lambda^2 + [n^8 - 2n^6 + n^4] = 0 \quad [18]$$

Since the characteristic equation is relatively easy to obtain, it furnishes a convenient basis for comparison with the results (equations of motion) given by other authors. To be consistent, in the comparisons that follow, quantities of the type $(1 + k)$ will be replaced by unity. Also, the displacements will be assumed to have the form of Equations [16].

Flügge (6) and Byrne (7) retain terms of the order $(z/a)^2$ as compared to one in the stress resultants [4] and strain-displacements relation [6], which results in the following characteristic equation when the displacements are independent of time.[12]

$$\lambda^8 - 2(2n^2 - \nu)\lambda^6 + \left[\frac{1-\nu^2}{k} + 6n^4 - 6n^2\right]\lambda^4 + [-4n^6 + 2(4-\nu)n^4 - 2(2-\nu)n^2]\lambda^2 + [n^8 - 2n^6 + n^4] = 0 \quad [19]$$

Comparison of Equations [18] and [19] reveals that retaining terms of the order $(z/a)^2$ in Equations [4] and [6] may result only in a small effect[13] in the equations of motion.

If, in the second of Equations [2], the term $\frac{Q_s}{a}$ is neglected as compared with the other terms, and at the same time, the expressions for the change of curvatures are simplified to read

$$\vartheta_x = -\frac{\partial^2 w}{\partial x^2}, \quad \vartheta_s = -\frac{\partial^2 w}{\partial s^2}, \quad \vartheta_{xs} = -2\frac{\partial^2 w}{\partial x \partial s} \quad [20]$$

then the resulting characteristic equation associated with the equations of motion is

$$\lambda^8 + \left[-4n^2 + \frac{3-\nu}{1-\nu}\gamma p^2\right]\lambda^6 + \left[6n^4 + \frac{1-\nu^2}{k} - \gamma p^2\left(\frac{3(3-\nu)}{1-\nu}n^2 + \frac{1}{k}\right) + \frac{2}{1-\nu}\gamma^2 p^4\right]\lambda^4 + \left[-4n^6 + \gamma p^2\left(\frac{3+2\nu}{k} + \frac{2n^2}{k} + \frac{3(3-\nu)}{1-\nu}n^4\right) - \gamma^2 p^4\left(\frac{4n^2}{1-\nu} + \frac{3-\nu}{(1-\nu)k}\right)\right]\lambda^2 + \left[n^8 - \gamma p^2\left(\frac{3-\nu}{1-\nu}n^6 + \frac{n^4}{k} + \frac{n^2}{k}\right) + \gamma^2 p^4\left(\frac{2n^4}{1-\nu} + \frac{2}{(1-\nu)k} + \frac{3-\nu}{1-\nu}\frac{n^2}{k}\right) - \frac{2}{(1-\nu)}\frac{1}{k}\gamma^2 p^6\right] = 0 \quad [21]$$

Although this type of approximation[14] leading to the characteristic Equation [21] has been justly used in special cases (9), its validity, in general, is questionable. In fact, comparison of Equations [17] and [21] indicates that the present approximation has left unaltered the terms involving time explicitly. It is the complicated form of these terms which gives rise to most of the practical difficulty encountered in the solution of vibration problems of shells.

In formulating a theory of shells, Vlasov (10) at first partially abandons assumptions (*c*) and (*d*) and retains terms of the order $(z/a)^2$ as compared to one in the stress resultants and the strain-displacement relations. Later, by simplifying his work, the resulting equations of motion fall within the assumptions of the classical theory, and the characteristic equation for cylindrical shells becomes[15]

$$\lambda^8 + \left[-4n^2 + 2\nu + \frac{3-\nu}{1-\nu}\gamma p^2\right]\lambda^6 + \left[6n^4 + \frac{1-\nu^2}{k} - (4+\nu)n^2 + 1 + \gamma p^2\left(-\frac{1}{k} - \frac{3(3-\nu)}{(1-\nu)}\frac{n^2}{k}\right) + \frac{2}{(1-\nu)}\gamma^2 p^4\right]\lambda^4 + \left[-4n^6 + (8-\nu)n^4 - 2n^2 + \gamma p^2\left(\frac{3(3-\nu)}{1-\nu}n^4 - 2(3+\nu)n^2 + \frac{2n^2}{k} + \frac{3+2\nu}{k}\right) + \gamma^2 p^4\left(-\frac{3-\nu}{(1-\nu)k} - \frac{4n^2}{1-\nu}\right)\right]\lambda^2 + \left[n^8 - 2n^6 + n^4 + \gamma p^2\left(-\frac{3-\nu}{1-\nu}n^6 + \frac{3-\nu}{1-\nu}n^2 - \frac{n^4}{k} - \frac{n^2}{k}\right) + \gamma^2 p^4\left(\frac{2n^4}{1-\nu} - \frac{4n^2}{1-\nu} + \frac{3-\nu}{(1-\nu)k}n^2 + \frac{2}{(1-\nu)k} + \frac{2}{(1-\nu)}\right) - \frac{2}{(1-\nu)k}\gamma^3 p^6\right] = 0 \quad [22]$$

It appears that there are only minor differences between Equations [17] and [22] and these are essentially in the terms involving p^2 in the coefficients of λ^2 and the last bracket.

Finally, we compare the characteristic Equation [17] with that of Kennard's recent paper (11) which is based on the work of Epstein (12). Kennard's simplified equations of motion[16] yield the following characteristic equation

$$\lambda^8 + \left[-4n^2 + \frac{3-\nu}{1-\nu}\gamma p^2\right]\lambda^6 + \left[6n^4 + \frac{1-\nu^2}{k} - \frac{4-\nu}{2(1-\nu)}n^2 + \frac{2+\nu}{2(1-\nu)} + \gamma p^2\left(-\frac{3(3-\nu)}{1-\nu}n^2 - \frac{1}{k}\right) + \frac{2}{1-\nu}\gamma^2 p^4\right]\lambda^4 + \left[-4n^8 + \frac{8-8\nu-3\nu^2}{2(1-\nu)}n^4 - \frac{(2+\nu)(2-3\nu)}{2(1-\nu)}n^2 + \gamma p^2\frac{3(3-\nu)}{1-\nu}n^4 - \frac{(4-\nu)(3-\nu)}{2(1-\nu)^2}n^2 + \frac{2n^2}{k} + \frac{3+2\nu}{k} + \frac{(2+\nu)(3-\nu)}{2(1-\nu)^2}\right) + \gamma^2 p^4\left(-\frac{3-\nu}{(1-\nu)k} - \frac{4n^2}{1-\nu}\right)\right]\lambda^2 + \quad [23]$$

[12] See equation (78), reference (6), p. 125.

[13] One should recall that replacing $(1 + k)$ by unity does not nullify the effect of retaining the $(z/a)^2$ terms; compare equations (11), reference (6), p. 118, with Equations [13] of this paper.

[14] Yuan's equation (6a), reference (8), may be obtained directly with this approximation; his characteristic equation is identical with Equation [21] of this paper when $p^2 = 0$.

[15] See table 2 of reference (10).

[16] Equations [22] of reference (11).

$$\left[n^8 - 2n^6 + n^4 + \gamma p^2 \left(-\frac{3-\nu}{1-\nu} n^6 - \frac{(4+\nu)(3-\nu)}{2(1-\nu)^2} n^4 - \frac{(3-\nu)(2-\nu)}{2(1-\nu)^2} n^2 - \frac{n^4}{k} - \frac{n^2}{k} \right) + \gamma^2 p^4 \left(-\frac{4-\nu}{(1-\nu)^2} n^2 + \frac{2+\nu}{(1-\nu)^2} + \frac{2n^4}{1-\nu} + \frac{(3-\nu)n^2}{(1-\nu)k} + \frac{2}{(1-\nu)k} \right) - \frac{2}{1-\nu^2} \gamma^3 p^6 \right] = 0 \quad \ldots\ldots\ldots\ldots\ldots\ldots [23]$$

As in the previous case, the minor differences between Equations [17] and [23] are in the terms involving p^2 in the coefficients of λ^2 and the last bracket. It is noteworthy that there is a close agreement between Vlasov's Equation [22] and Equation [23].

Conclusion

We have not succeeded in arriving at definite conclusions concerning the relative merits of the different approximations used by various authors in the classical theory of shells. However, on the basis of comparisons made, at least for cylindrical shells, there appears to be little advantage in going beyond Love's first approximation. Indeed, any true improvement of the theory beyond Love's first approximation should take into account the effect of shear deformation and transverse normal stress (1).

BIBLIOGRAPHY

1 "Notes on the Foundations of the Theory of Small Displacements of Orthotropic Shells," by F. B. Hildebrand, E. Reissner, and G. B. Thomas, NACA TN 1833, 1949.

2 "A Treatise on the Mathematical Theory of Elasticity," by A. E. H. Love, fourth edition, Dover Publications, New York, N. Y., 1944, chapter 24.

3 "The Equilibrium of Thin Elastic Shells," by A. E. Green and W. Zerna, *Quarterly Journal of Mechanics and Applied Mathematics*, vol. 3, March, 1950, pp. 9–22.

4 "Theory of Plates and Shells," by S. Timoshenko, McGraw-Hill Book Company, Inc., New York, N. Y., 1940, chapter 88.

5 "Note on the Expressions for the Strains in a Bent Thin Shell," by Eric Reissner, *American Journal of Mathematics*, vol. 64, 1942, pp. 768–772.

6 "Statie und Dynamik der Schalen," by W. Flügge, Edwards Bros., Inc., Ann Arbor, Mich., 1943.

7 "Theory of Small Deformations of a Thin Elastic Shell," by Ralph Byrne, Jr., Seminar Reports in Mathematics, University of California, Los Angeles, Calif., 1944.

8 "Thin Cylindrical Shells Subjected to Concentrated Loads," by S. W. Yuan, *Quarterly of Applied Mathematics*, vol. 4, 1946, pp. 13–26.

9 "Stability of Thin-Walled Tubes Under Torsion," by L. H. Donnell, NACA Report No. 479, 1933.

10 "Basic Differential Equations in General Theory of Elastic Shells," by V. S. Vlasov, NACA TM 1241 Translation, 1951.

11 "The New Approach to Shell Theory: Circular Cylinders," by E. H. Kennard, Journal of Applied Mechanics, Trans. ASME, vol. 75, 1953, pp. 33–40.

12 "On the Theory of Elastic Vibrations in Plates and Shells," by P. S. Epstein, *Journal of Mathematics and Physics*, vol. 21, 1942, pp. 198–208.

Free and Forced Vibrations of an Infinitely Long Cylindrical Shell in an Infinite Acoustic Medium[1]

By H. H. BLEICH[2] and M. L. BARON,[3] NEW YORK, N. Y.

The paper presents a general method for the treatment of free and forced-vibration problems of infinitely long thin cylindrical shells. Surprisingly simple results are obtained by utilizing the known and tabulated modes of the shell in vacuo as generalized co-ordinates describing the response of the shell. The frequencies of free vibrations of submerged shells are obtained, and the response of the shell and medium to sinusoidally distributed, periodic, radial forces is determined. The results indicate that there is a low-frequency range where no radiation occurs and a high-frequency range where energy is radiated. Free vibration, or resonance in the case of forced vibrations, occurs only in the low-frequency range. The results of the paper may be applied to obtain the response to arbitrarily distributed, periodic, or nonperiodic forces by expanding such forces in Fourier series and/or integrals. The results for free and forced vibrations are discussed in general and for the specific case of steel shells in water. Tables are provided to facilitate numerical computations. With limitations the method is also applicable to ring-stiffened shells, and to the case of a static pressure in the surrounding medium.

Nomenclature

The following nomenclature is used in the paper:

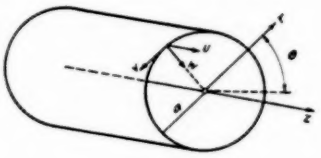

Fig. 1

θ, z, r = cylindrical co-ordinates, Fig. 1

u, v, w = longitudinal, tangential, and radial displacements of cylindrical shell, Fig. 1. Note that a positive displacement w is inward

U_k, V_k, W_k = coefficients defining shape of modes in vacuo, Equation [1]

$\phi_{u,k}$ $\phi_{v,k}$ ϕ_w = u, v, and w-components of displacement pertaining to generalized co-ordinate q_k, Equations [2] and [3].

k = 1, 2, 3 = subscript

a = radius of cylinder

C_k = coefficient

c = velocity of sound in medium

dA = element of surface area of shell

$F(r)$ = r-dependent function in expression for potential

$H_n^{(1)}, H_n^{(2)}$ = Hankel functions of first and second kind

i = $\sqrt{-1}$

L = length of longitudinal half wave of mode of vibration

M_k = generalized mass (co-ordinate q_k)

m = mass of shell per unit area

m_e = virtual mass of entrained medium

N, N_{ww}, N_{ee} = coefficients, see Equations [40], [46]

n = number of circumferential waves of mode of vibration

$P = P(t, \theta, z) = \cos n\theta \sin \frac{\pi z}{L} e^{i\Omega t}$ = external radial force (positive if outward)

p = pressure in medium

p_a = radial pressure of medium on cylinder

p_0 = static pressure in medium

Q_k = generalized force (co-ordinate q_k)

q_k = generalized co-ordinate

R = large value of the radius r

$S(t)$ = time dependent function in expression for potential

t = time

w_{st} = w due to static force

$\alpha_k = \frac{W_k^2}{U_k^2 + V_k^2 + W_k^2}$ = coefficient

$\beta, \bar{\beta}$ = see Equations [19], [37]

Δ = coefficient, see Equations [26], [30], [38], and Tables 1 and 2

ρ = mass density of medium

$\Phi = S(t)F(r) \cos n\theta \sin \frac{\pi z}{L}$ = potential function

Ω = frequency of free or forced vibration of shell surrounded by medium

ω_k = frequency of shell in vacuo

Introduction

Problems of vibrations of infinitely long cylindrical shells in an acoustic medium have been considered by Junger (1, 2, 3).[4] In the first two papers the assumption is made that the generators of the shell remain straight, leading to a plane problem. In the third paper the three-dimensional case is considered, but the complex interaction problem of shell and fluid is avoided by assuming that

[1] This paper is a result of investigations sponsored by the Office of Naval Research under Contract Nonr-266(08).

[2] Professor of Civil Engineering, Columbia University. Mem. ASME.

[3] Assistant Professor of Civil Engineering, Columbia University.

Contributed by the Applied Mechanics Division and presented at the Annual Meeting, New York, N. Y., November 29–December 4, 1953, of The American Society of Mechanical Engineers.

Discussion of this paper should be addressed to the Secretary, ASME, 29 West 39th Street, New York, N. Y., and will be accepted until July 12, 1954, for publication at a later date. Discussion received after the closing date will be returned.

Note: Statements and opinions advanced in papers are to be understood as individual expressions of their authors and not those of the Society. Manuscript received by ASME Applied Mechanics Division, March 27, 1953 Paper No. 53—A-37.

[4] Numbers in parentheses refer to the Bibliography at the end of the paper.

the shell has known displacements (functions of time and space), and then solving for the sound field. This treatment discloses the properties of the acoustic field but does not permit the determination of the response of the shell to external forces without further analysis. To obtain this response of the shell it is necessary to solve the wave equation simultaneously with appropriate equations describing the behavior of the shell. The purpose of the present paper is the solution of this general problem for the three-dimensional case.

In so far as the shell is concerned the approach used differs basically from the one used by Junger for the plane interaction problem. The present paper utilizes the modes of vibration of the shell in vacuo as generalized co-ordinates, while reference (2) expresses the displacements of the shell in Fourier series. It is believed that the mode approach is very much simpler than the alternative one, in part due to the fact that the modes in vacuo are already available in tabular form. The mode approach also is directly applicable to certain types of stiffened shells.

The emphasis of the present paper lies in the structural response of the shell, and the acoustical phases are considered secondary. However, to understand the structural response it was necessary to go into certain acoustical details, like radiating and non-radiating frequency ranges. The paper considers first the free vibrations of a submerged shell and then the forced vibrations caused by radial forces. By way of illustration the analysis is applied to cases of steel shells in water. The results obtained can be utilized for the solution of any dynamic problem of cylindrical shells.

Free Vibrations

The free and forced vibrations of a submerged, infinitely long, thin cylindrical shell are studied in this paper by considering the shell without the fluid as a separate structure responding to the applied forces combined with the dynamic forces exerted by the surrounding infinite acoustic medium. Using the modes of free vibration of the shell in vacuo as generalized co-ordinates, its response can be expressed in terms of the infinite number of these modes.

The frequencies and modes of vibrations of infinitely long thin cylindrical shells required for the purpose were determined in reference (4). The individual modes can be classified by the length L of the longitudinal half wave of the displacements and by the integral number n of circumferential waves. For each length L and number n there exist three frequencies $\omega_k (k = 1, 2, 3)$. The displacements of the modes corresponding to all three frequencies are sinusoidal, but the ratios of longitudinal, circumferential, and radial displacements, u, v, and w differ. Excluding the case $n = 0$, the displacements corresponding to the frequency ω_k may be written

$$\left.\begin{aligned} u &= U_k \cos n\theta \cos \frac{\pi z}{L} \\ v &= V_k \sin n\theta \sin \frac{\pi z}{L} \\ w &= W_k \cos n\theta \sin \frac{\pi z}{L} \end{aligned}\right\} \quad \ldots\ldots\ldots\ldots [1]$$

The modes defined in Equations [1] contain an arbitrary factor; only the ratios V_k/U_k and W_k/U_k can be determined and are contained in reference (4). It also might be mentioned that Equations [1] can be generalized by adding phase angles, which is equivalent to changing the origin of the co-ordinates θ and z.

The most general response of a cylindrical shell will be a combination of the modes for all values of L and n. However, in order to find for a submerged shell the frequencies and modes of free vibration of selected values L and n, one need consider only the three modes of shape, Equations [1], having the same parameters L and n. This simplification is due to the fact that the wave equation for the surrounding medium has a solution containing the factor $\cos n\theta \sin \pi z/L$, and the pressure belonging to such a solution does not excite modes of different values L or n.

Selecting the coefficients W_k in Equations [1] as generalized co-ordinates $W_k = q_k$, and using the abbreviations

$$\left.\begin{aligned} \phi_{u,k} &= \frac{U_k}{W_k} \cos n\theta \cos \frac{\pi z}{L} \\ \phi_{v,k} &= \frac{V_k}{W_k} \sin n\theta \sin \frac{\pi z}{L} \\ \phi_w &= \cos n\theta \sin \frac{\pi z}{L} \end{aligned}\right\} \quad \ldots\ldots\ldots\ldots [2]$$

the displacements u, v, and w can be expressed as functions of the three generalized co-ordinates q_1, q_2, q_3

$$u = q_1\phi_{u,1} + q_2\phi_{u,2} + q_3\phi_{u,3} \quad \ldots\ldots\ldots\ldots [3a]$$

$$v = q_1\phi_{v,1} + q_2\phi_{v,2} + q_3\phi_{v,3} \quad \ldots\ldots\ldots\ldots [3b]$$

$$w = (q_1 + q_2 + q_3)\phi_w \quad \ldots\ldots\ldots\ldots [3c]$$

The symbol ϕ_w in Equations [2] and [3] does not have a second subscript, as there is no difference in the w-displacements of the three co-ordinates q_k.

Owing to the inherent orthogonality between the displacements represented by the generalized co-ordinates, the equations of motion contain each only one of the co-ordinates q_k

$$M_k\ddot{q}_k + M_k\omega_k^2 q_k = Q_k \quad (k = 1, 2, 3) \quad \ldots\ldots [4]$$

where the generalized mass M_k is

$$M_k = \iint_A m(\phi_{u,k}^2 + \phi_{v,k}^2 + \phi_w^2)dA \quad \ldots\ldots [5]$$

In the case of free vibrations the generalized force Q_k is due solely to the radial pressure p_a of the medium on the cylinder at $r = a$

$$Q_k = \iint_A p_a\phi_w dA \quad \ldots\ldots [6]$$

Hence Equation [4] becomes

$$\ddot{q}_k + \omega_k^2 q_k = \frac{\iint_A p_a\phi_w dA}{m\iint_A (\phi_{u,k}^2 + \phi_{v,k}^2 + \phi_w^2)dA} \quad \ldots\ldots [7]$$

The integrals in Equations [5] to [7] are to be taken over the surface of a section of the cylindrical shell of length L.

The shell is assumed to be submerged in an acoustic medium, the velocity potential Φ for which is governed by the equation

$$\nabla^2\Phi = \frac{1}{c^2}\frac{\partial^2\Phi}{\partial t^2} \quad \ldots\ldots [8]$$

A solution of this equation suitable for the present problem is

$$\Phi = S(t)F(r)\cos n\theta \sin \frac{\pi z}{L} = S(t)F(r)\phi_w \quad \ldots\ldots [9]$$

where $S(t)$ and $F(r)$ are functions at our disposal. At the surface of the shell ($r = a$), the radial velocity of the shell must equal that of the medium

$$\dot{w} = -\frac{\partial\Phi}{\partial r}\Big]_{r=a} \quad \ldots\ldots [10]$$

Substituting Equations [3c] and [9] one obtains

$$(\dot{q}_1 + \dot{q}_2 + \dot{q}_3)\phi_w = -S(t)F'(a)\phi_w$$

or

$$S(t) = \frac{-(\dot{q}_1 + \dot{q}_2 + \dot{q}_3)}{F'(a)} \quad [11]$$

where

$$F'(a) = \frac{dF(r)}{dr}\Big]_{r=a}$$

The radial pressure exerted on the shell by the surrounding medium is the pressure at $r = a$

$$p_a = -\rho \frac{\partial \Phi}{\partial t}\Big]_{r=a} = -\rho \dot{S}(t)F(a)\phi_w \quad [12]$$

or substituting Equation [11]

$$p_a = \rho \frac{F(a)}{F'(a)} \phi_w(\ddot{q}_1 + \ddot{q}_2 + \ddot{q}_3) \quad [13]$$

Equations [6] and [7] become

$$Q_k = \rho \frac{F(a)}{F'(a)} (\ddot{q}_1 + \ddot{q}_2 + \ddot{q}_3) \int\int_A \phi_w^2 dA \quad [14]$$

and

$$\ddot{q}_k + \omega_k^2 q_k = \frac{\rho \alpha_k}{m} \frac{F(a)}{F'(a)} (\ddot{q}_1 + \ddot{q}_2 + \ddot{q}_3) \quad [15]$$

where

$$\alpha_k = \frac{\int\int_A \phi_w^2 dA}{\int\int_A (\phi_{u,k}^2 + \phi_{v,k}^2 + \phi_w^2) dA} = \frac{W_k^2}{U_k^2 + V_k^2 + W_k^2} \quad [16]$$

The last equation is obtained by substituting Equations [2] Numerical values of U_k, V_k, and W_k for various modes are given in the tables of reference (4).

The function $F(r)$ is obtained from Equation [8], which reads in full

$$\frac{\partial^2 \Phi}{\partial r^2} + \frac{1}{r}\frac{\partial \Phi}{\partial r} + \frac{1}{r^2}\frac{\partial^2 \Phi}{\partial \theta^2} + \frac{\partial^2 \Phi}{\partial z^2} = \frac{1}{c^2}\frac{\partial^2 \Phi}{\partial t^2} \quad [8a]$$

Assuming periodic solutions for the generalized co-ordinates q_k

$$q_k = C_k e^{i\Omega t} \quad [17]$$

Equations [9] and [11] give

$$\Phi = -i\Omega \frac{F(r)}{F'(a)} \phi_w(C_1 + C_2 + C_3) e^{i\Omega t} \quad [18]$$

Introducing the symbol

$$\beta = \sqrt{\frac{\pi^2}{L^2} - \frac{\Omega^2}{c^2}} \quad [19]$$

Equations [8a] and [18] lead to the differential equation

$$F''(r) + \frac{1}{r}F'(r) - \left(\beta^2 + \frac{n^2}{r^2}\right) F(r) = 0 \quad [20]$$

As boundary conditions we require that the velocity of the medium at $r = \infty$ vanishes in such a manner that the kinetic energy in the medium remains finite

$$r^{1+\epsilon} F(r)]_{r=\infty} = 0 \quad [21]$$

where $\epsilon > 0$ is a small number.

A solution of Equation [20] is

$$F(r) = H_n^{(1)}(i\beta r) \quad [22]$$

which satisfies Equation [21] provided the real part of β is positive.

Computing

$$F'(r) = i\beta \left[\frac{-n}{i\beta r} H_n^{(1)}(i\beta r) + H_{n-1}^{(1)}(i\beta r)\right] \quad [23]$$

and

$$\frac{F(a)}{F'(a)} = \frac{-a}{n - i\beta a \dfrac{H_{n-1}^{(1)}(i\beta a)}{H_n^{(1)}(i\beta a)}} \quad [24]$$

Equation [15] becomes

$$\ddot{q}_k + \omega_k^2 q_k = -\frac{\rho a}{2m} \alpha_k \Delta(\ddot{q}_1 + \ddot{q}_2 + \ddot{q}_3) \quad [25]$$

where

$$\Delta = \Delta(\beta a) = \frac{-2}{a}\frac{F(a)}{F'(a)} = \frac{2}{n - i\beta a \dfrac{H_{n-1}^{(1)}(i\beta a)}{H_n^{(1)}(i\beta a)}} \quad [26]$$

Substituting Equations [17] into [25], three homogeneous equations in the coefficients C_k are obtained

$$(\omega_k^2 - \Omega^2)C_k - \alpha_k \frac{\rho a}{2m} \Omega^2 \Delta(C_1 + C_2 + C_3) = 0 \quad (k = 1, 2, 3) \quad [27]$$

Nonvanishing solutions of these equations exist only if their determinant vanishes, which after evaluation leads to the frequency equation

$$\frac{\alpha_1}{\omega_1^2 - \Omega^2} + \frac{\alpha_2}{\omega_2^2 - \Omega^2} + \frac{\alpha_3}{\omega_3^2 - \Omega^2} = \frac{2m}{\rho a \Omega^2 \Delta} \quad [28]$$

valid for $n \neq 0$.

For the previously excluded case, $n = 0$, the cylindrical shell in vacuo has again three modes for each value L and n. One of these modes is, however, a purely torsional motion with displacement components $u = w = 0$. This mode is not excited by the radial forces from the surrounding medium, and only the two nontorsional modes need be considered. Instead of Equation [25] one obtains for $n = 0$

$$\ddot{q}_k + \omega_k^2 q_k = -\frac{\rho a}{2m} \alpha_k \Delta(\ddot{q}_1 + \ddot{q}_2) \quad [29]$$

where

$$\Delta = -2 \frac{iH_0^{(1)}(i\beta a)}{\beta a H_1^{(1)}(i\beta a)} \quad [30]$$

The frequency equation for $n = 0$ is

$$\frac{\alpha_1}{\omega_1^2 - \Omega^2} + \frac{\alpha_2}{\omega_2^2 - \Omega^2} = \frac{2m}{\rho a \Omega^2 \Delta} \quad [31]$$

The solution of the frequency Equations [28] and [31] is further discussed in a later section.

Forced Vibrations Due to Radial Forces

Any arbitrarily distributed radial force $P(t, \theta, z)$ can be expanded in a Fourier integral (or series) of terms

$$P(t, \theta, z) = e^{i\Omega t} \cos n\theta \sin \frac{\pi z}{L} = e^{i\Omega t} \phi_w \quad [32]$$

The following treatment will be restricted to the consideration of such individual terms, i.e., to force components $P(t, \theta, z)$ defined by Equation [32]. These forces P are counted positive if acting outward. Nonradial forces can be treated in a similar manner but will not be considered.

Equations [4] and [5] apply again, but Equation [6] for the generalized force Q_k must be replaced by

$$Q_k = \int p_a \phi_w dA - \int e^{i\Omega t} \phi_w^2 dA \quad [33]$$

Proceeding essentially in the same manner as before, using Equations [8] to [13] inclusive, and Equations [16] to [24] inclusive, the equations of motion for $n \neq 0$ become

$$\ddot{q}_k + \omega_k^2 q_k = -\frac{\rho a}{2m} \alpha_k \Delta(\bar{q}_1 + \bar{q}_2 + \bar{q}_3) - \frac{\alpha_k}{m} e^{i\Omega t} \quad (k = 1, 2, 3) \quad [34]$$

There is just one detail in the derivation of this equation which requires elucidation. The solution Equation [22]

$$F(r) = H_n^{(1)}(i\beta r)$$

does not satisfy the boundary Condition [21] for frequencies $\Omega > \pi c/L$ because the argument

$$a\beta = a\sqrt{\frac{\pi^2}{L^2} - \frac{\Omega^2}{c^2}}$$

becomes purely imaginary. The boundary Condition [21] is in this case replaced by the requirement that the potential function Equation [18]

$$\Phi = -\frac{i\Omega}{F'(a)} (C_1 + C_2 + C_3) e^{i\Omega t} F(r) \phi_w \quad [35]$$

represents an outgoing wave for large values of r. This condition is satisfied for

$$F(r) = H_n^{(2)}(\bar{\beta} r) \quad [36]$$

where

$$\bar{\beta} = \sqrt{\frac{\Omega^2}{c^2} - \frac{\pi^2}{L^2}} \quad \left(\Omega \geq \frac{\pi c}{L}\right) \quad [37]$$

and the positive sign of the square root applies. This leads to the value

$$\Delta = \Delta(\bar{\beta} a) = -\frac{2}{a} \frac{F(a)}{F'(a)} = \frac{2}{n - \bar{\beta} a \dfrac{H_{n-1}^{(2)}(\bar{\beta} a)}{H_n^{(2)}(\bar{\beta} a)}} \quad [38]$$

valid for $\Omega \geq \pi c/L$, while for $\Omega \leq \pi c/L$ Equation [26] remains in force.

Substitution of Equation [17]

$$q_k = C_k e^{i\Omega t}$$

in the equations of motion, Equation [34], leads to three nonhomogeneous linear equations for the coefficient C_k. Their solution is

$$C_k = \frac{\dfrac{\alpha_k}{\omega_k^2 - \Omega^2}}{m\left(\dfrac{\rho a}{2m} N\Delta - 1\right)} \quad [39]$$

where

$$N = \frac{\alpha_1 \Omega^2}{\omega_1^2 - \Omega^2} + \frac{\alpha_2 \Omega^2}{\omega_2^2 - \Omega^2} + \frac{\alpha_3 \Omega^2}{\omega_3^2 - \Omega^2} \quad [40]$$

Substituting the values C_k from Equation [39] into the Expression [18] for the potential function Φ and noting Equations [26], [32], and [38] lead to

$$\Phi = \frac{i\Omega a \Delta}{2m} \left[\frac{1}{\dfrac{\rho a}{2m} \Omega^2 \Delta - \dfrac{\Omega^2}{N}}\right] \frac{F(r)}{F(a)} P(t, \theta, z) \quad [41]$$

where the function $F(r)$ is given by Equations [22] and [36], respectively

$$F(r) = \begin{cases} H_n^{(1)}(i\beta r) & \text{if } \Omega < \dfrac{\pi c}{L} \quad [42a] \\ r^{-n} & \text{if } \Omega = \dfrac{\pi c}{L} \text{ and } n \neq 0 \quad [42b] \\ H_n^{(2)}(\bar{\beta} r) & \text{if } \Omega > \dfrac{\pi c}{L} \quad [42c] \end{cases}$$

Δ, β, and $\bar{\beta}$ are defined by Equations [19], [26], [37], and [38].

The pressure in the medium, $p = -\rho \partial\Phi/\partial t$, becomes

$$p = \frac{1}{1 - \dfrac{2m}{\rho a N \Delta}} \frac{F(r)}{F(a)} P(t, \theta, z) \quad [43]$$

The pressure p_a on the surface of the shell is

$$p_a = \frac{P(t, \theta, z)}{1 - \dfrac{2m}{\rho a N \Delta}} \quad [43a]$$

The knowledge of the coefficients C_k permits also the determination of the displacements of the shell. Of particular interest are the radial displacements w obtained from Equation [3c]

$$w = \frac{1}{m\Omega^2} \frac{P(t, \theta, z)}{\left[\dfrac{\rho a}{2m} \Delta - \dfrac{1}{N}\right]} \quad [44]$$

If one goes to the limit $\Omega \to 0$ this equation gives an expression for the deflection w_{st} under static loading $P(\theta, z) = \phi_w$

$$w_{st} = \lim_{\Omega \to 0} w = -\left[\frac{\alpha_1}{\omega_1^2} + \frac{\alpha_2}{\omega_2^2} + \frac{\alpha_3}{\omega_3^2}\right] \frac{P}{m} \quad [44a]$$

while a similar process for the pressure leads to the obvious result

$$\lim_{\Omega \to 0} p = 0$$

The expressions for the longitudinal and tangential displacements u and v due to the radial force $P(t, \theta, z)$ are somewhat more complicated

$$\left.\begin{aligned} u &= \frac{N_{uw}}{mN\Omega^2}\,\frac{\cos n\theta\,\cos\dfrac{\pi z}{L}\,e^{i\Omega t}}{\dfrac{\rho a}{2m}\,\Delta - \dfrac{1}{N}} \\ v &= \frac{N_{vw}}{mN\Omega^2}\,\frac{\sin n\theta\,\sin\dfrac{\pi z}{L}\,e^{i\Omega t}}{\dfrac{\rho a}{2m}\,\Delta - \dfrac{1}{N}} \end{aligned}\right\} \quad \ldots\ldots\ldots [45]$$

where

$$\left.\begin{aligned} N_{uw} &= \sum_{k=1}^{3} \frac{\alpha_k \dfrac{U_k}{W_k}\,\Omega^2}{\omega_k^2 - \Omega^2} \\ N_{vw} &= \sum_{k=1}^{3} \frac{\alpha_k \dfrac{V_k}{W_k}\,\Omega^2}{\omega_k^2 - \Omega^2} \end{aligned}\right\} \quad \ldots\ldots\ldots [46]$$

Equations [40] to [46], were derived for the case $n \neq 0$, but with exception of Equation [42*b*], they remain valid for $n = 0$ if the terms referring to the nonexisting frequency ω_3 are omitted when computing N, N_{uw}, and N_{vw} from Equations [40] to [46].

The degenerate solutions [42*b*] for $n = 0$ and for $n = 1$ do not satisfy Equation [21] and the total kinetic energy in the medium is in these cases not finite. This indicates that steady-state vibrations for $n = 0$ or 1 in an actually infinite medium are not possible if $\Omega = \pi c/L$. If one considers the infinite boundary of the medium as an approximation of a far boundary, $r = R$, the solution [42*b*] for $n = 1$ may be considered an approximation of physical meaning because the energy is then finite and the velocities at the boundary are small, as $1/R$. A similar reasoning does not apply for $n = 0$, because the longitudinal velocity $\partial\Phi/\partial z$ is not small for large values of r; the physical impossibility of this solution expresses itself in the fact that $\Delta = \infty$. To obtain a physical meaningful solution for $n = 0$ it is necessary to consider the actual conditions at the distant boundary.

To facilitate numerical computations, Tables 1 and 2 list the values of Δ occurring in Equations [41] to [46] for $n = 0$ to 4, inclusive.[5]

TABLE 1 VALUES OF Δ if $\Omega \leq \pi c/L$

$a\beta = a\sqrt{\frac{\pi^2}{L^2} - \frac{\Omega^2}{c^2}}$	$n = 0$	$n = 1$	$n = 2$	$n = 3$	$n = 4$
0	∞	2.000	1.000	0.667	0.500
0.1	4.928	1.952	0.997	0.666	0.4998
0.2	3.670	1.863	0.990	0.664	0.499
0.4	2.551	1.661	0.965	0.658	0.497
0.6	1.989	1.473	0.929	0.648	0.493
0.8	1.640	1.312	0.888	0.635	0.487
1.0	1.399	1.177	0.844	0.619	0.481
1.5	1.028	0.928	0.737	0.575	0.460
2.0	0.814	0.761	0.645	0.528	0.436
3.0	0.577	0.556	0.505	0.443	0.385
4.0	0.447	0.437	0.411	0.375	0.338
5.0	0.365	0.360	0.344	0.322	0.298
6.0	0.309	0.305	0.296	0.281	0.264
7.0	0.267	0.265	0.259	0.249	0.237
8.0	0.236	0.234	0.230	0.223	0.214
9.0	0.211	0.210	0.206	0.201	0.195
10.0	0.191	0.190	0.187	0.184	0.179

NOTE: Asymptotic expression valid for all values of n: $\Delta = \dfrac{4}{2\beta a + 1}$

Discussion of Frequency Equation

The discussion can be restricted to the frequency equation

$$\frac{\alpha_1}{\omega_1^2 - \Omega^2} + \frac{\alpha_2}{\omega_2^2 - \Omega^2} + \frac{\alpha_3}{\omega_3^2 - \Omega^2} = \frac{2m}{\rho a \Omega^2 \Delta} \quad \ldots\ldots [28]$$

as the case $n = 0$, Equation [31] may be obtained by substituting $\alpha_3 = 0$. This equation is transcendental, the parameter Δ being a transcendental function of the frequency Ω.

Number of Real Roots of Frequency Equation. The parameter Δ is actually a function of

$$a\beta = a\sqrt{\frac{\pi^2}{L^2} - \frac{\Omega^2}{c^2}} \quad \ldots\ldots\ldots\ldots [47]$$

and examination shows that the values of Δ are real if $a\beta$ is real, but that Δ becomes complex if $\Omega > \pi c/L$, so that $a\beta$ is imaginary. This leads to the question how many real roots Ω Equation [28] will furnish. The coefficients α_k and the frequencies ω_k on the left-hand side of Equation [28] being real, the entire left-hand side will always be real. As $(2m)/(\rho a)$ is also real, Equation [28] can have no real solution for Ω when $a\beta$ is imaginary, that is, any real root Ω must be below the limit $\Omega \leq \pi c/L$.

Further information on the number of real roots can be obtained by considering Equation [28] graphically. For $n \neq 0$, Fig. 2 shows in solid lines a typical plot of the values of the left-hand side of Equation [28] as function of Ω. Starting with a positive value for $\Omega = 0$, the plot shows vertical asymptotes for each of the values $\Omega = \omega_1$, ω_2, and ω_3. The right-hand side of Equation [28] is plotted in dashed lines, the intersections indicating roots of the frequency equation. As the right-hand side has real values only for $0 \leq \Omega \leq \pi c/L$ the curve ends at point E. The plot indicates that there are at least as many real roots Ω as there are frequencies ω_k of the system in vacuo which lie below

[5] Values of Δ for $n \leq 20$ can be obtained from reference (1) but only if $\Omega > \pi c/L$. The acoustic reactance and resistance ratios χ_n and θ_n shown in figs. 1 and 2 of reference (1) can be used to compute $\frac{1}{2}\,a\beta\Delta = \chi_n(a\beta) - i\theta_n(a\beta)$. For a limited number of ratios L/a, reference (3) contains curves giving the values of Δ as function of $a\Omega/c$.

TABLE 2 VALUES OF Δ if $\Omega \geq \pi c/L$

$a\beta = a\sqrt{\frac{\Omega^2}{c^2} - \frac{\pi^2}{L^2}}$	$n = 0$	$n = 1$	$n = 2$	$n = 3$	$n = 4$
0	$\infty - \pi i$	2.000	1.000	0.667	0.500
0.1	4.774−3.052 i	2.048−0.032 i	1.003−0.000 i	0.667−0.000 i	0.500−0.000 i
0.2	3.339−2.879 i	2.135−0.131 i	1.010−0.0003 i	0.669−0.000 i	0.501−0.000 i
0.4	1.974−2.479 i	2.250−0.530 i	1.045−0.005 i	0.676−0.0000 i	0.503−0.000 i
0.6	1.297−2.117 i	2.092−1.040 i	1.107−0.026 i	0.688−0.0002 i	0.508−0.000 i
0.8	0.908−1.820 i	1.684−1.383 i	1.196−0.082 i	0.708−0.0014 i	0.514−0.000 i
1.0	0.666−1.584 i	1.244−1.478 i	1.293−0.199 i	0.738−0.0051 i	0.523−0.0008 i
1.5	0.354−1.176 i	0.570−1.253 i	1.271−0.753 i	0.858−0.0547 i	0.559−0.0018 i
2.0	0.216−0.925 i	0.303−0.988 i	0.760−1.025 i	1.010−0.270 i	0.628−0.016 i
2.5	0.145−0.759 i	0.185−0.801 i	0.392−0.913 i	0.918−0.655 i	0.740−0.086 i
3.0	0.103−0.642 i	0.124−0.669 i	0.221−0.759 i	0.570−0.812 i	0.837−0.292 i
4.0	0.060−0.489 i	0.067−0.502 i	0.095−0.546 i	0.184−0.632 i	0.465−0.684 i
5.0	0.039−0.394 i	0.042−0.401 i	0.053−0.425 i	0.081−0.471 i	0.161−0.550 i
10.0	0.010−0.199 i	0.010−0.200 i	0.011−0.203 i	0.012−0.209 i	0.014−0.217 i

NOTE: Asymptotic expression valid for all values of n: $\Delta(a\beta) = \dfrac{4}{1 + 2ia\beta}$

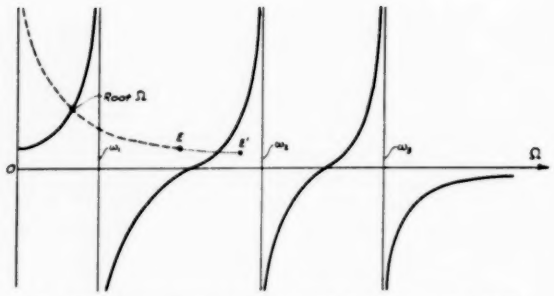

FIG. 2 ILLUSTRATION OF FREQUENCY EQUATION FOR $n \neq 0$

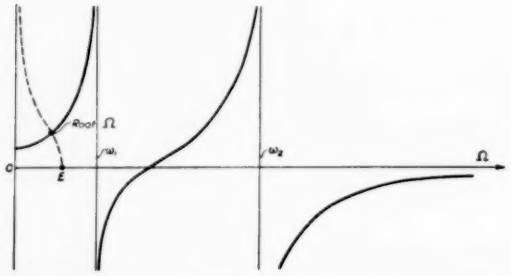

FIG. 3 ILLUSTRATION OF FREQUENCY EQUATION FOR $n = 0$

$\pi c/L$, and at the most one more. This latter case can occur if there is a further frequency ω_k just larger than $\pi c/L$, so that the end point falls in a position like E' in Fig. 2. If in particular all frequencies ω_k are larger than $\pi c/L$, there may be no real frequency at all. The case of no real root will occur only for mediums having very low density ρ.

For $n = 0$ somewhat similar conditions prevail, Fig. 3. In this case the end point E lies, however, on the Ω-axis, which results in the occurrence of one real root in all cases, even if $\omega_1 > \pi c/L$. An example of such a case is a steel shell in water vibrating with a half-wave length $L > a$.

It is also apparent from Figs. 2 and 3 that the lowest root Ω_1 of the frequency equation must be smaller than the frequency ω_1, while the next root Ω_2, if any, must lie between ω_1 and ω_2, and the highest root must be between ω_2 and ω_3. No root can lie above the highest frequency ω_3 in vacuo.

Attention is drawn to the fact that due to the orthogonality of the modes q_k of the shell in vacuo

$$\alpha_1 + \alpha_2 + \alpha_3 = 1 \quad \ldots\ldots\ldots\ldots\ldots\ldots [48]$$

As a rule, one, and for many configurations, two values α_k are quite small, indicating that the radial displacements of such modes are small. In such cases the coupling of the motion of the shell and the surrounding medium is slight, and the frequencies Ω of such modes will be very close to the frqeuencies ω in vacuo.

To simplify the numerical determination of the roots of the frequency equation, Table 1, giving values of Δ for real arguments $a\beta$, has been provided. After a frequency Ω has been obtained the shape of the mode can be determined by computing the coefficient C_k from Equation [27].

Effect of Compressibility. It is of considerable interest to consider the effect of the compressibility in order to determine when it might be neglected. The compressibility appears in the derivation of Equation [8] where the velocity of sound c occurs, and the solution for an incompressible fluid may be obtained by using $c = \infty$. This does not change the frequency Equation [28], but the argument $a\beta$ used in determining the term Δ in this equation is in this case

$$a\beta = \frac{a\pi}{L} \quad \ldots\ldots\ldots\ldots\ldots\ldots [49]$$

instead of the value given in Equation [47] which depended on the frequency Ω. Comparing Equations [47] and [49], it is apparent that the compressibility may be neglected only if $\Omega/c \ll \pi/L$.

If the compressibility is neglected the number of real roots Ω is always equal to the number of frequencies ω_k. It is obvious that roots higher than $\pi c/L$ found for the incompressible case are unreal.

Complex Roots of Frequency Equation. The fact that the number of real roots Ω of the frequency equation may be smaller than the number of frequencies ω_k in vacuo raises the question of the existence of complex roots in lieu of the missing real roots, and of the physical meaning of complex roots, if any. In order to have physical meaning the solution corresponding to a complex root Ω must represent an outgoing wave and must also decay with time.

In order to recognize the wave character of the solution it is convenient to use the potential function in the form Equation [36], employed previously for $\Omega > \pi c/L$

$$\Phi = Ce^{i\Omega t} H_n^{(2)}(\bar{\beta} r)\phi_n \quad \ldots\ldots\ldots\ldots\ldots\ldots [50]$$

To avoid incoming waves the real part of $\bar{\beta}$ must not be negative. Based on this expression one obtains a "wave-frequency equation," which is identical with Equations [28] or [31], except that the value Δ is a function of $a\bar{\beta}$ and must be computed from Equation [38] instead of Equation [26]. It is to be noted that the argument $a\bar{\beta}$ in Equation [38] will now be complex. A study of the potential Function [50] indicates that for complex roots Ω for which the time-dependent term $e^{i\Omega t}$ is damped, the term $H_n^{(2)}(\bar{\beta} r)$ becomes ∞ at $r \to \infty$. Such roots and the corresponding solutions appear at first to have no physical significance. It should be pointed out, however, that these complex roots and the corresponding solutions occur and have significance as "asymptotic solutions" in transient problems. In such cases the validity of the asymptotic solution is limited to finite values of r and the fact that $H_n^{(2)}(\bar{\beta} r)$ does become infinite at $r \to \infty$ is immaterial. For example, a heavy shell in a light medium, like air, is capable of slightly damped vibrations. The frequency equation in such a case has complex roots Ω the real parts of which are close to the frequencies ω_k in vacuo, while the imaginary parts are quite small. Expression [50] is then the approximation of a possible motion, valid in the range $t > T$ and $r < R$, where T must be selected so large that the transient effects of the initiation of the motion have passed outside the cylinder having the arbitrarily selected radius R.

The numerical values of complex frequencies Ω can be determined easily approximately if, either the imaginary part of Ω is small, or if $|\Omega|$ is large. If the imaginary part of Ω is small the value of $\Delta(a\bar{\beta})$ computed for the adjoining real part of Ω, found in Table 2, may be used. This procedure would be applicable for the foregoing case of a heavy shell in a light medium. If the absolute value of the frequency $|\Omega|$ is large such that the argument $|a\bar{\beta}| \gg 1$, the term $\Delta(a\bar{\beta})$ may be determined by using asymptotic expressions for the Hankel functions

$$\Delta(a\bar{\beta}) = \frac{4}{1 + 2ia\bar{\beta}} \quad \ldots\ldots\ldots\ldots\ldots\ldots [51]$$

Frequently it is permissible to neglect even the real part of the denominator in this equation, giving

$$\Delta(a\bar{\beta}) = -\frac{2i}{a\bar{\beta}} \quad \ldots\ldots\ldots\ldots\ldots\ldots [52]$$

These approximations apply for all values of n but give better results for small values of n. A measure of the degree of approximation can be obtained by comparing the results of Equations [51] and [52] with the values for real arguments $a\bar{\beta}$ in Table 2.

Virtual Mass. For $n \neq 0$ it is possible to simplify the frequency equation by neglecting the two higher modes, thus obtaining an approximate equation for the lowest frequency. This equation can then be interpreted in a simple manner using the concept of the "virtual mass" of the entrained medium.

The numerical values of ω_k and the values U_k, V_k, and W_k to compute α_k required in Equation [28] are given in reference (4). These values indicate that wi hin the range $1 \leqslant L/a \leqslant 10$ the first term of Equation [28], $\alpha_1/(\omega_1^2 - \Omega^2)$, is very much larger than the other two if $\Omega < \omega_1$; for L/a values near 1 this is so because α_2 and α_3 are small, for larger L/a values because ω_2^2 and ω_3^2 are very much larger than ω_1^2. Neglecting the terms with α_2 and α_3 leads after rearrangement to

$$\Omega^2 \left(1 + \frac{\alpha_1 \rho a}{2m} \Delta\right) = \omega_1^2 \ldots\ldots\ldots\ldots\ldots [53]$$

This indicates that the lowest frequency Ω of the submerged shell is equal to the frequency of a shell in vacuo whose mass has been increased by the virtual mass m_v of a portion of the medium vibrating with it

$$m_v = \alpha_1 \frac{\rho a}{2} \Delta \ldots\ldots\ldots\ldots\ldots\ldots [54]$$

Δ is a function of the frequency given by Equations [19] and [26], but if $\omega_1 \ll \pi c/L$ the effect of the frequency is negligible and Equation [49] for the incompressible case may be used instead of Equation [19]. m_v may be computed quickly by the use of Table 1.

The same approach can be used also for $n = 0$ but gives good results only if $L/a < 2$. For longer shells the second term in Equation [31] remains large and cannot be neglected, thus making the simple virtual mass concept inapplicable.

Steel Shells Submerged in Water. When applying the frequency equations to thin steel shells (say, $a/t > 30$) submerged in an infinite body of water, it is found that for ratios $1 \leqslant L/a \leqslant 10$ and $n > 1$, one and only one frequency in vacuo is lower than $\pi c/L$, while for $n = 0$, all frequencies ω_k are above this limit.[6] It follows that for $n = 0$ one and only one real root Ω exists; for $n > 0$ there is at least one root and, according to the previous discussion, the possibility of a second one. A second root Ω can only occur, see E' in Fig. 3, if the second frequency ω_2 is close to $\pi c/L$. Reference (4) shows that in the range $1 \leqslant L/a \leqslant 10$ the second frequency ω_2 is much larger than the limit $\pi c/L$, and there will therefore be just "one real frequency" for each value of n.[7] This frequency can be determined from the simplified Equation [53], except if $n = 0$ and $L/a > 2$.

Similar conditions prevail for ratios $L/a > 10$, except for $n \geqslant 2$, where for extremely large ratios, due to the effect of the bending stiffness of the shell, all the frequencies in vacuo may lie above $\pi c/L$, resulting in no real roots. In the limiting case $L = \infty$ only complex roots occur for any value of n. This case has been discussed independently in reference (5).

If $L/a < 1$ the foregoing result is expected to remain valid, unless the length of the half wave is so short, comparable to the thickness t, that all frequencies in vacuo lie above $\pi c/L$.

Complex roots of the frequency equation representing waves exist and can be determined approximately by using the asymptotic values for $\Delta(a\bar{\beta})$, Equation [52]. However, the solutions corresponding to the complex roots lack physical meaning, except as asymptotic solutions of transient problems discussed in the previous section. In the case of a steel shell in water where $1 \leqslant L/a \leqslant 10$, the asymptotic solution is a combination of the free vibration, corresponding to the real frequency Ω, and of damped wave motions corresponding to the complex roots Ω. If the motion is such that the undamped motion is at all excited, the asymptotic solution converges rapidly toward the undamped vibration of real frequency Ω, and the damped motions due to complex frequencies will give only unimportant contributions.

Discussion of Results for Forced Vibrations

Response of Shell and Medium. The most significant feature of the results of section Forced Vibrations Due to Radial Forces, is the fact that the response is entirely different for frequencies Ω of the applied force above and below the limit $\Omega = \pi c/L$. Different expressions, see Equations [42 *a–c*], apply in the two ranges, resulting in different physical behavior.

If $\Omega \leqslant \pi c/L$ the ratios $H_n^{(1)}(i\beta r)/H_n^{(1)}(i\beta a)$ and as a consequence the values of the coefficient $\Delta(a\beta)$, are real. Equations [43] to [45] indicate that in this case the pressure p and the displacements are in phase with the applied force P. There is no input of energy by the applied force and no radiation. It is of interest that the pressure p decreases very rapidly with increasing radius because $H_n^{(1)}(i\beta r)$ decreases like $e^{-\beta r}/\sqrt{r}$. As expected, the expressions for the pressure and displacements contain a denominator which vanishes if Ω becomes equal to one of the roots of the frequency equation for free vibrations, indicating resonance.

If the frequency Ω is sufficiently smaller than $\pi c/L$ the effect of the compressibility becomes unimportant and the approximate Equation [49] for $a\beta$ may be used. For low frequencies, $\Omega \lesssim \omega_1$, one can neglect the modes q_2 and q_3. The resulting equation can be interpreted by means of the virtual mass defined by Equation [54], indicating that the response is identical with that of a shell of increased mass $(m + m_v)$ in vacuo.

If $\Omega > \pi c/L$ conditions are quite different. The ratio $H_n^{(2)}(\bar{\beta}r)/H_n^{(2)}(\bar{\beta}a)$ is complex and the coefficient $\Delta(a\bar{\beta})$ also is complex. As a result, the pressure p and the displacements are not in phase with the applied force, the phase angle being such that the applied force supplies energy which is radiated. There are no real roots of the frequency equation above $\pi c/L$, and resonance does not occur in this range.

The range $\Omega > \pi c/L$ can be further subdivided in two distinct ranges if $n \neq 0$. Table 2 indicates that for small values of $a\bar{\beta}$ the imaginary part of Δ is very much smaller than the real one, while for large values of $a\bar{\beta}$ the opposite is true. The dividing line is quite sharp but depends on the value of n. For $n \geqslant 2$ it lies above $a\bar{\beta} = n/2$. This indicates that, particularly if $n \geqslant 2$, there is an extensive range of frequencies $\Omega > \pi c/L$ where radiation and damping are quite small. The decay of the pressure p as function of r is also different in the two ranges. If the radiation is large the pressure decays very slowly, approximately as $1/\sqrt{r}$. If the radiation is small, the pressure decays much faster, nearly as fast as in the nonradiating case (although for very large values of r the decay becomes again $1/\sqrt{r}$).

Considering the response as function of the forcing frequency Ω, a number of significant frequencies, in addition to frequencies of free vibrations, can be found by considering the denominators of Equations [43] to [45]. If the frequency Ω is equal to one of the frequencies ω_k in vacuo, $N = \infty$, and Equation [44] gives $p_a = P(t, \theta, z)$; the pressure in the medium is in this case equal to the applied pressure, as if the shell were nonexistent. This is physically understandable, because at such a frequency the shell

[6] The frequencies in vacuo for $1 \leqslant L/a \leqslant 10$ can be obtained from reference 1.

[7] This count excludes the frequency of the purely torsional mode of the shell for $n = 0$. This mode was excluded when deriving Equation [31] as it is not coupled with the surrounding medium.

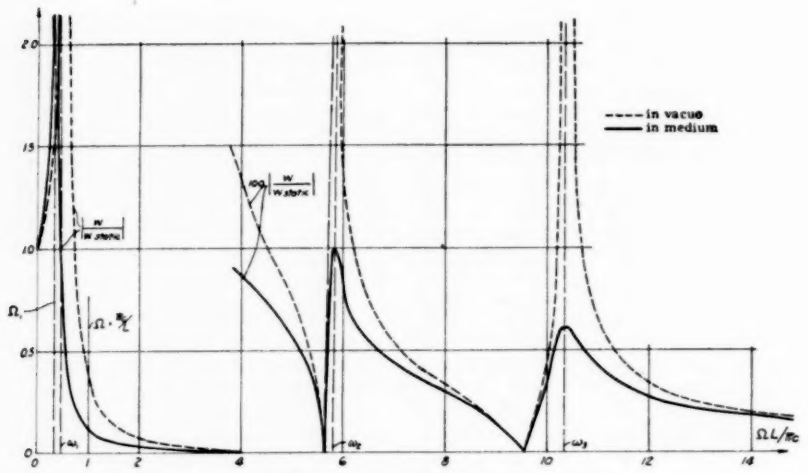

FIG. 4 RATIO $|w/w_{static}|$ FOR $n = 2$, $L/a = 4$, $\rho a/m = 4$
(ω = frequencies in vacuo.)

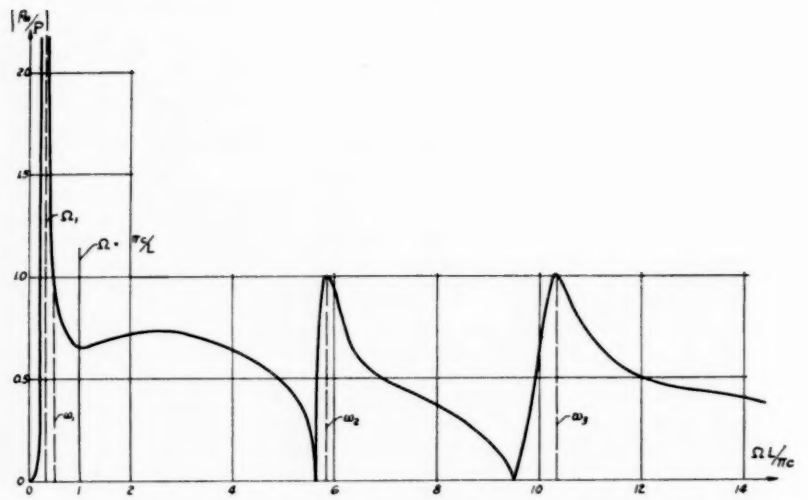

FIG. 5 RATIO $|p_a/P|$ FOR $n = 2$, $L/a = 4$, $\rho a/m = 4$
(ω = frequencies in vacuo.)

vibrates without requiring any outside force, and the entire applied force is transmitted to the medium.

Other significant values of the frequency Ω are those for which the term N vanishes. Consideration of Equations [40] and [46] shows that this occurs, in addition to the trivial value $\Omega = 0$, once between successive values of the frequencies ω_k in vacuo. If $N = 0$, both p and w vanish everywhere, indicating that there is no response at all of the fluid at such frequencies. This rather startling result is due to the fact that for these frequencies the three modes (or two modes if $n = 0$) interact in the manner of a vibration damper. If the longitudinal and radial displacements u and v are determined it is seen that they do not vanish; only w and p are zero. The frequencies at which this phenomenon occurs are necessarily the same as for the shell in vacuo.

At the end of the section mentioned, it has been pointed out that, and for what reason, the solution for $n = 0$ loses its meaning for $\Omega = \pi c/L$. The formulas for the response for frequencies very close to $\Omega = \pi c/L$ also must be used with caution, because they might be affected by the conditions at the distant boundaries of the medium.

Steel Shells in Water. Considering cases in the range $1 \leqslant L/a \leq 10$, there is for $n \geqslant 1$, one frequency in vacuo, ω_1, below $\pi c/L$, while the other two, ω_2, ω_3, are much higher. The frequency equation of the submerged shell has one real root, $\Omega_1 < \omega_1$, and two complex ones near ω_2 and ω_3.

Figs. 4 and 5 show the amplitudes of the radial response w and the maximum pressure p_a at the surface of the shell in nondimensional manner for a typical case, $n = 2$, $L/a = 4$, $\rho a/m = 4$. (The ratio $\rho a/m = 4$ indicates that the mass of the water displaced by the shell is 2.0 times the mass of the shell.) Fig. 4 shows in solid lines the amplification, i.e. the ratio $|w/w_{static}|$ of the amplitude of the displacement w to the static deflection of the shell as function of the ratio $\Omega L/\pi c$. Attention is drawn to the fact that the right half of the diagram is enlarged and shows $100|w/w_{static}|$. The same figure shows for comparison in dashed lines the response of the shell in vacuo. Fig. 5 shows the

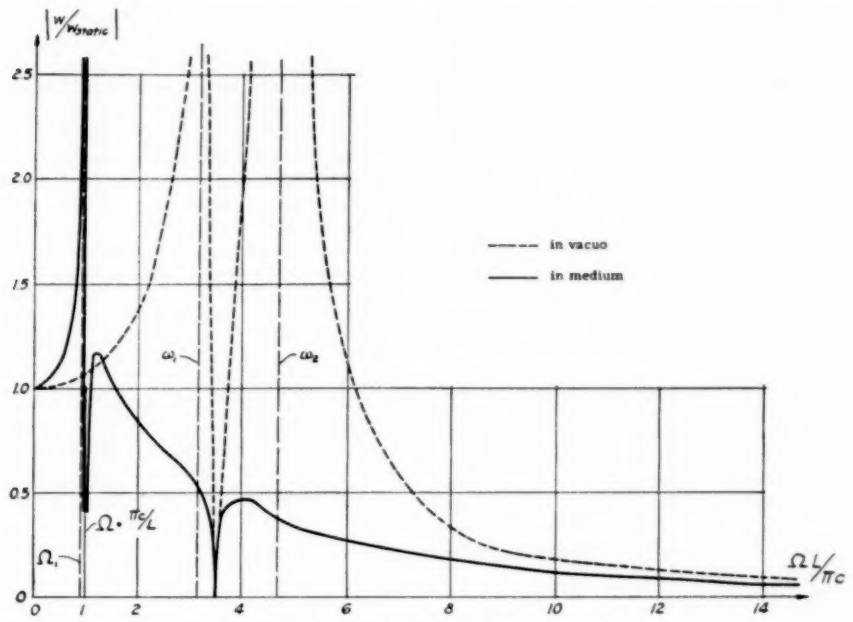

FIG. 6 RATIO $|w/w_{static}|$ FOR $n = 0$, $L/a = 4$, $\rho a/m = 8$
(ω = frequencies in vacuo.)

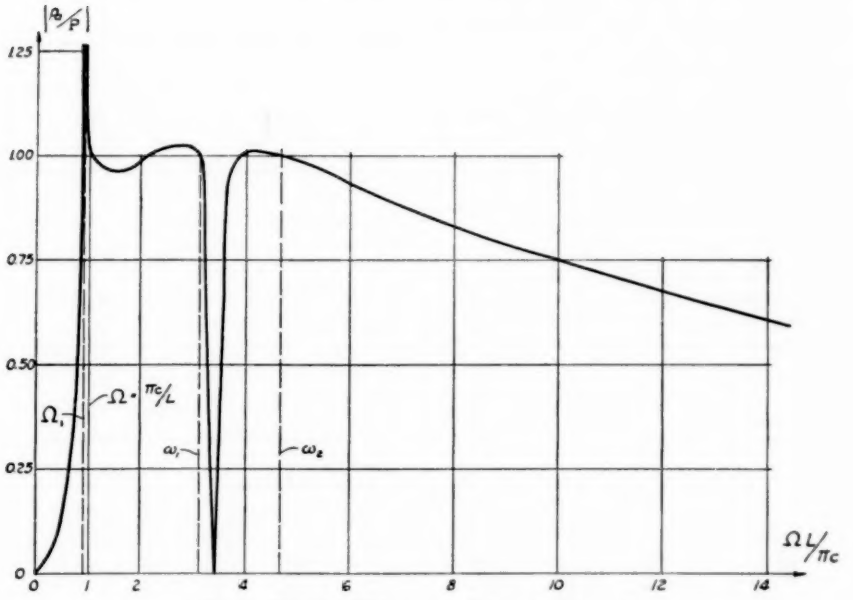

FIG. 7 RATIO $|p_s/P|$ FOR $n = 0$, $L/a = 4$, $\rho a/m = 8$
(ω = frequencies in vacuo.)

ratio of the peak values of the surface pressure p_s to the peak value P of the applied pressure $P(t, \theta, z)$.

The diagrams show clearly the previously mentioned fact that w and p become zero at two points, where $N = 0$, which is due to the vibration damper effect. The difference between the response in vacuo and in water for $\Omega L/\pi c > 1$, as shown in Fig. 4, is essentially that between an undamped and damped system, the response curve showing peaks near the undamped natural frequencies ω_k.

The principal point of interest in the response curve for the pressure, $|p_s/P|$, Fig. 5, is its saw-tooth pattern. There is the expected resonance at the one real root Ω_1, followed by a minor minimum near $\Omega L/\pi c = 1$; then, near ω_2 and ω_3, there are zero values followed closely by peaks of unit value. It is also of in-

terest that the pressure decreases with increasing frequencies only slowly, much slower than the response w.

Figs. 6 and 7 show the radial response w and the pressure p_s for the case $n = 0$. The difference between the responses w in vacuo and in water is much more pronounced than in the case $n = 2$. This is principally due to the fact that the only frequency Ω_1 of the submerged shell is very much lower than the fundamental frequency ω_1 of the shell in vacuo. Attention is drawn to the extreme narrowness of the peaks of the curves in Figs. 6 and 7 at the resonant frequency Ω_1. The response curve w near $\Omega L/\pi c = 1$ has been omitted, because at this point the solution for an infinite medium becomes meaningless. (See the last paragraph but one of section mentioned previously.)

Stiffened Shells. It is worth noting that the theory developed is applicable, approximately, to ring-stiffened shells provided the length L of the half wave is several times the stiffener spacing. In such a case modes of vibrations of the stiffened shell exist for which the displacements are approximately sinusoidal, so that the modes may be expressed again in the form of Equation [1]. If the frequencies and the shapes of the modes in vacuo are known[8] the previously derived formulas can be applied and furnish approximate results for stiffened shells. Such a treatment should give good approximations at low frequencies, while at high ones detail will be lost, because the vibrations of the shell between stiffeners have been neglected.

Effect of Static Pressure

The theory presented in earlier sections neglected the effect of a static pressure in the surrounding medium on the shell.

The effect of the static pressure on the medium is allowed for indirectly by the use of an appropriate value c for the velocity of sound, but the "buckling effect" of the static pressure on the shell does not appear in the previous derivations.

Consider the shell in vacuo on which an external pressure p_0 (smaller than the buckling one) is applied by an imaginary inertialess device. The modes of free vibrations and frequencies can be determined, furnishing a set of new modes having, in general, lower frequencies than in the case $p_0 = 0$. To account for the effect of the static pressure it is necessary to use these new modes and their frequencies in the previous analysis.

Provided p_0 is smaller (say, at least 10 per cent) than buckling pressure of the shell in the mode having the same half-wave length L and circumferential wave number n, the shape of the modes in vacuo for zero pressure and for a pressure p_0 will not differ substantially. One can conclude that this is the case by applying the reasoning used in reference (4)[9] to show that the shape of the modes in a thin shell will not be affected appreciably by its bending stiffness. It is therefore permissible to use the shapes of the modes without static pressure (given in reference 4) as approximation of the new modes, but new, corrected values ω_p for the frequencies must be used. The corrected frequencies ω_p can be found from Rayleigh's principle. If this is done it is found that even the frequencies change only very slightly, except the fundamental ones for $n \geqslant 1$. It is therefore sufficient to correct the fundamental frequencies for $n \geqslant 1$ and use the original ones for $n = 0$, and for the higher frequencies if $n \geqslant 1$.

The additional term in the expression for the potential energy due to a radial pressure p_0 is known from the theory of buckling (6)

$$\frac{p_0}{2}\int\int [w^2 - w_\theta^2 - u_\theta^2 - 2awu_x]d\theta\, dz \quad [55]$$

where the symbols are those of reference (4). To be able to apply the theory for the infinitely long shell to a shell of great, but finite length, it is of interest to be able to include also the effect of a longitudinal compression due to the pressure p_0 on the end surfaces. The additional contribution to the potential energy is

$$\frac{p_0}{2}\int\int -\frac{a^2}{2}[w_x^2 + v_x^2]d\theta\, dz \quad [55a]$$

Applying Rayleigh's principle, the corrected fundamental frequency is

$$\omega_p = \sqrt{\omega^2 - \frac{p_0}{am}B} \quad [56]$$

where, in the case of radial pressure only

$$B = \frac{(n^2-1)W_1^2 - 2\frac{a\pi}{L}W_1U_1 + n^2U_1^2}{U_1^2 + V_1^2 + W_1^2} \quad [57]$$

while for combined radial and longitudinal pressures

$$B = \frac{(n^2-1)W_1^2 - 2\frac{a\pi}{L}W_1U_1 + n^2U_1^2 + \frac{1}{2}V_1^2 + \frac{1}{2}\frac{a^2\pi^2}{L^2}W_1^2}{U_1^2 + V_1^2 + W_1^2} \quad [57a]$$

The values of B have been determined for $n = 1$ to 4, inclusive, and are listed in Table 3 for $1 \leqslant L/a \leqslant 10$. It will be noted that some of the values B for $n = 1$ are negative, indicating an increase of the frequency due to radial pressure only.

TABLE 3 VALUES OF B IN EQUATION [56]

	Radial pressure only				Combined radial and longitudinal pressure			
L/a	$n=1$	$n=2$	$n=3$	$n=4$	$n=1$	$n=2$	$n=3$	$n=4$
1.00	0.282	2.604	7.108	13.86	4.963	7.171	11.718	18.55
1.25	0.111	2.362	6.956	13.81	2.949	5.186	9.869	16.80
1.50	−0.0427	2.222	6.906	13.82	1.810	4.142	8.923	15.90
1.75	−0.0457	2.152	6.903	13.85	1.252	3.555	8.391	15.39
2.00	−0.212	2.126	6.922	13.89	0.763	3.207	8.071	15.07
2.25	−0.240	2.123	6.947	13.92	0.539	2.991	7.865	14.86
2.50	−0.248	2.132	6.973	13.95	0.405	2.851	7.726	14.72
2.75	−0.245	2.147	6.997	13.97	0.323	2.758	7.629	14.61
3.00	−0.236	2.165	7.019	13.99	0.273	2.693	7.559	14.53
3.50	−0.211	2.200	7.056	14.02	0.222	2.616	7.466	14.43
4.00	−0.185	2.231	7.083	14.04	0.202	2.574	7.410	14.36
5.00	−0.140	2.278	7.120	14.07	0.195	2.534	7.348	14.28
6.00	−0.107	2.310	7.143	14.08	0.201	2.518	7.316	14.24
7.00	−0.0842	2.330	7.157	14.09	0.209	2.511	7.298	14.21
8.00	−0.0672	2.345	7.166	14.10	0.215	2.507	7.286	14.20
9.00	−0.0547	2.356	7.173	14.10	0.221	2.505	7.278	14.19
10.00	−0.0452	2.364	7.178	14.10	0.225	2.503	7.273	14.18

[8] It is intended to treat engineering methods for the determination of these modes in a future paper.

[9] See the paragraph containing Eq. [20].

BIBLIOGRAPHY

1 "Radiation Loading of Cylindrical and Spherical Surfaces," by

M. C. Junger, *Journal of the Acoustical Society of America*, vol. 24, May, 1952, p. 288.

2 "Vibrations of Elastic Shells in a Fluid Medium and the Associated Radiation of Sound," by M. C. Junger, JOURNAL OF APPLIED MECHANICS, Trans. ASME, vol. 74, 1952, pp. 439–445.

3 "The Physical Interpretation of the Expression for an Outgoing Wave in Cylindrical Coordinates," by M. C. Junger, *Journal of the Acoustical Society of America*, vol. 25, January, 1953, p. 40.

4 "Tables for the Frequencies and Modes of Free Vibrations of Infinitely Long Thin Cylindrical Shells," by M. L. Baron and H. H. Bleich, published in this issue, pp. 178–184.

5 "Response of an Elastic Cylindrical Shell to a Transverse, Step Shock Wave," by R. D. Mindlin and H. H. Bleich, JOURNAL OF APPLIED MECHANICS, Trans. ASME, vol. 75, 1953, pp. 189–195.

6 "Stabilitätsprobleme der Elastostatik," by A. Pflüger, Julius Springer, Berlin, Germany, 1950, p. 130.

Tables for Frequencies and Modes of Free Vibration of Infinitely Long Thin Cylindrical Shells[1]

By M. L. BARON[2] and H. H. BLEICH,[3] NEW YORK, N. Y.

Tables are presented for the quick determination of the frequencies and shapes of modes of infinitely long thin cylindrical shells. To make the problem tractable, the shells are first treated as membranes without bending stiffness, and the bending effects are introduced subsequently as corrections. The underlying theory is based on the energy expressions for cylindrical shells.[4] The tables cover the following range: lengths of longitudinal half wave L from 1 to 10 radii a; number n of circumferential waves from 0 to 6. The results apply for Poisson's ratio $\nu = 0.30$.

Introduction

THE problem of the free vibrations of infinitely long thin cylindrical shells for the case of negligible bending stiffness has been considered by Rayleigh.[5] The solution is relatively simple, leading to a cubic frequency equation. While in many cases of practical interest the assumption of negligible bending stiffness is permissible, there also are situations where this is no longer sufficient. This paper is concerned with providing a procedure for the determination of the frequencies and modes applicable also when the bending stiffness is not entirely negligible. The full solution of the problem including bending effects being numerically rather complex, the following approximate approach is used which is found to give satisfactory results in the range of interest.

Considering the frequencies of the modes of a selected wave length, the use of the membrane theory will result in an error, the magnitude of which is not known. One can obtain an estimate of this error by computing an upper limit for the frequency from Rayleigh's principle. Using the shape of the mode determined from the membrane theory, one can compute a corrected frequency of a mode of this shape using an expression for the potential energy including the effect of the bending stiffness. This corrected frequency is necessarily an upper limit for the actual frequency and certainly will be a very good approximation to the actual one if the difference between it and the membrane frequency is small. However, it will be shown subsequently that in the range of interest, $h/a < 1/30$, the corrected frequency is always a very good approximation even if it differs substantially from the membrane frequency.

The procedure outlined in the foregoing lends itself well to the determination of the frequencies from tables. The frequencies and shapes of the modes according to the membrane theory were computed and tabulated for two variables: the longitudinal half-wave length L (from one radius to 10 radii), and the number n of circumferential waves (from 0 to 6). The frequency equation furnishes three roots for each geometry, and the ratios of the amplitudes of radial, tangential, and longitudinal motions were computed for each root. The ratios were then substituted in the expressions for the kinetic and potential energies, and the corrected frequencies determined. Owing to the fact that the differences between the squares of the corrected and membrane frequencies are proportional to the square of the thickness-radius ratio, h^2/a^2, only the respective constants need be recorded in the tables. Hence the determination of the corrected frequencies does not increase the number of variables in the tabulation which remains at two, the longitudinal half-wave length L, and the number of circumferential waves n.

The next section contains the fundamental equations on which the tables in the third section are based. The fourth section considers the important question of accuracy of the corrected frequencies indicating the validity of the tables for values $h/a < 1/30$. The last section finally contains a short discussion of the physical meaning of the results found. While not essential for the use of the tables, the discussion sheds light on the dependency of the frequencies and modes on the parameters L/a and n.

Fundamental Equations

Using cylindrical co-ordinates r, θ, and z, the displacement of any point of the shell is defined by its components, Fig. 1:

u = longitudinal displacement (positive in direction of z-axis)

v = tangential displacement (positive in direction of positive θ)

w = radial displacement (positive inward)

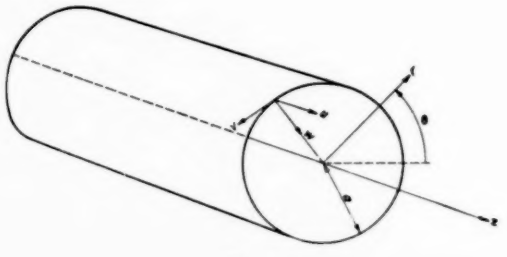

Fig. 1

[1] This paper is a result of investigations sponsored by the Office of Naval Research under Contract Nonr-266(08).

[2] Assistant Professor of Civil Engineering, Columbia University.

[3] Professor of Civil Engineering, Columbia University. Mem. ASME.

[4] "A Strain-Energy Expression for Thin Cylindrical Shells," by H. H. Bleich and F. DiMaggio, Journal of Applied Mechanics, Trans. ASME, vol. 75, 1953, pp. 448-449.

[5] "The Theory of Sound," by J. Rayleigh, Dover Publications, New York, N. Y., 1945.

Contributed by the Applied Mechanics Division and presented at the Annual Meeting, New York, N. Y., November 29–December 4, 1953, of The American Society of Mechanical Engineers.

Discussion of this paper should be addressed to the Secretary, ASME, 39 West 39th Street, New York, N. Y., and will be accepted until July 12, 1954, for publication at a later date. Discussion received after the closing date will be returned.

Note: Statements and opinions advanced in papers are to be understood as individual expressions of their authors and not those of the Society. Manuscript received by ASME Applied Mechanics Division, March 27, 1953. Paper No. 53—A-33.

Let

a = mean radius of cylindrical shell
h = thickness of shell
E = Young's modulus
$G = \dfrac{E}{2(1+\nu)}$ = modulus of rigidity
ν = Poisson's ratio
$N = \dfrac{\nu}{1-\nu}$ = elastic constant
m = mass of shell per unit of area
ω = circular frequency of vibrations

The strain energy P stored in the shell can be expressed[4] as a function of the displacements u, v, and w

$$P = P_1 + P_2 \quad \ldots\ldots [1]$$

where the first term P_1 is the membrane strain energy

$$P_1 = \frac{E}{2(1-\nu^2)}\frac{h}{a}\int\int\Big[a^2u_x^2 + (v_\theta - w)^2 + 2a\nu u_x(v_\theta - w) + \frac{1-\nu}{2}(u_\theta + av_x)^2\Big]dzd\theta \quad \ldots [2]$$

while the second term P_2 represents the strain energy of bending and coupling terms between membrane and bending strains[6]

$$P_2 = \frac{E}{24(1-\nu^2)}\frac{h^3}{a^3}\int\int\Big[a^4 w_{xx}^2 + (w_{\theta\theta} + w)^2 + \frac{1-\nu}{2}(aw_{x\theta} - u_\theta)^2 + \frac{3(1-\nu)}{2}a^2(v_x + w_{x\theta})^2 + 2a^2\nu w_{xx}(w_{\theta\theta} + v_\theta) + 2a^3 u_x w_{xx}\Big]dzd\theta \quad \ldots [3]$$

The subscripts indicate partial derivatives with respect to z or θ.

The expression for the kinetic energy is

$$T = \frac{am}{2}\int\int[\dot{u}^2 + \dot{v}^2 + \dot{w}^2]dzd\theta \quad \ldots\ldots [4]$$

Membrane Theory. When h is small, P_1 alone may be used as approximation of the total potential energy of the shell, leading to the membrane theory. Using Hamilton's principle the differential equations for this use can be obtained from the condition that the integral

$$J = \int_{t_0}^{t_1}(T - P_1)dt \quad \ldots\ldots [5]$$

shall be stationary. Substituting Equations [2] and [4] and applying the rules of the calculus of variations, the following set of simultaneous partial differential equations is obtained

$$\left.\begin{aligned} -\frac{a^2m}{2Gh}\ddot{u} + a^2u_{xx} + \frac{1}{2}(u_{\theta\theta} + av_{x\theta}) + aN(au_{xx} + v_{x\theta} - w_x) &= 0 \\ -\frac{a^2m}{2Gh}\ddot{v} - w_\theta + v_{\theta\theta} + \frac{a}{2}(u_{\theta x} + av_{xx}) + N(au_{x\theta} + v_{\theta\theta} - w_\theta) &= 0 \\ -\frac{a^2m}{2Gh}\ddot{w} - w + v_\theta + N(au_x + v_\theta - w) &= 0 \end{aligned}\right\} \quad \ldots [6]$$

[4] It is proper to call attention to the fact that the expression for the strain energy P_2 used may not be correct in the light of recent advanced shell theories.[7] However, the authors are satisfied that the effect of any corrected strain-energy expression in the range of the following tables is insignificant.

[7] "The New Approach to Shell Theory," by E. H. Kennard, JOURNAL OF APPLIED MECHANICS, Trans. ASME, vol. 75, 1953, pp. 33–40.

For convenience E and ν were expressed by the shear modulus

$$G = \frac{E}{2(1+\nu)}$$

and the constant

$$N = \frac{\nu}{1-\nu}$$

For infinitely long shells suitable solutions of Equations [6] are

$$\left.\begin{aligned} u &= U\cos n\theta\cos\frac{\pi z}{L}e^{i\omega t} \\ v &= V\sin n\theta\sin\frac{\pi z}{L}e^{i\omega t} \\ w &= W\cos n\theta\sin\frac{\pi z}{L}e^{i\omega t} \end{aligned}\right\} \quad \ldots\ldots [7]$$

where $n = 0, 1, 2, \ldots$ is an integral number indicating the number of circumferential waves, L is the length of the longitudinal half wave, and U, V, W are constants. Fig. 2 shows a typical displacement pattern.

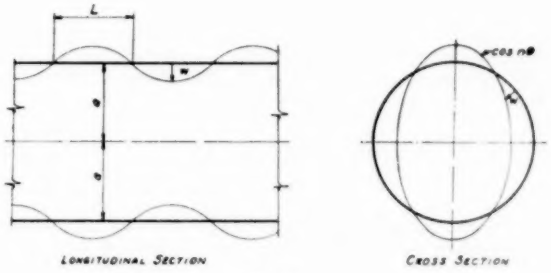

FIG. 2

Substitution of Equations [7] into [6] leads to three homogeneous equations for the three constants U, V, W

$$\left.\begin{aligned} [2(N+1)j^2 + n^2 - K^2]U - (2N+1)njV + 2NjW &= 0 \\ -[2N+1]jnU + [j^2 + 2(N+1)n^2 - K^2]V - 2(N+1)nW &= 0 \\ -2NjU + 2(N+1)nV - [2(N+1) - K^2]W &= 0 \end{aligned}\right\} \quad \ldots [8]$$

where

$$j = \frac{\pi a}{L} \quad \ldots\ldots [9]$$

$$K = \omega a\sqrt{\frac{m}{Gh}} \quad \ldots\ldots [10]$$

Nonvanishing solutions of Equations [8], and free vibrations, exist only if the determinant of Equations [8] vanishes. This leads to the frequency equation

$$(K^2 - j^2 - n^2)\,[K^2[K^2 - 2(N+1)(j^2 + n^2 + 1)] + 4(2N+1)j^2] + 4(2N+1)j^2n^2 = 0 \quad \ldots\ldots [11]$$

For given values of j and n, defining the wave lengths of the mode, Equation [11] furnishes three positive roots K^2, defining three mutually orthogonal modes of frequencies

$$\omega = \frac{K}{a}\sqrt{\frac{Gh}{m}} \quad \ldots\ldots [12]$$

Equation [11] was derived by Rayleigh.[8] The shape of the mode pertaining to a particular frequency can be found by computing the ratios of U, V, and W from Equations [8].

For the special case $n = 0$, the frequency Equation [11] separates into two factors

$$K^2 = j^2 \quad \ldots\ldots [13]$$

$$K^2\,[K^2 - 2(N+1)\,(j^2+1)] + 4\,(2N+1)\,j^2 = 0 \quad \ldots\ldots [14]$$

The modes pertaining to the Solution [13] are purely torsional vibrations of the cylinder ($U = W = 0$, $\alpha = 0$). The modes corresponding to the solutions of Equation [14] are combinations of radial and longitudinal motions, without tangential components ($V = 0$).

Correction of Membrane Frequency. A correction of the frequency obtained from the membrane theory to allow for the neglected term P_2 in the potential energy is now obtained from Rayleigh's principle. Using the shape of the mode, i.e., the values of the constants U, V, and W determined from Equations [8], a new corrected frequency ω_c is determined from the equality

$$T_{\max} = P_{1,\max} + P_{2,\max} \quad \ldots\ldots [15]$$

where the subscript "max" indicates the maximum value of the respective quantity.

Substituting Equation [7] into [4] (but using ω_c instead of ω) and integrating over a section of the shell of length L gives for $n \neq 0$

$$T_{\max} = m\omega_c^2 \frac{\pi a L}{4}\,[U^2 + V^2 + W^2] \quad \ldots\ldots [16]$$

The value of $P_{1,\max}$ must be equal to the kinetic energy of the vibrating membrane which follows from Equation [16] for $\omega_c = \omega$

$$P_{1,\max} = m\omega^2 \frac{\pi a L}{4}\,[U^2 + V^2 + W^2] \quad \ldots\ldots [17]$$

The value of $P_{2,\max}$ can be evaluated by substituting Equations [7] into [3], and the value of the corrected frequency ω_c may finally be computed from Equation [15]

$$\omega_c = \frac{K}{a}\sqrt{\frac{Gh}{m}\left(1 + \frac{\bar{K}^2}{K^2}\frac{h^2}{a^2}\right)} \quad \ldots\ldots [18]$$

where K is the root of the frequency Equation [11] and the constant $\bar{K}^2$ is given by the expression

$$\bar{K}^2 = \frac{1}{6(1-\nu)\left[1 + \left(\frac{V}{U}\right)^2 + \left(\frac{W}{U}\right)^2\right]}\left\{[(j^2+n^2)^2 - 2n^2 + 1]\left(\frac{W}{U}\right)^2 - (3-\nu)\,nj^2\left(\frac{V}{U}\right)\left(\frac{W}{U}\right) + \frac{3(1-\nu)}{2}j^2\left(\frac{V}{U}\right)^2 + [2j^2 - (1-\nu)\,n^2 j]\left(\frac{W}{U}\right) + \frac{(1-\nu)}{2}n^2\right\} \quad \ldots [19]$$

Equation [18] applies for any value of n. The range of ratios h/a for which Equation [18] gives sufficiently accurate results is discussed in the fourth section.

[8] Reference 5, p. 404.

Tables

The frequencies are determined from the approximate Formula [12], or if necessary, from the corrected Formula [18] as indicated at the head of the tables.

The shapes of the modes are defined by the ratios of the constants V/U and W/U which define the displacements according to Equations [7]. These ratios were used to determine $\bar{K}^2/K^2$ from Equation [19]. The ratios V/U and W/U describe the nature of a particular mode, whether it is principally longitudinal, tangential, or radial, or possibly mixed.

For any selected half-wave length L and any number n of circumferential waves the frequency equation has three roots corresponding to three modes. For $n = 1$, and similarly for $n = 2, 3 \ldots$ to 6, the factor K, the ratios W/U, V/U, and where required the ratio $\bar{K}^2/K^2$ are presented as functions of L/a for each value of n in separate tables. Each table is in three parts, headed "Lowest frequency," "Second lowest frequency," and "Highest frequency," respectively (Tables 2 to 7, inclusive). The tables cover the range from $L/a = 1$ to 10. For $h/a \leqq 1/30$, the two higher frequencies always can be computed from the approximate Equation [12], while the corrected Equation [18] may be required for the lowest frequency if $n > 1$. For this reason it was not necessary to give the coefficients $\bar{K}^2/K^2$ for the two higher frequencies.[9]

For the special case $n = 0$, the frequency equation also has three roots, Table 1. Owing to the division in torsional and nontorsional vibration the headings of the parts of this table differ from the others, but are self-explanatory. For $n = 0$, all frequencies can be determined from the approximate Equation [12], the correction according to Equation [18] is always insignificant.

Range of Applicability of Tables

The numerical results presented in Tables 1 to 7 can be used to examine the effect of the approximations used in obtaining the frequencies ω and ω_c.

The frequency ω_c, found from Rayleigh's principle, is an approximation of the actual frequency, ω_c being necessarily too high. The membrane frequency ω is a cruder approximation which is in most cases, but not always, lower than the actual frequency.[10] If the difference between ω_c and ω is small, we can expect that the error in ω_c will be even smaller than this difference, and use ω_c or ω depending on the requirements of accuracy of the problem.

Values of $\bar{K}^2$ for $n = 0$ and 1 are given in Tables 8 and 9 for three ratios of L/a. If these values are used to determine the corrected frequencies ω_c, it can be shown that the difference between ω and ω_c for an arbitrary maximum ratio $h/a < 1/30$ never exceeds 0.4 per cent for $n = 0$, and 0.7 per cent for $n = 1$. The use of the correction for $n = 0$ or 1 appears therefore unnecessary.

Applying Tables 3 to 7 and Equation [18], we find that for $n > 1$, the difference for the lowest frequency in each case is much larger than for the second lowest or highest frequency. The differences depend on the values $\bar{K}^2$ which are listed in Table 10 for the higher frequencies. Using an arbitrary maximum ratio of $h/a < 1/30$, the differences for the second lowest frequencies never exceed 1/40 of one per cent, and are still lower for the highest frequencies. The membrane frequencies therefore can always be used when computing any but the lowest frequency for

[9] A detailed discussion is given in the following section.

[10] This is due to the fact that the second term P_2 of the strain energy neglected in the membrane theory contains not only the energy of bending, but also coupling terms between membrane and bending strains. Owing to the coupling terms P_2 is capable of negative values, indicating that ω is not necessarily a lower limit for the actual frequency.

TABLE 1 FREQUENCIES FOR $n = 0$

Ratio, L/a	Torsional frequency $\omega = K/a\sqrt{Gk/m}$ Factor, K	Shape of mode, $U = W$	Lower nontorsional frequency, $\omega = K/a\sqrt{Gk/m}$ Factor, K	Shape of mode W/U	V/U	Higher nontorsional frequency, $\omega = K/a\sqrt{Gk/m}$ Factor, K	Shape of mode W/U	V/U
1.0	3.142	0	1.604	−9.510	0	5.338	+0.1052	0
1.25	2.513	0	1.599	−7.186	0	4.284	0.1392	0
1.5	2.094	0	1.592	−5.567	0	3.586	0.1797	0
1.75	1.795	0	1.582	−4.354	0	3.093	0.2297	0
2.0	1.571	0	1.569	−3.406	0	2.729	0.2936	0
2.25	1.396	0	1.551	−2.643	0	2.455	0.3783	0
2.5	1.257	0	1.525	−2.028	0	2.246	0.4931	0
2.75	1.142	0	1.490	−1.539	0	2.090	0.6497	0
3.0	1.047	0	1.445	−1.165	0	1.976	0.8580	0
3.5	0.8976	0	1.327	−0.7025	0	1.844	1.422	0
4.0	0.7854	0	1.201	−0.4760	0	1.783	2.101	0
5.0	0.6283	0	0.9869	−0.2862	0	1.736	3.495	0
6.0	0.5236	0	0.8309	−0.2073	0	1.718	4.825	0
7.0	0.4488	0	0.7158	−0.1642	0	1.709	6.093	0
8.0	0.3927	0	0.6282	−0.1368	0	1.704	7.308	0
9.0	0.3491	0	0.5595	−0.1177	0	1.700	8.496	0
10.0	0.3142	0	0.5042	−0.1035	0	1.699	9.661	0
∞	0	0	0	0	0	1.691	$U = V = 0$	

TABLE 2 FREQUENCIES FOR $n = 1$

Ratio, L/a	Lowest frequency $\omega = K/a\sqrt{Gk/m}$ Factor, K	Shape of mode V/U	W/U	Second lowest frequency $\omega = K/a\sqrt{Gk/m}$ Factor, K	Shape of mode V/U	W/U	Highest frequency $\omega = K/a\sqrt{Gk/m}$ Factor, K	Shape of mode V/U	W/U
1.0	1.428	−5.106	−21.14	3.357	+2.784	−0.6252	5.611	−0.3306	0.0144
1.25	1.322	−14.77	−40.01	2.813	2.048	−0.7310	4.628	−0.4236	0.0271
1.5	1.203	+39.13	+78.00	2.483	1.533	−0.7820	4.003	−0.5245	0.2503
1.75	1.082	10.51	16.88	2.266	1.161	−0.7819	3.584	−0.6350	0.3359
2.0	0.9682	6.756	9.352	2.109	0.8885	−0.7488	3.294	−0.7555	0.4389
2.25	0.8660	5.300	6.616	1.987	0.6870	−0.7014	3.088	−0.8856	0.5582
2.5	0.7761	4.537	5.271	1.886	0.5367	−0.6517	2.941	−1.024	0.6914
2.75	0.6979	4.078	4.503	1.799	0.4234	−0.6056	2.833	−1.167	0.8352
3.0	0.6300	3.778	4.023	1.724	0.3368	−0.5649	2.753	−1.315	0.9864
3.5	0.5193	3.430	3.490	1.599	0.2168	−0.4996	2.645	−1.615	1.301
4.0	0.4342	3.259	3.236	1.501	0.1406	−0.4505	2.579	−1.917	1.621
5.0	0.3150	3.159	3.077	1.363	0.0552	−0.3816	2.506	−2.515	2.257
6.0	0.2377	3.216	3.121	1.273	0.0128	−0.3336	2.469	−3.104	2.878
7.0	0.1852	3.352	3.256	1.212	−0.0096	−0.2972	2.447	−3.684	3.485
8.0	0.1478	3.535	3.443	1.169	−0.0219	−0.2679	2.434	−4.258	4.081
9.0	0.1205	3.747	3.661	1.138	−0.0287	−0.2438	2.424	−4.828	4.669
10.0	0.09990	3.980	3.899	1.114	−0.0322	−0.2236	2.418	−5.395	5.250
∞	0	$W = V$	$U = 0$	1.000	$V = W = 0$	$W = 3.72V$	2.391	$V = -W$	$U = 0$

TABLE 3 FREQUENCIES FOR $n = 2$

Ratio, L/a	Lowest frequency $\omega = K/a\sqrt{Gk/m\,(1 + K^2h^2/K^2a^2)}$ Factor, K	Factor, $(K/K)^2$	Shape of mode V/U	W/U	Second lowest frequency $\omega = K/a\sqrt{Gk/m}$ Factor, K	Shape of mode V/U	W/U	Highest frequency $\omega = K/a\sqrt{Gk/m}$ Factor, K	Shape of mode V/U	W/U
1.0	1.102	30.85	+11.57	+38.63	3.840	+1.394	−0.4434	6.357	−0.6626	+0.1726
1.25	0.9276	21.59	5.953	15.95	3.362	1.047	−0.4532	5.523	−0.8459	0.2530
1.5	0.7773	18.34	4.496	10.60	3.063	0.8176	−0.4409	5.523	−1.037	0.3453
1.75	0.6535	17.65	3.873	8.472	2.858	0.6590	−0.4193	4.704	−1.234	0.4459
2.0	0.5530	18.44	3.560	7.445	2.709	0.5453	−0.3950	4.491	−1.434	0.5515
2.25	0.4717	.....	3.399	6.918	2.595	0.4613	−0.3712	4.342	−1.637	0.6598
2.5	0.4056	23.19	3.324	6.654	2.506	0.3975	−0.3489	4.235	−1.840	0.7692
2.75	0.3515	.....	3.303	6.547	2.435	0.3480	−0.3283	4.156	−2.044	0.8788
3.0	0.3070	31.96	3.319	6.539	2.378	0.3087	−0.3096	4.095	−2.248	0.9883
3.5	0.2389	.....	3.421	6.706	2.292	0.2508	−0.2771	4.011	−2.656	1.206
4.0	0.1904	64.77	3.582	7.018	2.231	0.2107	−0.2500	3.956	−3.053	1.420
5.0	0.1283	127.0	4.006	7.869	2.155	0.1594	−0.2082	3.893	−3.868	1.842
6.0	0.09178	233.1	4.504	8.876	2.110	0.1282	−0.1777	3.858	−4.671	2.257
7.0	0.06871	400.8	5.042	9.965	2.083	0.1074	−0.1547	3.837	−5.470	2.667
8.0	0.05326	651.3	5.605	11.10	2.064	0.0925	−0.1368	3.824	−6.268	3.074
9.0	0.04245	1009	6.184	12.27	2.051	0.0813	−0.1225	3.815	−7.063	3.478
10.0	0.03461	1501	6.775	13.46	2.041	0.0725	−0.1108	3.808	−7.858	3.881
∞	0	.....	$W = 2V$	$U = 0$	2.000	$V = W = 0$	$W = -1.53V$	3.780	$V = -2W$	$U = 0$

TABLE 4 FREQUENCIES FOR $n = 3$

Ratio, L/a	Lowest frequency $\omega = K/a\sqrt{Gk/m\,(1 + K^2h^2/K^2a^2)}$ Factor, K	Factor, $(K/K)^2$	Shape of mode V/U	W/U	Second lowest frequency $\omega = K/a\sqrt{Gk/m}$ Factor, K	Shape of mode V/U	W/U	Highest frequency $\omega = K/a\sqrt{Gk/m}$ Factor, K	Shape of mode V/U	W/U
1.0	0.8130	107.0	+4.754	+17.32	4.458	+0.9414	−0.3161	7.425	−0.9903	+0.2140
1.25	0.6346	109.5	3.821	12.46	4.033	0.7238	−0.3021	6.729	−1.255	0.3044
1.5	0.5012	129.2	3.478	10.75	3.772	0.5830	−0.2816	6.327	−1.522	0.3995
1.75	0.4019	163.4	3.361	10.12	3.598	0.4860	−0.2603	6.075	−1.792	0.4965
2.0	0.3275	213.2	3.356	9.970	3.477	0.4158	−0.2403	5.908	−2.062	0.5937
2.25	0.2708	.....	3.415	10.09	3.388	0.3631	−0.2221	5.792	−2.332	0.6905
2.5	0.2270	371.4	3.516	10.36	3.322	0.3221	−0.2059	5.708	−2.602	0.7867
2.75	0.1926	.....	3.645	10.73	3.271	0.2894	−0.1915	5.646	−2.871	0.8821
3.0	0.1653	634.0	3.794	11.18	3.231	0.2628	−0.1787	5.599	−3.141	0.9768
3.5	0.1251	.....	4.134	12.20	3.173	0.2221	−0.1572	5.532	−3.678	1.164
4.0	0.09774	1638	4.509	13.34	3.135	0.1924	−0.1400	5.489	−4.215	1.350
5.0	0.06410	3631	5.324	15.80	3.088	0.1520	−0.1145	5.437	−5.285	1.717
6.0	0.04513	7138	6.186	18.41	3.062	0.1258	−0.0966	5.409	−6.354	2.080
7.0	0.03344	12810	7.075	21.10	3.046	0.1073	−0.0834	5.393	−7.421	2.441
8.0	0.02573	21400	7.981	23.83	3.035	0.0936	−0.0733	5.382	−8.488	2.801
9.0	0.02042	33800	8.898	26.59	3.028	0.0830	−0.0654	5.374	−9.553	3.159
10.0	0.01658	50900	9.822	29.37	3.022	0.0746	−0.0590	5.369	−10.62	3.517
∞	0	.....	$W = 3V$	$U = 0$	3.000	$V = W = 0$	$W = -0.79V$	5.346	$V = -3W$	$U = 0$

TABLE 5 FREQUENCIES FOR $n = 4$

	Lowest frequency $\omega = K/a\sqrt{Gh/m}\,(1 + \bar{K}^2h^2/K^2a^2)$				Second lowest frequency $\omega = K/a\sqrt{Gh/m}$			Highest frequency $\omega = K/a\sqrt{Gh/m}$		
Ratio,	Factor,	Factor,	Shape of mode		Factor,	Shape of mode		Factor,	Shape of mode	
L/a	K	$(\bar{K}/K)^2$	V/U	W/U	K	V/U	W/U	K	V/U	W/U
1.0	0.5982	387.0	+3.714	+15.90	5.177	+0.7191	−0.2308	8.690	−1.312	+0.2436
1.25	0.4422	515.1	3.409	13.83	4.806	0.5620	−0.2109	8.103	−1.653	0.3353
1.5	0.3356	736.8	3.371	13.38	4.586	0.4602	−0.1906	7.770	−1.996	0.4279
1.75	0.2614	1072	3.456	13.61	4.444	0.3894	−0.1724	7.563	−2.338	0.5201
2.0	0.2083	1553	3.607	14.17	4.348	0.3375	−0.1565	7.427	−2.680	0.6115
2.25	0.1694	.....	3.799	14.93	4.279	0.2978	−0.1428	7.333	−3.022	0.7020
2.5	0.1401	3100	4.019	15.81	4.229	0.2665	−0.1310	7.265	−3.363	0.7918
2.75	0.1177	.....	4.258	16.77	4.191	0.2412	−0.1209	7.214	−3.704	0.8809
3.0	0.1001	5739	4.511	17.79	4.162	0.2203	−0.1121	7.175	−4.045	0.9694
3.5	0.07486	.....	5.047	19.96	4.120	0.1879	−0.0976	7.121	−4.726	1.145
4.0	0.05799	16150	5.608	22.22	4.092	0.1639	−0.0864	7.086	−5.407	1.320
5.0	0.03736	37350	6.777	26.93	4.060	0.1305	−0.0700	7.045	−6.767	1.666
6.0	0.02634	75100	7.981	31.78	4.042	0.1085	−0.0587	7.022	−8.126	2.010
7.0	0.01944	137000	9.205	36.69	4.031	0.0929	−0.0506	7.008	−9.484	2.352
8.0	0.01493	230000	10.44	41.65	4.024	0.0812	−0.0444	6.999	−10.84	2.694
9.0	0.01183	366000	11.69	46.64	4.019	0.0721	−0.0395	6.993	−12.20	3.035
10.0	0.009586	555000	12.94	51.65	4.015	0.0649	−0.0356	6.989	−13.56	3.376
∞	0	.....	$W = 4V$	$U = 0$	4.000	$V = W = 0$	$W = -0.55V$	6.970	$V = -4W$	$U = 0$

TABLE 6 FREQUENCIES FOR $n = 5$

	Lowest frequency $\omega = K/a\sqrt{Gh/m}\,(1 + \bar{K}^2h^2/K^2a^2)$				Second lowest frequency $\omega = K/a\sqrt{Gh/m}$			Highest frequency $\omega = K/a\sqrt{Gh/m}$		
Ratio,	Factor,	Factor,	Shape of mode		Factor,	Shape of mode		Factor,	Shape of mode	
L/a	K	$(\bar{K}/K)^2$	V/U	W/U	K	V/U	W/U	K	V/U	W/U
1.0	0.4472	1304	+3.421	+17.38	5.972	+0.5852	−0.1728	10.08	−1.631	+0.2636
1.25	0.3183	2057	3.391	16.79	5.652	0.4618	−0.1528	9.573	−2.048	0.3540
1.5	0.2355	3294	3.529	17.35	5.466	0.3812	−0.1352	9.290	−2.465	0.4437
1.75	0.1802	5180	3.751	18.43	5.349	0.3247	−0.1204	9.116	−2.882	0.5325
2.0	0.1418	7918	4.021	19.77	5.271	0.2828	−0.1081	9.002	−3.299	0.6203
2.25	0.1142	.....	4.322	21.29	5.216	0.2505	−0.0978	8.923	−3.715	0.7073
2.5	0.09381	16920	4.643	22.91	5.176	0.2249	−0.0892	8.866	−4.131	0.7937
2.75	0.07835	.....	4.979	24.60	5.146	0.2041	−0.0819	8.823	−4.547	0.8796
3.0	0.06637	32590	5.325	26.35	5.123	0.1868	−0.0757	8.791	−4.963	0.9650
3.5	0.04933	.....	6.041	29.96	5.091	0.1597	−0.0656	8.746	−5.794	1.135
4.0	0.03805	95560	6.777	33.67	5.070	0.1396	−0.0578	8.717	−6.625	1.304
5.0	0.02458	225000	8.286	41.25	5.045	0.1114	−0.0466	8.682	−8.286	1.640
6.0	0.01715	458000	9.822	48.96	5.031	0.0928	−0.0390	8.663	−9.946	1.975
7.0	0.01265	837000	11.38	56.74	5.023	0.0795	−0.0336	8.652	−11.61	2.309
8.0	0.009690	1420000	12.94	64.57	5.018	0.0695	−0.0294	8.644	−13.26	2.642
9.0	0.007668	2260000	14.51	72.42	5.014	0.0618	−0.0262	8.639	−14.92	2.975
10.0	0.006221	3430000	16.08	80.30	5.011	0.0556	−0.0236	8.636	−16.58	3.308
∞	0	.....	$W = 5V$	$U = 0$	5.000	$V = W = 0$	$W = -0.42V$	8.620	$V = -5W$	$U = 0$

TABLE 7 FREQUENCIES FOR $n = 6$

	Lowest frequency $\omega = K/a\sqrt{Gh/m}\,(1 + \bar{K}^2h^2/K^2a^2)$				Second lowest frequency $\omega = K/a\sqrt{Gh/m}$			Highest frequency $\omega = K/a\sqrt{Gh/m}$		
Ratio,	Factor,	Factor,	Shape of mode		Factor,	Shape of mode		Factor,	Shape of mode	
L/a	K	$(\bar{K}/K)^2$	V/U	W/U	K	V/U	W/U	K	V/U	W/U
1.0	0.3418	3966	+3.383	+20.18	6.821	+0.4945	−0.1325	11.54	−1.948	+0.2770
1.25	0.2371	6990	3.531	20.84	6.543	0.3924	−0.1145	11.10	−2.442	0.3657
1.5	0.1725	12000	3.804	22.43	6.384	0.3253	−0.0998	10.86	−2.935	0.4532
1.75	0.1305	19760	4.140	24.44	6.286	0.2779	−0.0880	10.71	−3.428	0.5396
2.0	0.1019	31170	4.513	26.71	6.221	0.2425	−0.07843	10.61	−3.921	0.6252
2.25	0.0816	.....	4.911	29.12	6.176	0.2152	−0.07065	10.54	−4.414	0.7101
2.5	0.06679	69280	5.326	31.63	6.143	0.1934	−0.06420	10.49	−4.906	0.7945
2.75	0.05561	.....	5.752	34.21	6.118	0.1757	−0.05878	10.46	−5.398	0.8786
3.0	0.04701	136000	6.187	36.84	6.100	0.1609	−0.05417	10.43	−5.891	0.9623
3.5	0.03480	.....	7.076	42.20	6.074	0.1378	−0.04680	10.39	−6.875	1.129
4.0	0.02680	409000	7.981	47.66	6.056	0.1205	−0.04115	10.37	−7.859	1.295
5.0	0.01726	973000	9.822	58.75	6.036	0.09629	−0.03311	10.34	−9.826	1.626
6.0	0.01200	2000000	11.69	69.97	6.025	0.08020	−0.02769	10.32	−11.79	1.956
7.0	0.008849	3660000	13.56	81.25	6.019	0.06872	−0.02378	10.31	−13.76	2.285
8.0	0.006782	6220000	15.45	92.58	6.014	0.06012	−0.02084	10.30	−15.73	2.614
9.0	0.005367	9920000	17.34	103.9	6.011	0.05344	−0.01853	10.30	−17.69	2.942
10.0	0.004347	15100000	19.24	115.3	6.009	0.04809	−0.01670	10.30	−19.66	3.271
∞	0	.....	$W = 6V$	$U = 0$	6.000	$V = W = 0$	$W = -0.35V$	10.28	$V = -6W$	$U = 0$

TABLE 8 TYPICAL VALUES OF $\bar{K}^2$ FOR $n = 0$

$L/a =$	1	5	9
Torsional mode	2.467	0.0987	0.03046
Lower nontorsional mode	21.64	−0.0104	0.00095
Higher nontorsional mode	1.792	0.2407	0.2407

TABLE 9 TYPICAL VALUES OF $\bar{K}^2$ FOR $n = 1$

$L/a =$	1	5	9
Lowest frequency	24.354	0.0379	0.0029
Second lowest frequency	3.528	0.1015	0.0913
Highest frequency	2.561	0.2677	0.0808

TABLE 10 TYPICAL VALUES OF $\bar{K}^2$ FOR HIGHER MODES, $n > 1$

		$n =$ 2	3	4	5	6
Second lowest frequency	$L/a = 1$	5.106	6.791	8.560	10.302	11.91
	$L/a = 5$	0.5075	1.044	1.694	2.480	3.419
	$L/a = 9$	0.3884	0.8424	1.446	2.207	3.130
Highest frequency	$L/a = 1$	4.338	6.441	8.725	11.267	14.146
	$L/a = 5$	0.7658	1.851	3.466	5.580	8.182
	$L/a = 9$	0.5356	1.627	3.250	5.370	7.976

$n > 1$, and the values $\bar{K}^2/K^2$ were omitted from Tables 1 and 2 and parts of Tables 3 to 7 pertaining to the higher frequencies.

The determination of the lowest frequency for the cases $n = 2$ to 6 requires, in general, the use of the corrected value ω_c, although there are cases where the correction is negligible provided h/a is small. The tables applicable for these frequencies contain the values $\bar{K}^2/K^2$ for convenient computation of ω_c. It has been stated previously that the value ω_c will be a good approximation if the difference between ω_c and ω is small. Applying the appropriate tables one can ascertain quickly that this is only the case for a very limited part of the range, for small values of L/a, n, and h/a. If L/a is large, the difference may be several 100 per cent (in the extreme case several 1000 per cent) and this simple reasoning becomes inconclusive.

There is, however, another way to approach the problem, leading to the conclusion that the frequencies ω_c in the range considered here are good approximations despite the large differences between ω and ω_c. Let us assume the vibration problem would be solved accurately by Hamilton's principle using the complete Expression [1] for the strain energy. The solution would consist of three frequencies and corresponding modes. The two higher ones of these frequencies and their modes would be very close to the membrane frequencies and modes presented in the tables, because for these modes the portion P_2 of the strain energy is insignificant, as indicated by the small values of $\bar{K}^2$ in Table 10. The three modes of the exact solution must necessarily be orthogonal to each other, i.e.

$$\int\int ma\,[u_i u_k + v_i v_k + w_i w_k]\;dz d\theta = 0 \ldots\ldots [20]$$

where u_i, v_i, w_i, are the displacement of one mode, and u_k, v_k, and w_k of one of the other modes. Substituting the Expressions [7] one obtains three simple relations between the nine constants $U_i, V_i, W_i (i = 1, 2, 3)$

$$U_1 U_2 + V_1 V_2 + W_1 W_2 = 0 \ldots\ldots\ldots [21a]$$

$$U_1 U_3 + V_1 V_3 + W_1 W_3 = 0 \ldots\ldots\ldots [21b]$$

$$U_2 U_3 + V_2 V_3 + W_2 W_3 = 0 \ldots\ldots\ldots [21c]$$

Equations [21] apply also for the values U, V, and W of the membrane theory. If the shape of the two higher actual modes is very close to the membrane ones, the values U_2, U_3, V_2, V_3, W_2, and W_3 for the actual modes will be nearly identical with the respective values for the modes of the membrane. The values U_1, V_1, and W_1 for the actual modes and for the membrane ones satisfy the respective Equations [21] with nearly identical coefficients, indicating that the respective ratios V_1/U_1 and W_1/U_1 can differ only slightly. The shape of the lowest mode determined from the membrane theory and presented in the tables can therefore not differ substantially from the actual shape. As ω_c has been determined from Rayleigh's principle which gives excellent approximations for the frequency even if the selected shape of the mode is only a crude approximation, we have a right to expect that ω_c is a good approximation in the entire range covered by the tables.

To illustrate the accuracy of the tables in a case where ω and ω_c differ substantially the frequency was computed exactly for a rather extreme case, $n = 2$, $L/a = 10$, $h/a = 1/30$. Table 3 gives for this case

$$\omega = \frac{0.03461}{a}\sqrt{\frac{Gh}{m}} \quad \text{and} \quad \omega_c = \frac{0.05653}{a}\sqrt{\frac{Gh}{m}}$$

while the exact frequency was found

$$\omega_{ex} = \frac{0.05641}{a}\sqrt{\frac{Gh}{m}}$$

In spite of the large difference between ω and ω_c, the corrected value ω_c differs only 0.2 per cent from the exact value ω_{ex}, confirming the earlier reasoning.

Dependency of Frequencies on Parameters L/a, n, and h/a

An illustration of the dependency of the frequencies on the length of the half wave L/a and the number of circumferential waves n is presented in Figs. 3, 4, and 5, for the lowest, second lowest, and highest frequencies, respectively. The frequency factor K decreases as the ratio L/a becomes larger, indicating the decreasing rigidity of the shell. As a function of n the frequency factor K shows a certain anomaly; for the lowest frequency K decreases as n becomes larger, Fig. 3, while it increases for the two other frequencies, Figs. 4 and 5. It appears therefore that the two higher frequencies increase with increasing number of circumferential waves, while the fundamental frequency decreases if h/a is small so that the frequency depends essentially on K and only slightly on $\bar{K}^2$, see Equation [18].

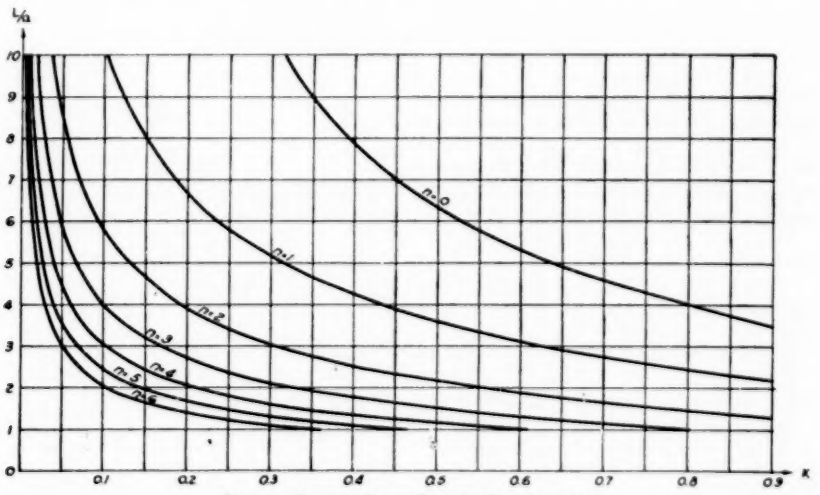

Fig. 3 Values K for Lowest Frequency

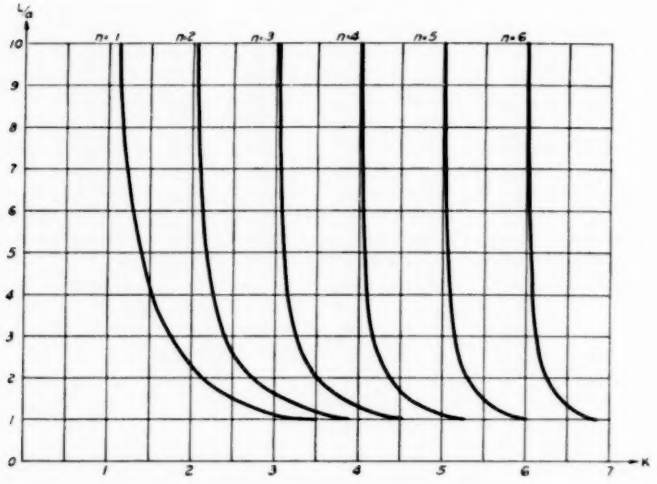

FIG. 4 VALUES K FOR SECOND LOWEST FREQUENCY

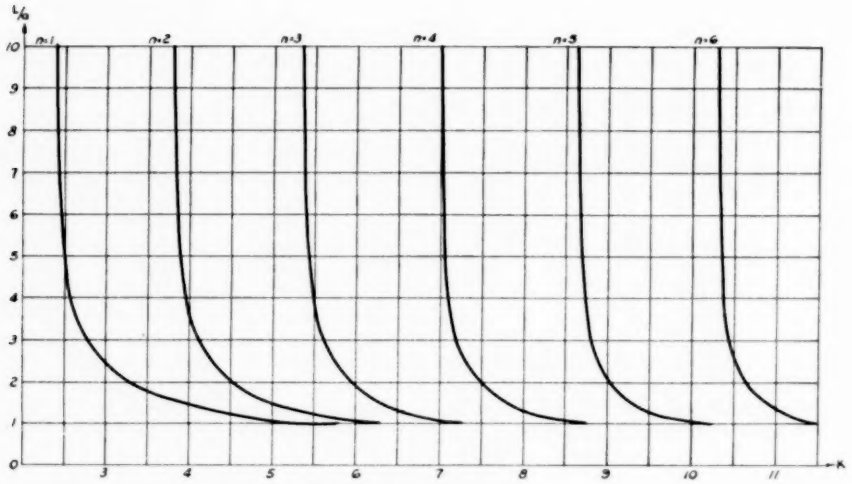

FIG. 5 VALUES K FOR HIGHEST FREQUENCY

The tendency of the fundamental frequency to decrease is ultimately arrested by a large increase in $\bar{K}^2/K^2$ for rising values of n.

The frequencies for $n = 0$ and 1, and the higher frequencies for $n > 1$ are proportional to $\sqrt{Gh/m}$ and increase with the square root of the thickness h. Because of the factor

$$\sqrt{1 + \frac{\bar{K}^2}{K^2}\frac{h^2}{a^2}}$$

the lowest frequencies for $n > 1$ increase faster with increasing h, the increase being very pronounced if L/a or n is large.

On the Thickness of Normal Shock Waves in a Perfect Gas

By A. H. SHAPIRO[1] and S. J. KLINE[2]

An approximate method for calculating the thickness of shocks in perfect gases, similar to the integral methods of ordinary boundary-layer theory, is formulated and leads to an explicit formula relating a shock-thickness Reynolds number to the Prandtl number, ratio of specific heats, and Mach number entering the shock. The method takes account of the variation of viscosity with temperature. The results of the approximate theory are in exact accord with the known exact solutions for (*a*) the case where the Prandtl number is 3/4 and the viscosity and heat conductivity are constant, (*b*) the case where the shock is very weak, and (*c*) the case where the gas has finite viscosity but zero conductivity. In addition, the approximate theory is in good agreement with results obtained on a differential analyzer showing the effects of Prandtl number and variation of viscosity with temperature. The results also are expressed in terms of the ratio of shock thickness to mean free molecular path in the inlet gas. This ratio is given in terms of the Prandtl number, ratio of specific heats, and shock strength. In the absence of relaxation effects, the numerical magnitudes suggest that the continuum theory is accurate for inlet Mach numbers below about 1.5, whereas for higher Mach numbers the continuum theory is indicative of general orders of magnitude.

Nomenclature

The following nomenclature is used in the paper:

c = speed of sound
c^* = critical speed of sound
c_p = specific heat at constant pressure
D = defined by Equation [19*b*]
F = $p_1 + \rho_1 u_1^2$
G = $\frac{k}{k-1} p_1 u_1 + \frac{1}{2} \rho_1 u_1^3$
k = ratio of specific heats
l = mean free molecular path
m = mass flow per unit area, ρu
M = Mach number, u/c
M^* = dimensionless velocity ratio, u/c^*
n = exponent in $\mu \sim T^n$
p = pressure
Pr = Prandtl number, $c_p\mu/\lambda$
R = gas constant
Rey = shock-thickness Reynolds number, $\rho_1 u_1 \delta/\mu^*$
Rey′ = modified shock-thickness Reynolds number, $\rho_1 u_1 \delta/\mu_1$
T = absolute temperature
T^* = critical value of T
T_0 = absolute stagnation temperature
u = velocity in x-direction
x = direction normal to plane of shock
δ = shock thickness, defined by Equation [10]
λ = coefficient of thermal conductivity
μ = coefficient of viscosity
ρ = mass density

$(\ )_1$ refers to conditions far upstream of shock
$(\ )_2$ refers to conditions far downstream of shock
$(\ )^*$ refers to values of properties evaluated at T^*

Introduction

Definition of Problem. Plane compression waves in perfect gases tend to become ever steeper as the result of the nonlinear interaction between pressure and inertia forces. This tendency is resisted, however, by the diffusive-type action of viscosity and heat conduction. The compression wave becomes stationary in form when the steepening tendencies of the pressure and inertia forces are exactly counterbalanced by the spreading tendencies of viscous forces and heat conduction. It is then called a "shock wave."

The purpose of this paper is to investigate by means of an approximate but simple theory the thickness of plane (i.e., one-dimensional) shock waves of stationary form in a gas and to determine the effects of Prandtl number, of specific heat ratio, of initial properties, of viscosity-temperature variation, and of shock strength on the shock thickness.

Previous Work. Rayleigh (1)[3] determined the structure of shock waves in (*a*) gases having constant coefficient of viscosity but zero coefficient of heat conductivity, and (*b*) in gases with constant heat conductivity but zero viscosity. Taylor (2) succeeded in taking account of both viscosity and heat conductivity by means of a linearizing assumption which limits the results to weak shocks. Employing the assumption that the Prandtl number is exactly 3/4, Becker (3), and later Puckett and Stewart (4), obtained explicit and exact solutions for plane shocks of any strength in a gas with constant values of specific heat, viscosity, and thermal conductivity. Thomas (5) extended Becker's work on the assumption that the viscosity varies as the square root of the absolute temperature and showed the importance of this variation for large shock strengths. Morduchow and Libby (6), using numerical integrations and the assumption of the Prandtl number being 3/4, showed the effects of different laws of variation of viscosity with temperature. Further numerical integrations, based on the actual variations with temperature of the properties of air, were carried out by Meyerhoff (7), who also investigated briefly the influence of Prandtl number. Von Mises (8) developed a comparatively simple method for determining between fairly narrow limits the thickness of the shock wave.

Present Approach to Problem. In all the foregoing investiga-

[1] Professor of Mechanical Engineering, Massachusetts Institute of Technology, Cambridge, Mass. Mem. ASME.

[2] Assistant Professor of Mechanical Engineering, Stanford University, Stanford, Calif. Mem. ASME.

Contributed by the Applied Mechanics Division and presented at the Annual Meeting, New York, N. Y., November 29–December 4, 1953, of The American Society of Mechanical Engineers.

Discussion of this paper should be addressed to the Secretary, ASME, 29 West 39th Street, New York, N. Y., and will be accepted until July 12, 1954, for publication at a later date. Discussion received after the closing date will be returned.

Note: Statements and opinions advanced in papers are to be understood as individual expressions of their authors and not those of the Society. Manuscript received by ASME Applied Mechanics Division, January 12, 1953. Paper No. 53—A-35.

[3] Numbers in parentheses refer to the Bibliography at the end of the paper.

tions the gas was treated as a continuum and the Navier-Stokes formulation of the state of stress at a point was employed. This formulation, it may be recalled, involves the assumptions that (*a*) the stress components are proportional to the rate-of-strain components, and (*b*) the "pressure" to be employed in the thermodynamic equation of state [$p = p(\rho, T)$] is the mean of the three principal stresses, thus making the second (rate-of-dilation) coefficient of viscosity exactly zero. In the energy equation a similar linear proportionality between heat flux and temperature gradient is assumed in the form of the Fourier law of heat conduction.

Now the results of the several theoretical investigations mentioned indicate that the dissipative zone of the shock is extraordinarily narrow, amounting to no more than a very few mean free molecular path lengths. Since the total changes in fluid properties occurring in this zone usually are quite large, it follows that the gradients in the shock zone are probably several orders of magnitude greater than in any other type of experiment we could hope to carry out. This immediately raises questions as to the validity of the continuum hypothesis and of the linear laws of viscosity and heat conduction. In addition, there come to mind such other questions as those relating to statistical equilibrium, thermal-relaxation effects, quantum effects, and dissociation effects.

In brief, the results of the theoretical investigations throw doubts on the assumptions underlying the theories. This is stated not to disparage the researches enumerated, for they have been fruitful, but rather to cast them in an appropriate light. That is, the continuum theories based on the Navier-Stokes equation must be regarded as supplying order-of-magnitude indications as well as useful information concerning trends produced by variations of important parameters.

Viewed in this light, approximate solutions of the Navier-Stokes equation may be almost as meaningful as "exact solutions." This will be particularly true when the approximate solution is in a closed algebraic form and the exact solution requires laborious numerical integrations. Since the exact solution in this case does require numerical integration (except for Prandtl number equal to 3/4), the closed approximate solution may well be more useful for many practical purposes.

The approximate method outlined in this paper for calculating the shock-wave thickness is similar in many respects to the integral-momentum method for the ordinary viscous boundary layer. In the latter method, (*a*) we satisfy the governing physical laws in the large, but violate them in the small except at a few points, and (*b*) we assume a "plausible" velocity profile, guided by the known boundary conditions and the ability to satisfy the exact equations of motion at a few points. In the method to be outlined, (*a*) we satisfy the governing physical laws in the large, i.e., for the shock as a whole, by introducing the Rankine-Hugoniot equations for the conditions far upstream and far downstream of the dissipative zone, (*b*) we do not attempt to satisfy the governing physical laws in the small, except at one point, and (*c*) we introduce an arbitrary but plausible velocity distribution in the dissipative zone, selected so as to satisfy the Rankine-Hugoniot conditions at plus and minus infinity and to satisfy the governing laws at one point in the interior of the shock zone.

It will be assumed that we are dealing with a perfect gas having constant specific heats.

Analysis

Governing Physical Equations. To analyze the details of the shock zone, we may examine the flow through a control surface of unit cross-sectional area perpendicular to the flow and of infinitesimal thickness dx.

Since we are dealing with a one-dimensional steady flow, the equation of continuity is

$$\rho u = \rho_1 u_1 = \rho_2 u_2 \equiv m = \text{const} \quad [1]$$

With the assumptions outlined previously for the Navier-Stokes stress formulation, the dynamic equation in one dimension may be written (9)

$$\rho u \frac{du}{dx} = -\frac{dp}{dx} + \frac{d}{dx}\left(\frac{4}{3}\mu \frac{du}{dx}\right) \quad [2]$$

Since, by Equation [1], the product ρu is equal to the constant m, Equation [2] immediately may be integrated to the form

$$mu + p - \frac{4}{3}\mu \frac{du}{dx} = F = p_1 + mu_1 \quad [3]$$

where the constant of integration F is evaluated in terms of conditions far upstream of the shock zone; there the fluid properties are uniform, and, accordingly, $du/dx = 0$.

Proceeding with the same assumptions as before, the energy equation may be written as (9)

$$\frac{d}{dx}\left(-pu + \frac{4}{3}\mu u \frac{du}{dx}\right) + \frac{d}{dx}\left(\lambda \frac{dT}{dx}\right) = \frac{\rho u}{k-1}\frac{d}{dx}\left(\frac{p}{\rho}\right) + \rho u \frac{d}{dx}\left(\frac{u^2}{2}\right) \quad [4]$$

In the light of Equation [1], this also may be integrated once, thus giving

$$pu - \frac{4}{3}\mu u \frac{du}{dx} - \lambda \frac{dT}{dx} + \frac{m}{k-1}\frac{p}{\rho} + m\frac{u^2}{2} = G = p_1 u_1 + \frac{m}{k-1}\frac{p_1}{\rho_1} + m\frac{u_1^2}{2} \quad [5]$$

where the constant of integration G is evaluated in terms of conditions far upstream, where both du/dx and dT/dx are zero. From Equation [1] and the relation $p = \rho RT$ it may be shown that $T = pu/Rm$. Inserting this into Equation [5], and making other minor rearrangements, the energy equation becomes

$$\frac{k}{k-1}pu - \frac{2}{3}\mu \frac{d(u^2)}{dx} - \frac{\lambda}{Rm}\frac{d}{dx}(pu) + \frac{mu^2}{2} = G$$

From Equation [3], however

$$pu = Fu - mu^2 + \frac{2}{3}\mu \frac{d(u^2)}{dx}$$

Eliminating pu from the foregoing pair of equations, and simplifying, we obtain a second-order, nonlinear, ordinary differential equation for u as a function of x

$$-\frac{2}{3}\frac{\lambda u}{Rm}\frac{d^2}{dx^2}(u^2) + \left(\frac{2}{3}\frac{\mu}{k-1} + \frac{\lambda}{R}\right)\frac{d(u^2)}{dx} - \frac{\lambda}{Rm}F\frac{du}{dx} - \frac{k+1}{k-1}\frac{mu^2}{2} + \frac{k}{k-1}Fu = G \quad [6]$$

Selection of Velocity Distribution. It remains to select a simple velocity distribution $u(x)$ which will approximate the exact solution to Equation [6]. We may be guided in this choice by the following requirements:

(*a*) At $x = \pm\infty$, the velocity gradient du/dx should vanish.

(*b*) Far upstream of the dissipative zone ($x = -\infty$), the velocity should be u_1.

(*c*) Far downstream of the dissipative zone ($x = +\infty$), the velocity should be u_2.

(*d*) The function $u(x)$ should vary monotonically, should be continuous, and should have continuous derivatives.

(*e*) Since requirements (*a*, *b*, *c*) demand a point of inflection ($d^2u/dx^2 = 0$), this point is, without loss of generality, arbitrarily placed at $x = 0$. This agrees with the known exact solution of Becker (3) for Pr = 3/4.

(*f*) To conform with the known exact solution of Becker (3) for Pr = 3/4, the velocity at the inflection point ($x = 0$) is set equal to $c^* = \sqrt{u_1 u_2}$. This is equivalent to the assumption that $\mathbf{M} = 1$ at the inflection point, $x = 0$.

After some casting about, a combination of two error integrals was found to conform satisfactorily to the foregoing criteria

$$x \leq 0: \qquad u = c^* + (u_1 - c^*)\,\mathrm{erf}\,(-x/b) \quad \ldots\ldots\ldots\ldots [7a]$$

$$x \geq 0: \qquad u = c^* + (u_2 - c^*)\,\mathrm{erf}\left(\sqrt{\frac{u_1}{u_2}}\,\frac{x}{b}\right) \quad \ldots\ldots\ldots [7b]$$

where b is a characteristic length soon to be associated with the shock thickness, and erf(x) is defined by (10)

$$\mathrm{erf}(x) \equiv \sqrt{\frac{2}{\pi}} \int_0^x e^{-t^2/2}dt. \quad \ldots\ldots\ldots\ldots [8]$$

This curve is seen from Fig. 1 to be in close agreement with Becker's exact solution. In order to determine how sensitive the results might be to the choice of velocity distribution, a symmetrical sine curve also was investigated. From Fig. 1 it is plain that the sine curve is a very crude approximation and that it does not quite satisfy requirements (*a*), (*b*), (*c*), and (*f*).

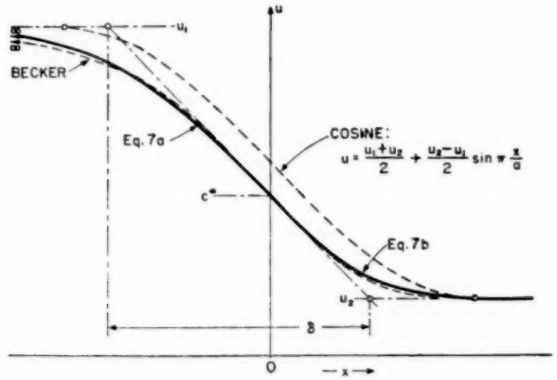

FIG. 1 COMPARISON OF BECKER'S EXACT VELOCITY DISTRIBUTION FOR Pr = 3/4, $\mathbf{M}_1 = 2.0$, AND $k = 1.4$ WITH ARBITRARY ERROR CURVE, EQUATIONS [7*a*] AND [7*b*], AND WITH A SYMMETRICAL COSINE CURVE

(In order to compare the curves easily, they all have the same slope at the inflection point.)

Shock-Thickness Reynolds Number. The velocity distribution, Equation [7], is as yet undetermined to the extent that the characteristic length b is unknown. We now evaluate the latter by requiring that Equation [6] be satisfied at one point, namely, at $x = 0$. Accordingly, we find from the properties of the error integral that

$$(u)_{x=0} = c^* \quad \ldots\ldots\ldots\ldots [9a]$$

$$\left(\frac{du}{dx}\right)_{x=0} = -\frac{u_1 - c^*}{b}\sqrt{\frac{2}{\pi}} = -\sqrt{\frac{2}{\pi}}\,\frac{c^*}{b}\,(\mathbf{M}_1^* - 1) \quad [9b]$$

$$\left(\frac{d(u^2)}{dx}\right)_{x=0} = -\frac{2c^*(u_1 - c^*)}{b}\sqrt{\frac{2}{\pi}} = -\sqrt{\frac{8}{\pi}}\,\frac{c^{*2}}{b}\,(\mathbf{M}_1^* - 1) \quad \ldots\ldots [9c]$$

$$\left(\frac{d^2}{dx^2}(u^2)\right)_{x=0} = \frac{4}{\pi}\,\frac{(u_1 - c^*)^2}{b^2} = \frac{4}{\pi}\,\frac{c^{*2}}{b^2}\,(\mathbf{M}_1^* - 1)^2 \quad [9d]$$

At this point it is convenient to define a characteristic thickness for the shock. This is defined in the usual manner as

$$\delta \equiv \frac{u_2 - u_1}{(du/dx)_{x=0}} \quad \ldots\ldots\ldots\ldots [10]$$

and has the geometrical significance indicated by Fig. 1. Combining this with Equation [9*b*], and recalling that $u_1u_2 = c^{*2}$, we may form the relation

$$\frac{\delta}{b} = \sqrt{\frac{\pi}{2}}\,\frac{\mathbf{M}_1^* + 1}{\mathbf{M}_1^*} \quad \ldots\ldots\ldots\ldots [11]$$

Thus Equations [9*b*], [9*c*], and [9*d*] may be expressed in terms of δ rather than b.

Equations [9*a*], [9*b*], [9*c*], and [9*d*] are now substituted into Equation [6], with b eliminated in favor of δ by means of Equation [11]. At the same time, since we are attempting to satisfy Equation [6] at $x = 0$, the transport properties are evaluated at the temperature T^* corresponding to $x = 0$; they are therefore denoted by the symbols μ^* and λ^*. How T^* is determined is discussed later.

After these substitutions have been made in Equation [6], the latter is in the form of a quadratic algebraic equation with δ as unknown. In the course of solving this equation, certain dimensionless groups appear quite naturally. The chief of these are the "shock-thickness Reynolds number," defined by

$$\mathrm{Rey} \equiv \frac{\rho_1 u_1 \delta}{\mu^*} = \frac{m\delta}{\mu^*} \quad \ldots\ldots\ldots\ldots [12]$$

and the Prandtl number, defined by

$$\mathrm{Pr}^* \equiv c_p{}^*\mu^*/\lambda^* \quad \ldots\ldots\ldots\ldots [13]$$

The following relations also are useful in simplifying the solution

$$\frac{F}{mu_1} = 1 + \frac{p_1}{\rho_1 u_1^2} = 1 + \frac{RT_1}{u_1^2} = 1 + \frac{1}{k\mathbf{M}_1^2} \quad \ldots\ldots [14]$$

$$\frac{G}{mu_1^2} = \frac{1}{2} + \frac{p_1}{\rho_1 u_1^2} + \frac{p_1}{(k-1)\rho_1 u_1^2} = \frac{1}{2} + \frac{1}{(k-1)\mathbf{M}_1^2} \quad [15]$$

It has been found convenient to express the results in terms of $\mathbf{M}_1^*$ rather than $\mathbf{M}_1$, where (11)

$$\mathbf{M}_1^* \equiv u_1/c^* \quad \ldots\ldots\ldots\ldots [16]$$

$$\mathbf{M}_1^2 = \frac{\frac{2}{k+1}\,\mathbf{M}_1^{*2}}{1 - \frac{k-1}{k+1}\,\mathbf{M}_1^{*2}} \quad \ldots\ldots\ldots\ldots [17]$$

and

$$c^* = \sqrt{\frac{2}{k+1}}\,c_0 \quad \ldots\ldots\ldots\ldots [18]$$

where c_0 is the stagnation speed of sound either far upstream or far downstream of the dissipative zone.

With the help of the auxiliary relations of Equations [12] to

[18], the solution of Equation [6] at $x = 0$ may be brought into the convenient and explicit form

$$\text{Rey} = \frac{D}{k+1}\frac{\mathbf{M}_1^* + 1}{\mathbf{M}_1^* - 1}\left[1 \pm \sqrt{1 + \frac{8k(k+1)}{3\text{Pr}^*}\frac{1}{D^2}\frac{(\mathbf{M}_1^* - 1)^2}{\mathbf{M}_1^*}}\right] \quad \ldots\ldots [19a]$$

where

$$D \equiv \frac{4}{3} + \frac{2k}{\text{Pr}^*} - \left(\frac{k+1}{2\text{Pr}^*}\right)\frac{\mathbf{M}_1^{*2} + 1}{\mathbf{M}_1^*} \quad \ldots\ldots [19b]$$

The selection of the sign preceding the radical in Equation [19a] is determined by the requirement that Rey be positive—thus, when D is positive the plus sign must be used, but when D is negative the minus sign must be used.

A word is now in order regarding the evaluation of μ^* and λ^*. If we choose to ignore the variation of μ and λ with temperature, then there is no difficulty, as μ^* and λ^* may be evaluated at the temperature T_1. When it is desired to make an improvement on this calculation, however, we may be guided by the exact solution for Pr = 3/4. In the latter case the adiabatic stagnation temperature T_0 is constant throughout the dissipative zone, and therefore $T^* = [2/(k+1)]T_0$. It seems reasonable to suppose that evaluating μ^* and λ^* at this same temperature for other values of Pr will provide a good approximation. Since this type of simplifying assumption is in keeping with the general purpose of the method outlined here, it will be adopted in what follows.

Results

Comparison With Exact Solution for Pr = 3/4. Puckett and Stewart (4) have put Becker's exact solution (3) for the case where Pr = 3/4 and μ and λ are constant into the form

$$(\text{Rey})_{\text{Pr}=3/4} = \frac{8k}{3(k+1)}\frac{\mathbf{M}_1^* + 1}{\mathbf{M}_1^* - 1} \quad \ldots\ldots [20]$$

When Pr* is set equal to 3/4 in Equation [19], it reduces to Equation [20], thus showing that the approximate method of this paper is in perfect agreement with the exact solution of Becker. This gratifying result suggests that the approximate method is likely to be reasonably accurate for other values of Prandtl number.

Very Weak Shocks. When $\mathbf{M}_1^*$ approaches unity, Equation [19] may be approximated by

$$(\text{Rey})_{\mathbf{M}_1^* \to 1} \cong \frac{4}{k+1}\left(\frac{4}{3} + \frac{k-1}{\text{Pr}^*}\right)\frac{1}{\mathbf{M}_1^* - 1} \quad \ldots\ldots [21]$$

Hence the thickness of weak shocks is inversely proportional to the strength of the shock, provided that the strength is measured by the fractional difference between the propagation speed of the shock and the propagation speed of a sound wave. Even for extremely weak shocks, however, the shock thickness at normal pressure and temperature is extremely small compared with the dimensions of physical objects. For example, in air at normal atmospheric conditions, with $\mathbf{M}_1^* = 1.05$, $k = 1.4$, and Pr* = 3/4, it is found that δ is only about 10^{-5} ft.

Taylor (2) has worked out the exact solution to Equation [6] for arbitrary values of Pr on the basis of the linearizing assumption that $\mathbf{M}_1^*$ is nearly unity. When arranged in the form of the shock-thickness Reynolds number, his solution proves to be identical with Equation [21]. This agreement lends added confidence in the accuracy of the approximate method of this paper.

Very Strong Shocks. For infinitely strong shocks, $\mathbf{M}_1^*$ attains a finite maximum given by $\sqrt{(k+1)/(k-1)}$. When this value is substituted into Equation [19], it is found that the shock-thickness Reynolds number of very strong shocks is finite and not zero. The numerical values of Rey for very strong shocks may be read from Fig. 2. (For remarks concerning the shock thickness itself, see the discussion accompanying Figs. 5 and 6.)

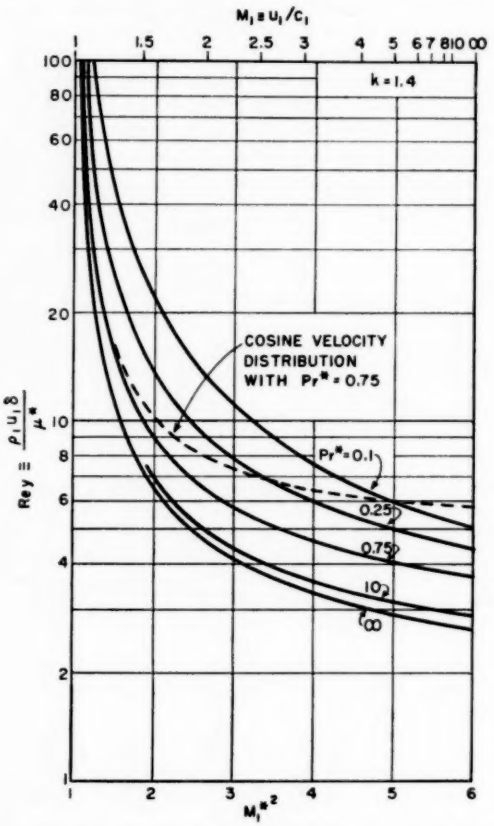

Fig. 2 Shock-Thickness Reynolds Number Versus $\mathbf{M}_1^{*2}$, for Various Values of Prandtl Number, and With $k = 1.4$
(Solid curves are for error-integral velocity distributions, and dashed curve is for cosine velocity distribution.)

Gas With $k = 1$. When k is set equal to unity in Equation [19], the latter may be reduced to the simple form

$$(\text{Rey})_{k=1} = \frac{4}{3}\frac{\mathbf{M}_1^* + 1}{\mathbf{M}_1^* - 1} \quad \ldots\ldots [22]$$

The most interesting feature of this result is that the shock-thickness Reynolds number is independent of Prandtl number, and hence the shock thickness itself is independent of the coefficient of thermal conductivity. This may be explained easily on physical grounds. In a gas with $k = 1$, the specific heats are infinite, and, therefore, finite changes in state occur with zero change in temperature. This means that the gas flows through the dissipative zone of the shock isothermally. Consequently heat conduction plays no role in the process, and the shock thickness is accordingly independent of λ.

Since, for $k = 1$, the results are independent of Pr, it follows that Equation [22] should be identical with Equation [20] when $k = 1$ is inserted into the latter. This is, in fact, the case.

Gases With Extreme Values of μ^* and λ^*. It is of some interest to examine the limiting cases where λ^* and μ^* take on ex-

TABLE 1 VALUES OF REY AND δ

	Pr = 0		Pr = ∞	
	$\mu^* \neq 0, \infty$; $\lambda^* = \infty$	$\mu^* = 0$; $\lambda^* \neq 0, \infty$	$\mu^* = \infty$; $\lambda^* \neq 0, \infty$	$\mu^* \neq 0, \infty$; $\lambda^* = 0$
Rey	∞	∞	$\frac{8/3}{k+1}\frac{M_1^*+1}{M_1^*-1}$	$\frac{8/3}{k+1}\frac{M_1^*+1}{M_1^*-1}$
δ	∞	$\frac{\lambda^*}{\rho_1 u_1 c_p^*}\frac{M_1^*+1}{M_1^*-1}\left(\frac{4k}{k+1}-\frac{M_1^{*2}+1}{M_1^*}\right)$	∞	$\frac{8/3}{k+1}\frac{\mu^*}{\rho_1 u_1}\frac{M_1^*+1}{M_1^*-1}$

treme values of either zero or infinity. The values of Rey and δ corresponding to four such combinations are summarized in Table 1.

It is seen that the shock-thickness Reynolds number is always infinite for Pr = 0 (zero viscosity or infinite conductivity) but is generally finite (except at $M_1^* = 1$) for Pr = ∞ (zero conductivity or infinite viscosity).

If either μ^* or λ^* is infinite, then the shock thickness becomes infinite, as might be expected from physical considerations.

When the gas has finite viscosity but zero conductivity, or finite conductivity but zero viscosity, the shock thickness is finite. These results are in accord with the exact results obtained by Rayleigh (1) and by Taylor (2), both of whom found that either finite viscosity alone or finite conductivity alone can account for the existence of finite compression waves of stationary form. Indeed, the formula for δ given in Table 1 for the case where $\lambda^* = 0$ is identical with the formula for δ calculated from Rayleigh's exact solution (1) for the case $\lambda = 0$; this constitutes still another exact agreement between the present approximate method and a known exact solution.

Effect of Mach Number. Fig. 2 shows that the shock-thickness Reynolds number decreases with ascending Mach number. For Mach numbers near unity this effect is very pronounced, but at high Mach numbers the shock-thickness Reynolds number is nearly constant. The shapes of the curves in Fig. 2 are typical of those for values of k between 1 and 5/3.

Effect of Prandtl Number. Fig. 2 (and Fig. 4) are typical of the effects produced by variations in Pr* for gases with k not too close to unity. The outstanding feature to be observed is that, for values of Pr* between, say, 3/4 and infinity, the shock-thickness Reynolds number is insensitive to variations in Pr*.

In fact, comparison of Table 1 with Equation [20] shows that

$$\frac{(\mathrm{Rey})_{\mathrm{Pr}^*=3/4}}{(\mathrm{Rey})_{\mathrm{Pr}^*=\infty}} = k$$

which establishes an upper limit to the decrease in Rey owing to an increase in Pr* for values of the latter between 3/4 and ∞. As the Prandtl number becomes small compared with unity, on the other hand, the shock-thickness Reynolds number rises sharply. In the range of real gases, however, where Pr* usually lies between 0.5 and 1.0, it is safe to say that the Prandtl number has only a minor effect on the shock thickness.

According to Fig. 3, the influence of Prandtl number is dependent upon the specific-heat ratio. For $k = 1.0$ the shock thickness is completely independent of Prandtl number. As k increases from unity, the effect of Prandtl number increases simultaneously.

Meyerhoff (7), who solved Equation [6] by means of a differential analyzer combined with numerical integration, reached the conclusion, "the shock-wave thickness (in air) for an initial Mach number of 2.0 is about 3 times greater for Pr = 0.657 than for Pr = 0.75." This conclusion is vastly different from the evidence of Fig. 2. A close examination of Meyerhoff's results reveals, however, that the comparison is between two shocks having the same value of $\rho_1 u_1$ but very different values of initial pressure and temperature. In particular, the inlet temperature for Pr = 3/4 was 0 C whereas for Pr = 0.657 it was 500 C. But if the shock-thickness Reynolds numbers, Rey, are formed using the viscosities corresponding to these temperatures together with the thicknesses measured directly from Fig. 3 of Meyerhoff's paper (7), it is found that Rey for the case of 0 C is 4 per cent greater than that for the case of 500 C. This difference of 4 per cent is (within the accuracy of taking slopes from Meyerhoff's Fig. 3) exactly what one would predict, owing to the differences in Pr* and k, from Figs. 3 and 4 of the present paper. Therefore Meyerhoff's result, properly interpreted, confirms the present theory as given in Figs. 3 and 4. The difference in shock-wave thickness noted by Meyerhoff is only minutely ascribable to the difference in Prandtl number and is principally the result of the difference in viscosity between the two cases investigated. In fact, the effect due to the difference in k, although small for this case, is still 3 times as large as the effect due to the difference in Pr. This example, incidentally, illustrates the value of working with the appropriate nondimensional parameter, the shock-thickness Reynolds number.

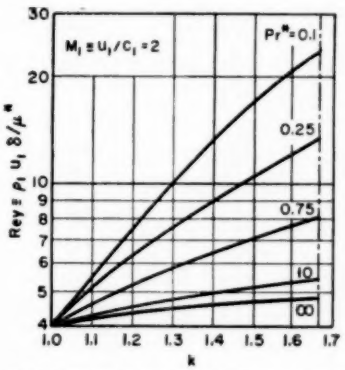

FIG. 3 SHOCK-THICKNESS REYNOLDS NUMBER VERSUS SPECIFIC-HEAT RATIO, FOR VARIOUS VALUES OF PRANDTL NUMBER, AND FOR $M_1 = 2$

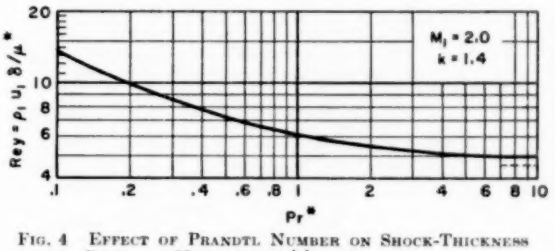

FIG. 4 EFFECT OF PRANDTL NUMBER ON SHOCK-THICKNESS REYNOLDS NUMBER, FOR $M_1 = 2$ AND $k = 1.4$

Effect of Specific-Heat Ratio. From Fig. 3 it is seen that the effect of k is substantial for gases with low Prandtl numbers, and that it is very small for gases with values of Pr* large compared with unity. In the range of real gases, i.e., for Pr* ≧ 3/4, a change in k from 1.0 to 5/3 acts to increase the shock-thickness Reynolds number about twofold.

Effect of Variation of Viscosity and Conductivity With Temperature. Although both μ and λ vary substantially with temperature, it is known that for real gases their variations are such that the Prandtl number depends only slightly on temperature. It has been noted already that, everything else being the same, the shock-thickness Reynolds number for known gases is insensitive to Prandtl number. Therefore we may investigate the effects of variations in viscosity and heat conductivity by considering only variations in viscosity for constant values of Pr*.

It is convenient to think of variations of viscosity with temperature as affecting the results in two ways; namely, (*a*) there are gradients in viscosity through the dissipative zone, and (*b*) in the center of the dissipative zone, where presumably viscosity is of most importance, the temperature (and hence the viscosity) is different from the value at the entrance to the shock. Effect (*a*) cannot be treated by the present analysis, but the effect (*b*) is easily taken into account.

We define a modified shock-thickness Reynolds number, Rey′, in terms of the inlet properties

$$\text{Rey}' \equiv \rho_1 u_1 \delta/\mu_1 \quad \ldots\ldots [23]$$

If we assume that the viscosity-temperature law may be represented by $\mu \sim T^n$, where n is an empirically determined constant, then

$$\text{Rey}' = \text{Rey}\,\frac{\mu^*}{\mu_1} = \text{Rey}\left(\frac{T^*}{T_1}\right)^n \quad \ldots\ldots [24]$$

From the laws of adiabatic flow (11)

$$\frac{T^*}{T_1} = \frac{2}{k+1}\left(1 + \frac{k-1}{2}\,\mathbf{M}_1^2\right)$$

Therefore

$$\text{Rey}' = \text{Rey}\left[\frac{2}{k+1}\left(1 + \frac{k-1}{2}\,\mathbf{M}_1^2\right)\right]^n \quad \ldots\ldots [25]$$

By means of Equation [25] the results given previously may easily be expressed in terms of Rey′ rather than Rey.

To illustrate the effects of viscosity variation, Fig. 5 shows how $\rho_1 u_1 \delta/\mu_1$ varies with inlet Mach number for Pr* = 3/4, k = 1.4, and for values of n of zero (constant viscosity), 0.5 (value from kinetic theory), and 0.768 (empirical value for air). It is seen that the variation of viscosity increases the shock thickness at all Mach numbers; this is explained physically by noting that the variation in viscosity with temperature makes the viscosity in the midst of the dissipative zone larger than the inlet viscosity, and this in turn increases the spreading tendencies of viscosity.

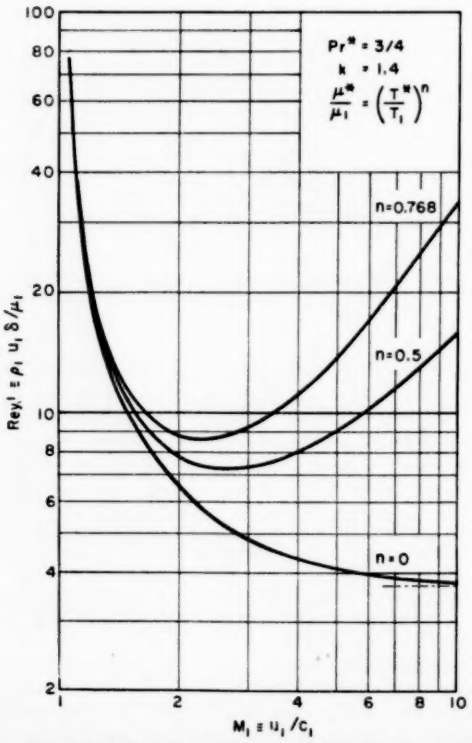

FIG. 5 EFFECT OF VARIATION OF VISCOSITY WITH TEMPERATURE ON SHOCK THICKNESS, FOR Pr* = 3/4, k = 1.4, AND SEVERAL VISCOSITY-TEMPERATURE LAWS

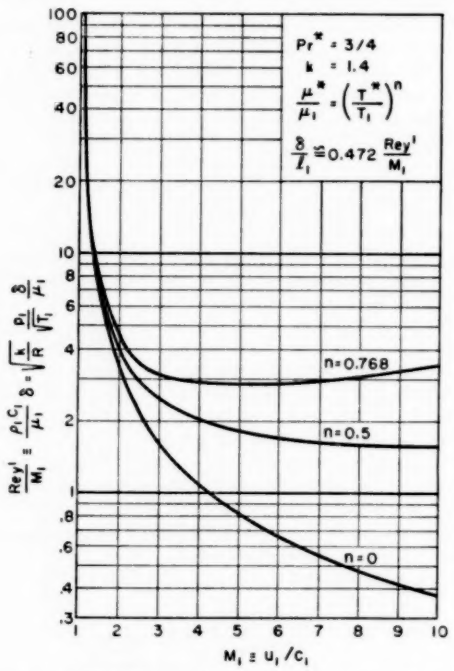

FIG. 6 REY′/$\mathbf{M}_1$ VERSUS $\mathbf{M}_1$ FOR Pr* = 3/4 AND k = 1.4
(The ordinate is proportional to shock thickness for fixed thermodynamic properties, and the abscissa is a measure of shock strength. The ordinate also is proportional to ratio of shock thickness to mean free molecular length in inlet gas.)

To illustrate the effects of viscosity variation, Fig. 5 shows how $\rho_1 u_1 \delta/\mu_1$ varies with inlet Mach number for Pr* = 3/4, k = 1.4, and for values of n of zero (constant viscosity), 0.5 (value from kinetic theory), and 0.768 (empirical value for air). It is seen that the variation of viscosity increases the shock thickness at all Mach numbers; this is explained physically by noting that the variation in viscosity with temperature makes the viscosity in the midst of the dissipative zone larger than the inlet viscosity, and this in turn increases the spreading tendencies of viscosity.

At high Mach numbers the effect of viscosity variation is especially pronounced. Whereas for the case of constant viscosity Rey′ constantly decreases with rising $\mathbf{M}_1$, in the case of variable viscosity the value of Rey′ falls to a minimum and then rises again, approaching infinity as $\mathbf{M}_1$ approaches infinity.

To show the effect of shock strength and of viscosity-variation on the shock thickness for fixed thermodynamic properties (p_1, T_1, ρ_1, μ_1, c_1) at inlet, Rey′/$\mathbf{M}_1$ is plotted against $\mathbf{M}_1$ in Fig. 6. According to kinetic theory, the ordinate of this chart is approximately twice as large as the ratio of shock thickness (δ) to mean free molecular path in the approach gas (l_1). Applying this rule to the values given by Fig. 6, it is evident that the continuum theory of the shock thickness is valid for very weak shocks but is only indicative of general orders of magnitude for strong shocks.

Morduchow and Libby (6), by integration of the exact Navier-Stokes equations, obtained results similar to those of Fig. 6.

They found (for $k = 1.4$ and $\mathrm{Pr} = 3/4$) that with values of n less than 0.5 the shock thickness (for constant p_1, T_1, and μ_1) decreases continuously with shock strength and approaches zero as $\mathbf{M}_1 \rightarrow \infty$; for n greater than 0.5 the shock thickness first decreases with $\mathbf{M}_1$ but passes through a minimum and then rises, tending toward infinity for $\mathbf{M}_1 \rightarrow \infty$; and for n equal to 0.5 the shock thickness decreases but approaches a finite limit as $\mathbf{M}_1 \rightarrow \infty$. The present theory, as embodied in Fig. 6, is seen to be in agreement with these conclusions. The quantitative values of δ/l_1 (found by comparing Fig. 6 of this paper with fig. 5 of reference 6) are also in excellent agreement with those of Morduchow and Libby, differing at most by a few per cent. From this we conclude that the important aspect of the viscosity-temperature variation is that the viscosity in the middle of the dissipative zone differs from the inlet viscosity. This is physically plausible because most of the viscous action occurs near the middle of the dissipative zone. In this respect the shock wave is similar to the viscous boundary layer near a solid surface; in the latter case it is known that the effects of viscosity variation across the boundary layer may be accounted for approximately by treating the problem as one of constant viscosity provided that the viscosity is taken as some mean viscosity in the dissipative zone.

The thickness of shocks advancing into gas of fixed pressure and temperature having $\mathrm{Pr}^* = 3/4$ and $k = 1.4$ varies with shock strength according to the following rules (see Fig. 6):

1 If the viscosity of the gas is constant, or if it varies only slowly with temperature, the shock thickness continually decreases as the shock strength increases.

2 If the viscosity of the gas varies with temperature as does air, the thickness at first decreases with rising shock strength, reaches a minimum at $\mathbf{M}_1 \leqq 5$, and then rises again, tending toward infinity as the shock strength becomes infinite.

Similar rules for other values of Pr^* and k may be derived by plotting Equations [19] and [25] after the manner of Fig. 6. It may be remarked incidentally that this method of plotting is perhaps the most illuminating, since it not only brings out most clearly the effects of the different variables, but simultaneously indicates the validity of the continuum theory through expressing the shock-wave thickness as a multiple of the molecular mean free path.

Effect of Assumed Velocity Distribution. It remains to be seen whether the results of the approximate method are sensitive to the choice of the assumed velocity distribution.

If, in place of Equation [7], the cosine function of Fig. 1 is substituted into Equation [6], then Equation [19] must be replaced by

$$\mathrm{Rey} = \frac{2}{k+1}\left(\frac{4}{3} + \frac{k-1}{\mathrm{Pr}^*}\right)\frac{\mathbf{M}_1^{*2}+1}{\mathbf{M}_1^{*2}-1}\left[1 + \sqrt{1 + \frac{\frac{8}{3}\frac{k(k+1)}{\mathrm{Pr}^*}}{\left(\frac{4}{3} + \frac{k-1}{\mathrm{Pr}^*}\right)^2}\left(\frac{\mathbf{M}_1^{*2}-1}{\mathbf{M}_1^{*2}+1}\right)^2}\right] \quad \ldots [26]$$

In Fig. 2 the dashed line represents this equation for $k = 1.4$ and $\mathrm{Pr}^* = 3/4$. For low Mach numbers, Equation [26] is seen to agree well with the exact solution and indeed reduces to Equation [20] as $\mathbf{M}_1^* \rightarrow 1$. At high Mach numbers, Equation [26] yields too large a value of shock thickness, but the maximum error (for $\mathbf{M}_1 = \infty$) is only 50 per cent.

This result shows that the approximate method yields correct orders of magnitude, provided that the assumed velocity distribution has the correct general shape in the midst of the dissipative zone. A similar conclusion is known to be valid for the integral methods of boundary-layer theory, namely, that the results are insensitive to the choice of assumed velocity profile.

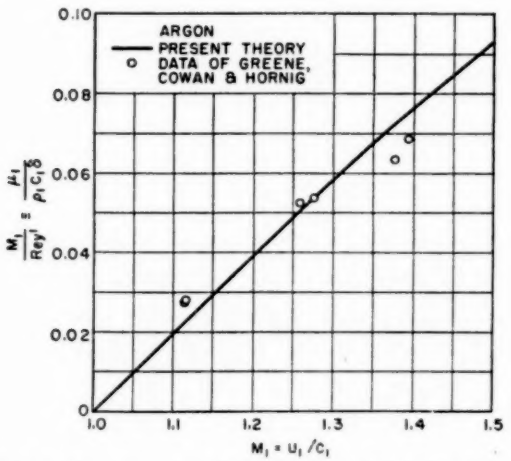

FIG. 7(a) COMPARISON OF PRESENT THEORY WITH EXPERIMENTAL RESULTS OF GREENE, COWAN, AND HORNIG—ARGON, WITH $k = 1.667$, $\mathrm{Pr}^* = 0.66$, AND $n = 0.816$

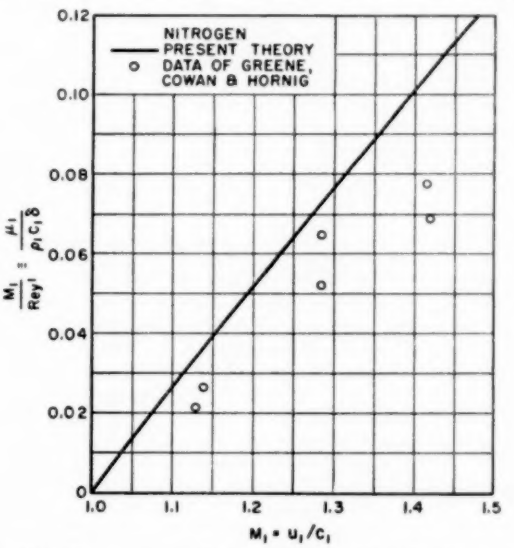

FIG. 7(b) COMPARISON OF PRESENT THEORY WITH EXPERIMENTAL RESULTS OF GREENE, COWAN, AND HORNIG—NITROGEN, WITH $k = 1.40$, $\mathrm{Pr}^* = 0.77$, AND $n = 0.756$

Comparison With Experiments. Figs. 7(a) and 7(b) show a comparison between the results of the present theory and the experimental data of Greene, Cowan, and Hornig (12). The latter, it should be noted, report the shock thickness as $(\rho_2 - \rho_1)/(d\rho/dx)_{\max}$; although this is not strictly comparable with δ as defined in the present paper, the difference should be quite small for weak shocks. The accuracy of the experimental shock thickness is claimed as ± 15 per cent.

For argon, Fig. 7(a), the deviation of the theory from the experimental data is within the experimental accuracy of the latter. For nitrogen, Fig. 7(b), on the other hand, the experimental value of δ is substantially in excess of the theoretical. It

is tempting to conclude that the difference in agreement between theory and experiment in the two cases arises from the fact that the nitrogen molecule, unlike the argon molecule, has a rotational degree of freedom and thus is subject to a nonequilibrium relaxation effect which tends to increase the shock thickness. However, in the present state of affairs this conclusion might be premature, as the combination of experimental errors and theoretical inadequacies might be in fact responsible for the striking differences between Figs. 7(*a*) and 7(*b*).

BIBLIOGRAPHY

1 "Aerial Plane Waves of Finite Amplitude," by Lord Rayleigh, Proceedings of the Royal Society of London, England, series A, vol. 84, 1910, p. 247.

2 "The Conditions Necessary for Discontinuous Motion in Gases," by G. I. Taylor, Proceedings of the Royal Society of London, England, series A, vol. 84, 1910, p. 371.

3 "Impact Waves and Detonation," by R. Becker, part 1, NACA TM, No. 505, 1929.

4 "The Thickness of a Shock Wave in Air," by A. E. Puckett and H. J. Stewart, *Quarterly of Applied Mathematics*, vol. 7, 1950, p. 457.

5 "Note on Becker's Theory of the Shock Front," by L. H. Thomas, *Journal of Chemical Physics*, vol. 12, 1944, p. 449.

6 "On a Complete Solution of the One-Dimensional Flow Equations of a Viscous Heat Conducting Compressible Gas," by M. Morduchow and P. A. Libby, *Journal of the Aeronautical Sciences*, vol. 16, 1949, p. 674.

7 "An Extension of the Theory of the One-Dimensional Shock-Wave Structure," by L. Meyerhoff, *Journal of the Aeronautical Sciences*, vol. 17, 1950, p. 775.

8 "On the Thickness of a Steady Shock Wave," by R. von Mises, *Journal of the Aeronautical Sciences*, vol. 17, 1950, p. 551.

9 "Modern Developments in Fluid Dynamics," by S. Goldstein, Oxford University Press, New York, N. Y., vol. 2, 1948.

10 "Tables of Functions With Formulae and Curves," by E. Jahncke and F. Emde, Dover Publications, New York, N. Y., 1945.

11 "Introduction to Theoretical Gas Dynamics," by R. Sauer, J. W. Edwards, Ann Arbor, Mich., 1947.

12 "The Thickness of Shock Fronts in Argon and Nitrogen and Rotational Heat Capacity Lags," by E. F. Greene, G. R. Cowan, and D. F. Hornig, *Journal of Chemical Physics*, vol. 19, 1951, p. 427.

Brief Notes*

On the recommendations of the Executive Committee of the ASME Applied Mechanics Division, it has been decided to initiate a section devoted to brief notes on technical matters in mechanics. These notes must not be longer than 750 words (about 2½ double-spaced typewritten pages, including figures) and will be subject to the usual review procedure prior to publication. After approval such notes will be published in the next issue of the Journal. The notes should be submitted to the Secretary of the ASME Applied Mechanics Division.

The Delayed Hot-Water Problem

By WALTER MUNK,[1] LA JOLLA, CALIF.

IT is a common source of annoyance that in houses where the hot-water heater is some distance from a faucet it may take a remarkably long time to get hot water after the faucet is turned on. After this initial delay the actual change from cold to hot water is relatively quick. It will be shown that the heat "front" advances at a velocity less, possibly much less, than that of the water, and that to a first approximation the heat front remains unsoftened.

The problem differs essentially from classical heat-flow problems. In its simplest form we assume a pipe extending from the hot-water heater at $x = 0$ in the positive x-direction. At $t = 0$, when the water is turned on, we have for the temperature $T = H(x)$ where $H(x)$ is a step function equal to T_{hot} for $x < 0$ and T_{cold} for $x > 0$. Subsequently $T = T_{hot}$ at $x = 0$ until the original hot-water supply is exhausted.

The water is well stirred, and $T(x)$ is taken as the temperature of both the water and pipe at a distance x from the heater.[2] The increase in heat content of pipe and water between x and $x + \delta x$ is $(c'm'\delta x + cm\delta x)\delta T$, where c' is the heat capacity of the pipe and m' its mass per unit length, and where c, m are the corresponding quantities for the water. This increase must equal the excess $qc(\partial T/\partial x)\delta x\delta t$ of heat inflow at x over outflow at $x + \delta x$ during δt, provided conduction in pipe and water is negligible. Here $q = mu$ is the mass flux at a mean velocity u (independent of x). Hence

$$(c'm' + cm)\frac{\partial T}{\partial t} = -cmu\frac{\partial T}{\partial x}$$

or

$$\frac{\partial T}{\partial t} + v\frac{\partial T}{\partial x} = 0$$

where

$$v = \frac{u}{1 + r}, \quad r = \frac{m'c'}{mc}$$

The solution satisfying the boundary conditions is

$$T = H(x - vt)$$

Thus the "heat wave" travels at a velocity v which is always less than the water velocity u. The reason for the delay is, of course, that the pipe has to be heated as well as the water. In the case of pipes with thick walls and small ID, the delay can be considerable. For ¾-in. heavy wrought-iron pipe $r = 0.91$, $v = 0.52u$. If the discharge is 6 cu in. per sec, it would take 50 sec to obtain hot water at a faucet 30 ft from the heater!

To the present approximation the hot water arrives suddenly. Actually, the heat front will be blurred, largely because the velocity of flow varies throughout the pipe, and the water is hotter in the middle of the pipe than against the walls.

Plastic Potential Theory and Prandtl Bearing Capacity Solution[1]

By R. T. SHIELD,[2] PROVIDENCE, R. I.

THE purpose of this note is to outline a method of showing that the Prandtl stress solution[3] to the plane-strain problem of a flat rigid punch (or footing) is valid for idealized, weightless soils with cohesion whose angles of internal friction are less than 75 deg. Since a kinematically admissible velocity field can be associated with the Prandtl stress solution,[4] limit analysis[5,6] shows that the Prandtl value[3]

$$p = c\cot\varphi[\exp(\pi\tan\varphi)\tan^2(\pi/4 + \varphi/2) - 1] \quad [1]$$

is an upper bound for the collapse value of the average pressure over the punch, where c is the cohesion and φ is the angle of internal friction of the soil. A statically admissible extension of the Prandtl stress field into the rigid region is found here, so that the value [1] is also a lower bound and therefore the true value of the average pressure.

In Fig. 1, *O-E* is the center line of the punch *O-A* indenting the surface *O-D* of the soil. The region *O-B-C-D* is composed of the Prandtl stress field of two regions of constant state, *O-A-B* and *A-D-C*, and a region of radial shear *A-B-C*. The Prandtl field is continued to the line of stress discontinuity *B-S-F* which is as yet unspecified. The stress field below this line is determined from the following conditions:

---

[1] Associate Professor, Scripps Institute of Oceanography, University of California.

[2] The case of different temperatures has been treated by Anzelius ("Partial Differential Equations of Mathematical Physics," by H. Bateman, Dover Publications, New York, N. Y., 1932, p. 123), and "Heat Transfer: A Liquid Flowing Through a Porous Prism," by T. E. W. Schumann, *Journal of The Franklin Institute*, vol. 208, 1929, p. 405.

* Discussion of papers in Brief Notes should be addressed to the Secretary, ASME, 29 West 39th Street, New York, N. Y., and will be accepted until July 12, 1954, for publication at a later date. Discussion received after the closing date will be returned.

NOTE: Statements and opinions advanced in papers are to be understood as individual expressions of their authors and not those of the Society. Manuscript received by ASME Applied Mechanics Division, November 13, 1953.

[1] The results presented in this paper were obtained in the course of research sponsored by the Office of Naval Research under Contract N7onr-35801 with Brown University.

[2] Research Associate in Applied Mathematics, Brown University. Now Senior Research Fellow, ARE Fort Halstead, Sevenoaks, Kent, England.

[3] "Über die Härte Plastischer Körper," by L. Prandtl, Nachrichten von der Königlichen Gesellschaft der Wissenschaften zu Göttingen, *Mathematisch-Physikalische Klasse*, 1920, pp. 74–85.

[4] "Mixed Boundary Value Problems in Soil Mechanics," by R. T. Shield, *Quarterly of Applied Mathematics*, vol. 11, 1953, pp. 61–75.

[5] "On Plastic-Rigid Solutions and Limit Design Theorems for Elastic-Plastic Bodies," by D. C. Drucker, H. J. Greenberg, E. H. Lee, and W. Prager, Proceedings of the First U. S. National Congress of Applied Mechanics, June, 1951, pp. 533–538.

[6] "Soil Mechanics and Plastic Analysis or Limit Design," by D. C. Drucker and W. Prager, *Quarterly of Applied Mathematics*, vol. 10, 1952, pp. 157–165.

Manuscript received by ASME Applied Mechanics Division, August 11, 1953.

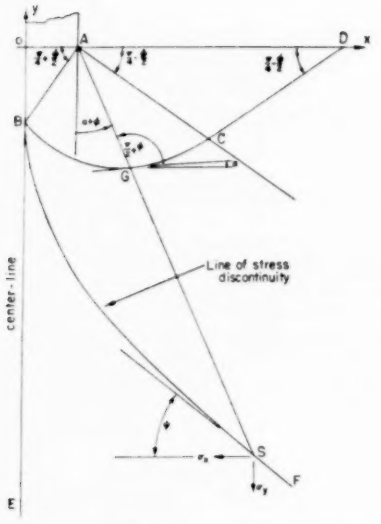

FIG. 1 AN EXTENSION OF PRANDTL STRESS SOLUTION FOR A FOOTING ON A SOIL

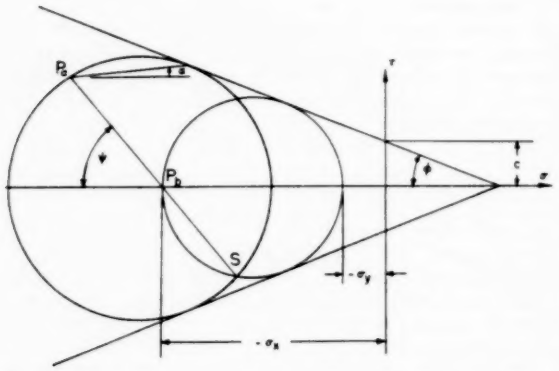

FIG. 2 MOHR'S CIRCLES FOR STATES OF STRESS AT POINT S IN FIG. 1

1 σ_x and σ_y are functions of y only and x only, respectively, and τ_{xy} is zero, satisfying the equilibrium equations and the symmetry condition across O-E.

2 In the immediate neighborhood of the line of discontinuity, the material is in a plastic state of stress. These conditions, together with the jump conditions[7] across the line of discontinuity, are sufficient to determine the stresses in the region B-E-F-S-B and to determine the line B-S-F.

Fig. 2 shows the Mohr's circles for the states of stress on either side of the line at a typical point S. It is found that, in region B-E-F-S-B, σ_x is a monotonic algebraically decreasing function of y, and σ_y is a monotonic algebraically increasing function of x. The yield condition is nowhere violated in this region if φ is less than 75 deg.

A perfectly plastic material may be considered as a soil for which $\varphi \to 0$. Designating the shearing stress on a plane of slip by k, it follows from the foregoing that the value $(2 + \pi)k$ is a lower as well as an upper bound for the collapse value of the average pressure in the indentation of such a material. A somewhat similar method has been used by Bishop[8] to show the validity of the "complete" solution to the V-notched bar problem for a perfectly plastic material.

[7] "Stress and Velocity Fields in Soil Mechanics," by R. T. Shield, Brown University Report A11-81 to the Office of Naval Research, December, 1952.

Comparison of the Hardening Produced in a Yield-Point Steel by Uniaxial Loading Under Static and Under Dynamic Conditions

BY D. B. HARRIS[1] AND M. P. WHITE[2]

IN a previous paper, one of the authors described a possible dynamic stress-strain relation for a metal with a well-defined yield point.[3] This was deduced from an analysis of permanent strains obtained in longitudinal impact tests on wires and short cylinders that were made by Professors Duwez and Clark.[4]

It was concluded,[3] among other things, that in a metal with a definite yield point the plastic deformation produced by uniaxial impact would propagate along the specimen in the form of a "shock wave," a traveling discontinuity of stress, strain, and particle velocity. Because of the large gradient of strain, it was believed that the degree of cold-working under dynamic loading would be more severe than for an equal strain produced statically. (The latter would be at least partly due to a uniform deformation occurring simultaneously over the entire length of specimen.) Consequently, it was stated, without proof, that in a metal with a yield point the hardening associated with a given uniaxial strain would be greater under dynamic conditions than under static.

This matter has recently been investigated at the University of Massachusetts. Low-carbon steel (0.04–0.05 C) wire, 0.100 in. diam annealed soft, was subjected to tensile impact at about 50 fps, stress being maintained for about 0.006 sec. Permanent strains varying from very small up to about 0.09 in each test piece resulted. At several locations, showing a longitudinal strain of 0.055, microhardness readings were made at random over the cross section, the readings being averaged.

Before testing, but after annealing, a 12-in. length of wire had been taken from the test specimen. This was stretched statically to a strain of 0.055 (at 0.02 ipm), sectioned, and its microhardness measured at several points. An annealed, unstretched piece of wire also was sectioned and the hardness measured. The results are given in Table 1.

TABLE 1 MICROHARDNESS OF TEST WIRES

Specimen	VHN	R_b
Unstrained	123.7	68.4
0.055 static	162.4	82.5
0.055 dynamic	212.0	93.7

[8] Private communication from J. F. W. Bishop to W. Prager, October, 1952.

[1] Research Engineer, E. I. Du Pont de Nemours and Co., Wilmington, Delaware.

[2] Head, Civil Engineering Department, University of Massachusetts, Amherst, Mass.

[3] "On the Impact Behavior of a Material With a Yield Point," by M. P. White, Trans. ASME, vol. 71, 1949, pp. 39–52.

[4] "An Experimental Study of the Propagation of Plastic Deformation Under Conditions of Longitudinal Impact," by P. E. Duwez and D. S. Clark, Proceedings of the ASTM, vol. 47, 1947, pp. 502–532.

Manuscript received by ASME Applied Mechanics Division, July 8, 1953.

It appears that plastic straining under longitudinal impact causes more severe working and greater hardening in annealed mild steel than does an equal static strain.

Acknowledgment

The authors wish to express their gratitude to the Research Corporation for financing this investigation, to Mr. A. S. Weissinger of the American Steel and Wire Company, for valuable advice as to materials, and to the American Steel and Wire Company of the United States Steel Corporation, for supplying the test specimens.

Note on the Problem of Vibrations of Slightly Curved Bars[1]

By ERIC REISSNER,[2] CAMBRIDGE, MASS.

THE following is concerned with an approximate analysis of the effect of curvature of a nearly straight beam on its dynamic behavior and, in particular, on its frequencies of vibrations. It is assumed that the center line of the beam is plane and the vibrations which are considered take place in this plane. It is further assumed that the ends of the beam do not move. The special case of this problem which is given if the center line of the beam is a circular arc has been considered by Den Hartog[3] and Waltking.[4] A summary of their results may be found in a recent monograph by Federhofer.[5] These earlier results for the circular-arc beam are more general than the present results for the same case, in so far as they do not depend on the nearly straightness of the beam.

Our principal result is the observation that under assumptions to be stated the effect of curvature of the given beam manifests itself for all practical purposes entirely through a relatively simple modification of the equation $(Dw'')'' + \rho w'' = q$, for the straight beam.

Basic Differential Equations

We take as equations of motion

$$N' = \rho u'' \quad M'' + (w_0'N)' = \rho w'' - q \ldots\ldots [1a, b]$$

and as stress strain relations

$$M = -Dw'', \quad N = C(u' + w_0'w') \ldots\ldots [2a, b]$$

In these equations $y = w_0(x)$ represents the undeformed center line of the beam, u and w are displacements in the directions of x and y, and N and M are stress resultant and couple. Furthermore, $D = EI$ and $C = EA$, where I and A are moment of inertia and area of the cross section of the beam, respectively. Equations [1] and [2] require for their validity that the square of the slope, $(w_0')^2$, be small compared with unity.[6]

Consideration is given to beams with immovable ends, that is, with the following boundary conditions

$$u(\pm L) = 0 \ldots\ldots [3]$$

Additional boundary conditions for w may be as in the problem of the straight beam.

The following simplifying assumption is now made: The effect of longitudinal inertia is negligible compared with the effect of transverse inertia. This means that we neglect the term $\rho u''$ in Equation [1]. We then have $N' = 0$ or

$$N = N_0 \ldots\ldots [4]$$

Combination of Equations [4] and [2b] gives $u' = (N_0/C) - w_0'w'$. From this, by integration and in view of the Boundary Conditions [3]

$$u(L) - u(-L) = 0 = N_0 \int_{-L}^{L} (1/C)dx - \int_{-L}^{L} w_0'w'\,dx$$

or

$$N_0 = \frac{\int_{-L}^{L} w_0'w'\,dx}{\int_{-L}^{L} (1/C)\,dx} \ldots\ldots [5]$$

Combination of Equations [1b], [2a], and [5] leads to the following integrodifferential equation for w

$$(Dw'')'' - \frac{w_0''}{\int_{-L}^{L} (1/C)dx} \int_{-L}^{L} w_0'w'\,dx + \rho w'' = q \ldots [6]$$

which is the principal result of this note.

Example 1

We consider free vibrations of a beam of uniform cross section (D = const, C = const) with center-line equation

$$w_0 = H \cos \alpha x, \quad \alpha = \pi/2L \ldots\ldots [7]$$

Setting $w = \cos pt\, W(x)$ we have as equation for W

$$W^{iv} - \frac{\rho p^2}{D} W = \left[\frac{H^2C\alpha^3}{2LD} \int_{-L}^{L} \sin \alpha x\, W'(x)\,dx\right] \cos \alpha x \ldots [8]$$

A particularly simple result is obtained for a beam with simply supported ends. Prescribing

$$W(\pm L) = W''(\pm L) = 0 \ldots\ldots [9]$$

we find that the solution corresponding to the first symmetrical mode of the straight beam is of the form

$$W = A \cos \alpha x \ldots\ldots [10]$$

Introduction of Equation [10] in Equation [8] leads to the relation

$$A\left[\alpha^4 - \frac{\rho p^2}{D} + \frac{H^2C\alpha^4}{2D}\right] = 0 \ldots\ldots [11]$$

or

$$\frac{\rho p^2}{D} = \left(\frac{\pi}{2L}\right)^4 \left[1 + \frac{CH^2}{2D}\right] \ldots\ldots [12]$$

The ratio D/C is the square of the radius of gyration i of the cross section. From this it is concluded that to the order of

---

[1] Supported by Office of Naval Research under Contract N5-ori-07834 with Massachusetts Institute of Technology.

[2] Professor of Mathematics, Massachusetts Institute of Technology.

[3] "The Lowest Natural Frequency of Circular Arcs," by J. P. Den Hartog, *Philosophical Magazine*, vol. 5, 1928, pp. 400–408.

[4] "Schwingungszahlen und Schwingungsformen von Kreisbogenträgern," by F. W. Waltking, *Ingenieur-Archiv*, vol. 5, 1934, pp. 429–449.

[5] "Dynamik des Bogenträgers und Kreisringes," by Karl Federhofer, Julius Springer, Wien, Austria, 1950.

[6] "Die Durchschlagskraft eines schwach gekrümmten Balkens," by K. Marguerre, Berliner Math. Ges. Sitzungsber, vol. 37, 1938, pp. 20–40.

Manuscript received by ASME Applied Mechanics Division, Sept. 25, 1953.

approximation here considered, the curvature correction is a function of the ratio of beam rise H to radius i, independent of the span $2L$ of the beam. Note that this correction is for a symmetrical mode of vibration. To the degree of approximation here considered there is no curvature correction for unsymmetrical modes. The frequency of the first symmetrical mode as given by Equation [12] equals the frequency of the first unsymmetrical mode when $H/i = (30)^{1/2} = 5.48$ and is higher than that frequency when H/i is greater than 5.48.

Example 2

Consider a simply supported uniform beam of span $2L$ with initial curvature given by

$$\left.\begin{aligned} w_0'' &= \sum_{n=0}^{\infty} A_n \cos \alpha_{2n+1} x + B_n \cos \alpha_{2n} x \\ \alpha_n &= n\pi/2L \end{aligned}\right\} \ldots\ldots [13]$$

Setting $w = \cos pt\, W(x)$ and $q = 0$ and integrating once by parts transforms Equation [6] as follows

$$W^{iv} + \frac{C}{D} \frac{\int_{-L}^{L} w_0'' W\, dx}{2L} w_0'' - \frac{\rho p^2}{D} W = 0 \ldots\ldots [14]$$

The solution W may be taken in the form

$$W = \sum_{n=0}^{\infty} X_n \cos \alpha_{2n+1} x + Y_n \sin \alpha_{2n} x \ldots\ldots [15]$$

Introduction of Equation [15] into [14] leads to the following system of equations

$$\left[\alpha_{2n+1}^4 - \frac{\rho p^2}{D}\right] X_n + \frac{1}{2} \frac{C}{D} A_n \Sigma (A_m X_m + B_m Y_m) = 0 \ldots [16a]$$

$$\left[\alpha_{2n}^4 - \frac{\rho p^2}{D}\right] Y_n + \frac{1}{2} \frac{C}{D} B_n \Sigma (A_m X_m + B_m Y_m) = 0 \ldots [16b]$$

Equations [16] imply the relation

$$\left\{1 + \frac{1}{2} \frac{C}{D} \sum_{n=0}^{\infty} \frac{A_n^2}{\alpha_{2n+1}^4 - \rho p^2/D} + \frac{B_n^2}{\alpha_{2n}^4 - \rho p^2/D}\right\} \cdot \Sigma (A_m X_m + B_m Y_m) = 0 \ldots [17]$$

As $$\Sigma A_m X_m + B_m Y_m = \int_{-L}^{L} w_0'' W\, dx$$

must be $\neq 0$ in order to have w_0'' affect the vibration problem, we conclude that the frequency equation for those frequencies which are affected by the initial curvature is of the form

$$\sum_{n=0}^{\infty} \left(\frac{A_n^2}{\rho p^2/D - \alpha_{2n+1}^4} + \frac{B_n^2}{\rho p^2/D - \alpha_{2n}^4} \right) = 2 \frac{D}{C} \ldots [18]$$

Effect of Longitudinal Inertia

The effect of longitudinal inertia may be shown to be negligible by an order-of-magnitude consideration.

We may add that a Rayleigh-Ritz analysis for Example 1, with $W = A \cos \alpha x$ and $U = B \sin 2\alpha x$, leads to the following modification of Equation [12]

$$\frac{\rho p^2}{D} = \left(\frac{\pi}{2L}\right)^4 \left[1 + \frac{1}{2} \frac{H^2}{i^2}\right] \left[1 - \frac{\pi^2}{64} \frac{H^2}{L^2}\right] \ldots [12a]$$

This confirms the result of the order-of-magnitude analysis that for shallow arches the effect of longitudinal inertia is negligible.

General Solution for Nonuniform Hinged-End Columns

By L. H. DONNELL,[1] CHICAGO, ILL.

CONSIDER an elastic hinged-end column of length l centrally loaded by end compressions P. Let the elastic axis be the x-axis, with origin at one end, and the principal axes of cross sections be in the y and z-directions. Moment equilibrium under a transverse deflection w in either the y or z-direction requires that

$$Pw = -EI\, d^2w/dx^2 \ldots\ldots [1]$$

where $I(x)$ represents the principal moments of inertia of cross sections about axes perpendicular to the deflection being considered. Then equilibrium and end conditions are satisfied if

$$w = \Sigma a_m \sin m\pi x/l \qquad (m = 1, 2, 3 \ldots)$$

$$I = I_0(\Sigma a_m \sin m\pi x/l)/(\Sigma m^2 a_m \sin m\pi x/l) \ldots\ldots [2]$$

and

$$P = \pi^2 E I_0/l^2 \ldots\ldots [3]$$

The coefficients a_m can be chosen to give the desired variation of I in Equation [2], and this expression seems to be general enough to represent any possible nonuniformity. The illustrations show variations in cross section which can be obtained with only two terms, for $m = 1, 3$ (Fig. 1), or $m = 1, 2$ (Fig 2). Any

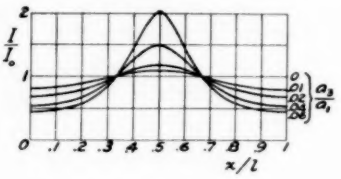

Fig. 1

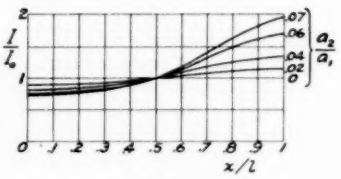

Fig. 2

given variation can be approximated as closely as desired by equating Expression [2] to the required value at each of as many sections as the number of terms used in the series, and solving the resulting system of simultaneous equations for I_0, to determine P. It should be sufficient to do this for a few sections, since general experience indicates that fine detail in the variation has little influence on the buckling load.

---

[1] Research Professor of Mechanics, Illinois Institute of Technology. Mem. ASME.

Manuscript received by ASME Applied Mechanics Division August 26, 1953.

Expression [2] is indeterminate for $x = 0$, $x = l$ but reduces to the determinate forms $I = I_0\Sigma ma_m/\Sigma m^3a_m$ and $I = I_0(\Sigma ma_m \cos m\pi)/(\Sigma m^3a_m \cos m\pi)$, respectively, at these points. If E varies as well as I the bending stiffness EI can be taken as a variable instead of I alone.

Method of Computing Principal Strains

By N. J. TALEB,[1] PRINCETON, N. J.

THE purpose of this note is to present a method for computing quickly the magnitudes and directions of principal strains if we are given ϵ_1, ϵ_2, ϵ_3 which are the magnitudes of the strains in three arbitrary directions such as 1, 2, 3 (see Fig. 1).

If ϵ_x and ϵ_y represent, respectively, the strains in the x and y-directions (see Fig. 2) and γ_{xy} represents the shearing strain, we then have[2]

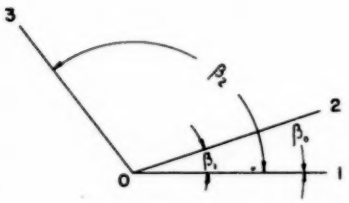

FIG. 1

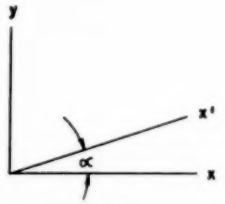

FIG. 2

$$2\epsilon_x' = (\epsilon_x + \epsilon_y) + (\epsilon_x - \epsilon_y)\cos 2\alpha + \gamma_{xy}\sin 2\alpha \quad [1]$$

where ϵ_x' is the strain along any axis, x'.

If x and y are rotated through an angle φ so as to coincide with the axes of principal strains, we get (see Fig. 3)

$$2\epsilon_x' = (\epsilon_1' + \epsilon_2') + (\epsilon_1' - \epsilon_2')\cos 2\alpha \quad [2][3]$$

where ϵ_1' and ϵ_2' are the principal strains.

At

$$\alpha = -\varphi,\ \epsilon_x' = \epsilon_1$$
$$\alpha = \beta_1 - \varphi,\ \epsilon_x' = \epsilon_2$$
$$\alpha = \beta_2 - \varphi,\ \epsilon_x' = \epsilon_3$$

In general

$$2\epsilon_i = (\epsilon_1' + \epsilon_2') + (\epsilon_1' - \epsilon_2')\cos 2(\beta_{(i-1)} - \varphi)$$
$$= (\epsilon_1' + \epsilon_2') + (\epsilon_1' - \epsilon_2')[b_{i-1}\cos 2\varphi + a_{i-1}\sin 2\varphi] \quad [3]$$

where

$$a_{i-1} = \sin 2\beta_{i-1}$$
$$b_{i-1} = \cos 2\beta_{i-1},\ i = 1, 2, 3$$

Equation [3] supplies us with three equations which when solved yield

$$\tan 2\varphi = \frac{(\epsilon_1 - \epsilon_2)(1 - b_2) - (1 - b_1)(\epsilon_1 - \epsilon_3)}{(\epsilon_1 - \epsilon_2)(a_2) - (a_1)(\epsilon_1 - \epsilon_3)} \quad [4]$$

[1] Graduate student, Princeton University.

[2] "Elements of Strength of Materials," by S. Timoshenko and G. H. MacCullough, D. Van Nostrand Co., Inc., New York, N. Y., third edition, 1949, p. 81.

[3] No shear acts at the principal planes.

Manuscript received by ASME Applied Mechanics Division, November 10, 1952.

$$\frac{\epsilon_1' - \epsilon_2'}{2}\cos 2\varphi = \frac{a_2(\epsilon_1 - \epsilon_2) - a_1(\epsilon_1 - \epsilon_3)}{a_2(1 - b_1) - a_1(1 - b_2)} \quad [5][4]$$

$$\frac{\epsilon_1' + \epsilon_2'}{2} = \epsilon_1 - (\text{right-hand side of Equation [5]}) \quad [6]$$

Illustrative Numerical Example

Let it be required to find the directions and magnitudes of the principal strains if it is given that (see Fig. 4)

$$\epsilon_1 = +100 \text{ units} \quad \epsilon_2 = +200 \quad \epsilon_3 = -50$$

$$\beta_1 = 60° \quad \beta_2 = 120°$$

$$a_1 = \sin 2\beta_1 = 0.866 = -a_2$$

$$b_1 = \cos 2\beta_1 = -0.500 = b_2$$

Substituting in Equation [4]

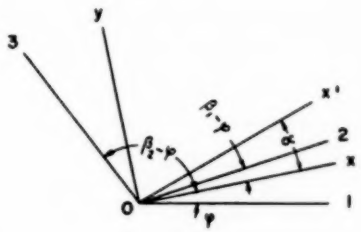

FIG. 3

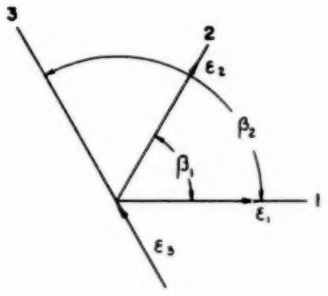

FIG. 4

$$\tan 2\varphi = \frac{-375}{-43.4} = 8.64 \quad \therefore \varphi = 41° 42', \frac{\pi}{2} + 41° - 42'$$

From Equation [5]

$$\frac{\epsilon_1' - \epsilon_2'}{2}\cos 2\varphi = +16.7$$

From Equation [6]

$$\frac{\epsilon_1' + \epsilon_2'}{2} = 83.3$$

$\therefore \epsilon_1' = +228.7$ units and acts at $\varphi = 41° - 42'$

[4] This numerator and the denominator in Equation [4] are the same.

$\epsilon_2' = -62.1$ units and acts at $\varphi = 41° - 42' + \frac{\pi}{2}$

Advantages of the method are as follows:

1 It is shorter than the usual methods.
2 By using Equation [4] one can get φ in one step.

Besides that one can find φ, ϵ_1', ϵ_2' without introducing a set of axes; x, y, find ϵ_x, ϵ_y, γ_{xy}, then proceed to find ϵ_1', ϵ_2' as is usually done.

Use of Double-Exposure Photography in Photoelasticity

By W. M. KOCH[1] and P. A. SZEGO,[2] HOUSTON, TEXAS

THE usual experimental setup for two-dimensional photoelasticity consists of a plane and a circular polariscope. As is well known, the plane polariscope produces both isoclinics (lines of constant direction of principal stress) and isochromatics (lines of constant difference between principal stresses), while the circular polariscope produces only isochromatics.

We have not been able to find reference in the literature to the fact that a pattern of isochromatics alone (without isoclinics) may be obtained with a "plane" polariscope by use of a doubly exposed photograph. To do this, take a first photograph through the plane polariscope arranged in the standard fashion. The intensity of light falling on the film willv ary as $\sin^2 2\omega \sin^2 \Delta$, where Δ is proportional to the difference between the principal stresses while ω is the angle between the plane of polarization and the direction of a principal stress. Now turn polarizer and analyzer, together, through 45 deg. The intensity will now vary as $\cos^2 2\omega \sin^2 \Delta$, provided ω is still measured from the original plane of polarization. Now if the film be doubly exposed, these two intensities add to give simply $\sin^2 \Delta$. Thus the resulting picture shows only isochromatics.

On trying this technique we found the isochromatics obtained by double exposure were somewhat sharper than those obtained with a circular polariscope. This we incline to attribute to the inevitable small imperfections in the quarter-wave plates of the circular polariscope.

[1] Reed Roller Bit Company. Mem. ASME.
[2] Assistant Professor of Mechanical Engineering, The Rice Institute.

Manuscript received by ASME Applied Mechanics Division, December 21, 1953.

Discussion

On Reinforced Circular Cutouts[1]

H. J. Weiss.[2] The author is to be commended for his work on the limit analysis of reinforcements of a circular cutout in a rectangular slab by a "hub" of general symmetric cross section. Attention should be drawn to the author's comments on the limitations of the analysis—that the hub was treated as a curved beam and shear force neglected. It would be useful to have experimental evidence to determine what effect the various factors neglected in the analysis have on the results.

Author's Closure

The interesting comments of Professor Weiss are very much appreciated. As yet, no experiments have been performed which would permit a direct evaluation of the beam-theory approximation. However, some experiments carried out by Vasarhelyi and Hechtman[3] have recently become available and have stimulated an extension of the theoretical results obtained in the paper under discussion.

The paper was primarily concerned with an analysis of the hub, while the slab was assumed to be in a homogeneous state of stress. It has been possible to extend the analysis to include stress concentrations in the slab. However, the curved-beam theory, with an accompanying neglect of shear, has been retained for the hub. Details of the theory may be found in a summary of some recent work by Hodge[4] and his associates. This summary also contains a comparison of the theoretical results with the experiments of Vasarhelyi and Hechtman. For each specimen considered, theoretical upper and lower bounds were obtained which differed by less than 20 per cent, and the experimental results were always between these two bounds.

Toroidal-Shell Expansion Joints[1]

R. A. Clark.[2] It is always gratifying to learn that experimental measurements are predicted accurately by a theoretical analysis, particularly when the theoretical analysis involves various approximations or idealizations, some of which may be difficult to justify completely. Certainly the measured stresses reported here correlate with theory as closely as could be expected. However, the deviation between results for the axial deflection does seem surprising, as the author states. Has the author investigated this point further? Any improvement in the theoretical results due to the inclusion of the direct strain term in Equation [16] of the paper is apparently too small to matter. Relaxing the condition that the tangent remain vertical at the inner edge, $\phi = -\pi/2$, might account for the discrepancy but it seems doubtful that this would furnish a sufficiently large correction.

Although the author does state that the problem at hand is closely allied to the bending of curved tubes, greater recognition might have been given to this fact. The two problems are actually mathematically identical, as had been noted by the writer.[3] Thus the solution of the present problem can be obtained from the solution of the problem of the bending of a curved tube by little more than a redefinition of the symbols. For instance, the quantity N_1/D_0, used in Equation [27] and graphed in Fig. 10 of the paper, is the "rigidity factor" for a curved tube, first introduced by von Kármán. Beskin[4] later extended von Kármán's results and, retaining up to six terms in the series, calculated coefficients which may be related to those in the present work. Actually, work of E. Reissner and the writer[5] has shown that a solution corresponding to the retention of two terms in the series is valid for values of μ up to about 10 and that for $\mu > 10$ the asymptotic solution is sufficiently accurate.

The author is to be complimented for devising the interesting comparisons shown in Figs. 12 to 14.

Author's Closure

The author agrees with Professor Clark's remark with regard to the fact that this problem develops to be mathematically identical to the problem of the bending of curved tubes even though the loadings and deformations in the two problems are markedly dissimilar.

Since the publication of this paper the author has had occasion to measure the strain on a toroidal-shell expansion joint with quite different dimensions from that reported in the paper. The dimensions of the stainless-steel shell were $a = 31.8$ in., $b = 1.75$ in., $h = 0.05$ in., which give a value of $\mu = 6.35$. The measured ratio of maximum bending stress to deflection was 0.11 $\frac{E}{a}$, which agrees very well with the curve in Fig. 14 in the author's paper.

The Rate of Growth of Vapor Bubbles in Superheated Water[1]

E. F. Lype.[2] Although the author's objective was to verify a theory on the dynamic stability of gas bubbles in water, his skillfully conducted experiments on the growth of vapor bubbles in superheated water are also a valuable contribution to our knowl-

---

[1] By E. Levin, published in the December, 1953, issue of the Journal of Applied Mechanics, Trans. ASME, vol. 75, pp. 546–552.

[2] Graduate Division of Applied Mathematics, Brown University, Providence, R. I.

[3] "Welded Reinforcement of Openings in Structural Steel Members," by D. Vasarhelyi and R. A. Hechtman, First Progress Report, Contract NObs-50238, University of Washington, Seattle, Wash., 1951.

[4] "Final Report on Yield Loads of Slabs With Reinforced Cutouts," by P. G. Hodge, Jr., Technical Report B11-22, Contract N7onr-35810, Brown University, Providence, R. I., 1953.

[1] By N. C. Dahl, published in the December, 1953, issue of the Journal of Applied Mechanics, Trans. ASME, vol. 75, p. 497.

[2] Assistant Professor of Mathematics, Case Institute of Technology, Cleveland, Ohio.

[3] "On the Theory of Thin Elastic Toroidal Shells," by R. A. Clark, *Journal of Mathematics and Physics*, vol. 29, 1950, p. 172.

[4] "Bending of Curved Thin Tubes," by L. Beskin, Journal of Applied Mechanics, Trans. ASME, vol. 67, 1945, p. A-1.

[5] "Bending of Curved Tubes," by R. A. Clark and E. Reissner, Advances in Applied Mechanics, II, Academic Press, New York, N. Y., 1951.

[1] By P. Dergarabedian, published in the December, 1953, issue of the Journal of Applied Mechanics, Trans. ASME, vol. 75, pp. 537–545.

[2] Senior Research Engineer, Armour Research Foundation of Illinois Institute of Technology, Chicago, Ill. Mem. ASME.

edge of the phenomena of phase transition and phase equilibrium of water.

It is known from diffusion experiments that the process of evaporation from a water surface occurs at a rate which is of the order of 1 per cent of what the conventional evaporation formula in the kinetic theory of gases predicts. On account of this extraordinary behavior of water in contrast to most other liquids, studies of bubbles in boiling water are of great importance. Such studies were previously available in Jakob's experiments of 1932, made with an average superheat temperature of 0.5 deg C.[3] We now have, thanks to the author's paper, experimental data for five additional superheat temperatures.

This makes it possible to examine a kinetic theory on the evaporation of water which was presented by the writer[4] at the Eighth International Congress for Mechanics in Istanbul, Turkey, August 20–28, 1952. According to this theory, the increase in the amount of vapor in the bubble is, per unit surface and time

$$G = \sqrt{\frac{gR}{2\pi}} \left(\frac{\sqrt{T'}}{v'} - \frac{\sqrt{T^s}}{v^s} \right) e^{-\frac{\Delta U''}{2RT'}} \quad \ldots\ldots [1]$$

The rate of growth of the radius of a spherical bubble is

$$\frac{dr}{dt} = Gv^s \quad \ldots\ldots [2]$$

where

r = radius of bubble
t = time
v^s = specific volume of saturated vapor at external pressure
G = evaporation coefficient
g = acceleration of gravity
R = gas constant for water vapor
T' = superheat temperature of liquid
T^s = saturation temperature of vapor at external pressure
v' = specific volume of saturated vapor at superheat temperature
$\Delta U''$ = internal energy of evaporation at superheat temperature

For a given external pressure, the rate of evaporation depends only on the superheat temperature. Then, the rate of growth of the radius has one constant value for each superheat temperature. From Equations [1] and [2], herewith, the rate of bubble growth can be calculated for the five superheat temperatures tested by the author. The result is shown in Figs. 1 to 5 of this discussion, where the straight line represents the slope of the r, t-curve, calculated for a saturation temperature of 100 C. The agreement between theory and experiment is very good. At the lowest superheat temperature, Fig. 1, the calculated bubble growth is slightly larger than the observed one; this seems to indicate that the barometic pressure during the experiment was somewhat larger than 760 mm. Some of the curves for higher superheat temperature, Figs. 3 and 4, show a faster growth of the bubble

[3] "Heat Transfer," by M. Jakob, John Wiley & Sons, Inc., New York, N. Y., vol. 1, 1949.

[4] "Liquid-Vapor Phase Transitions in Pseudo-Crystalline Fluids," by E. F. Lype, Eighth International Congress for Mechanics in Istanbul, Turkey, August 20–28, 1952.

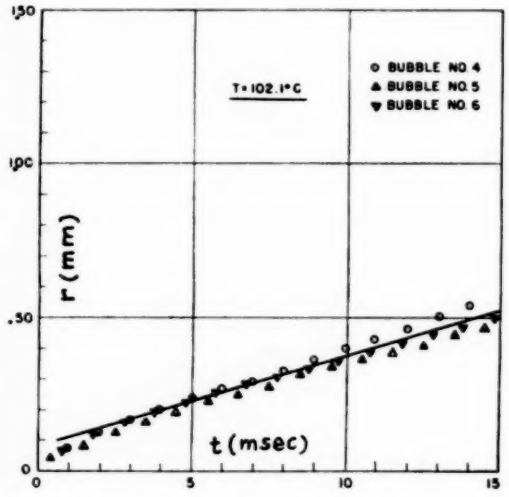

Fig. 2

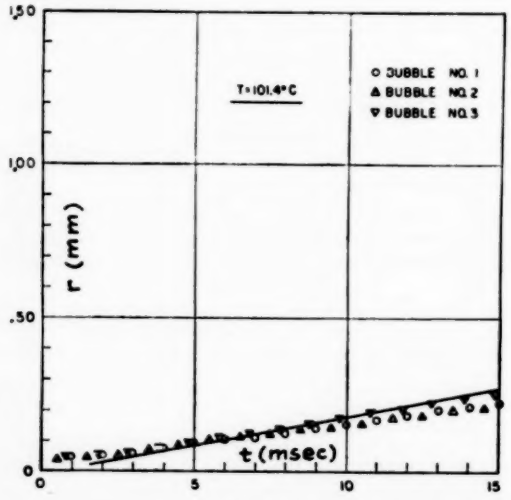

Fig. 1

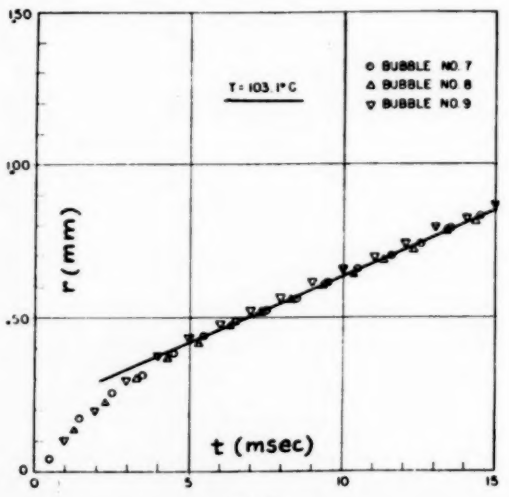

Fig. 3

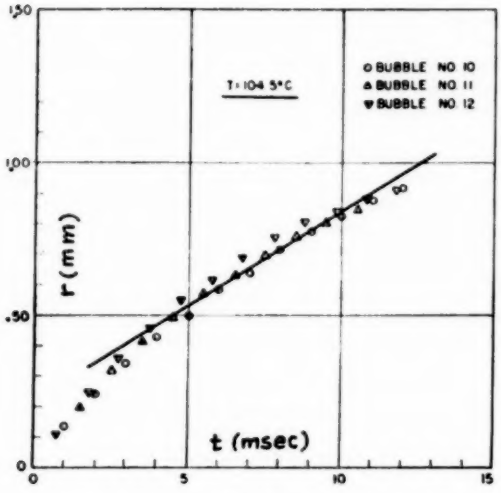

FIG. 4

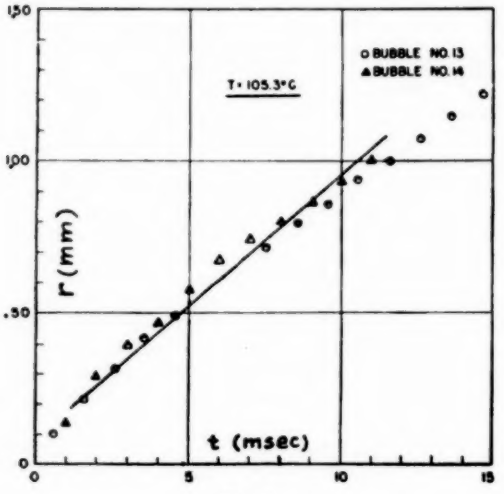

FIG. 5

during the first 3 millisec; this has not yet been explained from the viewpoint of the kinetic theory.

Thus the author's experimental findings can be explained by two theories, entirely unrelated to each other. The situation seems to be analogous to that encountered in other transport phenomena; namely, the macroscopic approach (the author's) provides a solution containing certain unspecified physical constants (thermal diffusivity and conductivity), while the microscopic approach (the kinetic theory) is based on a specific concept of the mechanism of the phenomenon and provides a solution which is entirely free of unspecified physical constants.

J. T. SINNETTE, JR.[5] The author is to be commended for his ingenuity in devising and applying this simple but elegant experimental technique to the confirmation of the importance of thermal diffusion in bubble growth as given by the theory of Plesset and Zwick. This investigation is typical of the excellent fundamental research on cavitation under the direction of Dr. Plesset, the need for which is becoming of increasing importance in a wide variety of applications including pumps, turbines, propellers, torpedoes, submarines, and in fact, wherever damage, loss of efficiency, or the production of noise by cavitation are of significance. The avoidance of serious cavitation in these machines and the accurate prediction of incipient cavitation are intimately tied to a better understanding of the mechanism of cavitation gained by such fundamental investigations as covered in the present paper.

The author's analysis gives a clear over-all picture of the mechanism of bubble growth in terms of the equation of motion with the driving forces based on a number of different assumed conditions. What the author calls "dynamic equilibrium" is based upon the ideal behavior of a bubble containing nondiffusing air and vapor at constant pressure. It is interesting to note the condition for stability of this dynamic equilibrium can be expressed in the form

$$p_a > \frac{2\sigma}{3R}$$

that is, for dynamic stability the air pressure in the bubble need only be slightly more than sufficient to support one third of the pressure difference resulting from surface tension, and may thus be quite small for moderate bubble size. Furthermore, for $\delta p > 0$, that is, for a superheated liquid, any bubble containing air will have two radii giving dynamic equilibrium, in which the smaller radii is dynamically stable and the larger unstable. (The two roots coincide when $p_a = 2\sigma/3R$ at equilibrium.) But below the boiling point, a bubble containing air has only one equilibrium radius and it is dynamically stable. These results can be derived easily from the relations given in the paper.

Although these considerations of dynamic equilibrium and stability are instructive, one must next consider how these results are modified when the equilibrium with dissolved gases is considered. As pointed out in the paper (and discussed more fully in the reference paper by Plesset and Epstein), a dynamically stable bubble is unstable when diffusion of dissolved gas is considered, and, if the liquid is not supersaturated with dissolved air, the air will diffuse out of the bubble into solution and the bubble will collapse. If, however, the liquid is supersaturated with dissolved air (or gas), as, for example, in a carbonated beverage or as is usually the case in a water tunnel operating appreciably below atmospheric pressure, there will exist just one unstable equilibrium radius at which the partial pressure of the dissolved gases plus the vapor pressure of the liquid will just balance the ambient pressure (p_∞) plus the collapsing pressure due to surface tension ($2\sigma/R$). For smaller radii, the bubble will collapse, while for larger radii the bubble will grow indefinitely by a combination of diffusion of gas and evaporation of liquid into the bubble. (Smaller bubbles may be stable if in contact with suitable solid particles or boundary shapes (author's reference 6) and may thus serve as nuclei for bubble growth if conditions are changed.)

The comparison between the extended Rayleigh theory and the Plesset-Zwick theory clearly shows the importance of thermal diffusion in limiting the rate of bubble growth and the experimental results confirm this conclusion.

The justification for neglecting diffusion of dissolved air perhaps warrants brief discussion. Clearly some diffusion of dissolved air is required to prevent the concentration of dissolved air from increasing indefinitely during boiling. If an equilibrium concentration is reached during boiling, the molal ratio (equal approximately to the partial pressure ratio) of air to water in the

[5] Staff consultant, U. S. Naval Ordnance Test Station, Pasadena, Calif.

final stages of bubble growth will be equal to this ratio in liquid phase. Since this ratio clearly was quite small in the experiments described, the neglect of the air in the dynamics of the bubble growth were fully justified.

The growth of a bubble supersaturated with dissolved gas at a temperature below the boiling point should differ in that here $\delta p < 0$ so that the driving force and the rate of growth are limited by the rate of diffusion of gas into the bubble. Nevertheless, it appears that the Plesset-Zwick theory with slight modification might be used to calculate bubble growth in this case also, inasmuch as the process is governed by the same diffusion equation but with a different diffusivity and somewhat modified boundary conditions. The experimental verification might be more difficult, however, because of the slower growth and hence larger effect of bubble translation during growth.

Author's Closure

The author is grateful to Dr. Lype and Mr. Sinnette for their complimentary remarks.

In view of Dr. Lype's comments on evaporation rates it seems appropriate to point out where the question of evaporation rates arises. The mechanism of bubble growth, as explained in detail in the paper, has to do with the growth of dynamically unstable vapor bubbles. These bubbles grow because at superheat temperatures the vapor pressure inside the bubble exceeds the external pressure on the vapor bubble. Thus one has the condition of the vapor of small density pushing against the very dense surrounding liquid so that the inertial effects of the liquid play a dominant role in affecting the rate of growth. Now the evaporation of the vapor into the bubble proceeds at a finite rate and if this rate is not sufficiently high to keep up with the rate of volume change in the bubble, the vapor in the bubble will behave more like a permanent gas causing a pressure deficiency. The rate of evaporation is estimated from kinetic theory which says that the mass of gas evaporated per unit area per unit time at an absolute temperature T for water is

$$G = 0.04\, p_v \sqrt{\frac{M}{2\pi BT}} \qquad [3]$$

where the factor 0.04 is the coefficient of evaporation for water based on experimental data as presented in a paper by Wyllie,[6] p_v denotes the vapor pressure for a vapor with molar mass M, and B is the gas constant. If one assumes that the vapor obeys the perfect gas law

$$p_v = \frac{\rho'}{M} BT$$

which is reasonably accurate in the temperature range near 100 C, Equation [3] may be written

$$G = 0.04\, \rho' \sqrt{\frac{BT}{2\pi M}} = V\rho'$$

where

$$V = 0.04 \sqrt{\frac{BT}{2\pi M}}$$

is the desired velocity to be associated with the rate of the evaporation process.

As an example, for a superheat temperature of 105 C, V is approximately 670 cm per sec which is much greater than the rate of increase of the bubble radius as determined by experiment and theory. Thus the assumption of p_v constant, in so far as evaporation rates are concerned, is reasonable. To sum up the concept of bubble growth as presented in the paper, it suffices to state that the rate of growth of the vapor bubbles is a dynamical process modified by the cooling of the bubble wall by evaporation. The finite evaporation rate of the water vapor is so much greater than the rates of bubble growth obtained that it lends credence to the assumption that the vapor pressure inside the bubble maintains a value corresponding to the temperature of the bubble wall. Thus the evaporation rate does not determine the rate of growth of these bubbles beyond strengthening the assumption mentioned.

Recent experiments on the rate of growth of vapor bubbles in various liquids have been performed at the Naval Ordnance Test Station as a continuation of the work presented in the paper. One of these liquids is carbon tetrachloride which is a nonpolar liquid with an evaporation coefficient equal to unity. The unpublished experimental results indicate agreement with the Plesset and Zwick theory which predicts a growth rate of vapor bubbles in carbon tetrachloride approximately one third as great as in water for the same amount of superheat, whereas Dr. Lype's formula (see his Equation [1]) based on evaporation rates would predict a growth rate for carbon tetrachloride nearly one thousand times greater than in water. In addition, Dr. Lype assumes that the vapor in the bubble is always at 100 C and that the liquid at the bubble wall is at the bulk liquid superheat temperature. This concept of a temperature discontinuity at the bubble boundary does not appear to be physically plausible. The slopes Dr. Lype indicates on the author's published graphs seem to indicate a rough agreement with the data. This agreement seems to be merely accidental since a check of Dr. Lype's coefficient of evaporation given as

$$e^{-\Delta U/2RT}$$

where ΔU is the internal heat of evaporation per mole, R is the gas constant, and T the absolute temperature, yields a value of approximately 0.002 for water at 100 C as compared with the previously mentioned experimental value of 0.04.

In connection with Mr. Sinnette's discussion on the problem of dynamic equilibrium of vapor or air bubbles, it should be pointed out that experimental and theoretical work is also continuing on this phase at the Naval Ordnance Test Station.

[6] "Evaporation and Surface Structure of Liquids," by G. Wyllie, Proceedings of the Royal Society, series A, vol. 197, 1949, p. 383.

Flexural Vibrations in Uniform Beams According to the Timoshenko Theory[1]

M. A. Dengler.[2] The author deduces the transverse response of uniform beams in accordance with the Timoshenko bending mechanism. Various sets of boundary conditions are included in the considerations. The general method employed for obtaining mathematical solutions is based on the classical principle of mode superposition. Solutions appear as power-series expansions which do have certain numerical advantages over the exact solutions obtained by the authors of reference (1) of the author's Bibliography, while on the other hand, it generally might be admitted that the exact traveling-wave approach conveys a deeper insight into the physical reality of the respective phenomena.

[1] By R. A. Anderson, published in the December, 1953, issue of the Journal of Applied Mechanics, Trans. ASME, vol. 75, pp. 504–510.

[2] Executive Editor (Acting), *Applied Mechanics Reviews*, Kansas City, Mo.

The contents of the paper are closely related to the analysis of J. Miklowitz (2). Results of all three investigations, the work of the present paper, and the works reported under references (2) and (1), are in excellent agreement. The idea to treat rotatory and shear deflections separately, instead of dealing directly with the Timoshenko differential equation in the total transverse displacement, is a favorable one. It simplifies the establishment of boundary conditions.

The writer notes that the author of the present paper does not mention the interesting and important investigation on the same subject by R. W. Leonard and B. Budiansky[3] and assumes that this was unintentionally omitted from the author's list of references.

The contents of this latter work are very close to those of the present paper. One of the three principal methods of solution employed in the latter reference is based on the classical mode superposition concept. The writer has not undertaken the task of comparing in detail the results of the present author and the authors of the NACA Technical Note.[3]

L. E. Goodman.[4] The author discusses a solution of the equations first developed by Professor Timoshenko to account for the influence of shear distortion and rotatory inertia on the vibrations of beams. The expression developed by the author for the corrected natural frequencies of a pin-ended beam (his Equation [55]) is exactly the same as one published previously by Goodman and Sutherland.[5] There is only a trivial difference in nomenclature. This earlier publication also points out the importance of the shear distortion at high frequencies and its Fig. 1[6] is essentially the same as the author's Fig. 1. The ordinate was chosen in a slightly different way, but to convert the ordinates of the curve given by Goodman and Sutherland one has only to multiply them by the corresponding abscissas and by π. They then become the same as those computed by the author, barring a slight numerical difference which is due to the fact that the earlier reference makes use of a shear-distortion coefficient $k' = 0.870$, while the author employs lower values of k'.

It is only a source of personal regret that the author has overlooked the fact that some of his results duplicate existing literature. But it is of importance to the profession as a whole that correct values of the coefficient k' be established. In practice, a poor choice of this coefficient may vitiate conclusions based on the Timoshenko equations, no matter how adroitly the solution is manipulated.

For this reason a discussion, necessarily abbreviated, of the determination of k' is appropriate.

That there is some excuse for confusion on this point is apparent from the number of different values for the same cross section which have been employed by writers in the past. Reference to these may be found in Civil Engineering Studies, Structural Research Series No. 12, of the University of Illinois. In his first (1921) paper on the subject, for example, Professor Timoshenko[7] used the value $k' = 0.667$ for a rectangular section. The coefficient k' is here defined as the ratio of the average shear stress on a cross section to the product of the shear modulus and the angle of shear at the centroid. The material of this paper is reproduced, almost unchanged, in the textbook to which the author refers (3).

In 1922, however, Professor Timoshenko[8] set $k' = 0.889$ in order to bring the predictions of his equations into closer agreement with the three-dimensional theory of the small vibrations of elastic bodies. Which value is better?

The numerical value of k' depends on the distribution of shear stress over the cross section of the vibrating beam. The difficulty in fixing k' arises from the fact that this distribution is a function not only of the shape of the cross section but of the frequency of vibration as well. In the lower modes the stress distribution for a thin rectangular beam differs little from the parabola of statics, but in the higher modes, where the corrections for shear and rotatory inertia are important, the shear-stress distribution is a maximum near the upper and lower surfaces and it is a minimum near mid-depth. In other words, at the higher modes a sort of "skin effect" dominates. If the shear-distortion coefficient is to be a constant it can make the approximate theory coincide with the exact three-dimensional theory at only one frequency.

By using a value of k' based on statics the author has elected to make the correspondence occur at zero frequency. In the cited references by Goodman and Sutherland,[5] and in the work of Mindlin to which they refer, as well as in a cogent paper by Mindlin and Deresiewicz,[9] it is pointed out that it is more logical to enforce agreement at the high-frequency end of the spectrum.

The two last-named authors call attention to the physical fact that as the frequency of excitation is raised to a value in the vicinity of the first thickness-shear mode of vibration, strong coupling between the flexural and thickness-shear modes will greatly affect the response of the beam. They conclude that it is desirable to choose k' so that the thickness-shear frequency calculated from the Timoshenko equations will agree with that calculated from the three-dimensional equations of small elastic vibrations, i.e., $k' = 0.822$ for a rectangular and $k' = 0.847$ for a circular cross section.

The author seems to have used $k' = 0.667$ for rectangular and $k' = 0.750$ for circular cross sections; these are simply the ratios of the average to the maximum shear stresses for a static stress distribution. In view of what has been stated in the preceding paragraphs, it is apparent that these values—or any others based on a static stress distribution—cannot give the best results which the Timoshenko equations are capable of achieving, especially in the higher modes. It would be interesting therefore to learn the nature of the "pure shear-vibration theory" whose predictions are apparently represented by the horizontal dashed lines in the author's Fig. 1.

Author's Closure

The author wishes to express his appreciation to Dr. Dengler and Professor Goodman for their interest in the paper and for their critical comments.

The author is grateful for the generous comments of Dr. Dengler and agrees that the exact traveling-wave approach permits a deeper physical insight into the wave phenomena. It

[3] "On the Traveling Waves in Beams," by R. W. Leonard and B. Budiansky, NACA TN No. 2874, January, 1953.

[4] Research Associate Professor of Civil Engineering, University of Illinois, Urbana, Ill. Assoc. Mem. ASME.

[5] Discussion of R. S. Ayre and L. S. Jacobsen paper, "Natural Frequencies of Continuous Beams of Uniform Span Length," by L. E. Goodman and J. J. Sutherland, Journal of Applied Mechanics, Trans. ASME, vol. 73, 1951, p. A-217, Equations [4].

[6] Ibid., p. 218.

[7] "On the Correction for Shear of the Differential Equation for Transverse Vibrations of Prismatic Bars," by S. P. Timoshenko, *Philosophical Magazine*, vol. 41, 1921, pp. 744–746.

[8] "On the Transverse Vibrations of Bars of Uniform Cross-Section," by S. P. Timoshenko, *Philosophical Magazine*, vol. 43, 1922, pp. 125–131.

[9] "Timoshenko's Shear Coefficient for Flexural Vibrations of Beams," by R. D. Mindlin and H. Deresiewicz, ONR Project NR 064-388, Tech. Report No. 10, Columbia University, New York, N. Y., June 1953

is regretted that the excellent work of Leonard and Budiansky was not acknowledged. The author's only plea in this regard is that the latter report appeared only a month before the present paper was submitted and escaped his notice. It should be noted that, although both papers present classical mode-superposition solutions, the technique of solution is different. The solution of Leonard and Budiansky was obtained with the Laplace-transform technique while that of the present paper was obtained with a separation of variables technique. The author feels that his statement of the solution especially permits physical insight into the vibration problem.

Although not a major part of the paper, the author regrets that he did not give proper credit for the previous derivation of the frequency equation predicted by the Timoshenko theory for the case of a pin-ended beam. The reference cited by Professor Goodman is acknowledged. To be scrupulously fair, it should be noted that the above frequency equation was presented but not discussed by Professor Timoshenko in his initial paper.[10]

It appears that the discussion has overlooked the main contribution of the paper which consists of the general solution for the flexural response of a beam having standard end conditions to an arbitrary transverse loading. The calculations and figures presented for the case of a pin-ended beam were considered to be an illustrative example revealing the nature of the response predicted by the theory. The author regrets he did not state that the important parameter k' was chosen for the static condition of the beam. The values of $E/k'G$ were chosen to be 4 and $3^{5}/_{9}$ for solid rectangular and circular cross sections for convenience in the calculations. It is not agreed that the nature of the response is particularly sensitive to the choice of k'. As is pointed out in the comprehensive and accurate discussion, the value of k' can be so chosen as to cause the lower set of Timoshenko frequencies to be in substantial agreement with that of the more exact three-dimensional theory. But it can be shown that such an adjustment of k' would not change the nature of the calculated illustrative example.

It was not the author's purpose to consider the optimum value for the parameter k'. However, it is felt that, contrary to the dogmatic assertions of the discussion, the optimum value of k' for the complete solution has not been established. It is essential to note that the empirical procedures for choosing the value of k' are only justified by the results. The values of k' cited in the discussion were chosen to cause the lower set of frequencies to agree with that of the more exact three-dimensional theory. If the interest is solely in the frequencies, there can be no objection to this procedure. For some purposes, the amplitudes associated with the frequencies may be at least as important as the frequencies. Apparently it has not been established that the values of k' cited in the discussion will result in the optimum correction for the amplitudes.

The author regrets having made a serious omission in not identifying the "pure shear-vibration theory" depicted in Fig. 1 of the paper. This theory results from the Timoshenko theory if the Young's modulus is allowed to become infinitely large. The theory predicts a pure transverse-shear motion which is approached asymptotically by the motion in the lower set of frequencies at short-wave lengths. The so-called pure shear-vibration theory is analogous to the Bernoulli-Euler theory which results from the Timoshenko theory if the shear modulus is allowed to become infinitely large and the rotatory inertia is neglected.

[10] "On the Correction for Shear of the Differential Equation for Transverse Vibrations of Prismatic Bars," by S. P. Timoshenko, *Philosophical Magazine*, vol. 41, 1921, pp. 744–746, equation [10].

Flexural Wave Solution of Coupled Equations Representing the More Exact Theory of Bending[1]

M. A. Dengler.[2] The idea to treat the lateral-deflection components of beams due to rotary inertia and shear separately and to establish and solve a system of two partial differential equations in these two variables instead of a single one for the total beam deflection, reveals physical insight into the nature of traveling-wave phenomena and possesses certain definite advantages in view of a reduction of the mathematical complexities.

Without the least intention to diminish the value of this statement, it might be added, however, that the difficulties of establishing boundary conditions which in the present paper are said to be inherent to the "total deflection approach" employed by the authors of reference (3) and others are somewhat overemphasized. It may be demonstrated, for example, in an absolutely exact manner and without mentionable mathematical difficulties involved, that the initial and boundary conditions of an infinite beam subjected to a Dirac impulse at the center [problem treated in reference (3)], are

$$y(x, 0) = 0; \quad y_t(x, 0) = 0; \quad y_{tt}(x, 0) = \frac{g}{\gamma A_0} q(x, 0)$$

$$y_{ttt}(x, 0) = \frac{g}{\gamma A_0} q_t(x, 0); \quad y(\infty, t) = 0$$

$$y_x(0, t) = 0; \quad y_{xxx}(0, t) = -\frac{1}{k'GA_0} q_x(0, t)$$

Here y stands for the total beam deflection, $q(x, t)$ is the external load per unit length, $q(x, t) = \delta(x)\delta(t)$, and the two Dirac functions involved are assumed to be in accordance with the following "continuity definition:" If there is a continuous function $f(x, \epsilon)$ such that $f(x, \epsilon) = 0$ for $|x| > \epsilon$ and $\int_{-\epsilon}^{\epsilon} f(x, \epsilon)dx = 1$ for any positive ϵ whatsoever small, then the limit function $\delta(x) = \lim_{\epsilon \to 0} f(x, \epsilon)$ is a Dirac function.

The boundary conditions listed in the foregoing hence are the "boundary conditions under the load" for the impact problem of reference (3) of the paper. One might now proceed with a double Laplace-transform approach (deducing transforms first with respect to time t and then with respect to distance x) instead of using the Fourier-transform analysis employed in reference (3). As long as one never deviates from the "continuity definition" of Dirac functions, no appreciable mathematical complication ever arises.

The specific problems dealt with in the paper are important and interesting. It is agreed that the mathematical method employed for solving them proves successful and permits a remarkably clear physical picture of the respective traveling-wave phenomena. The interpretation of the results of Uflyand, reference (2) of the paper, of course is correct. The writer assumes that the author of the paper has unintentionally failed to include in his list of references an important contribution to the subject by R. W. Leonard and B. Budiansky.[3]

[1] By J. Miklowitz, published in the December, 1953, issue of the Journal of Applied Mechanics, Trans. ASME, vol. 75, pp. 511–514.

[2] Executive Editor (Acting), *Applied Mechanics Reviews*, Kansas City, Mo.

[3] "On the Traveling Waves in Beams," by R. W. Leonard and B. Budiansky, NACA TN No. 2874, January, 1953.

Author's Closure

The author wishes to thank Dr. Dengler for his interest in the paper.

Dr. Dengler's remark, that the difficulties of establishing boundary conditions in the "total deflection approach" are overemphasized, comes as somewhat of a surprise to the author. In Dr. Dengler's own work the difficulties of defining proper boundary conditions at a beam cut, for the Timoshenko theory, was a subject of great concern.[4] In that work it is stated that the indefinite character of the boundary conditions was the primary reason for treating the infinite-beam problem by a method that did not require their definition. With this, and the Uflyand boundary condition errors reference (2), as examples, one can hardly refer to these difficulties as overemphasized.

Further, the author is not convinced that the suggested alternate approach, for the problem originally treated in reference (3), would lead to a correct solution. It is highly doubtful that one could justify the use of the stated conditions at $x = 0$. From Equations [2] of the paper it is obvious that

$$y_s(x, t) = y_{bx}(x, t) + y_{sx}(x, t)$$

where y_b and y_s are the bending and shear deflections, respectively. $y_s(0, t) = 0$ requires that $y_{bx}(0, t) = 0$, and $y_{sx}(0, t) = 0$, since obviously the special case where $y_{bx}(0, t) = -y_{sx}(0, t)$ is of no concern here. The author would agree that $y_{bx}(0, t) = 0$, but not that $y_{sx}(0, t) = 0$. In the limit (as $\epsilon \to 0$) the action of $q(x, t)$ tends toward that of a concentrated force at $x = 0$. In view of the relation for the shear force, Equation [3b] of the paper

$$S(x, t) = -k'A_0Gy_{sx}(x, t)$$

$y_{sx}(0, t)$, then, would not be zero.

Loss should not be made of the fact that the method of the paper leads to the solution of the infinite-beam problem of reference (3) in a more direct way than methods that employ the nonhomogeneous Timoshenko equation. Only a single Laplace transformation is involved. The moment transform $\bar{m}(x, p)$ of reference (3)[5] can be obtained by letting $S(0, t)$, in Equations [13] of the paper, be the Dirac function $\delta(t)$ with an associated impulse of magnitude A.

The author regrets not having seen the Leonard and Budiansky work[3] in time to comment in the paper on its important part in this subject.

Dynamic Stress-Strain Relations for Annealed 2S Aluminum Under Compression Impact[1]

J. D. Campbell.[2] The authors are to be congratulated on the interesting experimental work described in this paper, and it is gratifying to note the similarity between the authors' results and those obtained by the writer using a similar method of test.

The difference between the two dynamic stress-strain curves A and B in Fig. 4 of the paper appears to be not more than 10 per cent in strain at any stress. This corresponds to about 5 per cent in velocity in the curve of Fig. 2; i.e., to give agreement the curve of Fig. 2 should be raised by about 5 per cent. It appears from the points given in Fig. 2 that the curve could well be drawn rather higher, particularly near its upper end. Therefore it would be interesting to know the authors' estimate of the accuracy with which the experimental curves in Figs. 2 and 3 can be established.

The authors state that the difference between their three postulated stress-strain curves, Fig. 8, results from different rates of strain. It seems to the writer, however, that the difference is too large to be attributed to this cause. The authors estimated the minimum loading time in their tests to be about 2 microsec, and thus the mean rate of strain for the curve marked "5 per cent final strain" (Fig. 8) is about 25,000 sec^{-1}. The particle velocity for the "2 per cent final strain" curve is about half that for the "5 per cent final strain" curve; thus, assuming that the rise time is inversely proportional to the particle velocity, the mean rate of strain may be estimated to be about 5000 sec^{-1}. The authors also give the stress-strain curve for a strain rate of 0.040 per min, i.e., 0.00067 sec^{-1}. The following table thus gives the stress at 2 per cent strain at the three strain rates:

Strain rate, sec^{-1}	0.00067	5000	25000
Stress at 2 per cent strain, psi	8100	9500	10100

From this it will be seen that between the first and second columns the strain rate increases 7.5×10^6 times, and the stress about 17 per cent; the corresponding increases between the second and third columns are 5 times and 6 per cent. It seems unlikely that the second relatively small increase in log (rate of strain) could cause an increase of stress of the same order as that caused by the first very large increase.

Referring to the propagation distances of maximum strains quoted in Table 1 of the paper, it is difficult to see how the distance could be greater for a strain of 5 per cent than it is for a strain of 3.5 per cent; both sets of calculated distances show a reduction of distance as the strain increases. It appears, therefore, that accurate experimental determination of the distance is not possible; this is presumably due to the gradual fall of strain with distance shown in Fig. 7. The exact shape of the strain-distribution curve will depend on lateral inertia effects which are neglected in the theory.

E. H. Lee.[3] The authors are to be congratulated on the careful experimental measurements which provide new information concerning the dynamic response of metals. There still seem to be difficulties in interpreting the detail differences between the dynamic stress-strain curves associated with impacts with different maximum strain values. The interpretation given in the paper of having dynamic stress-strain relations which differ throughout the entire range of plastic strain is contradictory to the wave solution used, in which the front lower stress part of the wave is not influenced by the higher stress region following. This property is illustrated in Fig. 5 of the paper in which the front part of the wave applies for all three solutions.

As mentioned by the authors, the range of strain rate during a single impact is very wide. It is much wider than the average difference between impacts at the three strain values. This again suggests the difficulties involved in using three dynamic stress-strain curves. It must be borne in mind when considering the high stress-rate values at the impact surface estimated in the paper, that they are followed by a period during which high stress is maintained at almost constant magnitude. It may be that this period of maintained stress, which differs for each strain magnitude, has a more marked influence on the strain produced than the differences in initial loading rate.

---

[4] See particularly the paragraph following Equation [22], reference (3) of the paper, p. 183.

[5] See Equation [39].

[1] By J. E. Johnson, D. S. Wood, and D. S. Clark, published in the December, 1953, issue of the Journal of Applied Mechanics, Trans. ASME, vol. 75, pp. 523–529.

[2] Lecturer in Engineering Science, Oxford University, Oxford, England.

[3] Professor of Applied Mathematics, Graduate Division, Brown University, Providence, R. I. Mem. ASME

In spite of these difficulties in the present analysis, the writer feels that this paper advances our knowledge of this difficult question and hopes that the authors are undertaking further work to enable the problem of the detail of the strain-rate influence to be elucidated.

As a question of detail, it is not apparent from Fig. 8 that the elastic limit constant ϵ_0 differs for the three curves. Some information on this variation would help in assessing these results.

L. E. Malvern.[4] The authors have made a valuable addition to the existing information about a very puzzling phenomenon, the nature of the time dependence or rate dependence of the stress-strain relation in impact. The stress-time record at the impact end shows essentially constant stress until the arrival of unloading waves reflected from the free end of the specimen. This seems to indicate that the departure of the maximum stress and strain from the values predicted by the von Kármán theory, using the static stress-strain relation, cannot be explained by postulating a relaxation type of time dependence.

Some additional static compression of specimens cut from the constant residual-strain region of the bars used in the impact test might give further useful information. If in the further compression, the stress-strain curve is appreciably higher than the continuation of the original static curve, a dependence of the hardening on strain-rate history would be indicated, possibly due to greater disordering of the crystalline structure in the deformation under impact. Stress relaxation would be expected if the dependence is on instantaneous strain rate, rather than strain-rate history. But the uniformity of the residual strain for a considerable distance from the impact end seems to defy explanation on the basis of history dependence, since the strain-rate history varies greatly with distance from the impact end.

It would be desirable to have strain-time records obtained at stations on the specimen. For impact velocities much lower than most of those used by the authors, Sternglass and Stuart[5] have obtained such records for tensile impacts on specimens under initial tension.

Their results appear to show that in the transient response to impact, small plastic-strain increments are propagated at the elastic-wave velocity even when the initial tension is well into the plastic range. These results do not appear to be explainable either by a single dynamic stress-strain curve or by a family of curves as proposed in the present paper.

D. A. Stuart.[6] The authors are to be congratulated for their fine work and carefully written paper. However, the writer has some questions and comments which may concern, or be of interest in, their work.

It seems unfortunate that the authors did not determine the strain as a function of time in the test specimen. Using SR-4 strain gages, this procedure is not difficult and is extremely valuable. For example, using such a technique in the investigation of transient pulses in annealed copper, Sternglass and Stuart[5] have observed recoverable strains of a much larger magnitude than previously suspected. Obviously, any technique that measures only a permanent or plastic strain is incapable of obtaining such information concerning recoverable (elastic) deformations.

Also, the authors have indicated that the dynamic stress-strain curve for annealed 2S aluminum lies considerably above the static curve. In particular, it is stated that the overstress varies from zero to a maximum of 20 per cent of the stress at the highest attainable strain. It seems likely that such an effect is due to the strain rate and, if so, one would expect that the amount of allowable overstress would vary not only with the strain rate but also with the effective impact duration. It would be of interest to know whether such a variation of the amount of overstress with impact duration was observed or investigated. In addition, although it has been believed that face-centered cubic structures do not exhibit the phenomena of "delayed yield," preliminary experiments by H. Sack[7] have shown that annealed copper exhibits such an effect. In view of this fact, the change, if any, of the dynamic stress-strain curve with impact duration is of paramount importance.

Finally, since the von Kármán theory was derived with the assumption that the strain-rate effect is negligible, the writer has some question concerning the significance of the dynamic stress-strain curves obtained by applying the von Kármán theory to an experiment which deviates so widely from the assumptions of the theory. It is believed that a justification of this use of the theory is necessary.

Authors' Closure

The question raised by J. D. Campbell regarding the accuracy with which the experimental curves shown in Figs. 2 and 3 of the paper can be established may be answered as follows: Some purely elastic impact tests which were performed showed agreement between theoretical and experimental results within ± 1.2 per cent. Thus the authors conclude that the accuracies of stress and impact-velocity measurements are ± 1.5 per cent or better. The absolute error in the residual-strain measurements is ± 0.05 per cent strain or less which is determined by the sensitivity of the device employed to measure the specimen diameter. The additional scatter of the experimental points in Figs. 2 and 3 over and above their uncertainties may be attributed to slight variations in properties between the specimens. The authors feel that the data justify the conclusion that a slight but real difference exists between the two stress versus strain relations designated A and B in Fig. 4.

The modified stress versus strain relations given in Fig. 8 represent the consequences of the simplest hypothesis which the authors have found to be capable of describing the difference between the relations A and B of Fig. 4. At best, this hypothesis (the existence of an individual stress versus strain relation corresponding to each value of the maximum impact strain) can only be a rough approximation to reality.

The wave solution, represented in Fig. 5 of the paper, was constructed on the basis of stress versus strain relation A in Fig. 4. E. H. Lee correctly points out that, if the stress versus strain relations of Fig. 8, which depend upon the maximum impact strain, are accepted, completely separate wave solutions are required for each impact. Constructions to determine such wave solutions were made just to a sufficient extent that the theoretical distances of propagation of the maximum strains (as given in column B of Table 1) could be determined. The authors are of the opinion, in view of the relatively small differences between curve A of Fig. 4 and the curves of Fig. 8 and the amount of labor involved in making the complete construction for a wave solution, that the completion of such individual wave solutions was not worth while.

The values of the elastic limit constant, ϵ_0, and the constant,

---

[4] Assistant Professor of Mathematics, Carnegie Institute of Technology, Pittsburgh, Pa.

[5] "An Experimental Study of the Propagation of Transient Longitudinal Deformations in Elastoplastic Media," by E. J. Sternglass and D. A. Stuart, Journal of Applied Mechanics, Trans. ASME, vol. 75, 1953, pp. 427–434.

[6] Associate Professor of Materials, Cornell University, Ithaca, N. Y.

[7] Private communication from Professor H. Sack, Department of Engineering Physics, Cornell University, Ithaca, N. Y.

α, pertaining to the three stress versus strain relations given in Fig. 8 are listed in the following table:

Final strain, per cent	ϵ_0 Per cent	α 10^6 ips
2	0.045	−0.59
3.5	0.044	−0.21
5.0	0.043	−0.115

These values of ϵ_0 correspond to a considerable increase in the elastic limit of the material above the static value. However, no great quantitative significance should be attached to these values. By employing other more complex forms of relations between strain and velocity of propagation than the one used in the paper, the experimental data could be fitted equally well with other values of the elastic-limit strain. To determine the actual elastic-limit strain under impact conditions requires further experimental work in which more sensitive measurements of strains of that order are made. Such measurements are being made currently.

L. E. Malvern's suggestion, that the elevated stress versus strain relation under impact loading might be the result of an increased strain hardening due to greater crystalline disordering under impact conditions, is an interesting one. The difficulty of explaining the uniformity of residual strain near the impact end on the basis of such an hypothesis could be surmounted if it were assumed that the additional strain hardening was a fixed amount (at a given strain) and occurred discontinuously when the strain rate reached a certain critical value.

D. A. Stuart and L. E. Malvern have both inquired about strain versus time relations in the specimen. A few such measurements were made during the investigation, and the records of two of them are presented in the accompanying Figs. 1 and 2. Reliable values of the velocity of propagation as a function of strain cannot be derived from these records, as might be hoped, because the time scale is not sufficiently accurate. This is a result of insufficient frequency-response range of the amplification system employed in making these records.

The theoretical curves indicated in Figs. 1 and 2 were derived from the stress versus strain relation based upon the stress and particle-velocity measurements (curve *A* in Fig. 4) by means of the wave solution shown in Fig. 5. The difference between the experimental and theoretical values of the final strain indicated in Fig. 9 corresponds to the differences in strain at the appropriate stress between curves *A* and *B* of Fig. 4. Thus if theoretical strain versus time relations were derived on the basis of the stress versus strain relations given in Fig. 8, this discrepancy in Fig. 9 would disappear.

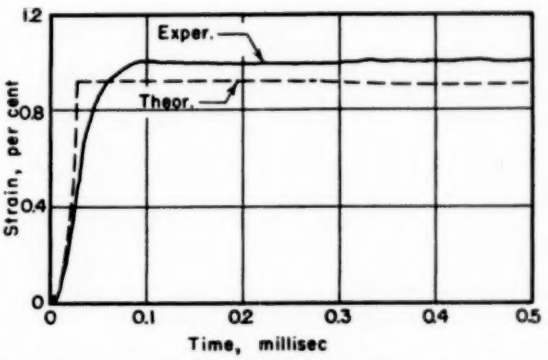

FIG. 1 STRAIN VERSUS TIME, 0.9 IN. FROM IMPACT END; IMPACT VELOCITY 44.7 FPS

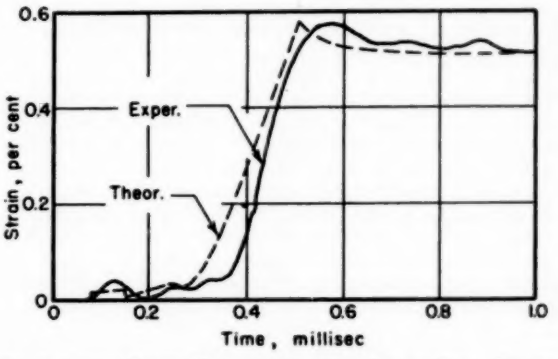

FIG. 2 STRAIN VERSUS TIME, 16.0 IN. FROM IMPACT END; IMPACT VELOCITY 69.8 FPS

The authors wish to express their appreciation for the stimulating discussions presented by Messrs. Campbell, Lee, Malvern, and Stuart.

Book Reviews

Methods of Theoretical Physics

METHODS OF THEORETICAL PHYSICS. By Philip M. Morse and Herman Feshbach. McGraw-Hill Book Company, Inc., New York, N. Y., vols. 1 and 2, 1953. Cloth, 6 × 9¼ in., figs., problems, appendix, glossary, tables, subject index, xxii and 1978 pp., two vols., $15 each vol.

REVIEWED BY A. ALI KHEIRALLA[1]

THIS outstanding contribution to the scientific literature of the English language may be recommended to all physicists, mathematicians, and engineers who are concerned with the solution of boundary-value problems. The book is, however, not a mere collection of isolated special methods but rather a masterly exposition at once broad in scope and deep in penetration into the fundamental unifying principles which form the basis of the practical techniques of this branch of modern theoretical physics.

The book is divided (about equally pagewise) into two volumes consisting of eight and five chapters. The first three chapters are largely devoted to introducing mathematical means of expression of physical phenomena. Fields and operators are discussed using vector-dyadic (to the exclusion of tensor) notation. Elastic deformation is introduced by means of the stress and strain dyadics. Equations of elastic waves, fluid motion, diffusion, and the electromagnetic field are derived physically. The characterization of physical problems by extremal properties is ably treated (from the physical viewpoint) in the chapter on variational principles.

Chapter four is an introduction to those basic concepts of the theory of functions of a complex variable which are most often used in physical applications. The fifth chapter is a presentation of the classical theory of ordinary differential equations classified according to singular points. The representation by series and integrals of the solutions is considered and their mathematical properties elaborated. Up to and including chapter five, the authors concentrate on presenting mathematico-physical background material. This is done in a concise and intuitively suggestive fashion. In chapter six, the actual methods of solution of boundary-value problems are discussed. Boundary conditions, the classification of partial differential equations and their difference equation analogs, the Sturm-Liouville problem, eigenfunctions, and the distribution of eigenvalues (spectra) are treated. Chapter seven on Green's function represents the first thorough discussion of this topic from a physical viewpoint in English technical literature. Starting from basic principles the concept is adapted to conditions of greater generality finally culminating in the abstract-vector form of Green's function.

The last chapter of the first volume is concerned with integral equations, their general properties, methods of solution, and relation to transforms based on their kernels. The Hilbert-Schmidt analysis in terms of eigenfunctions, eigenvalues, and Green's functions as well as the Fredholm theory and Wiener-Hopf method are presented.

The second volume opens with chapter nine which expounds perturbation and variational methods of obtaining approximate solutions (Ritz, WKBJ, and others). The tenth, eleventh, and twelfth chapters are devoted to applications of the techniques previously developed to a wide variety of instructive problems. Solutions of Laplace, Poisson, wave and diffusion equations under various boundary conditions in two and three dimensions are presented clearly and suggestively.

The final chapter of the second volume aims at a completely vector-dyadic representation and solution of the problems of physical (vector) fields. Here the vector wave and Laplace equations are solved by means of Green's dyadic. The concepts are applied to problems of radiation, scattering, vibrations, and elastic wave reflection.

Throughout the two volumes, the authors have sought to avoid the use of special tricks with a narrow range of applicability. Their purpose has been to present powerful general methods capable of attacking difficult problems under a wide variety of conditions. Special mention should be made of the recurrent emphasis on the wave impedance concept which should be of much interest to all concerned with the study of elastic or electromagnetic waves.

Above and beyond their value as a text, they contain material of extreme interest and applicability for those scientists and engineers who are engaged in research on boundary value problems.

[1] Lessells and Associates, Inc., Boston, Mass.

Applied Mechanics

ADVANCES IN APPLIED MECHANICS. Edited by Richard von Mises and Theodore von Kármán. Volume 3. Academic Press, Inc., New York, N. Y. 1953. Cloth, 6 × 9 in., x, and 324 pp., illus., $9.

REVIEWED by E. REISSNER[2]

THE present volume contains eight articles, of which five deal with fluid dynamics, one with plasticity, and two with mathematical methods. While the primary aim is the systematic exposition of isolated research results from recent literature, many of the articles appear to contain a certain amount of previously unpublished research. Referring for a more detailed analysis of the contents of the individual articles to *Applied Mechanics Reviews* and *Mathematical Reviews*, we may briefly describe them as follows.

A. I. Bellin surveys work dealing with the differential equation $d^2x/dt^2 = F(x, dx/dt, t)$ which is of importance in connection with forced nonlinear oscillations. G. F. Carrier undertakes to exemplify explicitly the mode of thinking associated with the use of boundary-layer techniques in theoretical work. The four different types of problems chosen as examples, which involve research results by the author, are a good indication of the power of this method which originates with Prandtl's famous study of fluid motion at high Reynolds numbers.

A paper by F. N. Frenkiel discusses diffusion under the influence of homogeneous turbulence. Hilda Geiringer offers an attractive and detailed exposition of much of what is known concerning plane stress and plane strain in plasticity. Gottfried Guderley elaborates the idea of Busemann and himself that the existence of transonic *potential* flow patterns for *some* profiles may be of limited physicial significance since for very slightly different profiles this same type of flow seems not to be possible.

H. Ludloff in an article entitled "On Aerodynamics of Blasts" reports on difficult and significant theoretical studies carried out previously by himself and by his coworkers. L. Rosenhead

[2] Professor of Mathematics, Massachusetts Institute of Technology, Cambridge, Mass.

briefly surveys much of the analytical work related to the existence of the Benard-von Kármán vortex street. He emphasizes the need for further research in various directions. Finally, O. Zaldastani reviews mathematical work on the problem of "the one-dimensional isentropic fluid flow."

The present book may be considered a worthy companion to the two earlier volumes and one hopes that further volumes will appear from time to time, as a storehouse for such expository accounts as experienced research workers in the field of applied mechanics find time to prepare.

Dynamics of Gases

GASDYNAMIK. By Klaus Oswatitsch. Springer-Verlag, Vienna, 1952. Cloth, 6½ × 9¼ in., xii and 456 pp., 300 figs., 3 tables, $18.60.

REVIEWED BY ASCHER H. SHAPIRO[3]

THAT the dynamics of compressible fluids has reached some degree of maturity is attested by the recent appearance of several books treating the subject in a more or less comprehensive fashion. The present work under review is a masterly treatment, in compact form, of a broad range of subjects in the field of gas dynamics.

The scope of the book is indicated by the following chapter outline, with the number of pages devoted to each chapter shown in parenthesis:

1 Thermodynamics (15). A review of thermodynamic principles.

2 Steady, One-Dimensional Flow (51). Principles; normal shocks; nonideal gas behavior; isentropic flow; nozzles; friction; energy addition; burning and detonation; moisture condensation.

3 Unsteady, One-Dimensional Flow (70). Governing integral and differential equations in Euler's and Lagrange's descriptions; internal ballistics; spreading of waves; potential and stream functions; small disturbances; steepening of wave fronts; compression shocks; isentropic motion; detonation; reflection of shocks; interaction of shocks and waves; reflection of shocks; nonisentropic motion; cylindrical and spherical shocks; plane isentropic waves; method of characteristics.

4 General Equations and Laws (24). Integral and differential equations of motion; similarity laws; vortex theorems; lift, circulation, drag, and thrust in steady flow.

5 Special Applications of Integral Laws (18). Mixing and sudden expansion; jets; cascades; propulsion systems.

6 General Equations and Special, Exact Solutions for Steady, Frictionless Flow (44). Basic equations of three-dimensional, plane, and axisymmetric flow; velocity potential and stream function; various co-ordinate systems; source and vortex flows; Prandtl-Meyer corner flow; conical flow; hodograph plane; various transformations; boundary conditions; aerodynamic forces; Prandtl's rule; sweepback.

7 Steady, Frictionless, Plane and Axisymmetric Subsonic Flow (33). Source and vortex singularities; linearized equations; Prandtl's rule for plane flow; Krahn's method; method of Janzen and Rayleigh; relaxation method; Kármán-Tsien formula; hodograph method.

8 Steady, Frictionless, Plane and Axisymmetric Supersonic Flow (72). Flow with small perturbations; oblique shocks and their interactions; conical flow; exact and approximate isentropic flow over profiles; hypersonic flow; nozzles; biplane; cascades.

9 Steady, Frictionless, Transonic Flow (37). Equations of transonic flow; similarity laws; nozzle flow; integral method; relaxation method; hodograph method.

10 Special Steady and Unsteady Space Flows (38). A variety of special problems relating to steady and unsteady flows, particularly over wings.

11 Flow With Friction (14). Compression shock; boundary layer equations; laminar boundary layer; relation between plane and axisymmetric boundary layers; turbulent boundary layer; effect of boundary layer on main flow; stability of boundary layer.

12 Survey of Experimental Methods and Analogies (15). Pressure and force measurements; optical methods; temperature measurements; wind tunnels; hydraulic analog; electrical analog.

The treatment of the subject matter is primarily theoretical, with an occasional reference to experimental results. In most portions of the book the mathematical background required is roughly that of the customary one-year graduate course in advanced calculus. Although the subject matter is inclusive, the treatment is condensed. For the foregoing reasons the work will most likely find its place as a reference book for professionals rather than as an introductory text.

The style of writing is clear and interesting, and the typography and figures are excellent.

In the reviewer's opinion this book will be an enduring reference work.

Methods of Mathematical Physics

METHODS OF MATHEMATICAL PHYSICS. By R. Courant and D. Hilbert. Vol. 1—First English Edition, translated and revised from the German original. Interscience Publishers, Inc., New York, N. Y., and London, England, 1953. Cloth, 6 × 9 in., xv and 561 pp., $9.50.

REVIEWED BY A. ALI KHEIRALLA[4]

THIS classic treatise which for 30 years has inspired and stimulated a whole generation of physicists, mathematicians, and engineers needs no introduction to those conversant with the German language. The translation of this brilliant exposition constitutes an acquisition of fundamental importance for English scientific literature. No review of this work would be complete without some mention of its striking literary style.

The book is especially distinguished by the attention and pedagogical skill devoted to establishing motivation on the part of the reader. It has set a high standard too often ignored by certain modern authors who, in their zeal to hide the fact that mathematics is born on scratch paper, pass by the golden mean of elegant presentation to settle on a barren and artificial edifice disfigured by the painstaking excisions of all motivating material and destined for a dusty disuse on the rearmost shelf of a public library. The unwarranted inference that this text is a compilation of scratch pads should by no means be made. Nothing could be more false. Beneath the surface of a singular expository style lies the ever visible deeper purpose of a nourishment to maturation of the mathematical intuition of the reader.

The material proper of this first volume is divided into seven chapters. The first chapter is devoted to the algebra of linear transformations and quadratic forms. The properties of vector spaces, linear dependence, completeness, the inequalities of Schwarz and Bessel, the orthogonalization of bases, matrices, and the extremal property of characteristic values are discussed. The next chapter deals with the representation of functions (regarded as vectors) by series (and integrals). Fourier series and

[3] Professor of Mechanical Engineering, Massachusetts Institute of Technology, Cambridge, Mass. Mem. ASME

[4] Lessells and Associates, Inc., Boston, Mass.

integrals, Legendre polynomials, and other orthogonal systems are treated. Chapter three is devoted to the topic of integral equations. Fredholm theory, Neumann series, and the Hilbert-Schmidt methods are presented suggestively. The next chapter on the calculus of variations constitutes a suggestive introduction to that subject. Starting from the simplest problems the methods are successively generalized in such a way as to encourage a deeper insight into the fundamental approaches of this field. The Euler (Lagrange) equations, Rayleigh-Ritz method, Legendre condition, the Euler expression as a gradient in function space, the transformation of variational problems, the variational derivation of the differential equations of physics, and a new section on reciprocal quadratic variational problems is included. Chapter five handles vibrations and the Sturm-Liouville problem. Green's functions and their applications and significance are thoroughly discussed. The next chapter deals with the applications of the approaches of the calculus of variations to eigenvalue problems. The distribution of eigenvalues is the main topic. Chapter seven discusses various special functions defined by characteristic value problems. The fundamental properties of Bessel, Legendre, Tchebycheff, Hermite, and Laguerre functions are presented. Spherical harmonics are treated and a new appendix on their transformations is included. Finally, a section on asymptotic expansions, the saddle-point method (of steepest descents) and the Darboux method conclude the chapter.

Worthy of particular note are the excellent supplementary sections at the ends of the chapters in which numerous well-chosen remarks and examples are used to stimulate the reader to further consideration of generalizations and interconnections of the material presented. In this manner not only is the way pointed to a wide supporting literature, but the reader also rapidly acquires the feeling for intuitive generalization which forms such a strong undercurrent throughout the work.

This translation should be especially welcomed in the many colleges and universities of the United States where the language barrier has often been the decisive factor in making it inaccessible to the general student public. It is also to be recommended to that great host of research workers whose mastery of the German language is not so perfect as to permit the complete understanding of a book in which no word is wasted.

Fluid Mechanics

FLUID DYNAMICS. Vol. 4. Proceedings of the Fourth Symposium in Applied Mathematics of the American Mathematical Society, held at the University of Maryland, June 22-23, 1941, Co-sponsored by The United States Naval Ordnance Laboratory. M. H. Martin, Editor; Editorial Committee: R. V. Churchill, Eric Reissner, A. H. Taub. McGraw-Hill Book Co., Inc., New York, N. Y., 1953. Cloth, 6¾ × 10 in., v and 186 pp., illus., $7.

REVIEWED BY G. K. BATCHELOR[5]

THE reviewer of a book of this kind has a well-nigh impossible task. For here are 14 unrelated papers on advanced fluid dynamics, all of them written in the terse style of a survey and demanding that the reader be almost a specialist. And when all 14 papers have been assessed, how shall an article about the whole group be made amusing and interesting? This reviewer confesses at once to failure and has fallen back on a catalogue of the contents of the book.

First one general query may be allowed. These papers are mostly good, and worth reading, since, being prepared for presentation at a gathering of fluid dynamicists, they are designed to enlighten and not solely to place on record a particular piece of work. But one wonders whether this is the proper publishing medium for them. Is there a good reason why the ordinary media, viz., the scientific and mathematical journals, could not cope with them, so justifying the addition of yet another occasional volume to the vast and alarmingly disorganized library of knowledge of fluid dynamics? It is not for me to say there is not a good reason, although I suspect that that is the case. However I do in all humility urge organizers of meetings like the one concerned to think seriously about the matter, because there is a growing tendency for scientists to unload onto congresses and symposia papers which they would otherwise have difficulty in publishing. Symposia have a definite role in current scientific life, and that role is concerned primarily with the spoken word.

Homogeneous turbulence is the subject of the first two papers, by S. Chandrasekhar and C. C. Lin, both papers being in the nature of reviews of contributions made by the authors in the few years prior to the symposium (which was held in 1951). Six papers are on high-speed flow, the first being an authoritative and illuminating discussion of the nonexistence of transonic potential flow by A. Busemann. R. E. Meyer contributes a short account (a full paper being published elsewhere) on waves of finite amplitude in ducts. T. Y. Thomas considers how the pressure distribution over the surface of curved profiles in supersonic flow may be explained by means of several hypotheses about the nature of the flow separation and the associated shock waves, although the significance of the hypotheses was not clear to this reader. In a short paper G. F. Carrier and K. T. Yen describe a method by which irrotational isentropic flows may be constructed, and M. H. Martin and W. R. Thickstun describe a particular case of transonic flow—as represented by Tricomi's equation—in which the sonic line looks like a Cornu spiral. Finally there is a short and clear discussion of nonuniform propagation of plane shock waves by J. M. Burgers.

The remaining papers do not fall so naturally into groups. A. E. Heins contributes a paper on some of the mathematical aspects of the theory of surface gravity waves. S. R. de Groot writes on the comparatively new subject of irreversible thermodynamic processes and discusses the connection with fluid dynamics; this article will appeal to those interested in the physical basis of the motion of fluids although it makes hard going for a newcomer to the subject. T. Theodorsen gives a brief exposition of propeller theory based on the velocity potential far downstream where the vortex lines all move backward at the same uniform velocity. A longish review of numerical methods, suitable perhaps for high-speed computing machines, in problems of conformal mapping is contributed by G. Birkhoff, D. M. Young, and E. H. Zarantonello; a new method for cases involving a free boundary at constant pressure is included. A numerical method of solving problems described in effect by Laplace's equation in two dimensions with conditions on the function or its derivative at an external boundary (such as steady unidirectional flow of a viscous flow under pressure gradient) is given by J. L. Synge; the method involves procedures similar to those used in the method of finite differences, but there is here the advantage that upper and lower bounds to the approximation are available at each stage. Lastly there is a clear account by A. Weinstein of the way in which problems of irrotational flow may be solved by the superposition of singularities representing sources and sinks; some recent developments make this method available for cases of axially symmetric flow with singularities off the axis.

It is this reviewer's impression that on the whole the papers have an expository standard higher than that found in journals. Libraries ought to have a copy of the book, but there does not seem to be much reason why individuals will want to purchase it.

[5] Lecturer in Mathematics, University of Cambridge, England.

Stress Concentration Design Factors

STRESS CONCENTRATION DESIGN FACTORS. By R. E. Peterson. John Wiley & Sons, Inc., New York, N. Y., 1953. Cloth, 9¼ × 11 in., x and 155 pp., 131 figs., $8.50.

REVIEWED BY HORACE GROVER[6]

THIS book is mainly a compilation of charts and relations useful in detail design of machine parts and structural elements.

The book is intended primarily "as a working tool—and therefore only enough background and references are given to enable the reader to explore the subject further if he so desires." Despite this modest preface, the introduction to "Definitions and Design Relations" contains a good summary of conventional methods of allowance for stress concentrations in design. This includes consideration of static loading, of loading under alternating stress, and of loading under combined static and alternating stresses. Illustrative numerical examples contribute to great clarity in this section.

There follow four sections on: Grooves and notches, shoulder fillets, holes in plates and Shafts, and miscellaneous design elements. The latter includes such items as: Shafts with keyways, gear teeth, press-fitted or shrink-fitted members, bolts and nuts, and so on.

Each of these sections contains, in addition to concise discussion, a series of charts of values of theoretical stress-concentration factors for various dimensional proportions of the notches under consideration. There are about one-hundred such charts in all: many of these charts cover a considerable range of dimensional parameters. This is the most extensive compilation of the kind known to this reviewer, and there are many indications of great care having been taken in the collection, evaluation, and presentation of the information.

Special attention has also been given to the format of the book as a "working tool." The charts are large, with full grids for readability. The helical binding permits opening so that any chart may be flat for easy abstraction of numerical values. Thumb tabs on the edge afford quick opening to charts likely to be used often.

This book should be of value and interest to anyone concerned with design allowance for stress concentration. For those who have frequent and varied problems of this nature, the book may be indispensable.

Heat Transfer

PROCEEDINGS OF THE GENERAL DISCUSSION ON HEAT TRANSFER, Sept. 11–13, 1951. The Institution of Mechanical Engineers, London, England; The American Society of Mechanical Engineers, New York, N. Y. Cloth, 8½ × 11 in., references, bibliography, figs., indexes, xiii and 496 pp., $10 from ASME Order Department, 29 West 39th Street, New York, N. Y.

REVIEWED BY CARL F. KAYAN[7]

THIS is indeed a rare compilation of international nature representing a panorama of heat-transfer activity in the various fields of scientific and engineering development. As such it is replete with a store of references accompanying the different papers which comprise two broad groups, namely (*a*) North American and (*b*) British, Commonwealth, and foreign papers.

The volume contains some 93 individual contributions. The symbols used are carefully indicated throughout, a relief to all readers. The papers cover a tremendous range of interest, from heat transfer in gun barrels to heat transfer as associated with vapor diffusion. The subjects deal with the developments in the mechanism of heat transfer and in the design of apparatus relating thereto, and are divided into five main sections, as follows:

1 Heat transfer with change of state
2 Heat transfer between fluids and surfaces
3 Conduction in solids and fluids
4 Radiation, instrumentation, measurement techniques, and analogies
5 Special problems such as heat transfer in turbine-blade cooling, in liquid metals, in gas turbines, and in piston engines, the mercury boiler, and so on.

The treatment of the various topics of the afore-mentioned classification in each case is handled in the two geographical groups indicated. At the Discussion in London, the papers were presented in general abstract by an official Reporter for the North American set, and by another official Reporter for the British, Commonwealth, and foreign offerings. In addition to the full record of the different papers in each of the five sections, there is also included at the end of each the formal discussions in London, the discussions in Atlantic City, N. J. (at the subsequent ASME Annual Meeting), and the authors' replies. The volume further records the proceedings at the official General Discussion dinner in London, as well as the formal James Clayton memorial lecture by Prof. A. P. Colburn, Mem. ASME, dealing with condensers of vapors and vapor mixtures.

Truly, as a mid-century publication covering a decade of development, the volume serves as a notable record to punctuate the progress in the field of heat transfer. It is a technological milestone in print. As such it well deserves a place in the library of all concerned with the engineering of heat-transfer equipment.

Bessel Functions and Formulas

BESSEL FUNCTIONS AND FORMULAE. Compiled by W. G. Bickley. Published for the Royal Society at the Cambridge University Press, New York, N.Y., 1954. Paper, 8½ × 11 in., 11 pp., 75 cents.

REVIEWED BY A. ALI KHEIRALLA[8]

THIS neatly printed, concise collection of formulas involving the Bessel functions of real and imaginary argument and integral order has been extracted from volume 10 of the British Association Mathematical Tables. Included are recurrence relations, series definitions, asymptotic expansions, auxiliary functions for small argument ($\chi^{-n}J_n(\chi)$ etc.) and for large argument ($e^{-\chi}K_n(\chi)$ etc.), zeros, addition formulas, related differential equations, a few integral representations, some integrals, the exponential generating function, and some expansions of elementary functions in series of Bessel functions of increasing (integral) order. Altogether there are 104 formulas listed. The collection should be of use as a ready reference to those basic formal properties of Bessel functions most often used in routine manipulations and computations.

---

[6] Chief, Applied Mechanics Division, Battelle Memorial Institute, Columbus, Ohio.

[7] Professor and Executive Officer, Department of Mechanical Engineering, Columbia University, New York, N. Y. Mem. ASME.

[8] Lessells and Associates, Inc., Boston, Mass.

Temperature Measurement

Temperature Measurement in Engineering. By H. Dean Baker, E. A. Ryder, and N. H. Baker. Vol. 1. John Wiley & Sons, Inc., New York, N. Y., 1953. Cloth, 6 × 9 in., vi and 179 pp., 83 figs., $3.75.

Reviewed by T. P. Torda[9]

THE first volume contains thirteen chapters, a name index, and a subject index. It is stated in the preface that "the object" of the book "is to provide in convenient nonmathematical form the information necessary to the engineer who wishes to measure temperature." The first four chapters of volume 1 are introductory with respect to the two-volume sequence, while the rest of the volume deals with thermocouple techniques. Specific references are given at the end of each of the chapters.

The first chapter deals with fundamental concepts of temperature and thermometers. It also discusses the various temperature scales used and shop standards for thermometry. In the second chapter the various thermometers are discussed in some detail. The third chapter deals with the planning of temperature measurements, the systematic and accidental errors involved. In the fourth chapter, some of the conditions are enumerated which affect temperature measurements. The fifth chapter treats the thermocouple thermometer. The thermoelectric power, multiple-metal circuits, parasitic thermoelectric and voltaic effects, the thermocouple wire, its testing and calibration, junction splices, insulation, and circuits for thermocouples are discussed. The sixth chapter gives a brief survey of indicating instruments. The seventh chapter deals with "design calculation techniques." It treats such subjects as thermal contact, nonuniform and time variable temperature, heat transfer, insulation, the influence of leads, and the installation. A numerical example is also included. The eighth chapter gives the various types of thermocouple junctions. The ninth chapter describes the techniques of drilling and preparing holes for the thermocouples. In the tenth chapter, protective coatings, heat and corrosion-resisting metals, plastics, refractories, and cements are discussed. The eleventh chapter gives useful hints about the leads, their cementing and sheathing. The technique for measuring temperature gradients is described in the twelfth chapter. Finally, a one-page "Conclusion to Volume I" is contained in chapter thirteen.

The book is what the authors set out to make it, namely: "The approach here has been to provide a comprehensive list of possible techniques,. . ." The great number of references included in the book will be quite useful to users of thermocouples. Reviewer thinks that the number of sections in the chapters should be reduced considerably.

[9] Professor of Aeronautical Engineering, University of Illinois, Urbana, Ill.

AN ASME PAPER

Its Preparation, Submission and Publication, and Presentation

To a large degree the papers prepared and presented under the ASME sponsorship are evidence by which its professional standing and leadership are judged. It follows, therefore, that to qualify for ASME sponsorship, a paper must not only present suitable subject matter, but it must be well written and conform to recognized standards of good English and literary style.

The pamphlet on "AN ASME PAPER" is designed to aid authors in meeting these requirements and to acquaint them with rules of the Society relating to the preparation and submission of manuscripts and accompanying illustrations. It also includes suggestions for the presentation of papers before Society meetings.

CONTENTS

PREPARATION OF A PAPER—

General Information—Style, Preferred Spelling, Length Limitation, Approvals and Clearances.

Contents of the Paper—Title, Author's Name, Abstract, Body of Paper, Appendixes, Acknowledgments, Bibliographies, Tables, Captions, Photographs, Other Illustrations.

Writing the Paper—Outline Tabulations, Tables, Graphs, Charts for Computation, Drawings, Mathematics, Accuracy, Headings and Numbering, Lantern Slides, Motion Pictures, Typing, Number of Copies.

SUBMISSION AND PUBLICATION OF A PAPER—

Intention to Submit Paper Required in Advance, Meeting Dates, Due Dates for Manuscript, Discussers, Review and Acceptance, Proofs, Advance Copies and Reprints, Discussion and Closure, Publication by Others.

PRESENTATION OF A PAPER—

Time Limit, Addressing Your Audience, Public Address Systems, Use of Slides.

REFERENCES—

References on Writing and Speaking, Engineering Standards.

Price 40¢. No discount allowed. *A remittance must accompany all orders for $5.00 or less. U. S. Postage Stamps are acceptable.*

THE AMERICAN SOCIETY OF MECHANICAL ENGINEERS

29 West 39th Street, New York 18, N. Y.

ASME PUBLICATIONS

METALS PROPERTIES

Here is specific information for the designer about the properties of metals with which he works—properties such as strength, hardness, machinability, electrical conductivity, thermal conductivity, etc. In convenient chart and table form, this book brings data on more than 200 metals in common industrial use—AISI steels, ASTM steels, cast copper alloys, aluminum alloys, die, magnesium, etc. It contains a practical kind of working data, from the cold-punch hardenability of steels to the weldability of aluminum alloys and hot-working temperatures of copper alloys.

Tabulated under each of the metals listed is such information as the chemical composition of the metal; its hardnesses, tensile strengths, and other characteristics; its industrial uses; treatment temperatures for forging, annealing, quenching, etc.; such technological properties as recrystallization temperature and hot-working temperature; and a great deal of other pertinent information.

449 pages $11.00*

METALS ENGINEERING—DESIGN

This book gives the design engineer quick access to the data he must have when working out specific designs. Comprising 45 sections and written by 45 well known authorities, it provides criteria for facing the over-all problems of selection of materials . . . facts on potential weaknesses of various metals and ways of making the metals strong . . . analysis of the specific problems of corrosion and the mechanical factors which influence corrosion . . . present knowledge of welding by nondestructive methods . . . special requirements of design and surface finish set up by plastic production . . . information on the design theory, design practice, experimental design, and the special requirements of aluminum and magnesium . . . equations for determining such factors as stress, creep, impact strength . . . results of tests available on the uses of residual stresses to improve fatigue performance, and the uses of flame hardening to increase resistance to fatigue failure . . . methods for making your structure or machine part stronger, such as shot peening, cold working, and case carburizing.

400 pages 360 Illustrations $10.00*

DESIGN DATA AND METHODS

This compilation—200 pages in length—includes formulas and methods of calculating stresses in beams, bars, columns, plates, shells, and cross heads; stress component formulas; procedures for computing stresses and deformations in pressure vessels; design data on press- and shrink-fitted assemblies and also for piping; factors of working stresses; analysis of values of tangential stress in thick-walled cylinders; numerical solution of problems of gas flow where pressure changes continuously; graphical and numerical procedures for method of characteristics for two dimensional supersonic flow; chart for oblique shock waves under water; accurate bearing calculations; and methods of treating and solving problems of vibration and of balancing rotating apparatus.

$4.00*

ASME TRANSACTIONS FOR 1953

Nowhere else will you find in a single volume so much valuable information on major trends and developments throughout the mechanical engineering field. Containing 256 papers, this massive reference places at your fingertips the experiences of over 400 experts, each a specialist in his field, with significant problems connected with aviation, applied mechanics, boiler feedwater treatment, fuels, gas turbine power, heat transfer, hydraulics, industrial instruments, lubrication, machine design, metal cutting, metal engineering, oil and gas power, production engineering, rubber and plastics, and steam generation. Discussions of the papers provide additional valuable data. Supplementing the text are hundreds of tables, graphs, charts, and photographs.

[illegible] pages Cloth Bound $15.00 ($7.50 to ASME members)

VISCOSITY OF LUBRICANTS UNDER PRESSURE

This new publication reviews and co-ordinates twelve experimental investigations made in England, Germany, Japan, Russia, and the United States over a period of thirty-five years. The tests were made on 148 lubricants comprising 29 fatty oils, 74 petroleum oils, 17 compounded oils, and 28 other lubricants. Data are co-ordinated by means of daily value lubricants with similar chemical composition or chemical structure are compared. The methods proposed for computing viscosity-pressure characteristics of oils with properties determined at atmospheric pressures are explained and illustrated. Practical examples such as experimental work on bearing friction functions, lubrication calculations, and additional information for engineers and research. Conclusions and recommendations are presented. Other chapters give the empirical computation of the temperature coefficients of viscosity, method of calculating pressure coefficients, a bibliography of 189 items, and symbols used.

[illegible]

* 10% Discount to ASME Members

THE AMERICAN SOCIETY OF MECHANICAL ENGINEERS 29 W. 39th St., New York 18, N. Y.